National Library of Canada
Acquisitions and Bibliographic Services Branch
395 Wellington Street
Ottawa, Ontario
K1A 0N4

Bibliothèque nationale du Canada
Direction des acquisitions et des services bibliographiques
395, rue Wellington
Ottawa (Ontario)
K1A 0N4

Your file Votre référence

Our file Notre référence

NOTICE

The quality of this microform is heavily dependent upon the quality of the original thesis submitted for microfilming. Every effort has been made to ensure the highest quality of reproduction possible.

If pages are missing, contact the university which granted the degree.

Some pages may have indistinct print especially if the original pages were typed with a poor typewriter ribbon or if the university sent us an inferior photocopy.

Reproduction in full or in part of this microform is governed by the Canadian Copyright Act, R.S.C. 1970, c. C-30, and subsequent amendments.

AVIS

La qualité de cette microforme dépend grandement de la qualité de la thèse soumise au microfilmage. Nous avons tout fait pour assurer une qualité supérieure de reproduction.

S'il manque des pages, veuillez communiquer avec l'université qui a conféré le grade.

La qualité d'impression de certaines pages peut laisser à désirer, surtout si les pages originales ont été dactylographiées à l'aide d'un ruban usé ou si l'université nous a fait parvenir une photocopie de qualité inférieure.

La reproduction, même partielle, de cette microforme est soumise à la Loi canadienne sur le droit d'auteur, SRC 1970, c. C-30, et ses amendements subséquents.

Canada

University of Alberta

Nonlinear Viscoelasticity and Microstructural Recovery of Block Copolymers Under Shear Deformation

by

Robert D. Spaans

A thesis
submitted to the Faculty of Graduate Studies and Research
in partial fulfillment of the requirements for the degree of

Master of Science

Department of Chemical Engineering

Edmonton, Alberta

Fall 1993

National Library of Canada
Acquisitions and Bibliographic Services Branch
395 Wellington Street
Ottawa, Ontario
K1A 0N4

Bibliothèque nationale du Canada
Direction des acquisitions et des services bibliographiques
395, rue Wellington
Ottawa (Ontario)
K1A 0N4

Your file Votre référence

Our file Notre référence

The author has granted an irrevocable non-exclusive licence allowing the National Library of Canada to reproduce, loan, distribute or sell copies of his/her thesis by any means and in any form or format, making this thesis available to interested persons.

L'auteur a accordé une licence irrévocable et non exclusive permettant à la Bibliothèque nationale du Canada de reproduire, prêter, distribuer ou vendre des copies de sa thèse de quelque manière et sous quelque forme que ce soit pour mettre des exemplaires de cette thèse à la disposition des personnes intéressées.

The author retains ownership of the copyright in his/her thesis. Neither the thesis nor substantial extracts from it may be printed or otherwise reproduced without his/her permission.

L'auteur conserve la propriété du droit d'auteur qui protège sa thèse. Ni la thèse ni des extraits substantiels de celle-ci ne doivent être imprimés ou autrement reproduits sans son autorisation.

ISBN 0-315-88111-9

Canada

University of Alberta

Release Form

Name of Author:	**Robert D. Spaans**
Title of Thesis:	**Nonlinear Viscoelasticity and Microstructural Recovery of Block Copolymers Under Shear Deformation**
Degree:	Master of Science
Year this degree granted:	Fall 1993

Permission is hereby granted to **The University of Alberta Library** to reproduce single copies of this thesis and to lend or sell such copies for private, scholarly, or scientific research purposes only.

The author reserves other publication rights, and neither the thesis nor extensive tracts from it may be printed or otherwise reproduced without the author's written consent.

Robert D. Spaans

(Student's signature)

Robert D. Spaans
15 Pavilion St.
Unionville, Ontario
Canada
L3R 1N8

Date : Aug. 26, 1993

University of Alberta

Faculty of Graduate Studies and Research

The undersigned certify that they have read, and recommend to the Faculty of Graduate Studies and Research for acceptance, a thesis entitled **Nonlinear Viscoelasticity and Microstructural Recovery of Block Copolymers Under Shear Deformation** submitted by **Robert D. Spaans** in partial fulfillment of the requirements for the degree of **Master of Science**.

M.C. Williams

M.C. Williams (Supervisor)

David T. Lynch

D.T. Lynch

Daniel Steigmann

D. J. Steigmann

Date : Aug. 26, 1993.

To My Parents

Who were the diligent and sacrificial

Agents of my Lord and Saviour

To whom I owe all that I am

Abstract

The rheology of ABA-type block copolymers was investigated by means of step-strain and dynamic-strain programs. Six grades of triblock copolymers were studied. They were: Dow Vector 8508-D—a poly[b-styrene-b-butadiene-b-styrene] (SBS) copolymer having a weight average molecular weight $\overline{M}_w$=69,427 and a styrene fraction ϕ_S=0.304, Dow Vector 4461-D—an SBS with $\overline{M}_w$=61,290 and ϕ_S=0.44, Dow Vector 2510-D—an SBS with $\overline{M}_w$=101,225 and ϕ_S=0.314, Shell Kraton 1101—an SBS with $\overline{M}_w$=76,000 and ϕ_S=0.289, Shell Kraton-D 1107—a poly[b-styrene-b-isoprene-b-styrene] (SIS) copolymer having $\overline{M}_w$=140,000 and ϕ_S=0.142, and Shell WRC-91-192—a poly[b-styrene-b-ethylene/butylene-b-styrene] (SEBS) copolymer with $\overline{M}_w$=67,000 and ϕ_S=0.298.

In step strain programs, test temperatures ranged from 90°C to 110°C, all of which were above the glass transition temperatures of the styrenic phases and below the separation temperatures of these polymers, so all were multiphase systems with each phase in the liquid state. Strain amplitudes (γ) ranged from 0.05% to 4%. A spectrum of relaxation times was derived from data on relaxation modulus (G_r) *vs.* time (t), and it was demonstrated that, under certain conditions of temperature and strain amplitude, the G_r(t) curve could not be fully described by a simple series of relaxing Maxwell elements. At high γ, G_r(t) dropped steadily in liquid-like fashion, while at lower γ a solid-like network response dominated. In some cases of minimal microstructural damage the stress relaxation was overtaken by a competing microstructural recovery process (driven by thermodynamic forces of

phase separation) which caused the modulus to pass through a minimum and then recover. Differences observed in the relaxation and recovery behaviour between polymer grades were primarily related to differences in the character of the interfacial diffuse phase (interphase). The recovery process was taken as evidence in favour of a true yield stress in liquid phase block copolymers.

Evidence for the yield stress was also derived from dynamic oscillatory strain testing, which covered the temperature range 25–97°C for Vector 8508-D. Above a critical stress amplitude, waveforms became nonlinear in a periodic and reproducible manner. The shapes of the waveforms suggested the initiation of many rapid relaxational processes above the critical stress amplitude.

Acknowledgments

I must begin by acknowledging my wife who has been a great source of support and encouragement. I thank her for putting up with me during some of these months.

Professor Michael C. Williams was an excellent instructor, motivator and overseer of the project. In addition, Dr. Leigh Wardhaugh gave me much patient instruction and sacrificed his time to train me on the equipment.

To the list I must add the men in the machine shop: Keith, Bob and Ron, each of whom put up with my stupid questions and helped a great deal. I must also thank Paul and Bob in the DACS Centre as well as Walter in the instrument shop for keeping the equipment running all these months and Kevin Dorma who also helped with numerous computer related problems. The help of Andy Guo in doing some analytical work for me is also appreciated, as well as the electron microscopy performed by Nilesh Oak.

The Faculty of Engineering greatly appreciates any cooperation with industry. Dr. Kevin Mackay at Dow Chemical Company U.S.A., and Dr. Geoff Holden at Shell Chemical Company are thanked for providing block copolymer samples.

Financial aid for the project was provided by NSERC operating grant number OGP0089809. Financial support for my expense was also graciously provided by an NSERC PGS1 graduate scholarship, as well as a Walter H. Johns Fellowship

and the Captain Thomas Farrell Greenhalgh Graduate Memorial Scholarship. My thanks are therefore also extended to the donors.

This document was prepared using the LaTeX document preparation system. Donald Knuth and Leslie Lamport are thanked for placing TeX and LaTeX in the public domain. As well, Donald Knuth is thanked for his LaTeX driver for the Gnuplot graphical package which was used for all but a very few figures in this document.

Contents

Chapter 1

Introduction 1

Chapter 2

Introduction to Polymer Rheology 4

2.1 Hindered Polymer Motion 4

2.2 Stress Relaxation 5

2.3 Small Amplitude Oscillatory Shear Flow 8

2.4 Shear Rate Dependence of Viscosity 14

2.5 Molecular Weight Dependence of Viscosity 17

2.6 Glass Transition 17

2.7 Time-Temperature Superposition 18

2.8 Thixotropy 19

Chapter 3

Review of Literature 21

3.1 Thermodynamics of Phase Separation 21

3.1.1 Two Phase Model 22

3.1.2 Three Phase Model 23
3.1.3 Interphase Free Energy Barrier 27
3.2 Microstructure 29
3.3 Nonlinear Mechanical Properties 31
3.3.1 Network Characteristics 31
3.3.2 Effect of Molecular Architecture 33
3.3.3 Plastic-to-Rubber Transition 33
3.3.4 Mechanisms of Mechanical Failure 36
3.3.5 Microstructural Repair 36
3.4 Rheology 37
3.4.1 Steady Shear Flow 37
3.4.2 Dynamic Strain Testing 40
3.4.3 Yield Stress 51

Chapter 4

Equipment and Methods; Rheological Testing **54**

4.1 Sensitivity 54
4.2 Modes of Operation 56
4.2.1 Dynamic Oscillatory 56
4.2.2 Dynamic Transient 58
4.2.3 Steady Mode 58
4.3 Auto-Zeroing of Motor 60
4.4 Alignment 60
4.5 Sample Gap 61

4.6 Autotension 62

4.7 "Internal" Data Acquisition and Analysis 62

4.8 "External" Data acquisition 63

4.9 Sample Formation 63

4.10 Temperature Control 64

4.11 Sample Loading 65

Chapter 5

Materials **66**

Chapter 6

Results 1; Stress Relaxation Experiments **76**

6.1 Step Strain Tests 76

6.1.1 SBS1 76

6.1.2 SBS2 93

6.1.3 SIS 99

6.1.4 SBS3 and SEBS 104

6.2 Step Rate Tests 104

Chapter 7

Results 2; Nonlinear Waveforms **110**

7.1 Strain Sweep 110

7.2 Frequency/Temperature Sweep 111

7.3 Waveforms 112

Chapter 8

Results 3; Phase Transition **143**

Chapter 9

Discussion **148**

9.1 Theory 148

9.1.1 Yield Stress 148

9.1.2 Phase Transition 153

9.2 Stress Relaxation Experiments 154

9.2.1 SBS1 155

9.2.2 SBS2 163

9.2.3 SIS 165

9.2.4 Peak Moduli 166

9.2.5 Relaxation Times 167

9.2.6 SBS3 and SEBS 174

9.3 Step Rate Tests 175

9.4 Nonlinear Waveforms 175

9.5 Phase Transition Phenomena: A Speculative Discussion 182

References **185**

Appendix A

Calibrations **195**

A.1 Torque 195

A.2 Gap 199

A.3 Circulation Jacket 199

Appendix B

Compression Mold 205

Appendix C

Graphical Curve Fitting 208

Appendix D

Copyrighted Materials 213

List of Tables

4.1 Staging area components. 56

5.1 Summary of polymers used. 67

6.1 Conditions for step strain tests on SBS1. 77
6.2 Peak stress and modulus for SBS1. 87
6.3 Conditions for step strain tests on SBS2. 93
6.4 Peak stress and modulus for SBS2. 98
6.5 Conditions for step strain tests on SIS. 100
6.6 Peak stress and modulus and final torque for SIS. 101
6.7 Final modulus for SIS at 90°C. 104

7.1 Actual γ° *vs.* nominal γ_N° for frequency/temperature sweep on SBS1. 115

A.1 Normal torque range calibration. 197
A.2 Low torque range calibration. 198
A.3 Tool expansion calibration. 200
A.4 Circulation jacket temperature calibration. 203

List of Figures

1.1 Triblock copolymer of the ABA type; end blocks are of the same chemical structure. 1

2.1 Step strain (a) and stress relaxation (b) in typical liquid polymers. . . 6

2.2 Maxwell spring and dashpot. 7

2.3 Strain input and shear stress measurement in a parallel plate rheometer; taken, with permission, from [60]. 9

2.4 In-phase shear stress response of an elastic solid to sinusoidal strain input. 10

2.5 Out-of-phase shear stress response of a Newtonian fluid to sinusoidal strain input. 11

2.6 Shear stress response of a viscoelastic fluid. 12

2.7 Typical shear rate or frequency dependence of viscosity for polymer melts 14

2.8 Stress-strain rate relationship for a fluid exhibiting a yield stress σ_y and constant "plastic" viscosity above zero shear rate. 16

2.9 Frequency dependence of viscosity for yield stress materials. 17

2.10 Loss and storage modulus *vs.* temperature for a single phase polymer. 18

3.1 Model of phase-separated microstructure for lamellar domains (top) and normal spherical or cylindrical domains (middle), showing the composition profile of minor component S (bottom) assuming a step change to 50% in the interphase. ΔT (or ΔR for cylindrical morphology) is the interphase thickness and D is the inter-domain spacing. 24

3.2 (a) Composition profile across the mixed interphase of thickness ΔR. The profile may be asymmetric, as shown. (b) Thermodynamic force profile corresponding to composition profile. The total barrier force F_A^i described in the text is the sum of the F_{Ak}^i acting on all units in the interphase. (c) Withdrawal of A block from domain core into matrix of B. Friction coefficients of four different types are indicated. 28

4.1 Staging area of the RMS 800. 55

4.2 Strain *vs.* time in four sequential zones as programmed in the step rate mode. 59

5.1 DSC heating scan of SBS1 showing two distinct transitions. 68

5.2 DSC heating scan of the polystyrene-rich glass transition region in SBS1. 68

5.3 Loss modulus as a function of temperature (heating run) for SBS1. . 69

5.4 DSC heating scan of microphase transition region in SBS1. 70

5.5 DSC heating scan of SBS2 showing three distinct transitions. 71

5.6 DSC heating scan of the styrene-rich glass transition region in SBS2. 71

5.7 DSC heating scan of microphase transition region in SBS2. 72

5.8 DSC heating scan of SIS showing four distinct transitions. 73

5.9 DSC heating scan of the glass transition region in SIS. 74

5.10 DSC heating scan of microphase transition region in SIS. 74

5.11 DSC heating scan of diblock transition region in SIS. 75

6.1 Stress relaxation experiments for SBS1 at 90°C. 78

6.2 Strain and stress irregularities, $\gamma_N = 4\%$. 80

6.3 Strain and stress irregularities, $\gamma_N = 0.05\%$. 81

6.4 Relaxation modulus $G_r(t)$ for SBS1 at 90°C, $\gamma_N = 1\%$ and 4%. . . . 83

6.5 Relaxation modulus $G_r(t)$ for SBS1 at 90°C, $\gamma_N = 0.05\%$ to 0.3%. . . 84

6.6 Relaxation modulus $G_r(t)$ for SBS1 at 100°C. 86

6.7 Relaxation modulus $G_r(t)$ for SBS1 at 110°C. 89

6.8 Temperature dependence of $G_r(t)$ for SBS1 at γ_N=0.1%. 90

6.9 Temperature dependence of $G_r(t)$ for SBS1 at γ_N=0.2%. 91

6.10 Temperature dependence of $G_r(t)$ for SBS1 at γ_N=1%. 92
6.11 Temperature dependence of $G_r(t)$ for SBS1 at γ_N=4%. 92
6.12 Torque relaxation for SBS2 at 110°C, γ_N = 0.1%. 94
6.13 Torque relaxation for SBS2 at 110°C, γ_N = 0.2%. 95
6.14 Torque relaxation for SBS2 at 110°C, γ_N = 0.4%. 95
6.15 Torque relaxation for SBS2 at 110°C, γ_N = 0.4%; no external data logging. 96
6.16 Torque relaxation for SBS2 at 110°C, γ_N = 1%; no external data logging. 96
6.17 Relaxation modulus $G_r(t)$ for SBS2 at 110°C. 97
6.18 Relaxation modulus $G_r(t)$ comparison for SBS1 and SBS2 at 110°C, γ_N = 1%. 98
6.19 Relaxation modulus $G_r(t)$ for SIS at 110°C, γ_N° = 0.1% to 4%. 102
6.20 Relaxation modulus $G_r(t)$ for SIS at 90°C, γ_N = 0.1% to 4%. 103
6.21 Relaxation modulus $G_r(t)$ for SIS at 90°C, γ_N = 0.1% to 0.2%. . . . 105
6.22 Relaxation modulus $G_r(t)$ for SIS at 90°C, γ_N = 0.4% to 4%. 105
6.23 Stress relaxation for SBS1 at 90°C after step strains at 1×10^{-4} rad/s *vs.* linear time. 108
6.24 Stress relaxation for SBS1 at 90°C after step strains at 1×10^{-4} rad/s *vs.* logarithmic time. 109

7.1 Strain sweep on SBS4, at 30°C and ω=1 rad/s. 111
7.2 Strain sweep on SBS1, at 30°C and ω=1 rad/s. 112
7.3 Dynamic viscosity frequency/temperature sweep on SBS1 γ_N° =0.5%. 113
7.4 η'' frequency/temperature sweep on SBS1, γ_N° =0.5%. 114
7.5 Run 2: Dynamic stress response of SBS1 at 25.6°C; γ_N° =γ° =2%, ω=1 rad/s. 117
7.6 Run 2: Dynamic stress response of SBS1 at 25.6°C; γ_N° =γ° =2%, ω=1 rad/s from 30 to 45 seconds. 118
7.7 Run 2: Dynamic stress response of SBS1 at 25.6°C; γ_N° =γ° =2%, ω=1 rad/s from 50 to 65 seconds. 118
7.8 Run 1: Dynamic stress response of SBS1 at 25.6°C; γ_N° =γ° =2%, ω=0.1 rad/s. 119

7.9 Run 3: Dynamic stress response of SBS1 at 25.6°C; $\gamma_N^o = \gamma^o = 2\%$, ω=10 rad/s. 119

7.10 Run 5: Dynamic stress response of SBS1 at 25.6°C; $\gamma_N^o = \gamma^o = 2\%$, ω=0.01 rad/s. 120

7.11 Run 6: Dynamic stress response of SBS1 at 43.2°C; $\gamma_N^o = \gamma^o = 2.5\%$, ω=0.1 rad/s. 121

7.12 Run 7: Dynamic stress response of SBS1 at 43.2°C; $\gamma_N^o = \gamma^o = 2.5\%$, ω=1 rad/s. 122

7.13 Run 8: Dynamic stress response of SBS1 at 43.2°C; $\gamma_N^o = \gamma^o = 2.5\%$, ω=10 rad/s. 122

7.14 Run 10: Dynamic stress response of SBS1 at 43.2°C; $\gamma_N^o = \gamma^o = 2.5\%$, ω=0.01 rad/s. 123

7.15 Run 11: Dynamic stress response of SBS1 at 60.5°C; $\gamma_N^o = \gamma^o = 2.5\%$, ω=0.1 rad/s. 124

7.16 Run 12: Dynamic stress response of SBS1 at 60.5°C; $\gamma_N^o = \gamma^o = 2.5\%$, ω=1 rad/s. 125

7.17 Run 13: Dynamic stress response of SBS1at 60.5°C; $\gamma_N^o = \gamma^o = 2.5\%$, ω=10 rad/s. 125

7.18 Run 14: Dynamic stress response of SBS1 at 60.5°C; $\gamma^o = 1.89\%$, ω=100 rad/s. 126

7.19 Run 15: Dynamic stress response of SBS1 at 60.5°C; $\gamma_N^o = \gamma^o = 2.5\%$, ω=0.01 rad/s. 126

7.20 Run 16: Dynamic stress response of SBS1 at 96.7°C; $\gamma_N^o = \gamma^o = 2.9\%$, ω=0.1 rad/s. 128

7.21 Run 17: Dynamic stress response of SBS1 at 96.7°C; $\gamma_N^o = \gamma^o = 2.9\%$, ω=1 rad/s. 128

7.22 Run 18: Dynamic stress response of SBS1 at 96.7°C; $\gamma_N^o = \gamma^o = 2.9\%$, ω=10 rad/s. 129

7.23 Run 20: Dynamic stress response of SBS1 at 25.6°C; $\gamma_N^o = \gamma^o = 2\%$, ω=0.1 rad/s, second cycle. 130

7.24 Run 21: Dynamic stress response of SBS1 at 25.6°C; $\gamma_N^o = \gamma^o = 2\%$, ω=1 rad/s, second cycle. 131

7.25 Run 22: Dynamic stress response of SBS1 at 25.6°C; $\gamma_N^o = \gamma^o = 2\%$, ω=10 rad/s, second cycle. 131

7.26 Run 27: Dynamic stress response of SBS1 at 25.6°C; $\gamma_N^o = \gamma^o = 3\%$, ω=10 rad/s, second cycle. 132

7.27 Run 29: Dynamic stress response of SBS1 at 45.4°C; $\gamma_N^o = \gamma^o = 3\%$, ω=0.1 rad/s, second cycle. 133

7.28 Run 30: Dynamic stress response of SBS1 at 45.4°C; $\gamma_N^o = \gamma^o = 3\%$, ω=1 rad/s, second cycle. 133

7.29 Run 31: Dynamic stress response of SBS1 at 45.4°C; $\gamma_N^o = \gamma^o = 3\%$, ω=10 rad/s, second cycle. 134

7.30 Run 34: Dynamic stress response of SBS1 at 60.5°C; $\gamma_N^o = \gamma^o = 3\%$, ω=0.1 rad/s, second cycle. 134

7.31 Run 35: Dynamic stress response of SBS1 at 60.5°C; $\gamma_N^o = \gamma^o = 3\%$, ω=1 rad/s, second cycle. 135

7.32 Run 36: Dynamic stress response of SBS1 at 60.5°C; $\gamma_N^o = \gamma^o = 3\%$, ω=10 rad/s, second cycle. 135

7.33 Run 38: Dynamic stress response of SBS1 at 60.5°C; $\gamma_N^o = \gamma^o = 3\%$, ω=0.01 rad/s, second cycle. 136

7.34 Run 39: Dynamic stress response of SBS1 at 96.5°C; $\gamma_N^o = \gamma^o = 3.5\%$, ω=0.01 rad/s, second cycle. 137

7.35 Run 40: Dynamic stress response of SBS1 at 96.5°C; $\gamma_N^o = \gamma^o = 3.5\%$, ω=0.1 rad/s, second cycle. 138

7.36 Run 41: Dynamic stress response of SBS1 at 96.5°C; $\gamma_N^o = \gamma^o = 3.5\%$, ω=1 rad/s, second cycle. 138

7.37 Run 42: Dynamic stress response of SBS1 at 96.5°C; $\gamma_N^o = \gamma^o = 3.5\%$, ω=10 rad/s, second cycle. 139

7.38 Run 43: Dynamic stress response of SBS1 at 96.8°C; $\gamma_N^o = \gamma^o = 5\%$, ω=0.01 rad/s, second cycle. 140

7.39 Run 44: Dynamic stress response of SBS1 at 96.5°C; $\gamma_N^o = \gamma^o = 5\%$, ω=0.1 rad/s, second cycle. 141

7.40 Run 45: Dynamic stress response of SBS1 at 96.8°C; $\gamma_N^o = \gamma^o = 5\%$, ω=1 rad/s, second cycle. 141

7.41 Run 46: Dynamic stress response of SBS1 at 96.8°C; $\gamma_N^o = \gamma^o = 5\%$, ω=10 rad/s, second cycle. 142

8.1 SBS4 solvated with 5 base oil, G' and η' strain sweep at 30°C and 1 rad/s. 144

8.2 Dynamic moduli SBS4 solvated with 5 base oil temperature sweep at 10 rad/s. 145

8.3 Dynamic viscosities for SBS4 solvated with 5 base oil temperature sweep at 10 rad/s. 145

8.4 SBS4 solvated with 5 base oil η^*–frequency/temperature sweep. . . . 146

9.1 Eyring rate model for (a) homopolymer segment with no imposed stress, (b) homopolymer segment with imposed stress, (c) block copolymer segment junction with imposed stress. σ is an imposed stress and $\sigma_A \equiv \frac{1}{2}\sigma/n_A$, where n_A is the molar density of A units. $\Delta\mu_A$ is a chemical potential difference. 151

9.2 Stress relaxation curves for typical homopolymers. 154

9.3 σ(t) for SBS1 at 90°C and γ=0.1% modeled as two competing exponentials. 157

9.4 Graphical fit of relaxation times for SBS1 at 90°C and γ=1%. 168

9.5 Graphical fit of short time relaxation for SBS1 at 90°C and γ=1%. . 169

9.6 Graphical fit of relaxation times for SBS1 at 90°C and γ=4%. 170

9.7 Graphical fit of relaxation times for SBS1 at 100°C and γ=1%. 170

9.8 Graphical fit of relaxation times for SBS1 at 110°C and γ=4%. 171

9.9 Graphical fit of relaxation times for SBS2 at 110°C and γ=1%. 172

9.10 Graphical fit of relaxation times for SIS at 110°C and γ=1%. 172

9.11 Graphical fit of short time relaxations for SIS at 110°C and γ=1%. . 173

9.12 Graphical fit of relaxation times for SIS at 90°C and γ=1%. 174

A.1 Transducer calibration set-up. 196

A.2 Tool expansion calibration. 201

A.3 Circulation oven temperature calibration. 204

B.1 Compression mold (a); heater base. 206

B.2 Compression mold (b); 50 mm die assembly. 207

C.1 First (longest) relaxation fit to G_r(t) for SBS1 at 1% strain and 90°C. 209

C.2 Second relaxation fit to G_r(t) for SBS1 at 1% strain and 90°C. 210

C.3 Third relaxation fit to $G_r(t)$ for SBS1 at 1% strain and 90°C. 211
C.4 Fourth relaxation fit to $G_r(t)$ for SBS1 at 1% strain and 90°C. 211
C.5 Composite of relaxations fit to $G_r(t)$ for SBS1 at 1% strain and 90°C. 212

Nomenclature

a_T	shift factor
B	subscript or superscript denotes polybutadiene
c_s	critical solution concentration (mol/l)
E	energy
E	subscript denotes engineering
E'	storage modulus in tension (Pa)
E''	loss modulus in tension (Pa)
E^*	complex modulus in tension (Pa)
ΔE	activation energy (J/mol)
f	overall fraction of interphase
G	shear modulus (Pa), or Gibbs free energy (J/mol)
G'	storage modulus in shear (Pa)
G''	loss modulus in shear (Pa)
G^*	complex modulus in shear (Pa)
G_r	relaxation modulus in shear (Pa)
ΔG	free energy difference (J/mol)
H	height (gap spacing) (mm)
ΔH	enthalpy difference (J/mol)
I	subscript or superscript denotes polyisoprene
K	Kelvin degrees

M_c	critical molecular weight for entanglement onset, or molecular weight between crosslinks (g/mol)
MW	molecular weight (g/mol)
$\overline{M}_w$	weight average molecular weight (g/mol)
$\overline{M}_n$	number average molecular weight (g/mol)
PB	polybutadiene
PI	polyisoprene
PS	polystyrene
R	radius of platens
ΔR	interphase thickness
S	subscript or superscript denotes polystyrene
SB	styrene-butadiene diblock copolymer
SBR	random copolymer of styrene and butadiene
SBS	styrene-butadiene-styrene triblock copolymer
SI	styrene-isoprene diblock copolymer
SIS	styrene-isoprene-styrene block copolymer
SEBS	styrene-(ethylene/butylene)-styrene block copolymer
ΔS	entropy difference (J/mol·K)
t	time (s)
T	temperature (°C or K)
T_g	glass transition temperature (°C or K)
T_s	separation temperature (°C or K)
ΔT	interphase thickness (Å)
V_m	molar volume (m^3/mol)

Greek Letters

γ	shear strain
γ_N	commanded (steady) shear strain
$\dot{\gamma}$	strain rate, usually in shear (s^{-1})
γ^o	dynamic (shear) strain amplitude
γ_N^o	commanded dynamic (shear) strain amplitude
δ	phase angle (degrees)
δ_i	solubility parameter of component i $(cal/cm^3)^{1/2}$
$\Delta\delta$	solubility parameter difference, $\delta_i - \delta_j$ $(cal/cm^3)^{1/2}$
ε	tensile strain
ε_E	engineering tensile strain
η	non-Newtonian viscosity (Pa·s)
η_o	zero shear rate limiting Newtonian viscosity (Pa·s)
η'	dynamic viscosity, out of phase with γ (Pa·s)
η''	in-phase viscosity function (Pa·s)
η^*	complex viscosity $= \eta' - i\eta''$ (Pa·s)
θ	angle of rotation (rad)
λ	relaxation time (s)
μ	Newtonian viscosity (Pa·s)
μ_i	chemical potential $= \left(\frac{\partial G}{\partial N_i}\right)_{N_j,T,P}$ (J/mol)
ρ	density (kg/m^3)
σ	stress (Pa)
σ_y	yield stress (Pa)
ϕ_i	volume fraction of component i
ϕ_I	overall volume fraction of the interphase
ω	frequency (s^{-1})

Chapter 1

Introduction

Block copolymers are polymeric chains having two or more monomer constituents grouped in large segments or blocks which are covalently bonded to other segments to form a single linear chain. In Figure 1.1 a triblock copolymer, *i.e.* one with three segments, is depicted with end blocks consisting of the same chemical units. These are known as ABA type copolymers.

The production of block copolymers was first announced by the Shell Chemical Company (U.S.A.) in 1965. Since then they have found application in many commercial products such as shoe soles, blend compatabilizers and adhesives.

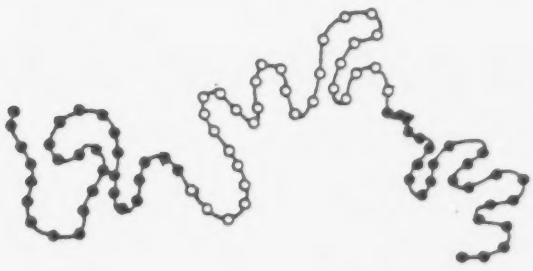

Figure 1.1: Triblock copolymer of the ABA type; end blocks are of the same chemical structure.

Block copolymers are produced by anionic polymerization techniques. Each block is formed separately and then chemically joined to its neighbouring block. The result is that the blocks contain no random sections and that each block has a narrow molecular weight distribution, or low polydispersity.

Because of chemical incompatibility between the covalently bonded blocks, segments of like kind coalesce at temperatures below some critical "separation temperature" T_s. For a triblock copolymer of the ABA type, as depicted in Figure 1.1, having a rubbery center block and glassy end blocks at room temperature the resulting material is known as a "thermoplastic elastomer" and behaves like a crosslinked rubbery solid.

The crosslinked elastomeric character is due to the network structure of these polymers. The end blocks trapped in glassy domains act as multi-junction crosslink points and the entanglements in the rubbery center blocks, which are prevented from slipping off by the network structure, enhance the strength of the rubbery phase. This gives the material most of the useful physical properties of vulcanized rubbers: high resilience, high tensile strength, highly reversible elongation and high abrasion resistance [21].

All of these properties are achieved without chemical crosslinking. Above the glass transition temperature of the dispersed phase (assuming no crystallinity), this two phase liquid system will flow under high enough stresses, so that these materials can be formed into useful products using conventional polymer processing technology. Upon cooling the network structure is reformed. This is unlike conventional vulcanizates, which are thermosets, *i.e.* degrade upon reheating and thus cannot be reformed. The temperature reversibility of the network structure leads to the "thermoplastic" in the name.

The rheology of these multi-phase materials has been an area of active investigation since their discovery and has presented many interesting questions to researchers. The rheology can be used as a probe of the microstructure, right

down to molecular dimensions. It can also be used to investigate the relationship between stress, strain and structure as well as the role of strain as a thermodynamic variable.

The rheology clearly has an important role to play in understanding the processing of these materials. The amazing utility of polymers in the marketplace stems largely from our ability to tailor the properties to our applications. While control over these properties is not absolute, processing history joins chemical structure as an important factor in determining end properties. With highly structured materials which display marked shear history dependence such as block copolymers it is possible to choose the shear history to achieve a wide range of properties. Other complex features of the rheology of these materials are also important to the processing characteristics and final properties. These include yield stresses, strongly non-Newtonian viscosity - shear rate relationships, high melt elasticity, and temperature as well as shear induced phase transitions.

Chapter 2

Introduction to Polymer Rheology

A few definitions should be covered before discussing the rheology of polymers.

Rheology The study of the deformation of matter.

Flow Deformation without a limit imposed by the material.

Solid A material which will not flow, *i.e.* the molecular character or microstructure of a solid material imposes a limit on deformation.

Liquid Any material which will flow (gases excepted).

2.1 Hindered Polymer Motion

Polymeric materials consist of long chain molecules which hinder the motions of their neighbouring chains. Two models have been used extensively to explain this hindrance behaviour.

The earliest was the entanglement model. Polymer molecules are thought to loop around each other and hinder each other in moving. Therefore, to move any one polymer molecule it is necessary to move several others because of the restricting entanglements ([61] p.191).

The reptation model begins by envisioning each polymer molecule to be contained in a tube formed by its surrounding neighbours. In order to move, the polymer molecule must diffuse down the tube. Individual segments may move by "reptating", *i.e.* moving in a fashion similar to a snake. Motion of the entire molecule is possible only by cooperative motion of several subsections of the chain, which would be made more probable and directional by the existence of an imposed stress. The small probability of cooperative motion in such long chains is the source of the high viscosities of polymers. This model overcame some fundamental objections to the entanglement model, since polymer molecules are not flexible enough to loop around each other in the manner usually depicted in conceptual diagrams. It would not actually be possible to tie a knot in a polymer molecule. However, the reptation model has yet to prove its utility in a quantitative way to the extent that the entanglement model has [61].

2.2 Stress Relaxation

When a polymer liquid sample is subjected to a step strain as in Figure 2.1 (a) the stress response is similar to that depicted in Figure 2.1 (b). The immediate response, similar to an elastic solid, is a jump in stress. This is followed by a viscoelastic response which is a relaxation of the imposed stress over time. The stress will approach zero stress asymptotically. This behaviour is known as viscoelasticity.

When the strain is first imposed the polymer molecules store this strain because they cannot untangle, or diffuse, quickly enough to relieve the stress. Over time the molecules are able to diffuse and disentangle so as to relieve the stress. Small

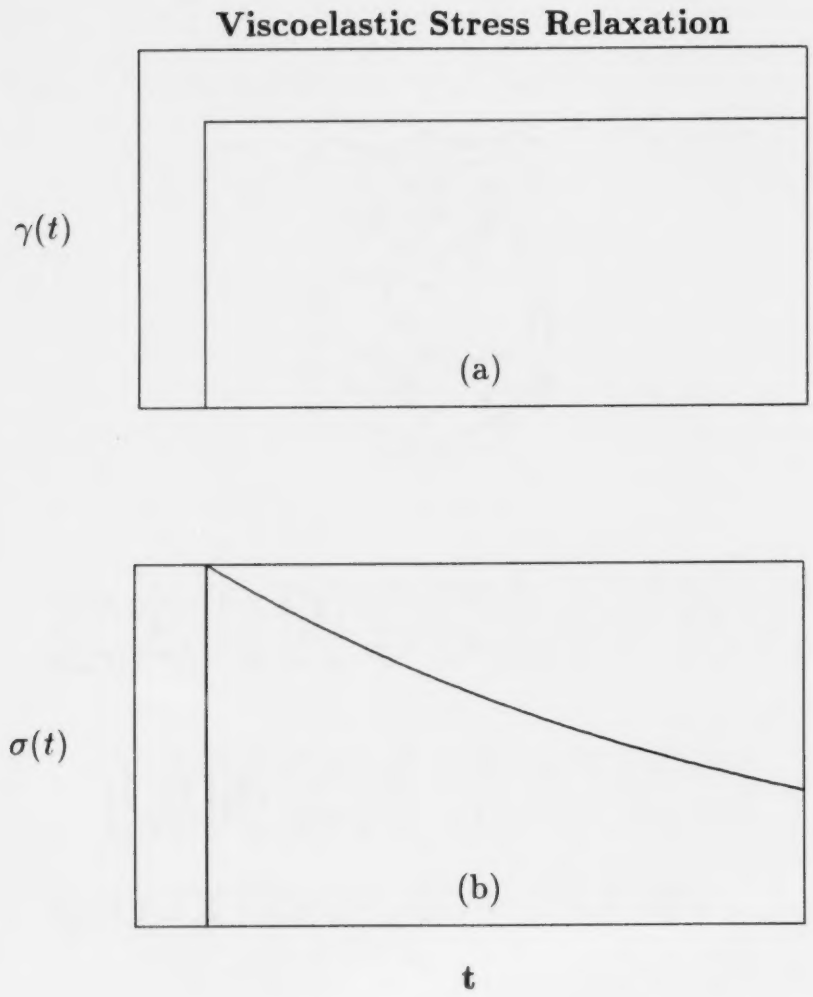

Figure 2.1: Step strain (a) and stress relaxation (b) in typical liquid polymers.

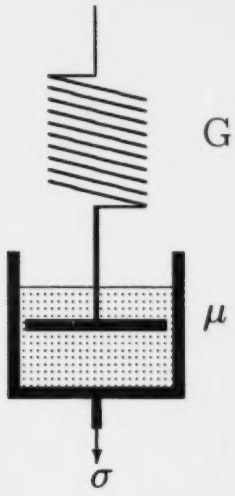

Figure 2.2: Maxwell spring and dashpot.

molecules, such as water, have very short relaxation times, on the order of 10^{-15} seconds or less, so that it is not possible to observe the stress relaxation behaviour of low molecular weight liquids.

Viscoelasticity can be modeled qualitatively if the material is thought of as a Hookean spring with modulus G and a dashpot containing a Newtonian viscous liquid with viscosity μ[1] coupled in series so that both components bear the same stress (Figure 2.2). A quantitative representation of this "Maxwell Model" behaviour is ([71] p.158):

$$\sigma + \lambda \frac{\partial \sigma}{\partial t} = \mu \frac{\partial \gamma}{\partial t} \tag{2.1}$$

$$\textit{where the relaxation time } \lambda \equiv \frac{\mu}{G}. \tag{2.2}$$

For the experiment depicted in Figure 2.1, $\gamma = 0$ for $t < 0$, $\gamma = \gamma_o$ for $t \geq 0$.

[1] In this manuscript, the symbol μ is used to denote *Newtonian* viscosities only, while the symbol η is used to denote non-Newtonian viscosities.

The time dependent stress is then

$$\sigma(t) = \sigma(0)e^{-t/\lambda} = \gamma_0 G e^{\frac{-t}{\lambda}}. \tag{2.3}$$

The Maxwell model cannot successfully be used for fitting data, mainly because it contains only one relaxation time while real polymers would have a spectrum of relaxation times because each chain has many relaxation modes and any polydispersity would broaden the spectrum even further. However, the Maxwell model is qualitatively correct and more complex models of linear viscoelasticity will not be discussed here.

2.3 Small Amplitude Oscillatory Shear Flow

In a concentric disk rheometer a sample can be subjected to an oscillatory shear strain as depicted in Figure 2.3. The bottom platen oscillates while the top platen transmits torque to a transducer which measures the stress output. A perfectly elastic solid (the Hookean spring with no dashpot in the Maxwell model) would respond to a sinusoidal strain input with an in-phase sinusoidal stress output (Figure 2.4), according to

$$\sigma = G\gamma(t) = G\gamma_o \sin \omega t. \tag{2.4}$$

An inelastic, Newtonian fluid which obeys Newton's law of viscosity would, if subjected to a sinusoidal strain input, respond with an out-of-phase sinusoidal stress output (Figure 2.5)

$$\sigma = \mu \frac{\partial \gamma}{\partial t} \equiv \mu \dot{\gamma} = \mu\gamma_o\omega \cos \omega t. \tag{2.5}$$

When shear rate $\frac{\partial \gamma}{\partial t}$ is zero, stress is also zero. When shear rate is a maximum, stress is also a maximum. As a result, the phase lag between stress and strain is 90°. A viscoelastic liquid will respond with a phase lag between 0 and 90° (Figure 2.6). Therefore, an oscillatory strain input of angular frequency ω

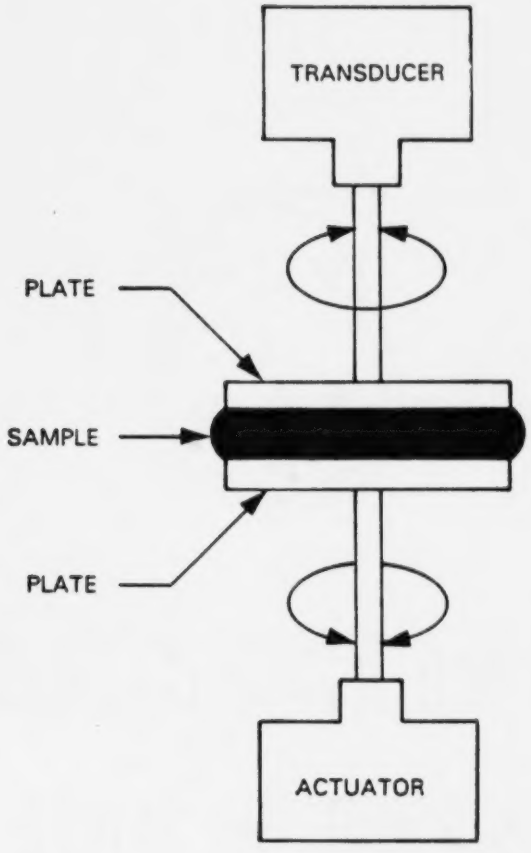

Figure 2.3: Strain input and shear stress measurement in a parallel plate rheometer; taken, with permission, from [60].

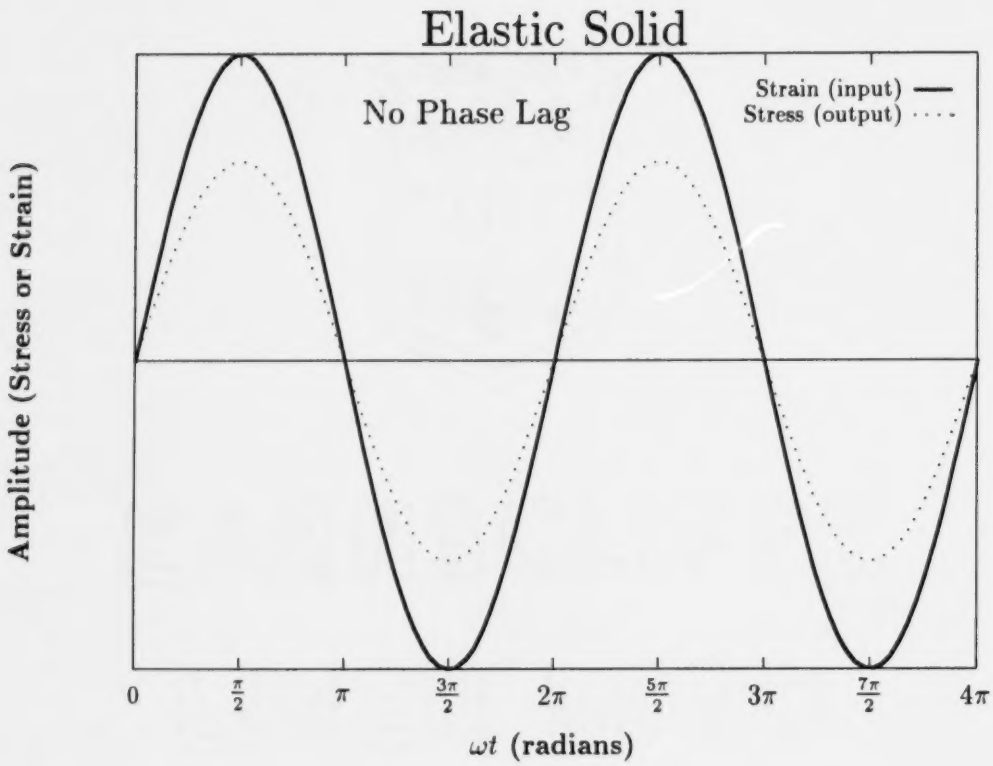

Figure 2.4: In-phase shear stress response of an elastic solid to sinusoidal strain input.

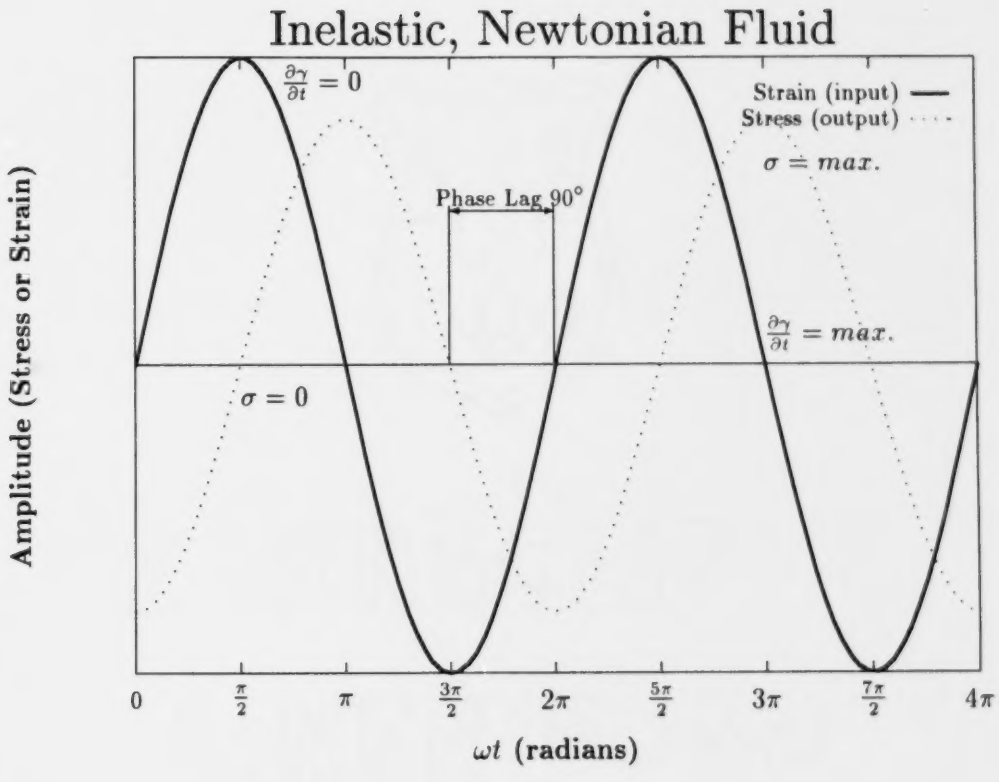

Figure 2.5: Out-of-phase shear stress response of a Newtonian fluid to sinusoidal strain input.

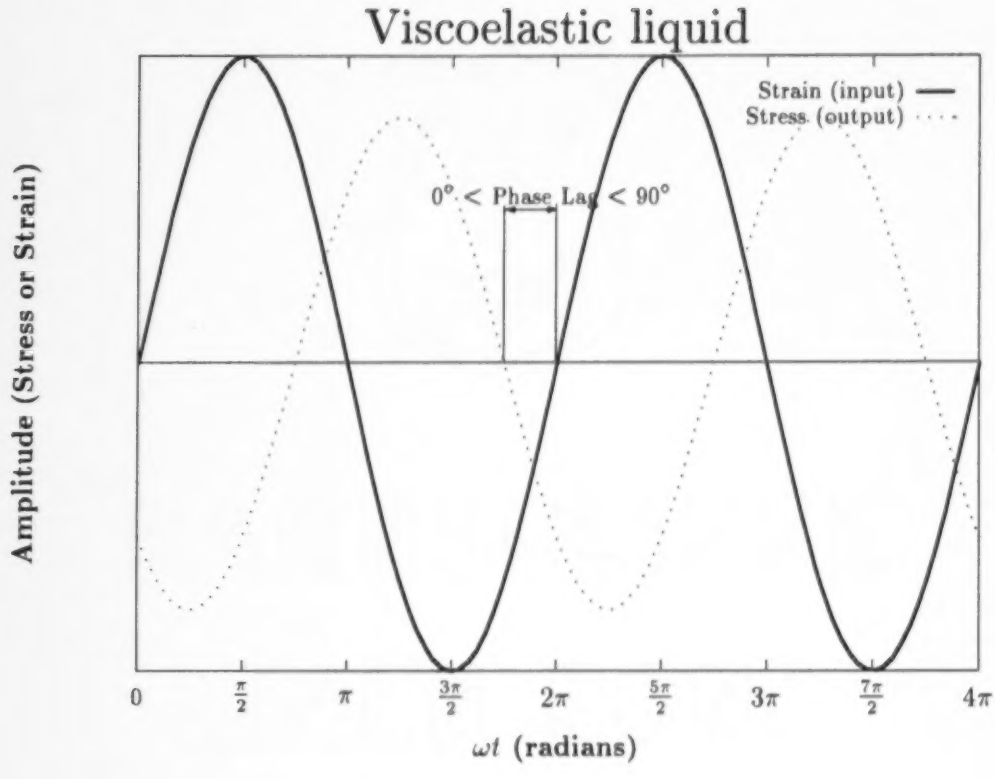

Figure 2.6: Shear stress response of a viscoelastic fluid.

$$\gamma = \gamma_o \sin \omega t \tag{2.6}$$

results in a sinusoidal stress output which lags behind the strain by a phase angle δ

$$\sigma = \sigma_o \sin(\omega t + \delta). \tag{2.7}$$

Rewriting Equation 2.7 by means of the trigonometric identity [$\sin(\alpha + \beta) = \sin\alpha\cos\beta + \cos\alpha\sin\beta$] we obtain

$$\sigma = (\sigma_o \cos\delta) \sin\omega t + (\sigma_o \sin\delta) \cos\omega t \tag{2.8}$$

so that the stress consists of two components: one in phase with the strain ($\sigma_o \cos\delta$) and the other 90° out of phase ($\sigma_o \sin\delta$). Both σ_o and δ are functions of ω.

Two material properties can now be defined:

Storage modulus (in phase): $G' \equiv \frac{\sigma_o}{\gamma_o} \cos\delta$ and

Loss modulus (out of phase): $G'' \equiv \frac{\sigma_o}{\gamma_o} \sin\delta$

so that

$$\sigma = \gamma_o [G' \sin\omega t + G'' \cos\omega t]. \tag{2.9}$$

Two viscosity functions can then be defined as:

$$\eta' \equiv \frac{G''}{\omega} \tag{2.10}$$

$$\eta'' \equiv \frac{G'}{\omega}. \tag{2.11}$$

Alternatively, the entire development above can be done in complex numbers ($e^{i\omega t}$). Then the complex shear modulus and the complex viscosity are

$$G^* = G' + iG'' \tag{2.12}$$

$$\eta^* = \eta' - i\eta''. \tag{2.13}$$

Normally these functions are determined at various strain amplitudes in order to determine the range of strains at which the measured properties do not change

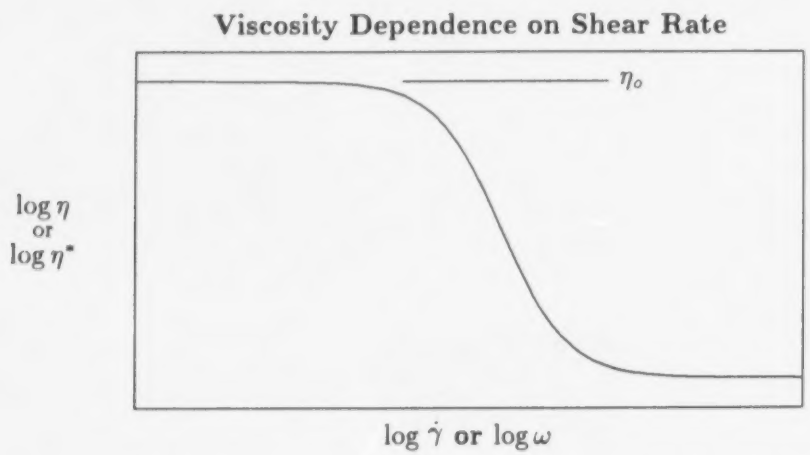

Figure 2.7: Typical shear rate or frequency dependence of viscosity for polymer melts .

with amplitude. This is known as the linear region and is by definition the region in which the microstructure of the tested material is not affected by the test. Properties tested in the linear region are known as "linear viscoelastic properties".

2.4 Shear Rate Dependence of Viscosity

For a Newtonian fluid, shear stress is directly proportional to shear rate at all shear rates and thus viscosity ($\mu \equiv \sigma / \dot{\gamma}$) is a constant when plotted against $\dot{\gamma}$. Polymers do not behave in such a simple fashion. A typical single phase polymer melt exhibits a non-Newtonian viscosity $\eta(\dot{\gamma})$ relationship like that depicted in Figure 2.7. Similar variation of $\eta'(\omega)$ and $|\eta^*(\omega)|$ ($\equiv \eta^*$ hereafter) is seen, with $\eta^*(\omega)$ usually very close to $\eta(\dot{\gamma})$. The high initial plateau is known as the low shear limiting viscosity, or Newtonian limit, and the low plateau at high shear rates is known as the upper Newtonian limit.

Figure 2.7 can perhaps best be understood by first considering the case of steady

shear flow. The high Newtonian limiting viscosity is a manifestation of the hindered motion of the polymer chains due to entanglements, requiring high shear stresses to pull them apart. In the transition region where viscosity drops off with increasing shear rates the entanglement network is gradually disrupted. In this region a process of disentanglement and re-entanglement is occurring, but as the shear rate increases disentanglement dominates to an increasing degree. At high shear rates the entanglement network is disrupted to its largest degree and the shear stress once again becomes proportional to shear rate so that the viscosity is constant. This is the primary explanation, though contributions from orientation and other factors also exist.

In small amplitude oscillatory shear testing a similar relationship is seen between dynamic viscosity and frequency. Low frequencies are a probe of long range structure because they correspond to the longest relaxation times which are related to long range cooperative motions. Long range motions in a polymer melt are difficult because of the hinderance of surrounding chains. Cooperation between many segments of a chain must occur for motion of a chain to occur and thus viscosity is high at low frequencies. At higher frequencies shorter range motions are detected corresponding to movements of smaller segments of a chain which is easier and thus viscosity is lower. At high frequencies a point is reached at which the relaxation time corresponding to the movement of a single subunit of the chain is indicated. This is the shortest range motion of the chain, requiring the least time and least cooperation and thus the viscosity again levels off with increasing frequency.

For multi-phase systems exhibiting a yield stress the behaviour of Figure 2.7 is not observed. Yield stress materials will not flow under imposed stresses lower than the yield stress σ_y, so that

$$\dot{\gamma} = 0 \qquad \sigma < \sigma_y \tag{2.14}$$

$$\sigma = \sigma_y + \mu_p \dot{\gamma} \qquad \sigma \geq \sigma_y. \tag{2.15}$$

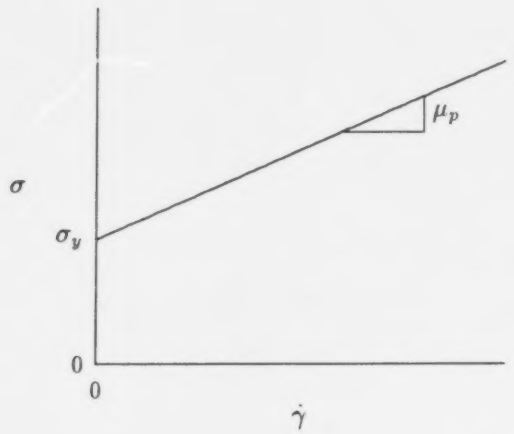

Figure 2.8: Stress-strain rate relationship for a fluid exhibiting a yield stress σ_y and constant "plastic" viscosity above zero shear rate.

In Equation 2.15, which is represented in Figure 2.8, the relationship between stress and strain rate at stresses above σ_y is linear. In general this would not be true. However, proceeding with this simple model

$$\eta = \frac{\sigma}{\dot{\gamma}} = \frac{\sigma_y}{\dot{\gamma}} + \mu_p. \tag{2.16}$$

The behaviour of a fluid obeying Equations 2.15 and 2.16 in dynamic oscillatory shear is shown in Figure 2.9. As lower frequencies are approached, corresponding to longer range structure, the viscosity increases without limit since the yield stress implies that flow (that is, long range motion) will not occur below some fixed stress. The result is a curve approaching a slope of -1 at low frequencies. The long range structure is therefore a network solid.

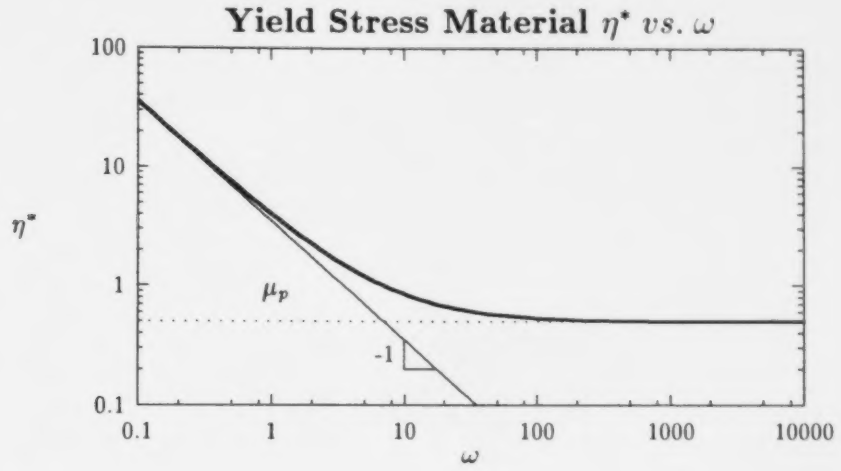

Figure 2.9: Frequency dependence of viscosity for yield stress materials.

2.5 Molecular Weight Dependence of Viscosity

It is found that limiting viscosities η_o of polymer melts, when plotted logarithmically against molecular weight, increase linearly with a slope of 1 until a critical molecular weight M_c at which point the slope changes abruptly to a steeper linear relationship. The slope of the curve above M_c has been measured quite universally to be 3.4. M_c is interpreted as the molecular weight at which a long-range entanglement network is established, due to the probability that there can exist at least two entanglements per polymer chain when the chains become this long.

2.6 Glass Transition

Amorphous polymer molecules in the melt state change position by thermally activated segmental jumps. Upon cooling, the amount of free volume decreases and these jumps occur less frequently because less space is available to receive the

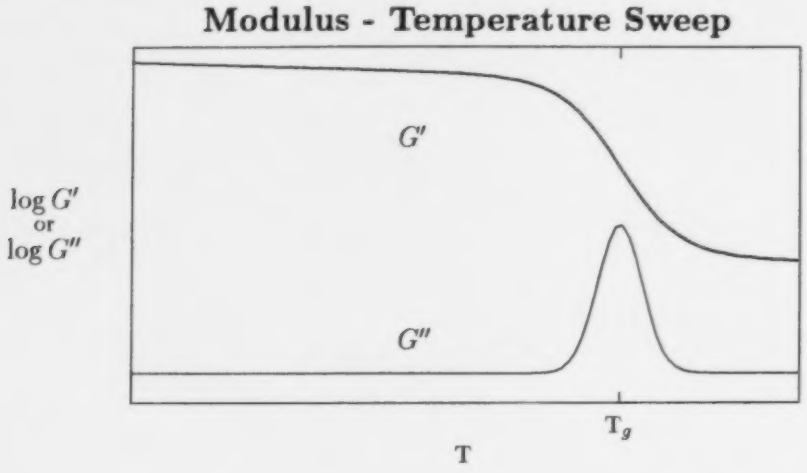

Figure 2.10: Loss and storage modulus *vs.* temperature for a single phase polymer.

jumping segment. When a temperature is reached at or below which there is a limiting free volume fraction, the segmental jumps cease entirely [49]. This point is called the glass transition temperature (T_g). A temperature sweep of G' and G'' reveals temperature transitions of a material (Figure 2.10). On cooling from the rubbery state, the glass transition temperature is identified as that at which G' increases rapidly (about 3 orders of magnitude) and G'' goes through a maximum.

2.7 Time-Temperature Superposition

If stress relaxation experiments such as that depicted in Figure 2.1 are performed at various temperatures, it is found that the relaxation processes are faster at higher temperatures. This is because polymer relaxations are activated processes. Therefore, time and temperature have equivalent effects on polymers. By using an Arrhenius temperature dependence for the viscosity and a rubberlike linear temperature dependence for the modulus ([71] p.162), both valid when $T \geq$

T_g+100°C,

$$\lambda(T) = \frac{\mu(T)}{G(T)} = \frac{C_1\, e^{\Delta E/RT}}{C_2\, \rho(T) \cdot T} \approx C_o\, e^{\Delta E/RT}. \tag{2.17}$$

It is therefore possible to accelerate relaxational processes by raising the temperature. This provides long time relaxational data from experiments of shorter duration. Data on $G_r(T)$ from higher temperature experiments can be shifted along the time axis by a constant shift factor a_T defined by

$$\lambda_T = a_T\, \lambda_{T_o} \tag{2.18}$$

which gives (when $T \geq T_g$+100°C)

$$a_T = exp\frac{\Delta E}{R}\left[\frac{1}{T} - \frac{1}{T_o}\right]. \tag{2.19}$$

When T is in a lower range ($T_g \leq T \leq T_g$+100°C) the shift factor for all amorphous polymers has been empirically found to follow a simple relationship known as the Williams-Landel-Ferry (WLF) equation

$$\log a_T = \frac{-17.44\,(T - T_g)}{51.6 + (T - T_g)}. \tag{2.20}$$

The two constants are related to the free volume fraction of the amorphous material at T_g ([71] p.163).

In the temperature range above $T_g + 100$°C the Eyring rate theory better predicts relaxation processes since at high temperatures free volume is not a limiting factor and so the molecule will move as fast as the energy supplied. At lower temperatures a polymer segment must wait a long time to find an element of free volume into which to jump.

2.8 Thixotropy

It remains now only to say a few words about thixotropy. Thixotropy is a decrease in the rheological properties of a material over time with concurrent

deformation. This is commonly seen in multiphase materials like block copolymers. If the structure is broken down during deformational processes such as shearing, which occurs in almost all processing steps, then the properties can be profoundly affected. Reproducible properties may be difficult to obtain commercially and reproducible results may be difficult to obtain experimentally.

Chapter 3

Review of Literature

3.1 Thermodynamics of Phase Separation

Understanding the thermodynamics of block copolymers is prerequisite to understanding their microstructure as well as their mechanical and rheological behaviour. Chemical incompatibility between block segments A and B of an AB or ABA block copolymer causes segments of like chemical structure to coalesce causing microphase separation. These microphases, while distinct, are covalently bonded through the segment junctions. Therefore, adhesion between these distinct phases in block copolymers is unlike the adhesion in any other multi-phase system. Stresses are easily transferred from the matrix, whether it be composed of the A or B segments, to the dispersed phase; however, enthalpic forces oppose stresses which tend towards remixing of the blocks, *i.e.* domain destruction. It is easy to see then how the thermodynamics of phase separation dominates the mechanical and rheological properties of these materials.

Early thermodynamic models [50, 42, 6, 47, 46, 36] proposed a two phase structure in these materials. A major advancement was the realization that a third, mixed phase of significant dimension exists in the microstructure [43, 44, 30, 51].

The importance of this mixed phase, or interphase, in interpreting the rheological and mechanical properties of these materials will become evident as we review the literature.

3.1.1 Two Phase Model

Meier [50] developed a model for phase separation in diblock copolymers assuming the existence of spherical domains of A in a continuous matrix of B with a well defined surface between the phases. The criterion for phase separation was that the Gibbs free energy difference ΔG between the random mixture of block copolymer segments and the domain system be negative.

This ΔG was separated into several entropic and enthalpic contributions. The first was the "placement entropy" ΔS_p. This was a decrease in the entropy relative to the random reference state caused by forcing the A-B junction to lie at the interface. ΔS_p was evaluated from a lattice model. The "restricted volume" entropy difference ΔS_v, evaluated by chain statistics, arose from the restriction of the A and B segments to the inside and outside of the domains respectively. The "elastic entropy" difference ΔS_{el} arose from the perturbation of chain dimensions in the domain system from their random-flight values.

The enthalpy difference ΔH between the domain and random systems was evaluated as the heat of mixing of a simple mixture of A and B molecules, despite the fact that the component blocks are joined together. The residual interaction of the A and B segments at the domain surface was treated as a surface free energy G_s and characterized by an interfacial tension γ. Using this model Meier proceeded to define a criterion for phase separation in terms of a critical molecular weight (M_s) at a given composition. Although it is true that $M_s = M_s(T, \phi_A)$, Meier made no mention of a temperature correlation in this initial work. The incorporation of a temperature correlation was an innovation of the model of Leary and Williams

[43, 44] which will be discussed next.

3.1.2 Three Phase Model

A major advance in the understanding of block copolymer thermodynamics was the recognition by Leary and Williams [43, 44] that the model must incorporate a third mixed region which they termed the "interphase". This region is of significant dimensions and influences the properties profoundly.

The model of Leary and Williams, like that of Meier, began with a random mixture of A and B polymer segments as the reference state. However, Leary and Williams considered triblock copolymers and did not restrict the model to spherical geometries. Rather, one of five geometries could be chosen and the change in the Gibbs free energy between the reference state and the phase separated state was calculated. All five of the geometries considered had been experimentally observed, the evidence for which will be reviewed in section 3.2. They were:(1) spherical or (2) cylindrical domains of component A in a matrix of B, (3) lamellar domains of both A and B, and (4) spherical or (5) cylindrical domains of B in a matrix of A. The phase separated states for structures 1 or 2 and 3 are shown in Figure 3.1. The letter S is used in Figure 3.1 to denote the end-block component, previously referred to as A. A very common commercial block copolymer is poly[b-styrene-b-butadiene-b-styrene], thus ABA becomes SBS. Here, ϕ_S represents the volume fraction of polystyrene blocks as a function of distance. The model first assumed a step change in ϕ_A (or ϕ_S) with the interphase having a 50-50 composition.

In order for a phase separated structure to exist, the change in Gibbs free energy,

$$\Delta G = \Delta H - T\Delta S, \tag{3.1}$$

from the reference state would have to be negative, and the equilibrium structure would be that with the largest negative ΔG.

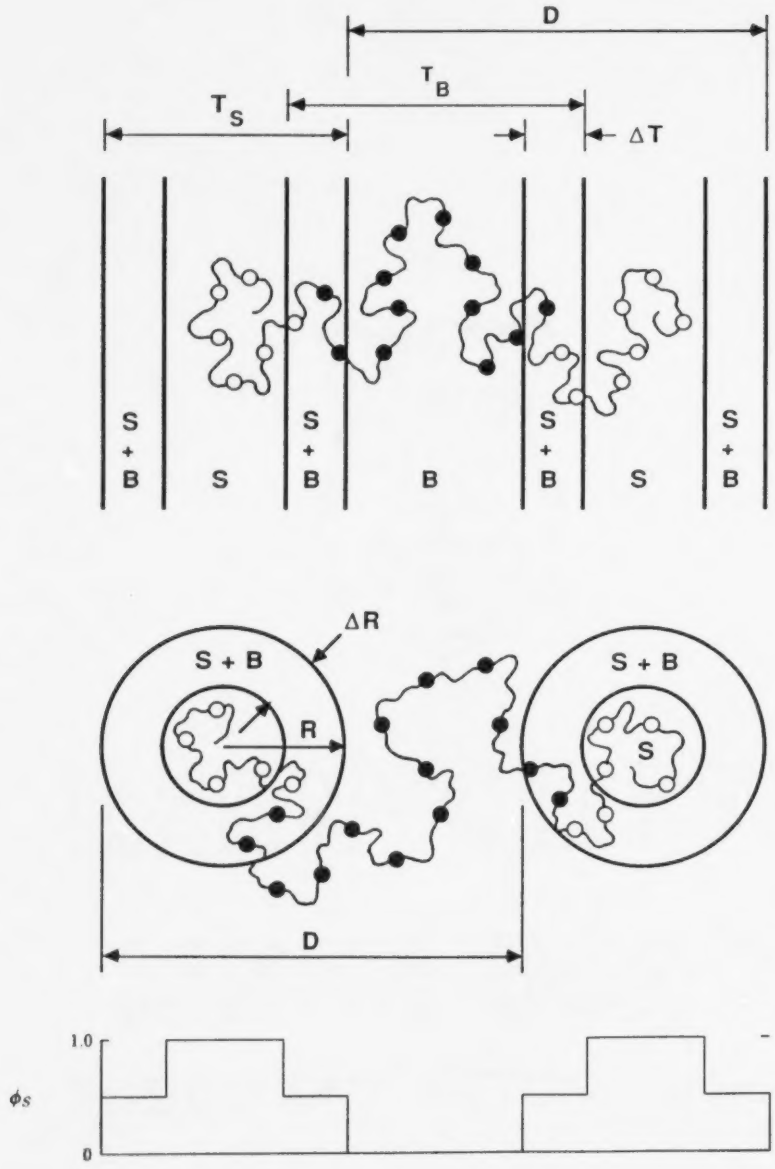

Figure 3.1: Model of phase-separated microstructure for lamellar domains (top) and normal spherical or cylindrical domains (middle), showing the composition profile of minor component S (bottom) assuming a step change to 50% in the interphase. ΔT (or ΔR for cylindrical morphology) is the interphase thickness and D is the inter-domain spacing.

The enthalpy of demixing was obtained from Scatchard-Hildebrand regular solution theory:

$$\Delta H = -V_m \phi_A \phi_B (\delta_A - \delta_B)^2 + f V_m \overline{\phi'_A \phi'_B} (\delta_A - \delta_B)^2 \tag{3.2}$$

where the first term represents complete demixing and the second term corrects for that exaggeration in terms of the mixed interphase. Here $\overline{\phi'_A \phi'_B}$ is the volume averaged product of the volume fractions of A and B in the interphase and f is the overall volume fraction of the interphase. V_m is the molar volume and δ_i is the solubility parameter of component i. This model did not require any knowledge of the domain surface free energy which would be unknown and unmeasurable.

The entropy of phase separation was thought of as arising from three contributions:

$$\Delta S_{total} = \Delta S_1 + \Delta S_A + \Delta S_B. \tag{3.3}$$

Here, ΔS_1 was considered as the entropy change resulting from one of the A-B junctions of a polymer molecule being forced to reside in the mixed region while ΔS_A and ΔS_B resulted from forcing A and B segments respectively to reside either in a pure A or pure B domain or in the mixed region.These terms could be generated from chain statistics; however, the mathematical details are beyond the purview of the present work.

Since the transition from a randomly mixed state to a phase separated state is a first order transition, a critical temperature for domain formation could be determined by letting $\Delta G = 0$, so that

$$T_{critical} = \left. \frac{\Delta H}{\Delta S} \right|_{\Delta G = 0}. \tag{3.4}$$

Leary and Williams then coined the phrase "separation temperature" or T_s. This designation will be used for the order-disorder transition temperature in much of this work, regardless of whether the transition under consideration is from a disordered

to an ordered state or the other way around, in which case it might more accurately be described as the "homogenization temperature".

The model predicted that T_s is directly proportional to the square of the solubility parameter difference $(\delta_A - \delta_B)^2$ as well as the molecular weight and the product of the volume fractions of the A and B components. Model predictions of T_s were compared to experimental values [45] obtained from differential scanning calorimetry (DSC) and laser light transmittance as well as electron microscopy and mechanical properties. It was found to be qualitatively correct in every case and in several cases to be accurate to within 10 K.

The model also permitted calculation of ΔT, the interphase thickness, and planar repeat distance D for lamellar structures. Henderson and Williams [34] applied the model to planar morphologies and found that ΔT generally increases with increasing ϕ_A, although at very large and very small ϕ_A there is no phase separation. D was found to increase with increasing molecular weight as $M^{0.50}$ to $M^{0.75}$.

The influence of various interphase composition profiles $\phi_A(x)$, where x is dimensionless distance through the interphase, was also considered [33]. The step change in composition used for simplicity in the Leary-Williams model was rather unrealistic. As mentioned earlier, the second term in equation 3.2 is dependent on the volume averaged product of the volume fractions of A and B in the interphase. This is where the choice of interphase composition profile influences the model. That choice was predicted to have significant effect on the separation temperature as well as the interphase thickness. The model was also extended to consider incomplete demixing of the A and B components within the homogeneous domains (since data suggested some dilution in the glassy phase) as well as asymmetric composition profiles [33]. It was shown that no conditions led to a true equilibrium with any mixing within the domains (implying that data represented a state of kinetically controlled entrapment of B within A, as A vitrified upon cooling), and also that an interphase slightly rich in the end block component A was preferred, as experimental

evidence showed [32].

It should be noted that the Leary-Henderson-Williams model predicts that such physical properties as T_s and ΔT are dependent on molecular weight. Model predictions can be calculated for any given molecular weight ; however, comparison with experiment may be difficult because all real polymer samples have some finite polydispersity ($PD \equiv \overline{M}_w/\overline{M}_n$) and thus represent a continuous spectrum of molecular weights. Since T_s is proportional to molecular weight, a PD of 1.1 for a polymer having a predicted T_s of 400 K would result in a 40 K transition range. This led Spontak and Williams [68] to use continuous thermodynamics to investigate the effects of PD on microstructures of block copolymers. It was found that $T_s = T_s(PD) = T_s(1)$ + linear increase with PD. Direct application of the model is sometimes complicated by the fact that it predicts *equilibrium* properties, while the microstructure of a given experimental sample may not be at equilibrium due to kinetic effects or solvent effects or sample strain history.

3.1.3 Interphase Free Energy Barrier

Theoretical predictions of the influence of the interphase on block copolymer properties were first expounded by Henderson and Williams [31]. An explanation of the model rightly belongs in a discussion on block copolymer thermodynamics. We begin by considering a triblock (ABA) copolymer which is phase separated, *i.e.* $T < T_s$. Figure 3.2 shows a mixed interphase separating a pure A domain and a pure B matrix. The composition profile across the interphase is shown in Figure 3.2 (a) as $\phi_A(r)$.

If some macroscopic force is imposed on the sample then individual chains will also experience some local stress field which in general would be difficult to predict from the macroscopic stress. However, we need only consider the force on a single chain for now. The total force on a chain will be the sum of frictional as well as

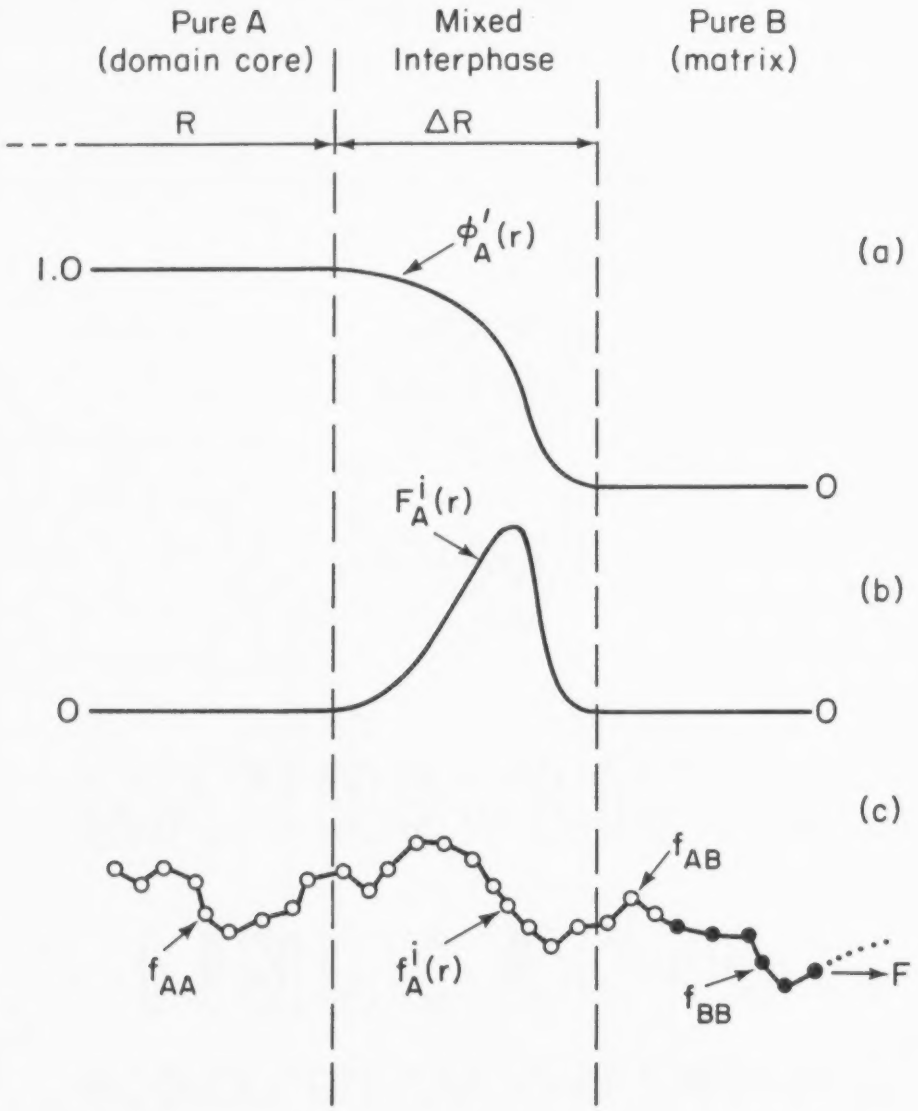

Figure 3.2: (a) Composition profile across the mixed interphase of thickness ΔR. The profile may be asymmetric, as shown. (b) Thermodynamic force profile corresponding to composition profile. The total barrier force F^i_A described in the text is the sum of the F^i_{Ak} acting on all units in the interphase. (c) Withdrawal of A block from domain core into matrix of B. Friction coefficients of four different types are indicated.

interphase thermodynamics forces, $F = F^f + F^i$. Four terms contribute to the friction: drag on B segments moving through B matrix (F^f_{BB}), drag on A segments through A domain (F^f_{AA}), drag on A segments moving through B matrix (F^f_{AB}) and drag on each type of segment in the interphase with varying composition (F^{fi}). These are all represented in Figure 3.2 (c).

The composition profile in Figure 3.2 (a) corresponds to a chemical potential variation $\mu_A(r)$. An interphase barrier force therefore exists which is the negative gradient of the chemical potential

$$F^i_A(r) = -\nabla\mu_A \tag{3.5}$$

which is shown in Figure 3.2 (b). Each of the A-chain units ($k = 1, 2, \ldots, n$) in the interphase feels a local force $F^i_{Ak} = -\nabla\mu_{Ak}$ so that the total barrier force is

$$F^i_A = \sum_k^n F^i_{Ak}. \tag{3.6}$$

If the external force on the chain is less than F^i_A then block pull-out will not be possible and then no flow can occur, which would explain the absence of a limiting viscosity η_o at low $\dot{\gamma}$ and establishes the theoretical basis for a liquid yield stress σ_y.

Two more points should be noted.

(1) The shape of the interphase composition profile is predicted to have a major influence on the rheology.

(2) The chemical potential μ_A can be expressed in terms of the solubility parameter difference $\delta_A - \delta_B$ and therefore rheological properties should be strongly dependent on $\delta_A - \delta_B$.

3.2 Microstructure

As mentioned in Section 3.1 thermodynamic forces cause microphase separation of a block copolymer below some critical T_s. The nature of these microphases

has been the subject of much investigation. Electron micrographs from Meier [50] of a styrene-isoprene (SI) diblock copolymer having 17 wt % styrene revealed the presence of spherical polystyrene (PS) domains in a matrix of polyisoprene (PI).

Beecher *et al.* [5] observed spherical domains in a styrene-butadiene-styrene (SBS) triblock copolymer of 28 wt% styrene content. These samples were solvent cast and it was found that the choice of solvent had a significant effect on the observed morphology. Samples cast from a 9:1 mixture of tetrahydrofuran and methyl ethyl ketone (THF/MEK) displayed polystyrene domain interconnectivity. Casting from a mixture of benzene and *n*-heptane resulted in very few connections and smaller domain diameters. The use of carbon tetrachloride as casting solvent resulted in very diffuse domain boundaries. It was explained that in casting from THF/MEK, a neutral solvent mixture for SBS (*i.e.* , one which is equally good for both chemical constituents of the polymer chains), the THF would evaporate first. Since MEK is a better solvent for PS, this would leave the PB unswollen and the PS end blocks would aggregate into spherical domains swollen with MEK, causing impingement between PS domains and resultant connectivity.

Inoue *et al.* [36], studying diblock copolymers of styrene and isoprene observed a systematic change in structure with increasing styrene content for polymers cast from the same solvent, namely toluene. A 20/80 PS/PI block copolymer revealed a structure of PS spheres in a matrix of PI. Increasing the ratio to 40/60 or 50/50 PS/PI resulted in an alternating lamellar structure. For a composition of 70/30 PS/PI the structure changed to that of spheres of PI in a matrix of PS. Casting solvent effects were also observed. A 40/60 composition cast from cyclohexane, a solvent which is almost equally good for both components, revealed rod-like or cylindrical PS microstructure. The same sample cast from MEK, a good solvent for PS, showed PS connectivity, although not as regular a structure as the lamellar case. Samples cast from CCl_4 and *n*-heptane, poorer solvents for PS, showed less PS domain continuity.

Uchida *et al.* [73] studied the microstructure of triblock copolymers of styrene and isoprene (SIS) cast from toluene. A styrene content of 9.5% resulted in a structure of spherical styrene domains in a matrix of polyisoprene. Increasing the styrene content to 23% and 47% changed the structure to that of rods of styrene and alternating lamella of styrene in polyisoprene respectively. A 72% styrene SIS had a structure of PI spheres in a PS matrix. Solvent effects were also observed. As the solvent became more selective to polyisoprene the PI domains in general became larger in dimension.

Spontak *et al.* [70] examined SBS copolymers having a styrene content of 30%. Both solvent cast and microtomed samples were photographed. Microtomed sections showed lamellar morphology while toluene cast samples showed cylindrical PS morphology with a diffuse interphase. Using computerized image enhancement of one PS cylindrical domain viewed end-on, one could clearly see the interphase, and its dimensions corresponded to predictions from the Leary-Henderson-Williams theory. Quantitative transmission electron microscopy was also used [69] on a stained sample (the stain blackened butadiene regions stoichiometrically) to acquire the shape of the volume-fraction composition profile across the interphase. An asymmetric profile was measured and found to be rich in styrene ($\approx$54%), similar to the findings of others [33].

3.3 Nonlinear Mechanical Properties

3.3.1 Network Characteristics

Holden *et al.* [21] and Bishop and Davidson [7], studying triblock copolymers SBS and SIS, proposed a two phase structure in these materials with the middle block phase constituting a continuous three dimensional matrix and dispersed end blocks serving as multi-junction points. They demonstrated that the elastic modulus (G)

could be accurately predicted from classical rubber elasticity theory if the middle block is a rubbery polymer such as polybutadiene (PB) or polyisoprene (PI) and the end block is a glassy thermoplastic. Classical rubber elasticity theory predicts

$$G = \frac{\rho RT}{M_c}, \tag{3.7}$$

where M_c is the molecular weight between crosslinks. While the junctions between chains in block copolymers are not chemical crosslinks, it was found that if the network is considered as a classical rubber then from both elastic modulus and solvent swelling data Equation 3.7 predicts M_c to be the molecular weight between entanglements of the homopolymer center block rather than the total molecular weight of the center block. Because the ends of the chains are trapped in the glassy domains, these entanglements can slide along the center blocks but cannot slip off, thus forming functionally effective crosslinks.

The effect of the microdomains was accounted for by modelling the material as a rubber containing hard filler particles. Because the bonding between the "filler" and the matrix is highly effective, the result is an increase in tensile strength. Bishop *et al.* [7] further pointed out that because the entanglements which form the crosslinks can slide along the chain the result is a more equitable distribution of stresses which also contributes to the high tensile strength of the materials. As a result the tensile strengths of SBS and SIS block copolymers were shown to be much higher than either of their respective homopolymers of similar crosslinking density. However, as shown by Holden *et al.* [21], a triblock copolymer having rubbery end blocks, namely BSB, has low tensile strength unless it is chemically vulcanized. They also demonstrated that at higher temperatures the PS domains in SBS or SIS become fluid and can be disrupted by applied stress, but upon cooling they become hard again, once again immobilizing the ends of the PB middle section.

Brunwin *et al.* [8] obtained tensile properties for an SBS with ϕ_S=0.40 and proposed that the high Young's modulus indicates that at low extension the PS

domains cannot move independently of each other. Therefore, the PS domains must interact with each other to form a loosely bound continuous phase of PS. Both stress and extension at break were shown to decrease with increasing temperature which they attributed to the softening of the PS domains.

3.3.2 Effect of Molecular Architecture

Holden *et al.* [21] concluded that the polystyrene content in a solid SBS or SIS polymer is the controlling factor in determining the tensile properties, that molecular weight has little or no effect. In tensile tests both initial modulus and ultimate tensile strength increased with increasing ϕ_S at a constant molecular weight. However, I have found, during the current study, that in shear testing of fluid samples molecular weight has a profound effect on relaxation times. Morton *et al.* [54] found that both the stress values and the ultimate strength are not dependent on the absolute PS block length, but rather on the polystyrene content. The polydispersity of the elastic block was also found to influence the tensile strength, with more highly monodisperse samples having higher strength. The polydispersity of the end blocks was shown to have no effect.

3.3.3 Plastic-to-Rubber Transition

Holden *et al.* [21] observed that the stress-strain curve of a 13% styrene SBS behaved like that of an undercured conventional vulcanizate while a 27.5% PS SBS acted like a conventional vulcanizate. SBS polymers having 30-53% PS exhibited a yield at low strains followed by drawing and then an elastic extension. At 65% styrene content a very high yield stress was observed followed by a short draw and immediate break. Morton *et al.* [54] observed a plastic yield point at low elongations as well as marked hysteresis only for polymers having 40% or greater PS content and attributed this to the formation of a semicontinuous PS phase which was irreversibly

disrupted after the first stretch. Beecher *et al.* [5] performed repetitive cyclic loading and observed a plastic yield at 3% elongation in the first extension cycle for a 28% styrene SBS cast from THF/MEK. The second cycle response was more like a vulcanized elastomer. Samples cast from other solvents showed no yield point. As explained in section 3.2 this solvent mixture causes PS continuity. This continuity is irreversibly broken during the first extension cycle. The breakage of PS domain interconnections was observed with electron microscopy.

Diamant *et al.* [17] performed tensile tests on SBS samples of varying composition and observed sample necking corresponding to a yield point at low strains ($\gamma = 1$ to 5%) in samples containing 29% and 48% styrene cast from THF/MEK. The magnitude of the yield stresses (σ_y) followed a simple proportionality to w_s^2. No yielding or necking was observed in samples containing 27% styrene. Properties in the necked region were rubbery, while those of the material prior to necking were glassy. Diamant [29] termed this the "plastic to rubber (PR) transition." He also suggested that the PR transition occurs when the PS continuity breaks, at low engineering strain

$$\varepsilon_E = (L - L_0)/L_o \tag{3.8}$$

where L is the length of the gage section and L_o is its original value, since second cycle tests did not display yield phenomena. However, the stress-strain curves for second cycle tests all displayed rubbery behaviour and all were significantly lower than their first cycle values. Therefore, molecular-scale networking was maintained, but glassy continuity was not.

Samples containing 27% PS did not exhibit yielding; however, the height of the second cycle stress-strain curve was only 1/2 of the first cycle values. In samples of this composition both spheres and cylinders could coexist and it was proposed that phase continuity existed through the latter. This rather weak continuity would be breaking progressively during the test and so no catastrophic yield was observed. Second cycle stress-strain curves were very similar for 29% and 27% styrene samples

since the truncated cylinders in 29% samples had much the same filler effect as the spherical domains in a 27% styrene SBS.

Samples of 29% PS cast from pure MEK did not exhibit yielding despite the fact that MEK is a better solvent for PS than THF/MEK. Comparing the interphase gradients, obtained by a rheological technique which will be reviewed in Section 3.4.2, it was seen that the interphase gradient for MEK cast samples was much lower (*i.e.*, the interphase was much broader) than for THF/MEK cast samples. It was therefore proposed that when the interphase composition is locally steep the classical case of a two phase system is approximated and all domains are in mechanical register and fail together, thus causing macroscopic yielding. However, if the interphase is diffuse then the domains fail individually and no macroscopic yielding would be observed.

Adding a low molecular weight polystyrene [14] (low enough that the chains could fit entirely in the original PS domains) to a 0.27 PS copolymer in order to raise the total PS composition to 48% created the yielding phenomenon in these samples. However, the stress-strain curves for these samples were consistently lower than the corresponding 0.48 PS SBS.

Blending 1% of a random styrene-butadiene copolymer (SBR) (thought to be of low enough molecular weight to be localized almost entirely within an expanded interphase) into a 0.48 PS SBS dropped the first cycle yield stress by 16% although the overall styrene content had dropped by only 0.3%. After addition of 10% SBR the yield stress vanished and strength properties were significantly reduced, indicating that PS connectivity had been entirely disrupted by growth of the interphase. The reduction in height of the stress-strain curves was explained in terms of the thermodynamic force barrier which was described in Section 3.1.3 of the current work. The addition of SBR, which was shown by rheological methods (see Section 3.4.2) to reside in the interphase, would lower the resistance to motion of a styrene block through the interphase into an incompatible phase.

3.3.4 Mechanisms of Mechanical Failure

The magnitude of ε_E at break was found by Diamant *et al.* [17] to be correlated with the middle block (rubbery) molecular weight. Strain, not stress, was the correlating factor because stress is affected by geometrical factors and filler content. The mechanisms of failure were proposed to be:

1) Chain pull-out, where PS end blocks pull out of their domains. The molecular weight of the styrene blocks is not a relevant parameter because it is the interfacial energy barriers which establish the level of force necessary. Long range microstructure would therefore also not have an influence.

2) Bond breakage.

3) Thermodynamic effects. The applied force acts to remix the two phases. Therefore, the thermodynamic balance is upset and a mechanically induced phase remixing occurs. In this view, failure occurs because viscous flow commences locally when microphase separation is destabilized and the anchoring glassy domains cease to exist.

3.3.5 Microstructural Repair

Diamant and Williams [15] also investigated the recovery of block copolymers from large tensile deformations. Samples of 0.27 PS, 0.29 PS and 0.48 PS were first stretched to 300% elongation (thus fracturing any PS-phase continuity) and then allowed to recover at various temperatures. There was found to be an initial rapid recovery due to the elastomeric character of the PB. The extent of this rapid recovery is limited by convergence of the glassy residues. Further recovery, which is much slower, involves repair of the microdomains by diffusional processes. Recovery at higher temperatures is more rapid for two reasons. The first is the stronger elastomeric forces, since rubbery modulus is proportional to temperature. The second cause can be understood if the interphase is considered as a series of shells

within each other like layers of an onion. Each shell has an average composition and a T_g corresponding to this composition. The composition profile is higher in ϕ_S, corresponding to higher T_g, closer to the centers of the microdomains. At higher temperatures the surface, or outermost dimension, of the glassy core (PS core + interphase fraction which is glassy) moves in closer to the PS core and thus the fraction of glassy material in the polymer sample is reduced.

In cycling tensile tests [16] with amplitudes which exceeded the PR transition, some strain recovery always occurred during the slack period of about 2-4 seconds between complete release of tension and build up of tension for the next cycle. The non-zero strain which remains after release of tension is termed "set". The amount of set did not vary significantly among the three different polymers strained to 400% or 600%, but there was a systematic increase of set (*i.e.* , some flow) on each cycle. It was found that some glassy continuity was even recovered during slack time by what could only be a diffusional process.

3.4 Rheology

The review of the literature on the rheology of block copolymers is restricted largely to that of triblock copolymers. This review has been divided into separate discussions on steady shear flow and small amplitude dynamic testing. Strictly speaking the preceding discussion on nonlinear mechanical properties could also be classified under rheology since rheology is "the study of the deformation of matter."

3.4.1 Steady Shear Flow

Holden *et al.* [21], studying the steady shear properties of SBS and SIS copolymers, found that they could flow as thermoplastics above the T_g of the end block. The melt viscosities were found to be much higher than those of

the constituent homopolymers of the same total molecular weight. Activation energies (ΔE) for flow were found to vary with temperature. At high temperatures ΔE approached that of the rubbery block and at low temperatures that of the thermoplastic block. Additional energy absorption, giving higher activation energies, is indicated in the flow process because the flow of block copolymers requires the movement of end blocks through the chemically incompatible matrix. As the styrene content was increased the viscosity was observed to pass through a maximum. This may have been due to morphological transitions through the composition spectrum, and further complicated by the effects of sample history. The influence of these two factors will be demonstrated by the results of the present work. None of the block copolymers studied displayed Newtonian behaviour at low shear rates as do homopolymers. Two distinct viscosity-shear rate relationships were seen for the same SBS sample with ϕ_S=0.39. To explain this it was proposed that if the styrene content is between 26% and 74% then by geometry either phase could be continuous and under shear a phase inversion could occur from one to the other continuous phase.

Paul *et al.* [55] studied the viscosity-shear rate relationship for SBS copolymers dissolved in solvent. The $\eta(\dot{\gamma})$ curves reduced to a single master curve. Hence, all solutions were homogeneous. Several solvents were investigated and it was found that a solvent having a solubility parameter $\delta_{solvent}$ closest to the average between δ_{PB} and δ_{PS}, and thus permeating all the polymer equally, resulted in a minimum η_o/η_s ratio.

Chung and Gale [9] were the first to report Newtonian behaviour of a block copolymer in bulk. Using a rotational viscometer they studied an SBS copolymer of molecular weight ($\times 10^{-3}$) 7-43-7. Above 175°C a limiting Newtonian viscosity was observed under steady shear testing. At 125°C, 140°C and 150°C steady shear testing could not be performed because of the high elasticity at these temperatures, even at the lowest shear rate attainable. These authors attributed this to a change

in microstructure from a multiphase to a homogeneous state above 175°C.

Vinagradov *et al.* [74] studied the steady shear viscosity of a 30% PS SBS block copolymer using a capillary rheometer. In the region of σ=3×10^3 to 3×10^4 N/m^2 the curve of $\dot{\gamma}$ (σ) had a slope close to 45°—a "pseudo-Newtonian" flow of the material was observed. At higher shear stresses a distinctly pronounced non-Newtonian flow was witnessed. With increasing σ this flow ended with a spurt, *i.e.* slippage of the material along the capillary walls because of the transition to the forced high-elastic state. Activation energy of viscous flow was shown to be considerably higher than for PB. Flow curves for SBS could be well described by a temperature invariant curve in the coordinates $\log(\eta/\eta_o)$ *vs.* $\log(\dot{\gamma} \cdot \eta_o)$ between 110°C and 170°C for a polymer of MW=8×10^4 and $\phi_S = 0.304$ if η_o was the value in the "pseudo-Newtonian" region, although this temperature range was below T_s. Thixotropic effects were strongly visible. When $\dot{\gamma}$ was increased gradually from 10^{-3} to 10^0 s^{-1} and then stepped immediately down to 10^{-3} again the second curve showed lower σ values. After relaxation for 3-4 hours the shear stress returned to the original value. This was attributed to a supra-molecular structure which breaks down under shearing. The structure recovers after removal of the load.

The IUPAC Working Party on "Structure and Properties of Commercial Polymers" [72] studied shear stress measurements on SBS copolymers after cessation of steady shear flow. Shear stress was observed to relax to a constant residual stress which was independent of the rate of previous shear at a constant duration of shear but dependent upon the duration of previous shear at a given shear rate. Residual shear stress (which is perhaps related to σ_y) increased with increasing shear duration. These observations were interpreted to suggest that all residual stress is developed during the shear process and that the unsheared material does not exhibit a yield stress. The authors made reference to a study in which viscous flow was observed at shear stresses below 10 Pa at 150°C and advanced this as additional evidence against the existence of a liquid yield stress. However, this latter study was never

published in a peer reviewed journal.

Soong *et al.* [67] measured shear stress growth curves for SBS copolymers and their blends with short chain SBR (MW=3600). Addition of 1% SBR resulted in a significant lowering of the stress growth curve. The concept of a thermodynamic force barrier caused by the interphase composition gradient and lowered by swelling of the interphase with added SBR was invoked to explain these results.

3.4.2 Dynamic Strain Testing

Linear Viscoelasticity as a Structural Probe

Holden *et al.* [21] drew evidence for a two phase structure in block copolymers from plots of viscous damping (loss modulus, G'') *vs.* temperature. Random copolymers of styrene and butadiene (SBR) showed a single maximum in a viscous damping curve while SBS block copolymers showed two peaks with a broad high plateau in between. As peak position corresponds to T_g, the first peak, below 200 K, corresponds to the polybutadiene phase T_g^B while the second peak, close to 100°C, corresponds to the polystyrene phase T_g^S.

Beecher *et al.* [5] studied the damping *vs.* T curves for SBS cast from different solvents. Samples cast from THF/MEK had the largest and best defined PS peak and a relatively low intermediate plateau. A mixture of benzene and heptane as solvent in the same SBS resulted in a $G''(T)$ curve with a high intermediate plateau. The use of CCl_4 resulted in a broad damping peak near 30°C and a lowering of the PS peak which these authors interpreted as indicating an incomplete separation of PS from the PB phase.

Kraus *et al.* [41] examined the viscoelastic properties of SBS polymers cast from four solvents, all equally good for PS but only 2 being good solvents for PB. Solvents that were poor for PB resulted in $E'/G' \gg 3$, while $E'/G' = 3$ is normal for

rubbery materials. This was interpreted as evidence for interconnectivity of PS chains resulting from solvent selection. Compression molded samples also displayed large E'/G' ratios and viscoelastic properties of compression molded samples were found to be orientation dependent.

Kraus and Rollman [40] plotted the viscous damping *vs.* temperature curves of SBS and SIS polymers of varying molecular weights. The polystyrene loss maximum was displaced toward lower temperatures as molecular weight decreased while the PB or PI maxima remained fixed except at the lowest molecular weight. The glass transition temperature of high polymers does decrease with decreasing molecular weight caused by introduction of additional free volume to the system by the chain ends; however, model predictions showed that this was not sufficient to explain the T_g shift observed. The viscoelastic behaviour was modeled by considering the mixed interlayer as consisting of sublayers of continually varying composition, each having the properties of a compatible blend or random copolymer, assuming a symmetric $\phi_S(x)$ with $\phi_{S_{total}} = 0.5$. The resulting curves failed to reproduce the shift in the PS loss peak with decreasing MW. It was proposed that if the profile is asymmetric with $\phi_{S_{total}} > 0.5$ then as block length decreases the interlayer (or interphase) would feed preferentially from the PS domains which would then disappear first. The resulting loss maxima showed the correct qualitative shapes.

Diamant *et al.* [13] examined the $G''(T)$ curves of SBS copolymers of varying molecular weights and styrene contents cast from various solvents. Data collected showed a high G'' plateau which was solvent dependent. A strictly two phase system would produce a $G''(T)$ with a very low plateau between the two major peaks. Therefore, it was concluded that only the existence of a major interphase in which $\phi_I(x)$ varied continuously from the PB rich to the PS rich regions would explain these observations. The interphase was modeled as a large number of these layers having different compositions and hence different T_g's. From this, the interphase composition profiles for each polymer-solvent pair were extracted. Higher styrene

contents, as well as casting solvents more preferential to PS resulted in broader, more diffuse interphases.

The same authors examined the linear viscoelastic properties of blends of PS and SBR in SBS copolymers [14]. Adding PS of low molecular weight (< MW of PS end block) to a 0.27 PS SBS in order to raise the total ϕ_s to 0.48 raised the G' and G'' plateau regions very close to those of 0.48 PS SBS. This implies that the linear properties (*i.e.*, the structure preserving properties) of a blend are governed primarily by the total PS content as long as the phase separated nature is maintained. The blend plateau did drop off relative to that of the 0.48 PS SBS as the T_g of polystyrene was approached. The elevation of the G'' plateau is associated with the volume fraction of the interphase. The elevation of G' is associated with the extent of glassy-phase continuity, being lowest for dispersed PS spherical domains, larger for microstructures of interconnected cylinders, and finally greatest for lamella. Using a structural model it was found that the best fits to the data assumed some intrusion of the PS additive into the interphase. The blend had a large PS rich phase and a larger interphase than the unblended material.

Blending a low molecular weight SBR with 0.48 PS SBS also changed the shape of the $G''(T)$ plateau. The plateau region showed a broad peak from -40 to +30°C. The peak (and hence T_g) of PS was unchanged and the T_g for the PB phase was shifted upwards by only 3°C. This was insufficient to suggest that all of the SBR resided in the PB matrix. The T_g of pure SBR of this composition and MW would be between -47°C and -67°C. Therefore, it was concluded that the bulk of the SBR resided in the interphase rather than forming a separate phase.

Microphase Transition

Chung and Gale [9] were the first to report a rheological transition at a critical temperature for a bulk block copolymer. Dynamic modulus plots as a function of

angular frequency at 175°C showed drastically different behaviour than those at lower temperatures. A sharp decrease of G' with decreasing angular frequency was observed, similar to the behaviour of homopolymers. Dynamic viscosity *vs.* angular frequency curves also levelled off to a Newtonian limit at 175°C while curves at 150°C and lower did not. It was concluded that the polymer underwent a change in flow mechanism from a highly elastic to a Newtonian behaviour with negligible elasticity at a critical temperature.

Pico and Williams [56, 58] reported a similar rheological transition. They used a solvent to plasticize the polymer, which they predicted would lower the separation temperature [59]. This was confirmed experimentally [57].

Gouinlock and Porter [22] measured the dynamic properties of a 7-43-7 SBS copolymer over a range of temperatures. A profound rheological transition was witnessed at around 146°C. Above this temperature an abrupt decrease in dynamic properties was witnessed. The discontinuity decreased in magnitude as frequency was increased. The transition was attributed to a weakening and/or loss of the crosslink structure due to a sharp increase in phase miscibility and/or the attainment at or above the transition temperature of an easily disrupted dispersed phase. The narrowness of the transition suggested that miscibility was the major factor. The transition was found to be thermally reversible. It was postulated that complete disappearance of the phase separated morphology may not have occurred since easily disruptable domains, not controlling viscous response, might conceivably yield the same results. The extraction of PS segments from domains was predicted to involve long range configurational rearrangements and long relaxation times. Therefore, domain disruption would increase with decreasing frequency and increasing temperature.

Chung and Lin [10] reported results identical to those of Gouinlock and Porter. They also showed the abrupt increase in phase angle as the transition temperature was passed. The transition was from low phase angles indicating highly elastic

behaviour to high phase angles indicating highly viscous behaviour.

Han and Kim [25] reported a rheological technique for determining the separation temperature of block copolymers. For homopolymers, plots of G' *vs.* G'' are independent of temperature. Therefore, for a block copolymer when $T < T_s$, G' *vs.* G'' (over ω) gives *non*-superimposing curves, while at $T > T_s$ these curves superimpose. This temperature dependence disappears first at high ω. Han and Kim, in contradiction to Gouinlock and Porter, concluded from this that structure breakdown is more rapid at higher frequencies. Han *et al.* [24] confirmed the method of Han and Kim by comparison with small-angle X-ray scattering techniques and found that T_s values determined by both methods agreed to within 10°C.

Time-Temperature Superposition of Relaxational Processes

In Section 2.7 some principles of time-temperature superposition were reviewed. If it is possible to shift curves so that relaxational data at short times and high temperatures superimpose on data at long times and lower temperatures, such that a single master curve can be constructed, then we say that time and temperature are "equivalent" variables.

Beecher *et al.* [5] applied time-temperature superposition, in the range from -50°C to +80°C, to a block copolymer with $\overline{M}_n$=76,000 and ϕ_S=0.28. They concluded that time and temperature could be treated as equivalent variables for relaxational processes, and that the fit of the WLF equation was very good at temperatures less than 0°C.

Shen and Kaelbe [64] examined experimental values of the time-temperature shift factor a_T at varying temperatures for an SBS block copolymer. From these shift factors it was found that WLF behaviour was followed, with modified constants, only in the vicinity of the T_g of either major phase. In between the two T_g's of the homopolymer blocks a different curve was followed. The WLF equation assumes

a constant free volume fraction below T_g and then a constant thermal expansion coefficient for fractional free volume above T_g. Due to the two phase character of block copolymers the "effective" fractional free volume will depend upon the phase which contributes the molecular mechanism for stress relaxation response. It was postulated that in the broad central region of response between -60°C and 80°C the molecular mechanisms for stress relaxation are contributed by an interfacial phase that intervenes between the PB matrix and the PS domains. In this region the difference between the test temperatures and the inflection temperatures[1] was found to be a constant. This indicated that shear relaxation occurs in successive interior shells of higher $T_i \approx T_g$ as the test temperature is raised above -60°C. This is consistent with a continuously varying composition profile in a diffuse interphase having high ϕ_S closer to the PS domains.

In a later publication, Shen and Hansen [65] examined the viscoelastic behaviour of a homogeneous block copolymer. Isothermal stress relaxation data were shifted into viscoelastic master curves which followed the classical WLF equation. The $T_i \approx T_g$ was slightly higher than for homopolystyrene.

Arnold and Meier [2] constructed master curves of reduced viscosity η_r *vs.* reduced frequency[2] ω_r for SBS block copolymers which showed two distinct slopes. Plots of a_T *vs.* 1/T fell on one of two lines. It was proposed that the rheology of ABA block copolymers is dominated by the interplay of processes tending to disrupt and to reform the network and domain systems. Three distinct states were described, which were thought to depend on the rate of deformation. At very low deformation rates there would be a state where the molecular network is essentially intact. At intermediate rates the three dimensional network would be disrupted.

[1]The inflection temperature was derived from the viscoelastic master curve obtained by superposing isothermal modulus-time curves at a series of temperatures. It was the temperature at which the modulus was found to be 10^9 dynes/cm^2 at a relaxation time of 100 sec, and corresponded approximately to the glass transition temperature.

[2]$\eta_r = \frac{\eta'}{a_T}\left(\frac{T^O}{T}\right)\left(\frac{\rho_O}{\rho}\right)$ and $\omega_r = \omega a_T$, where T^O is a reference temperature.

Domains and aggregates of many molecules would still occur but they would not be linked together. At high deformation rates the aggregates would be disrupted and the system would behave as an assemblage of individual, non-aggregated molecules. Therefore, the theory would predict a network response at low shear stress levels (including a yield stress), an intermediate region of shear stress where η would be much higher than expected for molecules of the given MW, and finally a region at high shear stresses where the behaviour would be typical of ordinary thermoplastics of the same MW.

As mentioned above, shift factor data fit two distinct curves, one for PS fractions >35% and one for fractions <31%. This was interpreted as reflecting two different types of domain structure in the low-frequency response region. One structure was proposed to have a semicontinuous PS phase where the thermal properties of PS dominate, and the other to have dispersed PS domains, so that the bulk thermal properties are more like those of PB. The product of the reduced viscosity $(\eta'_r)_c$ and frequency $(\omega_r)_c$, where c represents the point of transition from one slope to the next, was found to be constant, leading to the conclusion that the transition from microphase to thermoplastic behaviour occurs at a constant stress and is essentially independent of temperature.

Futamura and Meineckie [20] studied ABA block copolymers with differing center blocks but the same end blocks, namely styrene. The activation energies (ΔE) for dynamic viscosities were found to increase with increasing solubility parameter difference between the center block and end block. The relaxation time associated with the long-range motion of chains was found to increase with increasing incompatibility ($\Delta\delta$) between the endblock and the center block, indicating that the energy of mixing of the two blocks is the major contribution to the melt rheology.

Gouinlock and Porter [22] prepared frequency-temperature master plots (reduced dynamic viscosity *vs.* reduced frequency, see footnote on previous page) for SBS copolymers. These curves showed two branches below a critical reduced

frequency. Data at temperatures below T_s fell on the upper branch while data at $T > T_s$ fell on the lower branch. Low-T master curves displayed excellent frequency-temperature superposition in spite of an assumed gradual change in phase morphology with temperature. These authors proposed that at low T, where the interphase is relatively small, T-dependence of dynamic properties is dominated by the homopolymer activation energy for the block composing the continuous phase (PB, in those cases). However, as the transition is approached and styrene block diffusion into the interphase region continues, the activation energy for the polystyrene homopolymer assumes increasing importance. Near T_s and at higher T, where complete molecular miscibility occurs, the ΔE tends to level off midway between the values for the constituent homopolymers. Therefore, the overall effect of the polystyrene component on copolymer behaviour increases with miscibility of the PS block with the continuous phase, that is, with the extent of the interphase region.

The fact that superposition of high and low temperature reduced η' and G' values was possible above a critical frequency, and that shift factors were not discontinuous at the transition temperature, was taken to imply that at high reduced frequencies (higher frequencies being a probe of shorter range motions) PS blocks present in phase separated micro domains have the same effect on dynamic properties as they do when dispersed on a molecular scale.

Chung and Lin [10] also found two characteristic branches of the η'/a_T *vs.* $a_T\omega$ master curve at low reduced frequencies. η' was found to be a strong function of ω in the upper branch but independent of ω in the lower branch. Their results indicated a constant flow activation energy below T_s and a constant, but lower, activation energy above T_s whereas Gouinlock and Porter [22] reported a flow activation energy smoothly decreasing from low to high temperatures. The present author notes that the data of Chung and Lin showed more scatter than that of Gouinlock and Porter.

Domain Orientation and Disruption, and Transient Structures

Weill and Pixa [77] reported that triblock copolymers with a cylindrical morphology form a lattice structure of hexagonally packed cylinders. Orientation in processing was found to align these cylinders. As a result, mechanical properties tested perpendicular to the direction of flow are different than those tested parallel to the direction of flow.

Akovali *et al.* [1] found that immediately after stretching an SBS copolymer through the plastic-to-rubber transition the E'(T) curve was lowered while the $E''(T)$ curve remained unchanged. Annealing at 110°C for 2 hours restored the initial curves, except for the appearance of a small peak in E'' around -40°C which they attributed to a growth in the interphase.

Kelterborn and Soong [38] followed the same procedure but found that the E''(T) curves before and after stretching and subsequent annealing were identical. No small peak in $E''(T)$ appeared. After elongation to 300% and release at various temperatures, G' and G'' measured under shear at the temperature of elongation for two SBS polymers were followed with time. For a 0.48 PS polymer G' curves recovered faster at 35°C than at 60°C, opposite to what would be expected for an activated process. Unlike the behaviour of the 0.48 PS polymer, the recovery of a 0.29 PS polymer was faster at the higher temperature.

Two models of structure breakdown were proposed. The first was PS block pull-out which was termed "disorderly" structure breakdown. The second was void or crack formation, termed "clean" structure breakdown. Structures broken disorderly would reform slower than those broken cleanly because diffusion of blocks back into domains is a relatively slow process. Segment pull-out would happen more at higher temperatures and crack formation more at lower temperatures. More domains would be expected to fracture when PS continuity is low and more segments pulled out when continuity is high because of the greater stress required to break the PS

continuity.

In a 0.48 PS sample, PS continuity is high and it was proposed that two structure breakdown processes occur at both test temperatures. At 35°C clean break would dominate while at 60°C disorderly breakdown would dominate. The clean break (35°C) would heal faster, hence the unexpectedly more rapid recovery. A 0.29 PS copolymer has low styrene continuity and thus clean break would always dominate. Healing of the clean break is an activated process and therefore would happen faster at higher temperatures.

Results showed a significant change in G' and a small change in G'' upon initial stretching and release. G'' is sensitive to the amount of interphase and its composition profile, while G' is relatively independent of the interphase and sensitive to long-range phase continuity. Therefore, it was concluded that breakdown does not involve the interphase to a great extent. The small change in G'' throughout these experiments also suggested that the interphase is not strongly involved in recovery, either, which seems to be a process of restoring phase continuity when $T < T_g$.

Sivashinsky *et al.* [66] studied stress transients following a sudden imposition of shear flow for two SBS copolymers at temperatures above T_g of PS. All stress curves exhibited a maximum corresponding to a yield point. It was shown that fragmentation of the PS continuity is not the dominant process of structure breakdown at these temperatures since a 0.29 PS copolymer exhibited higher yield values than a 0.48 PS copolymer, despite having lower PS continuity. Block pull-out was proposed as the dominant process at high temperatures. Small aggregates of different sizes may flow as separate entities, and dislocated PS blocks may join blocks in other aggregates. The 0.29 PS copolymer exhibited greater total recovery of stress than the 0.48 PS copolymer. This was consistent with the large central PB block of the 0.29 PS copolymer sustaining much of the elastic deformation.

Morrison and Winter [52, 53] studied the effect of unidirectional rotational shear on the structure of triblock copolymers. Both SBS and SIS copolymers with initially

cylindrical morphology were studied. Cylinders were found to align locally in a hexagonal array to form grains with a common director varying randomly from grain to grain.

Storage modulus of the unsheared samples approached a low-ω plateau, indicating a kind of network behaviour. For SBS, after shearing G' and G'' were lower for all frequencies. At strains less than 5.0 the moduli dropped with increasing strain, while at strains above 5.0 the moduli increased and eventually ($\gamma = 28.6$) returned to their unsheared values. At 160°C this recovery occurred preferentially at high frequencies, while at 180°C the recovery occurred over the entire frequency range. SAXS measurements indicated macroscopic orientation in the flow field.

For SIS, post shear G' and G'' decreased with increasing strain at all frequencies until saturation, but the trend did not reverse itself at higher strains. No orientation was observed at low stresses, while at high stress SAXS measurements did indicate orientation.

It was proposed that for SBS, with a $T_s > 180$°C, the microphase separation energy is too high to be completely overcome by flow. Therefore, large sections of the structure remain intact within the flow. Grains deform and rotate as units. A mixture of phase disruption and granular flow would occur. Calculation of flow energy ($\sigma\gamma$) *vs.* energy of mixing at 160°C showed that domain disruption may be possible at the stress-strain combinations used but that complete homogenization would not be achieved. Well placed grains, *i.e.* those nearly aligned in the flow direction, would be stretched and rotated into the flow direction, producing macroscopic orientation. Poorly aligned grains such as those initially perpendicular to flow direction would rotate at low strains and then dissolve at high strain. The drop in moduli over the whole frequency domain at 160°C was interpreted to support this mixed model since this implies some microphase mixing as well as less entanglement. At higher T the recovery is more complete since there is greater molecular mobility and slightly reduced microphase separation energy.

For the SIS copolymer used in this study, the "desire" to microphase separate, as characterized by the magnitude of the microphase-separation energy, is lower than for the SBS which was used. Though $\Delta\delta$ is higher for PS–PI than PS–PB, the molecular weight of the SBS is considerably higher, leading to higher T_s. Therefore, the material does not achieve a high degree of order and thus G' and G'' decrease with increasing strain, but instead of recovering at higher strains it saturates at low values of G' and G''. The degree of microphase separation of these materials is thus permanently altered by flow.

Hugenberger and Williams [35] measured complex viscosities of block copolymer solutions. A critical solution concentration (c_s) was defined for a fixed T, above which samples would be microphase separated. Samples were shown to be very sensitive to shear history. Samples of $c \geq c_s$, despite being microphase-separated, exhibited a limiting η_o (indicating liquid-like behaviour) when loaded into a viscometer while being in a structured state. The same samples loaded above T_s (*i.e.*, T was raised until $c < c_s(T)$) and allowed to cool below T_s displayed solid-like behaviour, presumably because the structure was never subjected to shearing disruption. Shearing above some critical strain amplitude caused a lowering of the η' and η'' curves which was more severe at higher frequencies. Even a single cycle oscillation above the critical strain amplitude caused drastic microstructural damage.

Nonsinusoidal stress response curves were observed at high strain amplitudes. Low ω curves were symmetrical while at higher ω the curves became asymmetrical. As ω was increased still further the stress outputs again became sinusoidal.

3.4.3 Yield Stress

In our discussion of nonlinear mechanical properties (section 3.3) much was said about plastic-to-rubber yielding. This is not the same phenomenon as the

liquid phase yield stress which is to be discussed here, since the former involves breakage of solid interconnections between glassy domains. Liquid yield stress refers to a resistance to flow in a system where both phases are liquids, *i.e.* above T_g. Homopolymers, being viscoelastic, do not exhibit a true yield stress since any finite stress will cause a relaxation, however slow, which will eventually relieve the stress. The theoretical basis for the existence of a yield stress in block copolymers was established by Henderson and Williams [31]. Any force that is lower than that imposed by the interphase free energy barrier would not cause flow.

The work of the IUPAC working Party on "Structure and Properties of Commercial Polymers" has already been discussed (Section 3.4.1). Reference was made to a study wherein flow was observed at stresses as low as 10 Pa and it was concluded that no yield stress exists. However, as mentioned earlier, the study never appeared in a peer reviewed journal and nothing is known about the conditions of testing. Masuda *et al.* [48], working with a solution of SI diblock copolymers in *n*-tetradecane, which is a good solvent for the PI block but a nonsolvent for the PS block, also found that the shear stress after cessation of flow did not relax to the zero level, but left a considerable residual stress.

Diamant *et al.* [13] observed a high temperature plateau above 100°C in the G''(T) curves of SBS copolymers. The component homopolymers showed no such plateau, being homogeneous liquids. These data were interpreted to indicate a solid-like structure in the melt above the softening point of the PS phase which is probably a manifestation of a yield stress arising from thermodynamic forces associated with the interphase.

De Kee *et al.* [12] measured yield stresses of SBS copolymers in solution, with $c > c_s$, using a quasi-static technique. Yield stresses from 1 to 20 Pa were measured and found to decrease with increasing temperature and decreasing concentration. Yield stresses also decreased with each shearing.

Kotaka and White found that an SB diblock copolymer in a selective solvent

(one which is good for the PB phase but a nonsolvent for the PS phase) exhibited a yield stress with thixotropic character. Bauer and Meerlander [4] observed yield stresses in SI diblock copolymers in solution using solvents selective to the PI phase.

Watanabe *et al.* [76] found that diblock copolymer solutions in selective solvents exhibited higher-order odd harmonics, or nonsinusoidal stress response, in small amplitude oscillation. They concluded that these results suggested the existence of a yield stress. Steady shear experiments also suggested a Bingham-type flow model. In general, systems having ordered macrolattice structures (phase separation) showed nonlinear "viscoplasticity," and those having disordered structures showed linear viscoelasticity. The plasticity of the phase separated systems was attributed to the driving force for the macrolattice formation.

Hansen and Williams [27] measured yield stresses of bulk solvent cast SBS copolymers using a constant stress rheometer in the temperature range $T_g < T < T_s$. Yield stresses ranged from 50 to 420 Pa, depending on molecular weight, composition and casting solvent, as well as temperature, and were found to be larger for samples with higher T_s (at constant T) and to decrease with increasing T. For a sample tested above T_s, σ_y vanished, though it was evidently present at lower T. The above observations are consistent with LHW theory since polymers with a higher T_s would resist more strongly any mixing of the incompatible chemical blocks which would be necessary for flow to occur.

Han *et al.*, studying bulk SIS [23] and SBS [26] copolymers, observed evidence for yield stresses in dynamic data. Plots of $\log \eta'$ *vs.* $\log \omega$ at low values of ω did not level off but curved upward towards a slope of -1. Above a critical temperature (T_s) the same plots levelled off to a Newtonian limit. Pico and Williams [56, 58] performed the same experiments with SBS solvated with a neutral solvent, demonstrating the same phenomena.

Chapter 4

Equipment and Methods; Rheological Testing

The Rheometrics RMS 800 Mechanical Spectrometer was used for all rheological testing. The RMS 800 is essentially a rotational rheometer which can be operated with many geometries: cone and plate, parallel plates, cup and bob, and others. For this project, 50 mm diameter parallel plates were used exclusively. The bottom plate, or platen, is connected to a motor which is capable of a range of displacements with different time dependencies which will be described below. The top platen is connected to a force rebalance transducer capable of measuring both torque and normal force. A labelled diagram of the staging area in the rheometer is given in Figure 4.1 showing transducer, thermocouple and oven. An explanation of the parts is given in Table 4.1. It will be very helpful to refer to these as you read this section.

4.1 Sensitivity

The manufacturer's quoted torque range for the mid-range transducer (used exclusively in this project) is between 2 and 2000 g·cm. However, it is found that

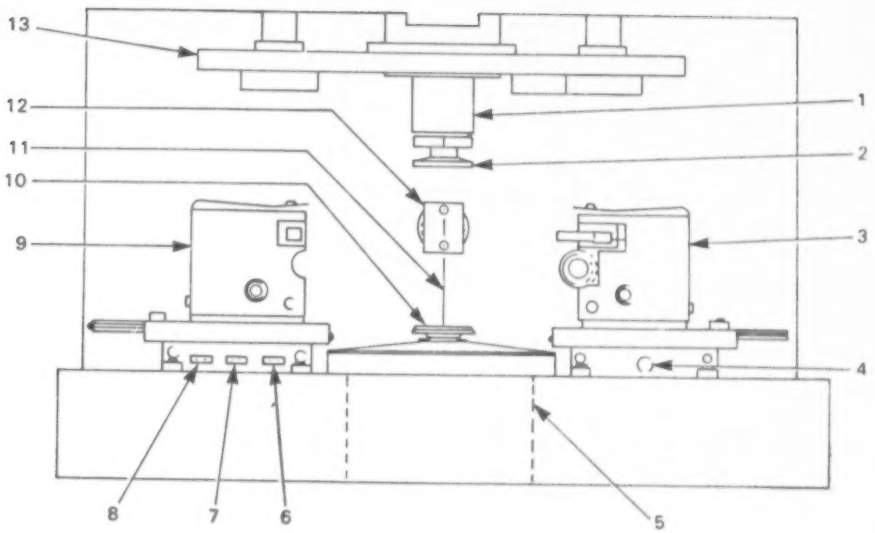

Figure 4.1: Staging area of the RMS 800.

Table 4.1: Staging area components.

1	Transducer.
2	Transducer anvil on which upper platen is mounted.
3,9	Right and left halves of oven.
4	Oven light.
5	Motor.
6,7,8	Thermocouple receptacles.
10	Motor anvil on which lower platen is mounted.
11	Tool thermocouple.
12	Heater gun.
13	Platform or quill which houses the transducer and can be raised or lowered by the stepper motor.

torques lower than 2 g·cm can be reliably measured. Torques as low as 1 g·cm can be accurately measured while torques down to 0.3 g·cm can be statistically differentiated from zero, but not accurately measured. This was determined by a calibration using known weights. The method and results are described in Appendix A Section A.1.

4.2 Modes of Operation

The modes used in this experimental program are described below.

4.2.1 Dynamic Oscillatory

The bottom platen can be displaced torsionally in a sinusoidal pattern at frequencies ranging from 10^{-3} to 10^{2} radian/s, with displacements down to 1.25

$\times 10^{-5}$ and up to 0.5 radians. Stress and strain are both measurable signals. In dynamic oscillatory mode several sweeps can be performed as described below

Single

This mode executes a single test at the specified frequency, strain amplitude and temperature. One and one half cycles are performed before the input (strain) and output (stress) waves are fitted to a sinusoid, thereby generating the amplitude ratio and phase lag. These quantities are then used to calculate automatically the rheological functions described in Section 2.3. At the end of every test the motor automatically returns to the same zero position.

Strain Sweep

In this mode the amplitude of the oscillation is sequentially increased (or decreased) between user-selected limits. One and one half cycles are executed before a sinusoidal function is fit to the input (strain) and output (stress) signals. Strain is calculated using

$$\gamma = \frac{\theta R}{H}$$
$$\%\gamma = \gamma \times 100\% \tag{4.1}$$

where γ = strain, θ = angular displacement in radians,
R = radius of platens, H = sample thickness = platen separation.

In the parallel plate geometry Equation 4.1 gives the strain at the outer boundary of the disk, which is also the maximum strain. The sample between the plates is experiencing nonhomogeneous strain which approaches zero at the centreline.

Frequency Sweep

Similar to the strain sweep, frequency of oscillation is sequentially increased (or decreased) between user-selected limits.

Temperature Sweep

A single test can be performed at each of a series of sequential temperatures in a user-selected range. Temperature control is achieved by a convection oven which uses either air or nitrogen as the heating medium, or else by a circulation jacket. The user can select a thermal soak time to achieve temperature steady state before each test is performed. Both environmental chambers will be discussed in the section on temperature control (4.10).

Frequency/Temperature Sweep

A frequency sweep is performed at each temperature in a temperature sweep.

4.2.2 Dynamic Transient

Dynamic transient tests are step strain tests like that described in Section 2.2 and Figure 2.1 which facilitate the measurement of relaxation times. The motor rotates the bottom platen at maximum motor speed to a fixed angular displacement corresponding to a user-selected strain. Stress and strain signals can be measured against time.

4.2.3 Steady Mode

The bottom platen connected to the motor can be rotated at a constant rate ranging from 10^{-3} to 10^{2} radians/s in either the clockwise or counter-clockwise

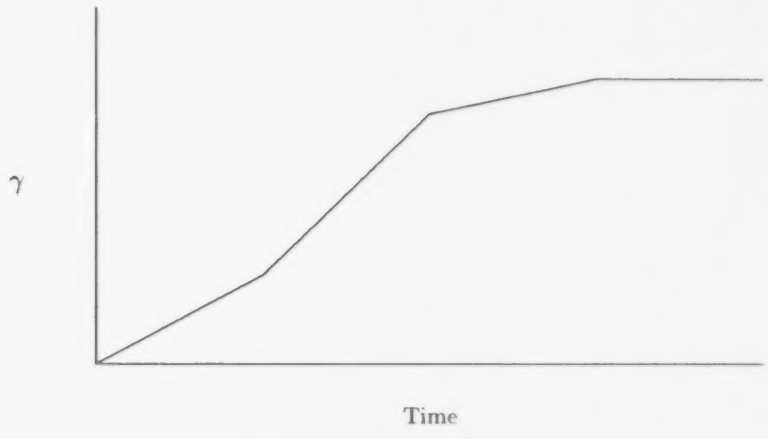

Figure 4.2: Strain *vs.* time in four sequential zones as programmed in the step rate mode.

direction. Stress and normal force, rather than stress and strain, are the measurable signals in steady mode.

Transient

The term "steady transient" seems like a conflict of terms. This mode is also known as the "step rate" mode, and allows the measurement of stress and normal force during four sequential constant shear rate zones. This is not the same as a rate sweep, wherein the shear rate is sequentially varied with a return to the zero position, and to zero strain rate, between each $\dot{\gamma}$. Rather, in the step rate mode the strain rate is changed to its programmed value in the next zone (presumably instantaneously) immediately after the end of the previous zone. This is schematically shown in a plot of $\gamma(t)$ in Figure 4.2. A negative strain rate results in a rotation in the opposite direction and a zero strain rate results in a constant angular displacement.

4.3 Auto-Zeroing of Motor

In dynamic oscillatory mode the motor to which the bottom platen is connected has a fixed zero position. Each time the motor is turned on or a test is ended (even between tests in a sweep) the motor returns to this zero position. In steady mode there is no fixed zero, but rather the motor chooses a zero point each time the motor is turned on and moves to this zero point. The zero is always in close proximity to the position of the motor when it was off.

In dynamic oscillatory mode each test begins in the direction of rotation opposite to that of the previous test. For example, in a strain sweep from 1 to 5% in 1% intervals 1, 3 and 5% would be started in the clockwise direction while 2 and 4% would be started in the counterclockwise direction. The same would be true of isolated single tests provided that the rheometer was not turned off between tests, or the computer control unit reset. In dynamic transient mode and in steady mode the user may select the direction of rotation.

4.4 Alignment

In a parallel plate rheometer it is important that the bottom and top platens be aligned very precisely. This is because the stress is calculated from the geometry and torque. The greatest stress contribution is from the outer edges of the platens. The effects of a small error in either parallelism (commonly referred to as flatness), or concentricity of the platens would be greatest near the edges where they would cause the greatest error in the stress calculation. The following alignment specifications are given in the RMS 800 manual. The flatness of the platens must be within $\pm$ 0.0003 inches from zero, that is, total error must not exceed 3 tenths of one thousandth of an inch from high to low point. Similarly the platens must be concentric to within a $\pm$ 0.001 inch error. For our equipment we ensured a flatness and concentricity

alignment within one half to two tenths of one thousandth of an inch.

4.5 Sample Gap

Because precise knowledge of the platen separation (commonly referred to as the "gap") is essential for strain calculation, it is important that it be known accurately. The platform assembly holding the transducer, to which the upper platen is attached, can be raised and lowered automatically by a stepper motor. All components are so well machined that the alignment of the platens does not change significantly with the position of the platform. A metal block on the platform pushes against the armature of a dial gauge which is marked in 2 micron (2×10^{-6} m) increments. Position of the platform can therefore be measured accurately to within 1 micron.

The gap is zeroed by lowering the platen until a positive normal force is registered on the analogue meter, indicating that the upper platen has touched the lower platen. The outer dial on the dial gauge can then be rotated until the needle shows zero displacement.

Due to thermal expansion of the platens the gap is not constant with temperature. This can be compensated for in two ways.

1. The gap can be zeroed at the planned test temperature.

2. If the sample is to be tested at several temperatures then the gap can be corrected, by employing the thermal expansion of the platens. In an automatic temperature sweep the autotension mode can be used so that the upper platen moves up with increasing temperature. The rheometer control computer senses the change in the gap by a magnetic indicator on the dial gauge. For manual temperature sweeps a calibration of gap change with temperature was done

by zeroing the gap at a range of temperatures. This calibration is given in Appendix A Figure A.2 and Table A.3.

4.6 Autotension

The autotension mode maintains a constant normal force on the transducer within a user-defined window (the autotension window, given in percent of full scale). Positive normal forces, that is in the upward direction, are relieved by raising the platform and hence the upper platen. Negative normal forces are relieved by lowering the platform. This is particularly useful in temperature sweeps to ensure that the transducer is not forced off scale in the normal direction as this could cause damage to the transducer.

4.7 "Internal" Data Acquisition and Analysis

The RMS-800 Mechanical Spectrometer is interfaced with a dedicated electronics console/computer controller. The electronics are proprietary, but it is known that this unit contains an analogue to digital converter capable of converting the $\pm$10V full scale signals from the transducer (both normal force and torque) and from the motor (displacement) into a signal in bits. In dynamic oscillatory mode input (strain) and output (stress) signals are fit to sinusoidal functions by proprietary software. In dynamic transient mode, data is collected at 512 equally spaced (in time) points in each of four time zones of user-selected duration between 1 second and 130,000 seconds. Typically the first zone is the shortest when the most rapid relaxations are occurring. For example, zone 1 may extend from 0 to 1 second, zone 2 from 1 to 11 seconds, followed by zones of 100 and 3600 seconds.

4.8 "External" Data acquisition

Using a 486 DOS based personal computer with an analogue to digital conversion card installed, one can aquire directly the waveforms of the input and output signals. The card, purchased from Keithley Metrabyte, has 16 bit resolution and software selectable ranges of ± 10V, ± 5V, ± 2.5V and ± 1.25V. Sampling rate is user-selectable from 0 to 47.5 KHz on one channel, and up to 8 channels can be read. However, channels are read sequentially, so sampling rate per channel is halved when reading 2 channels, quartered when reading 4 channels and so on. Furthermore, the card does not have the "sample and hold" feature. Therefore, data streamed to the disk must be plotted against two independent time axes, each channel lagging behind the previous channel by one sampling period.

4.9 Sample Formation

"Solid" polymer samples were compression molded into disks using a mold fabricated in-house. The specifications are given in Appendix B. Samples were 5 centimetres in diameter and roughly 2 millimetres thick. The mold was evacuated using a vacuum pump and controlled with an Omron E5CS temperature controller. The temperature setpoint for all copolymers was 225°C. Samples were molded for varying lengths of time (the timing started when the heater temperature first reached the set point) under a ram force of 2 tons in a platen press. With SBS1[1] and SBS4, 45 minutes heat soak was sufficient to cause interdiffusion of the polymer granule boundaries and eliminate all visible air bubbles, thus forming uniform samples. However, with SBS2, SBS3 and SIS 1 1/2 hours were necessary to obtain a sample with few trapped air bubbles. In order to facilitate sample removal, the mold disk surfaces were sprayed with a teflon-based mold release agent (Crown 66075 Dry Film

[1]See Chapter 5 and Table 5.1 for an explanation of these acronyms.

Lubricant & Mold Release Agent)[2] prior to loading of the granulated polymer.

4.10 Temperature Control

A gun heater protrudes from the back of the rheometer to within one or two centimetres of the platens. An insulated jacket closes around the platens and the gun heater. The heater operates by forced air or nitrogen if provided. The temperature range of this convection oven is from ambient to 500°C. Thermal control is taken from a platinum resistance thermometer (prt) positioned just beneath the lower surface of the bottom platen approximately one centimetre in from its outer edge. The control scheme is proportional and integral plus derivative. Quoted stability is ± 0.5°C when equilibrated. In practice it is found to be stable to within 0.1 to 0.2°C. Measurement of sample temperature is possible from a thermocouple located next to the prt or from a thermocouple which protrudes from the center of the motor through the center shaft of the lower platen and rests in a divot on the underside of the bottom platen in its center. This thermocouple is known as the "tool thermocouple" and the temperature so measured is known as the "tool temperature". To achieve subambient temperatures, the convection oven must be switched with a liquid circulation jacket. The gun heater and high temperature jacket are removed and the circulation jacket installed to close around the platens. A silicon oil is circulated through the jacket halves by a Haake F3 circulator/heater and refrigeration unit with temperature range of -30 to +105°C, which results in a range of -25 to +100°C at the platens. A calibration of sample temperature *vs.* tool temperature using the circulation jacket is given in Appendix A Figure A.3 and Table A.4.

[2]Crown Industrial Products: Whitby, Ontario L1N 5V3

4.11 Sample Loading

Molded samples were loaded by the following procedure. Platens were preheated to 185–190°C at a gap of about 2 mm. The platens were then opened and the sample was placed on the lower platen. A glass rod was then rolled over the sample to cause adhesion to the lower platen and exclude any air trapped beneath. The top platen was then lowered to contact the sample until the normal force was approximately 50% of full scale. If this did not result in good contact with the sample over the whole area of the top platen (*i.e.*, if there were any spaces around the edges) then the sample and platens were heated to 190°C[3] while in autotension mode. This caused the platen to move downwards as the sample relaxed until the gap was closed. The sample was then cooled and allowed to equilibrate at the test temperature.

[3]Note, with SBS2 and SIS only a 30% normal force and 170°C loading temperature were used.

Chapter 5

Materials

Several triblock copolymers from different manufacturers were used in this study. The properties of each are summarized in Table 5.1 and explained below.

Three styrene - butadiene - styrene block copolymers provided by Dow Chemical Company U.S.A. were used in this investigation. All three were monodisperse (1.02 < polydispersity < 1.03) and all molecular weights quoted are peak molecular weights from a GPC trace performed by Dow and confirmed by light scattering to be very close to weight average molecular weight.

The first of the Dow materials listed in Table 5.1 is Vector 8508-D which will be referred to as SBS1 in the remainder of this document. The molecular weight of SBS1 was quoted to be 69,427 and styrene weight fraction was quoted as 30.4%. The microstructure was predicted to be cylindrical and this was confirmed by an electron micrograph prepared by another researcher.

A trace from a differential scanning calorimeter (Figure 5.1) reveals the temperature transitions in the material. There are two distinct transitions that are immediately obvious in this trace. One is between 50°C and 70°C and the second is between 240°C and 250°C. The first is the glass transition of the styrenic dispersed phases. An enlargement of this region (Figure 5.2) shows a transition at

Table 5.1: Summary of polymers used.

Designation	Center Block	Overall $\bar{M}_w$	ϕ_S (%)	T_s (°C) [predicted]
Dow Copolymers				
SBS1	butadiene	69,427	30.4	243 [240]
SBS2	butadiene	61,290	44	255 [265]
SBS3	butadiene	101,225	31.3	[482]
Shell Copolymers				
SBS4	butadiene	76,000	28.9	[317]
SEBS	ethylene/butylene	67,000	29.8	[839]
SIS	isoprene	140,000	14	260 [240]

about 60°C-70°C. This is quite low, as the T_g for polystyrene is normally quoted to be in the region of 100°C. There is a molecular weight dependence in T_g, and the molecular weight of the styrene blocks ($\bar{M}_w$ = 10,500) is low enough to display such effects; however the molecular weight dependence alone is not strong enough to cause such a large shift in T_g. Diamant *et al.* [13] showed that plasticization of the glassy phase by the rubbery matrix blocks can cause such a shift. Therefore, ϕ_S in the glassy domains is less than 1.

Below the T_g of the dispersed phases is a gradual, concave downwards transition extending from -70°C (or lower) to +60°C. This is not normally seen in polymers and is quite different from the straight baseline seen above T_g. This must be a gradual transition revealing the change from glassy to liquid character of a diffuse interphase of continuously varying composition. If the interphase consisted of one or several discrete compositions then this region would show up as several discrete steps showing distinct second order transitions.

A plot of $G''(T)$ also reveals temperature transitions. Transitions are revealed by a peak in the curve of loss modulus *vs.* temperature. Figure 5.3 is a temperature sweep of modulus from - 25°C to 100°C. The large peak with a maximum at

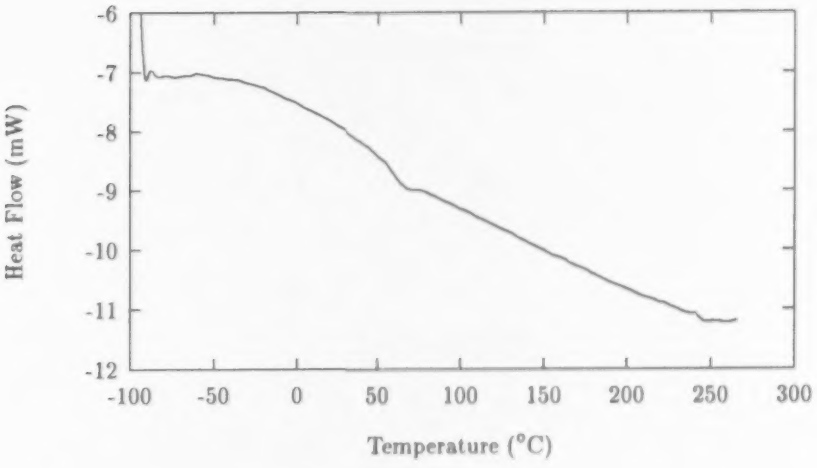

Figure 5.1: DSC heating scan of SBS1 showing two distinct transitions.

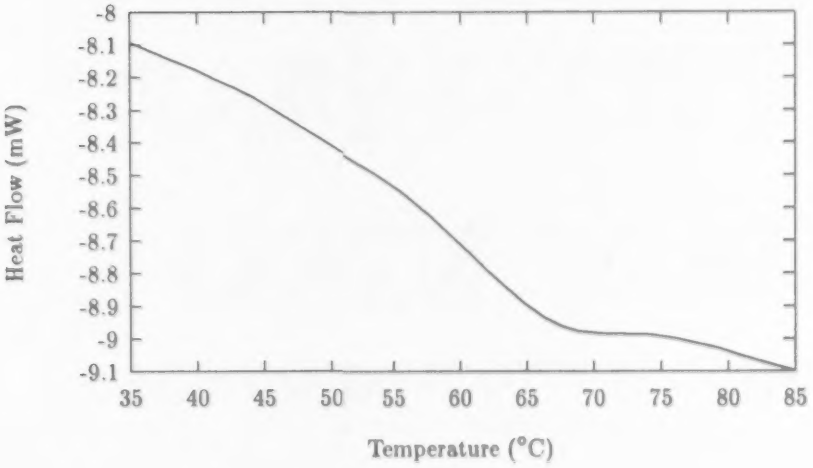

Figure 5.2: DSC heating scan of the polystyrene-rich glass transition region in SBS1.

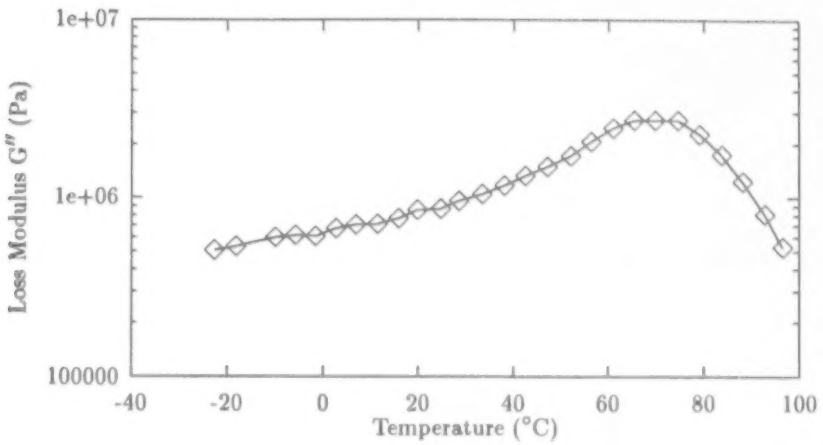

Figure 5.3: Loss modulus as a function of temperature (heating run) for SBS1.

65°C to 75°C indicates the glass transition of the dispersed phase. This transition is difficult to pinpoint because of the breadth of the transition. With the DSC the transition was seen between 60°C and 70°C, but T_g's for homopolymers can usually be accurately determined to within 2 or 3°C. However, Diamant *et al* [13] demonstrated that the mechanical loss peak for pure PS was much sharper than that corresponding to the PS phase in an SBS copolymer. At lower temperatures the loss modulus begins to level out to a plateau which Diamant showed can be represented by the superposition of many peaks, each corresponding to the glass transition of a slice of the interphase with some local average composition.

The Leary Theory prediction for the separation temperature T_s [43, 44, 45] for an SBS polymer with the same block molecular weights as SBS1 is 240°C. The second transition in the DSC trace (Figure 5.1), between 240°C and 250°C, has been enlarged in Figure 5.4 and reveals T_s to be around 243°C. A straight baseline has been superimposed on the data plot in order to demonstrate that there is a trough present here; however, it is difficult to determine where precisely the baseline should be drawn, or whether it would even be straight.

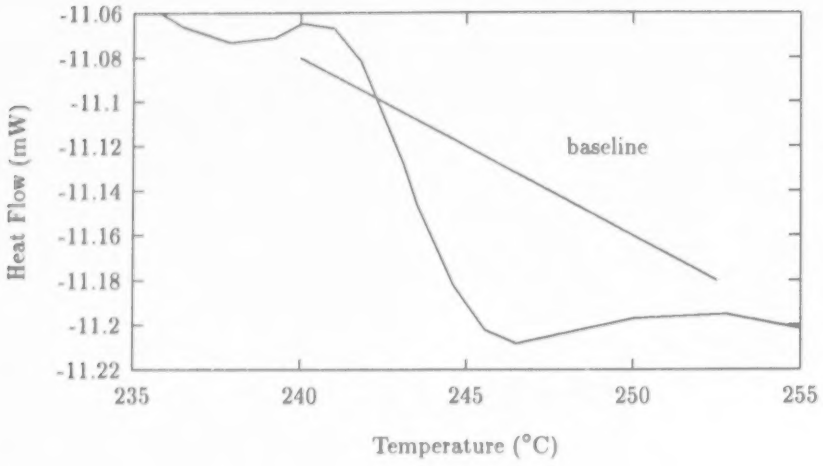

Figure 5.4: DSC heating scan of microphase transition region in SBS1.

Another Dow SBS polymer used in this study was Vector 4461-D and will be referred to as SBS2. The molecular weight was 61,290 and styrene weight fraction was 44%. Figure 5.5 reveals the thermal transitions in this material. The glass transition temperature of the dispersed phase (Figure 5.6) is very close to that of the corresponding phase in SBS1. The separation temperature is slightly higher than SBS1, being about 255°C (Figure 5.7). A calculation based on Leary Theory predicted T_s in the vicinity of 265°C. Another transition is evident in this trace at about -95°C which is the glass transition of the butadiene phase. This transition is not seen in Figure 5.1 because the scan was started at just above -100°C and the T_g of polybutadiene was lost in the response from the initial heating.

Another Dow SBS polymer used (SBS3) was Vector 2510-D with molecular weight of 101,225 and styrene weight fraction of 31.3%. The predicted T_s is 480°C, much higher than could be reached before significant degradation of the polymer occurs.

One SBS polymer from Shell Chemical Company, Kraton 1101, was also used

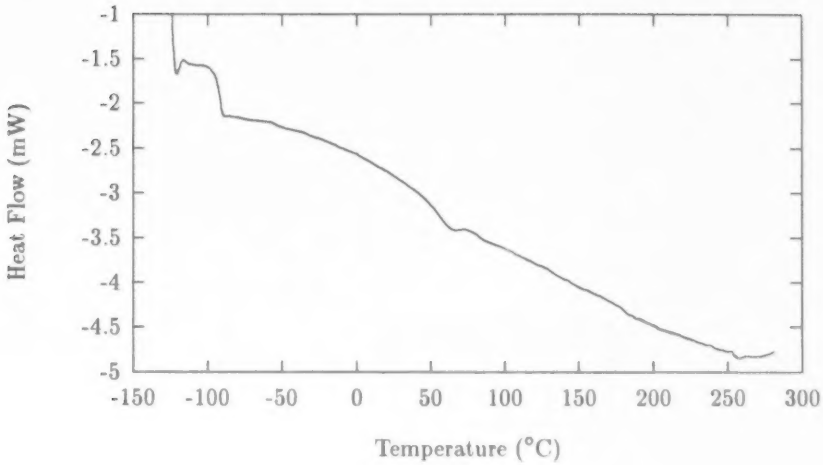

Figure 5.5: DSC heating scan of SBS2 showing three distinct transitions.

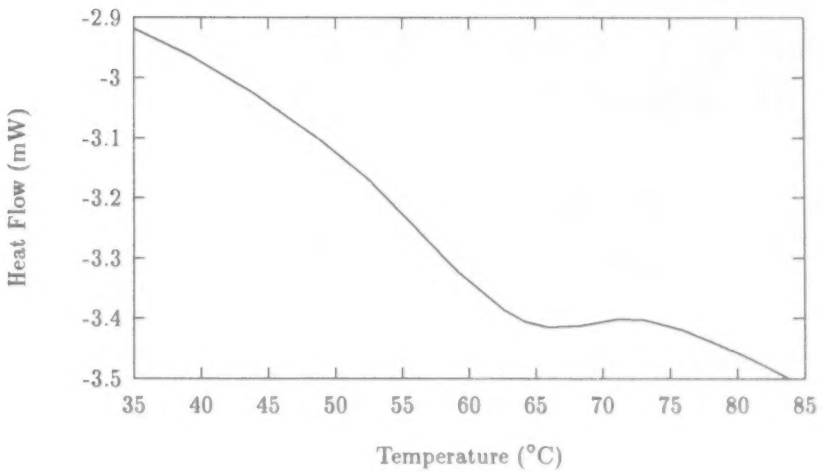

Figure 5.6: DSC heating scan of the styrene-rich glass transition region in SBS2.

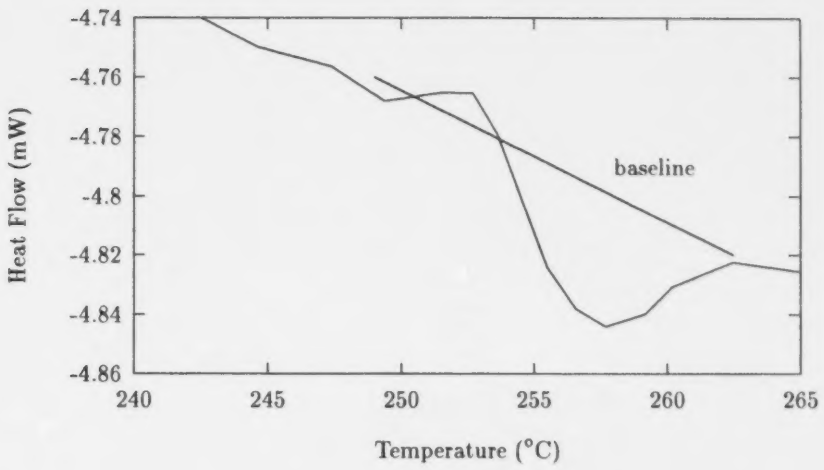

Figure 5.7: DSC heating scan of microphase transition region in SBS2.

in this study and will be referred to as SBS4. The molecular weights of the S-B-S blocks were 11-54-11 $\times 10^3$. The age of the sample was not known precisely as it had been transported from another lab at the University of California at Berkeley where studies on the rheology of block copolymers have been going on for many years. However, the sample had been kept in a sealed brown glass bottle and a small subsample was found to dissolve completely in cyclohexane, indicating that it was not crosslinked and thus probably close to being preserved.

A block copolymer with a random ethylene/butylene center block and styrenic end blocks, also provided by Shell Chemical Company, was used and will be referred to as SEBS. The molecular weight was 67,000 and the styrene content was 30%.

The last copolymer studied was a styrene-isoprene-styrene triblock produced by the Shell Chemical Company, marketed under the name Kraton-D 1107. This will be referred to as SIS. The block molecular weights were 10-120-10 $\times 10^3$, so that the styrene content was just over 14%. This also was an old sample brought from California and stored in sealed brown glass bottles. However, a small sample was

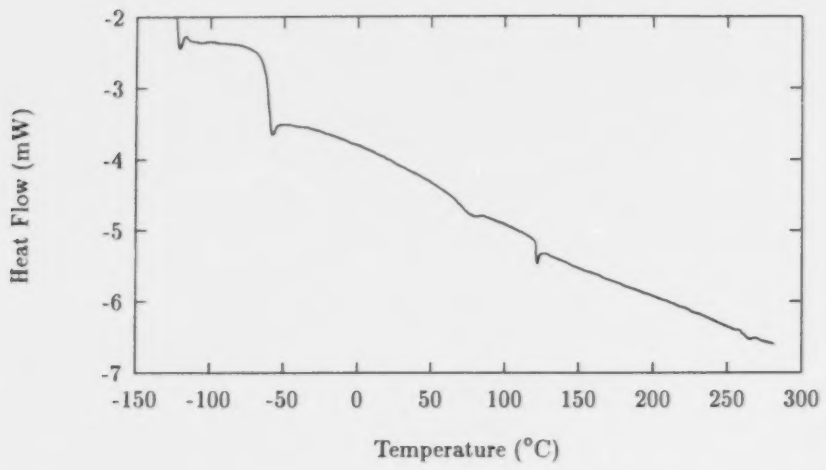

Figure 5.8: DSC heating scan of SIS showing four distinct transitions.

found to dissolve completely in THF.

The DSC trace (Figure 5.8) reveals four distinct temperature transitions in SIS. The first, around -60°C is the T_g of polyisoprene. At about 73°C is the T_g of the styrenic dispersed phase (Figure 5.9). The separation temperature is revealed to be about 260°C (Figure 5.10), slightly higher than the calculation, based on Leary Theory, of 240°C.

The last transition, at about 120°C (Figure 5.11), may be the separation temperature of a dispersed phase formed by diblock copolymers. The Shell block copolymers are known to contain a significant fraction (as high as 15 or 20%) of uncoupled diblocks [19]. Such diblock chains would have an average molecular weight of 130,000 (missing only one endblock of molecular weight 10,000) and a lower styrene fraction (roughly 7.3%) than the triblocks. Shifting T_s linearly according to Leary and Williams [44] results in a predicted T_s of only 11°C. However, Henderson and Williams [34] predicted that T_s of diblock copolymers would be higher than that of triblock copolymers of the same molecular weight and fractional styrene content.

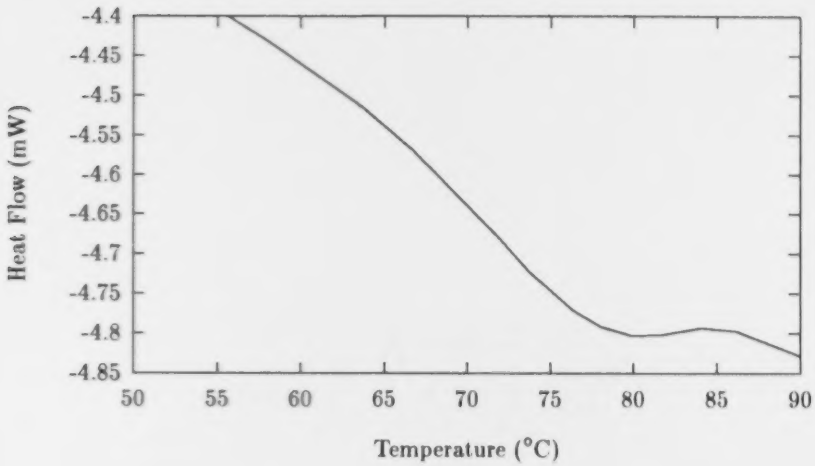

Figure 5.9: DSC heating scan of the glass transition region in SIS.

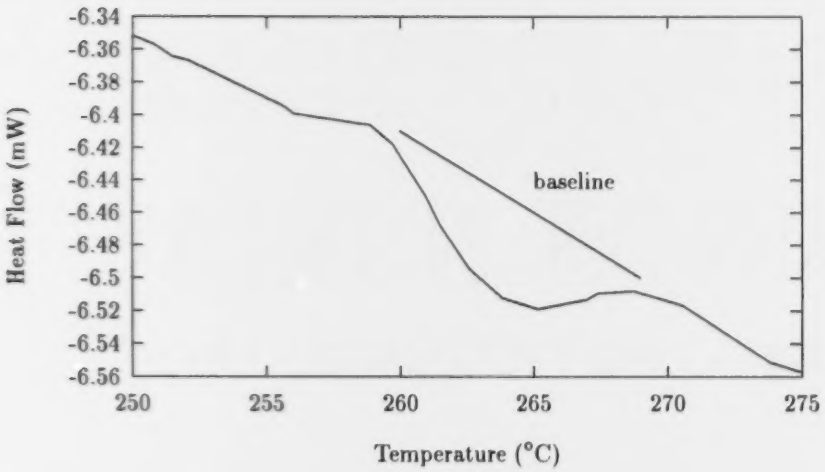

Figure 5.10: DSC heating scan of microphase transition region in SIS.

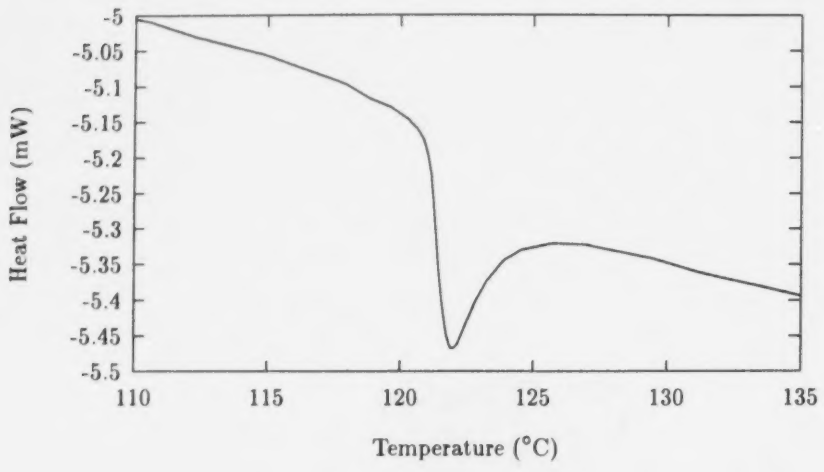

Figure 5.11: DSC heating scan of diblock transition region in SIS.

The magnitude of this difference depends greatly on the character of the interphase and on the styrene content. Furthermore, the diblock present need not form an entirely separate phase, but could instead form a phase of predominantly diblocks with some triblock. It is unknown how this would affect T_s. Thermodynamic theories have not addressed this question to date.

Chapter 6

Results 1; Stress Relaxation Experiments

6.1 Step Strain Tests

A series of step strain and stress relaxation experiments were performed on the triblock copolymer samples listed in Table 5.1, excepting SBS4. The results of these tests are presented in this chapter. The discussion of their meaning and significance is deferred to a later chapter. It should be noted here that the rheometer control arbitrarily defines one direction of rotation as positive torque (and hence stress and modulus) and the other as negative torque. All stress and modulus values reported here were therefore multiplied by -1 to facilitate logarithmic graphing. Step strain tests were performed using nitrogen as the convection heating gas and with a new sample for each test.

6.1.1 SBS1

The dynamic transient mode on the RMS 800 was used to perform several step strain tests on SBS1. The first test temperature set point was 90°C at which

polystyrene or polybutadiene would be completely fluid ($T_g < 90°C$) and exhibit stress relaxation $\sigma \rightarrow 0$ at long times. True temperatures and strain amplitudes, as opposed to set points, as well as gap spacings for each test on SBS1 are given in Table 6.1. The sampling zones, as described in Section 4.7, were chosen as 1, 10, 100 and 14,400 seconds and the strain amplitude was varied from 0.05% to 4%. The results of stress relaxation *vs.* time are given semilogarithmically in Figure 6.1, plotted against linear time.

Table 6.1: Conditions for step strain tests on SBS1.

Commanded Strain (%)	γ (actual, in %)	Gap (mm)	Temperature (±0.1°C)
Temperature Set Point = 90°C			
0.05	0.05	1.911	90.9
0.1	0.093	1.902	90.9
0.2	0.192	1.886	90.6
0.3	0.292	1.890	90.8
1	0.955	1.834	90.4
4	3.86	1.887	90.7
Temperature Set Point = 100°C			
0.1	0.085	1.770	100.8
0.2	0.183	1.713	100.5
0.4	0.377	1.637	100.8
1	0.955	1.604	100.5
4	3.84	1.819	100.8
Temperature Set Point = 110°C			
0.2	0.197	1.535	110.9
0.4	0.382	1.474	110.7
1	0.954	1.735	109.7
4	3.84	1.899	110.0

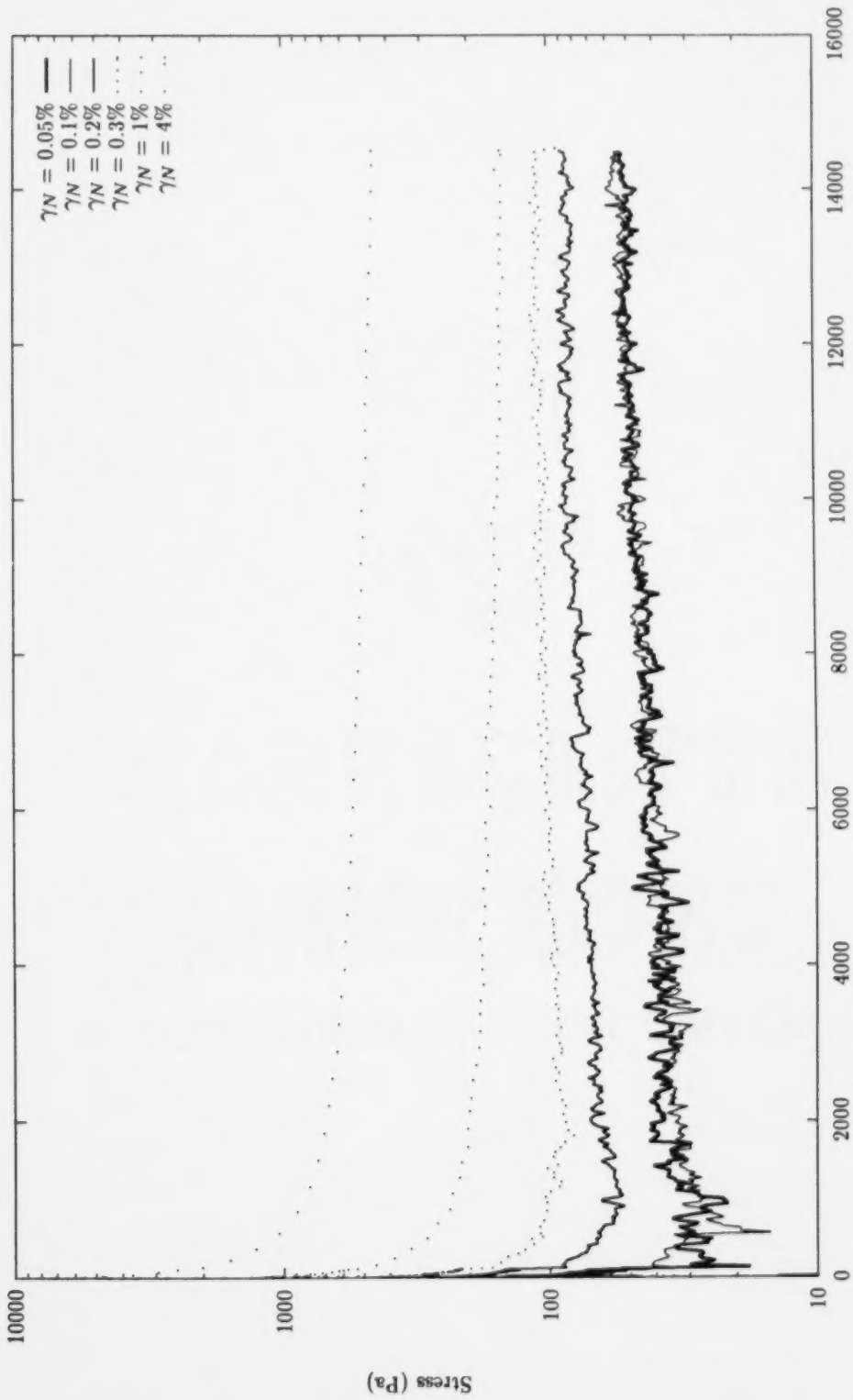

Figure 6.1: Stress relaxation experiments for SBS1 at 90°C.

Plotting both stress and strain against a logarithmic time scale for commanded strains (γ_N) of 4% (Figure 6.2) and 0.05% (Figure 6.3) reveals irregularities in the strain at short time scales which resulted in jumps in the stress. This was diagnosed as a logic error in the rheometer control. Referring to Figure 6.2 it can be seen that with a commanded strain of 4% the platen first moved rapidly to a strain of roughly 3.5% and then leveled off until the 1 second mark at which time it jumped to 3.86%. This level it maintained for the remainder of the test except for a brief drop back to its pre-1-second level occurring at 10 seconds and a slight blip at about 100 seconds. In Figure 6.3 the commanded γ was 0.05%. The platen first moved rapidly to a strain of around 0.28% and then levelled off, again until the 1 second mark and then moved rapidly to the set-point of 0.05% until the 10 second mark where it briefly jumped to its pre-1-second level. At 100 seconds another blip is seen in the strain, but for the greatest duration of the test the 0.05% level was maintained. Only for 0.05% and 0.1% commanded strain did the strain initially go to a higher-than-commanded strain.

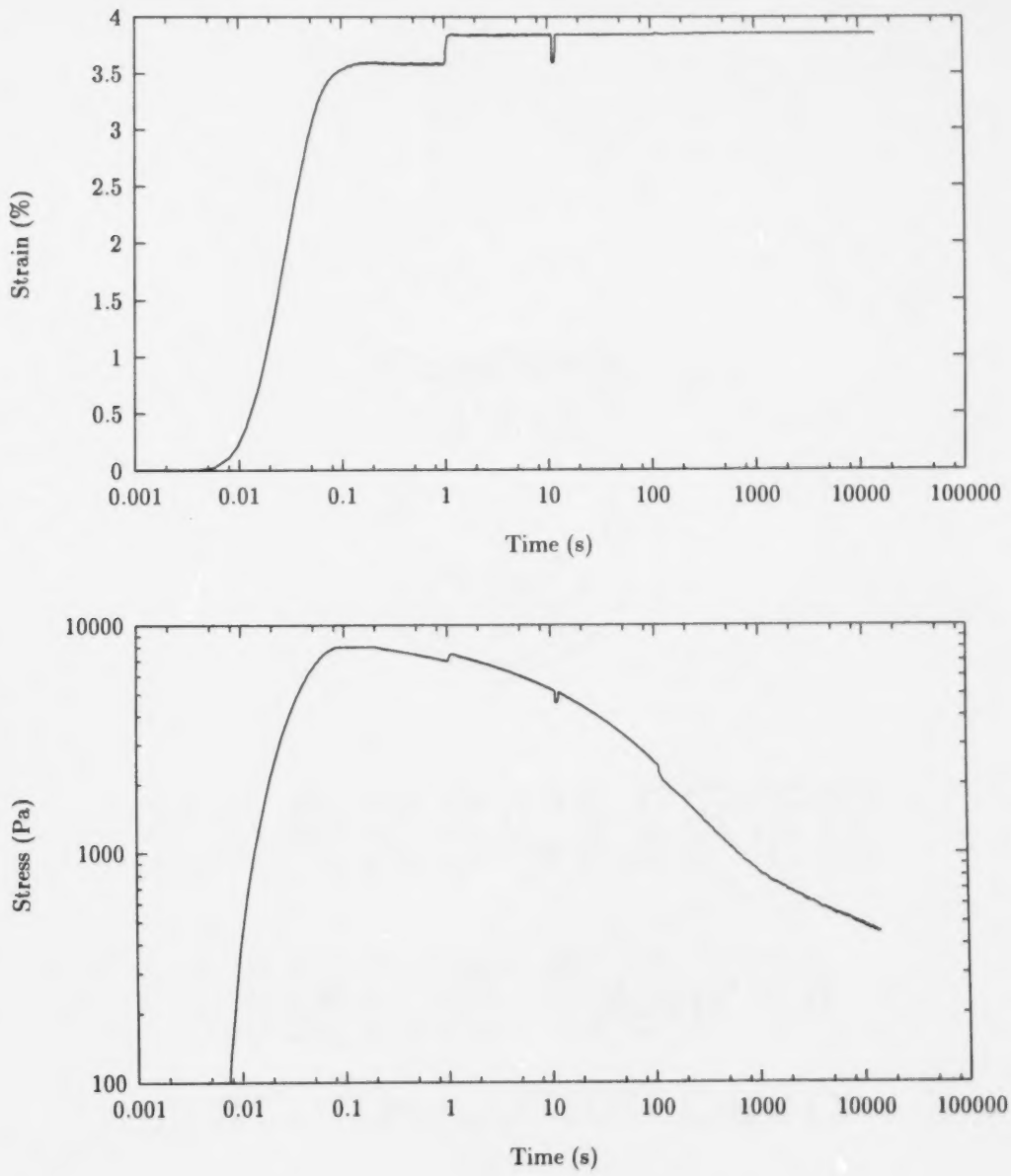

Figure 6.2: Strain and stress irregularities, $\gamma_N = 4\%$.

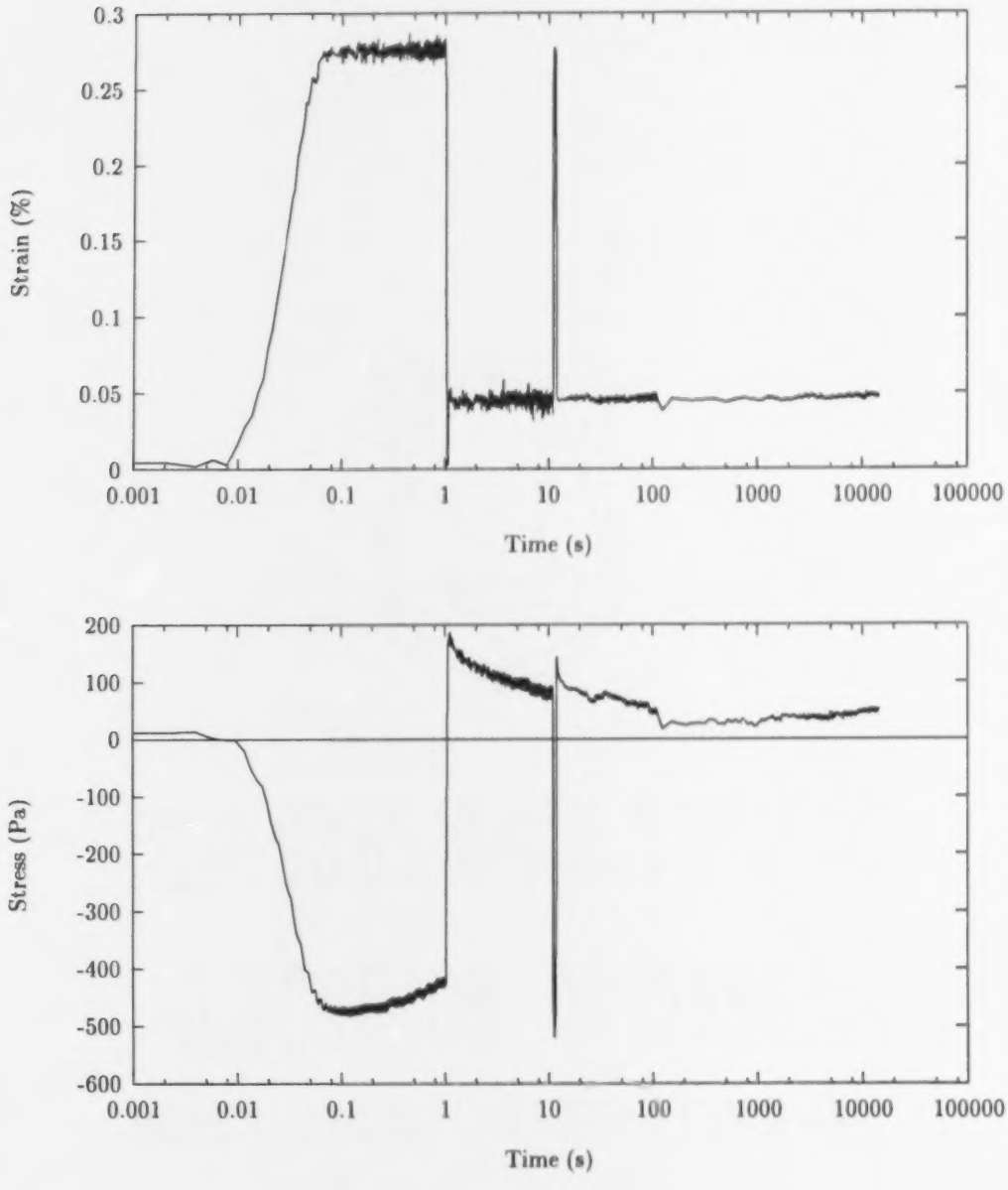

Figure 6.3: Strain and stress irregularities, $\gamma_N = 0.05\%$.

In both cases, and indeed in each of the test cases not shown here against a logarithmic time scale, these jumps in strain occurred at the end of each sampling zone of 1, 10 and 100 seconds. It seems that after the command from the rheometer control logic to change sampling rates is executed there is either a spurious voltage or a logic trip-up which causes the platen to "forget" where it should be. Furthermore, before the end of the first sampling zone the rheometer control does not quite know where the platen should be. The reader will have to forgive this personification of a rheometer as I know of no other way to describe it.

To overcome this problem, it was decided for all succeeding tests to use only one sampling zone for the duration of each test. However, since each test lasted for 14,500 seconds and the rheometer only takes 512 samples in each zone this would result in a rather low sampling rate. This way, all of the short time data would be lost as the changes would be occurring far too fast. Therefore, the short time data was obtained through external data acquisition. The voltage signals directly from the servo and transducer were digitized for the first 150 seconds of each test and converted later to stress and strain. It was found that by using only one sampling zone no strain irregularities resulted, either at short or long time scales; however, the strain imposed by the motion of the bottom platen γ was never quite the commanded, or nominal strain γ_N. External data logging was performed at 1.024 KHz which corresponds to 512 samples in a 1 second zone, *i.e.* the fastest sampling rate of which the RMS hardware is capable.

Returning to Figure 6.1, we note first that strains of 1 and 4% (commanded) result in stress relaxation curves with familiar shapes, very similar to that in Figure 2.1 (b). However, each is levelling off with very long relaxation times. The curves do not quite have slopes of zero, but are very gradual. Commanded strains from γ=0.05% to γ=0.3% result in stress transients which go through a minimum and recover some stress gradually. Such behaviour is not seen in polymers which are homogeneous in their microstructure.

As stress is not a material property the data were plotted as relaxation modulus

$$G_r(t) = \frac{\sigma}{\gamma} \tag{6.1}$$

vs. time. The results for γ_N=1 and 4% are shown separate (Figure 6.4) from the γ_N=0.05 to 0.5% results (Figure 6.5) as the plot becomes quite confusing if they are all shown together.

Referring to Figure 6.4, the modulus resulting from a 1% commanded step strain is initially 2×10^5 Pa, relaxing to about 1.6×10^4 Pa after 14,500 seconds. The modulus at 4% commanded strain is initially higher than the 1% modulus being about 3.2×10^5, but relaxes to a level lower than that of the 1% modulus at long times. As these curves do not superimpose at any time it is clear that these are nonlinear viscoelastic responses. Both curves are still relaxing at the end of the test, although are concave upwards and so are levelling off. Whether they would reach a plateau if left long enough is unknown.

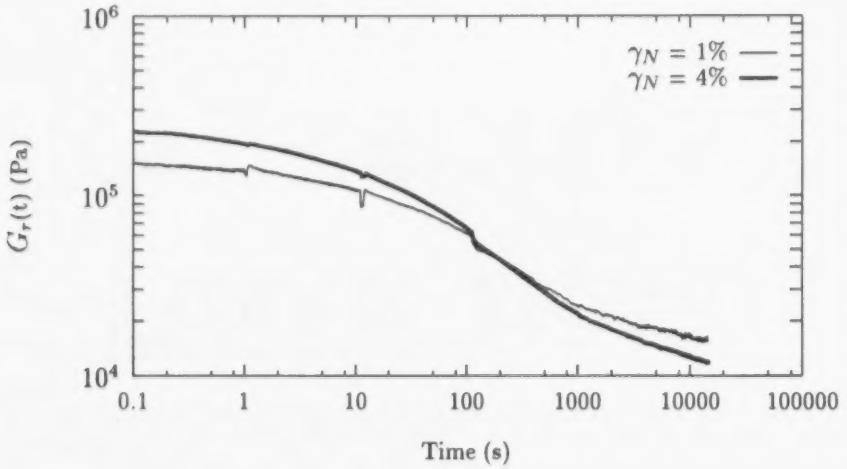

Figure 6.4: Relaxation modulus $G_r(t)$ for SBS1 at 90°C, γ_N = 1% and 4%.

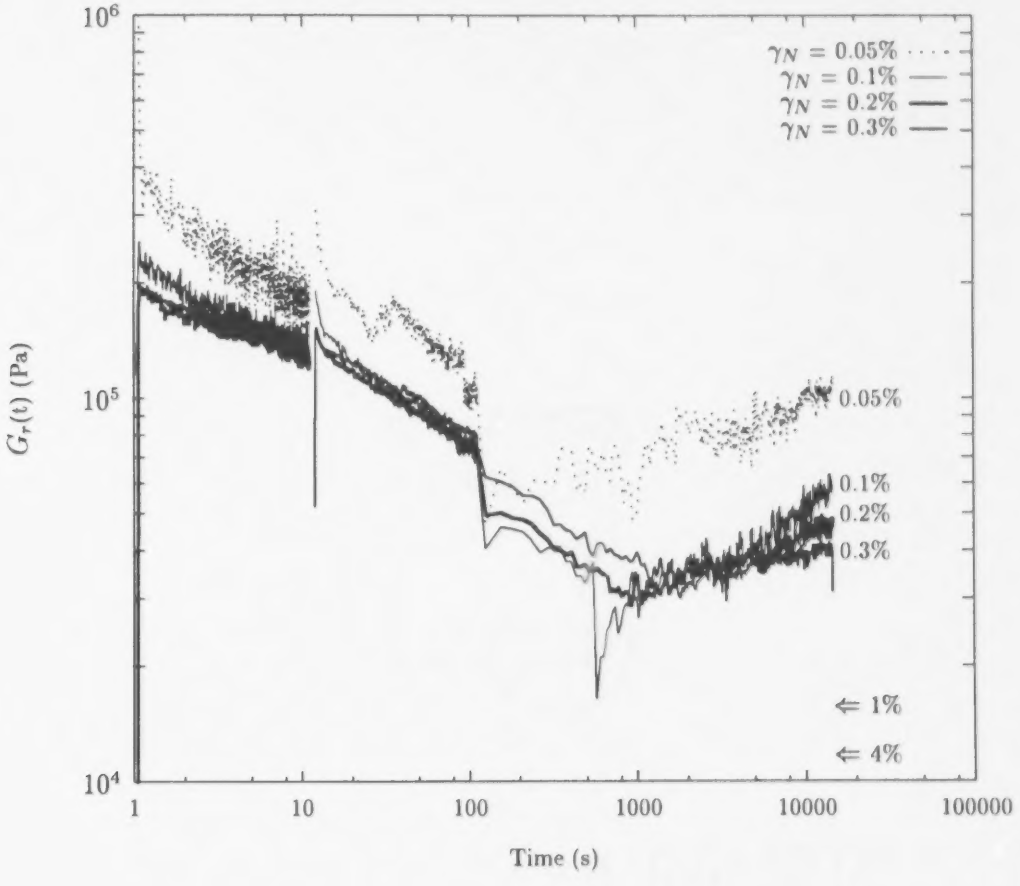

Figure 6.5: Relaxation modulus $G_r(t)$ for SBS1 at 90°C, γ_N = 0.05% to 0.3%.

The modulus as a function of time at lower strains is much different qualitatively. At γ_N=0.05% (Figure 6.5) the initial modulus is about 3.5×10^5 Pa which then relaxes to below 6×10^4 Pa at 100 seconds but then begins to recover, reaching 1×10^5 Pa by 14,500 seconds. The shapes of the curves for γ_N=0.1, 0.2 and 0.3% are very similar to γ_N=0.05%. However, there is a drastic drop in initial modulus from the γ_N=0.05% level. For γ_N=0.1% the initial modulus is about 2.2×10^5 Pa and for γ_N=0.2 and 0.3% is just under 2×10^5 Pa. From 2 to 10 seconds these curves are

practically coincident, but at long times the recovery is different. The final recovered modulus (where "final" means end-of-test, rather than indicating that some stable end state has been reached) is lower in each case for higher strains. The rate of stress recovery at 14,500 seconds as shown by the slope of the curve is also higher for lower strains. This may mean that the higher strains would eventually recover to the same level, but would take longer. The drop in final modulus from 0.05% to 1% commanded strain is much larger than from 0.1 to 0.2% although the proportional change in strain amplitude (a doubling of γ_N) is the same. The final moduli for γ_N=1 and 4% are indicated by the arrows on the same plot. The trend of lower final modulus for higher strains is followed.

At 100°C (Figure 6.6) a single sampling zone of 14,500 seconds was used as explained earlier. The relaxation modulus behaviour is qualitatively quite similar to that at 90°C. The modulus at γ_N=0.2% crosses over the modulus at 0.4% and the modulus at 0.1% crosses over the 1% modulus at short times (under 40 seconds). This indicates that the peak moduli were higher for lower strains. This is confirmed by the short time data collected externally and compiled in Table 6.2.

For γ_N=0.1% the modulus begins at 2.66×10^5 Pa, passing through a minimum below 1×10^4 and then recovering to over 6×10^4 by 14,500 seconds. The curve has not plateaued by this time, but a slight levelling off of the slope is observed. The modulus at γ_N=0.2% also passes through a minimum and then recovers, even seeming to reach a plateau at 6×10^3 seconds. The curve appears to drop again after this, however a slight "wave" is also observed in other curves such as γ_N=0.2% at 110°C (Figure 6.7) between 6×10^3 and 1×10^4 seconds, and this could explain the apparent drop. Furthermore, a foreshortened perspective of the curve will show that it levels off again after the drop. At γ_N=1% the modulus is levelling off to a plateau, although the curve does not reach a slope of zero on this time scale. The 4% curve begins relaxing with a concave upward curvature at short time scales and then turns downwards at longer times.

Figure 6.6: Relaxation modulus $G_r(t)$ for SBS1 at 100°C.

Table 6.2: Peak stress and modulus for SBS1.

Commanded Strain (%)	Peak Stress (Pa)	Peak Modulus (Pa)
Temperature Set Point = 100°C		
0.1	226	2.66×10^5
0.2	440	2.40×10^5
0.4	812	2.15×10^5
Temperature Set Point = 110°C		
0.2	393	1.99×10^5
0.4	670	1.75×10^5
4	>8000 (off scale)	$>2.08\times10^5$

Again the trend of lower final modulus with higher initial strain is followed, except in the case of 0.4% commanded strain. This curve is concave downwards and relaxing rapidly at long times, dropping well below the others. However, it should be noted from Table 6.1 that the sample gap for the test was anomalously small. The import of this will be discussed later.

At 110°C (Figure 6.7) the same trends in general are followed. From Table 6.2 the peak modulus at γ_N=0.2% is higher than that for γ_N=0.4%; however, the peak modulus for γ_N=4% is higher than either of the others. Short time data at 1% was unfortunately lost.

Relaxation moduli at γ_N=0.2, 0.4 and 1% pass through a minimum in each case and then recover. The final moduli at γ_N=0.2 and 0.4% are higher than that at γ_N=1%. However, at 0.4% the modulus is higher than at 0.2% commanded strain, contrary to the trend established at 90 and 100°C. At 4% commanded strain the curve is concave downwards and relaxing quickly at long time scales.

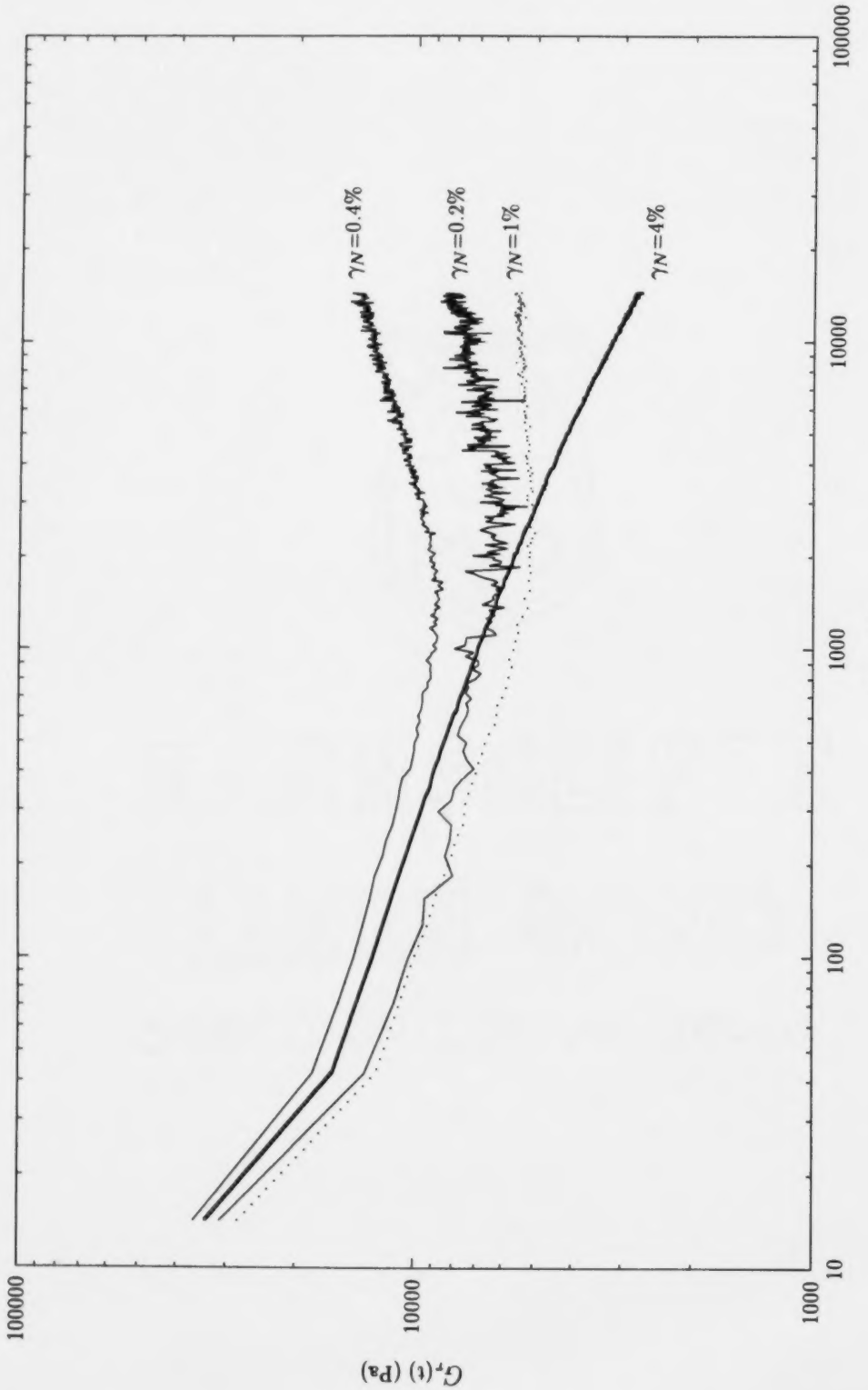

Figure 6.7: Relaxation modulus $G_r(t)$ for SBS1 at 110°C.

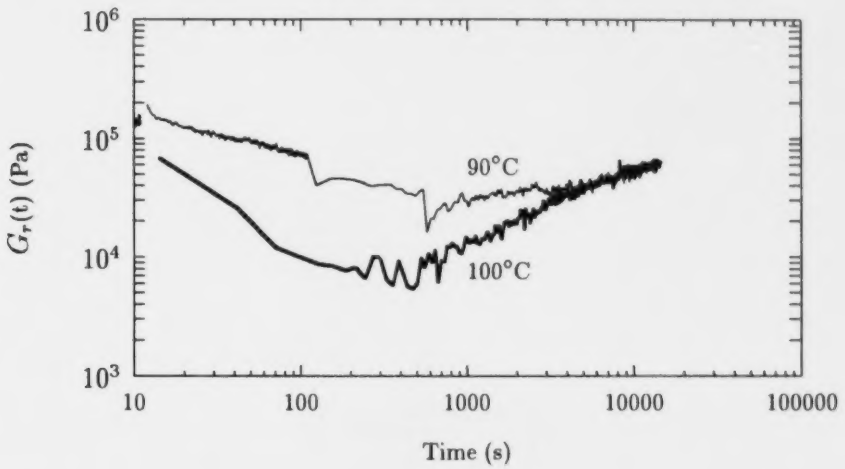

Figure 6.8: Temperature dependence of $G_r(t)$ for SBS1 at γ_N=0.1%.

Temperature Dependence

In Figure 6.8 $G_r(t)$ curves at 2 different temperatures are compared for SBS1 at constant γ_N=0.1%. With only a 10°C temperature variation there is a profound change in the relaxation behaviour. First it is noted that no amount of shifting along the time axis or the G_r axis will cause these two curves to superimpose, so that time-temperature superposition will not yield a single master curve. Both curves pass through a minimum, but the test at 90°C results in a minimum modulus roughly 3 times that at 100°C. While the 100°C curve does indicate more rapid initial relaxations, dropping to a lower modulus than that at 90°C, it also recovers more rapidly, the two curves becoming coincident from roughly 3500 seconds until the end of the test at 14,500 seconds.

For step strains of γ_N=0.2% the resulting $G_r(t)$ curves are compared at temperatures of 90°C, 100°C and 110°C in Figure 6.9. Again it is noted that no shifting along the time axis will yield a master curve, although the three *shapes* are quite similar. The drastic change in modulus over this narrow temperature range is

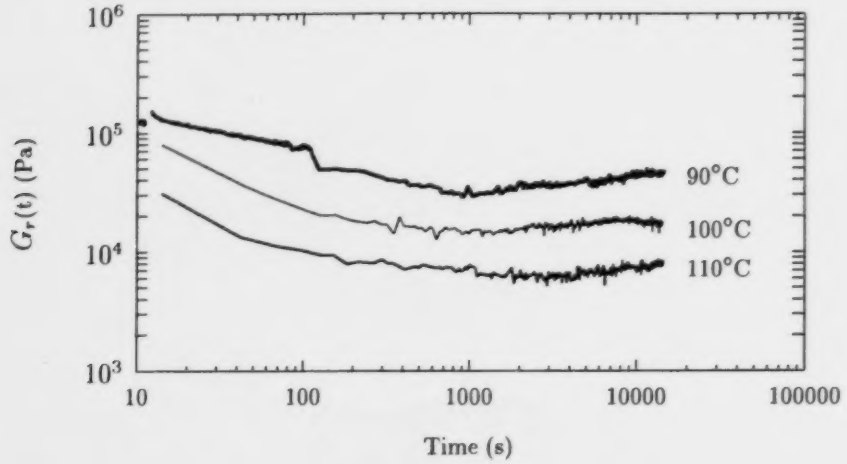

Figure 6.9: Temperature dependence of $G_r(t)$ for SBS1 at γ_N=0.2%.

again noted as the G_r values (at some fixed time) vary by a factor of 7.

Figure 6.10 shows the comparison of curves at the same three test temperatures but for γ_N=1%. At the end of the test the 90°C curve is still sloping downwards, the 100°C curve appears to have levelled out while the 110°C curve has begun to recover. At 110°C there should be greater molecular mobility resulting in more rapid relaxations, as well as recoveries.

When γ_N=4%, failure seems inevitable everywhere in this temperature bracket, as seen in Figure 6.11, which compares the $G_r(t)$ curves again at 90°C, 100°C and 110°C. Here we see for the first time curves which would come close to superimposing if shifted along the time axis. For example, the portion of the curve at 90°C between roughly 1200 s and 12000 s is parallel to the section between 100 s and 1000 s on the curve at 100°C, which in turn is parallel to the section of the curve at 110°C between 40 s and 400 s. In each case, the upswings in the curves proceeding to shorter times just preceding these sections are also close to parallel.

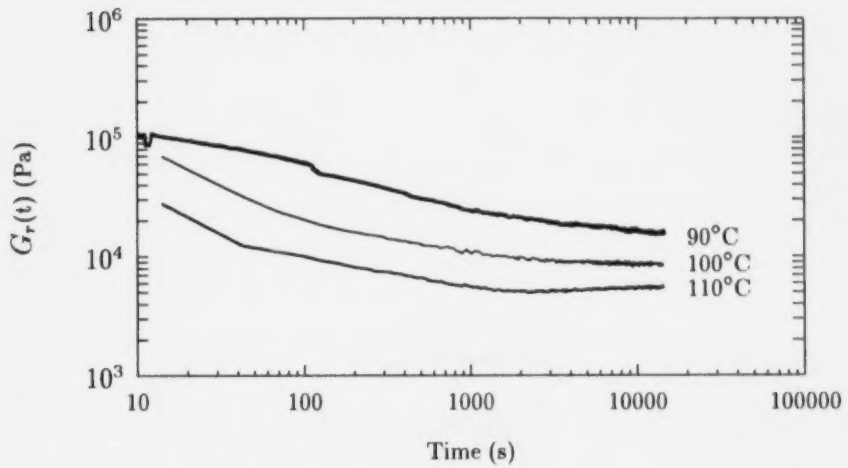

Figure 6.10: Temperature dependence of $G_r(t)$ for SBS1 at γ_N=1%.

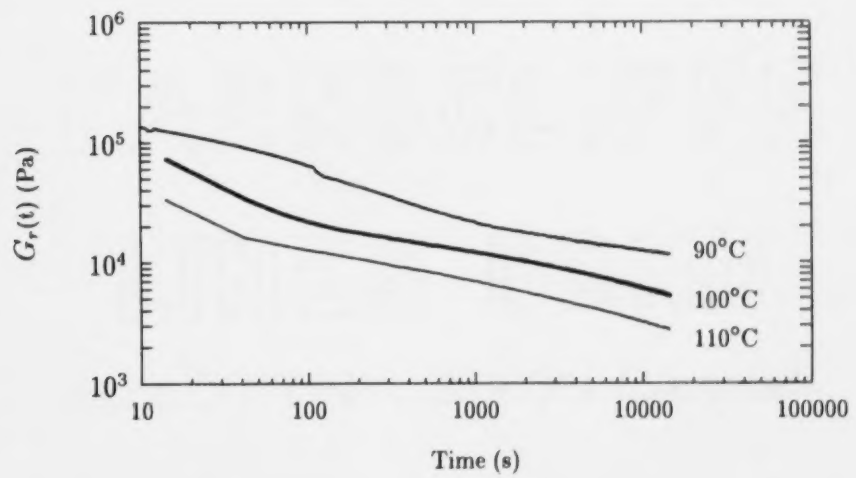

Figure 6.11: Temperature dependence of $G_r(t)$ for SBS1 at γ_N=4%.

Table 6.3: Conditions for step strain tests on SBS2.

Commanded Strain (%)	γ (actual, in %)	Gap (mm)	Temperature (±0.1°C)
0.1	0.080	1.823	110.5
0.2	0.185	1.905	110.6
0.4	0.382	1.928	110.6
0.4†	0.388	1.910	109.9
1†	0.955	1.881	109.7

†No external A/D used.

6.1.2 SBS2

For tests on SBS2 at 110°C, torque rather than stress, is plotted against time in Figures 6.12 through 6.16. Also, while initial torques were much higher, torque is only plotted between the limits of 2 and -2 g·cm as these are the manufacturer quoted limits of sensitivity of the transducer. Note that torques of less than 2 g·cm have been shown to be reliable measurements (see Appendix A), but for the moment we need not consider those arguments. True temperatures and strains, as opposed to set-points, are given in Table 6.3.

At γ_N=0.1 to 0.4% (Figures 6.12 to 6.14) the torque drops rapidly to zero and actually crosses over to a torque of opposite sign. The crossover at zero torque occurs at short times, being 200, 600 and 1100 seconds respectively for 0.1, 0.2 and 0.4% commanded strain. After crossing over to negative values the torque levels out to a constant value. That is, the noise in the data oscillates around a constant average. However, it was noticed on the strip chart record during one such test that when the external data logging ended there appeared to be a sudden drop in the signal as seen by a skip in the pen. Therefore, the test at 0.4% commanded strain was repeated without any external data acquisition. The result, in Figure 6.15, shows that torque drops rapidly after the initial step strain to zero and the

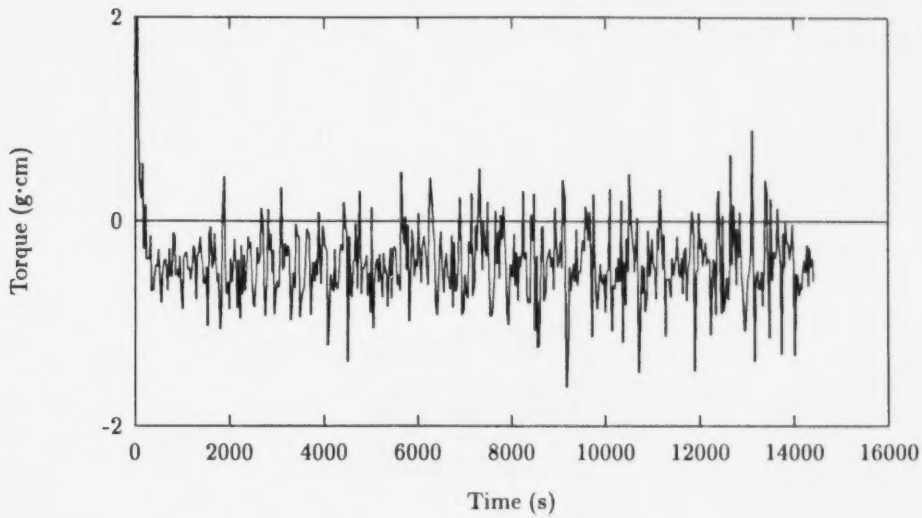

Figure 6.12: Torque relaxation for SBS2 at 110°C, γ_N = 0.1%.

noise oscillates around zero, remaining at that level. The same is true for a test at γ_N=1% (Figure 6.16) although the torque takes longer to relax to zero.

The external data logging system draws a current off of the same cable that supplies the internal signal. It appears that when the external data logging ends there is a spurious voltage which causes an electronic shift in the baseline. In tests on SBS1, torque did not drop off so rapidly and so was at a higher level when the external system shut off. Therefore, when the external data logging ended the shift in the baseline, which amounted to less than 1g·cm of torque or less than 4 Pa in stress, did not cause such a significant error.

Relaxation modulus as a function of time is plotted in Figure 6.17 for SBS2 at 110°C and γ_N=0.1 to 1%. For γ_N=0.1% and 0.2% external data logging had been used as discussed above, but not for γ_N=0.4% and 1%. Curves superimpose closely for the 0.4% and 1% cases, while the others follow closely within the bounds of the noise. All four curves display a near-linear decrease through the entire time range.

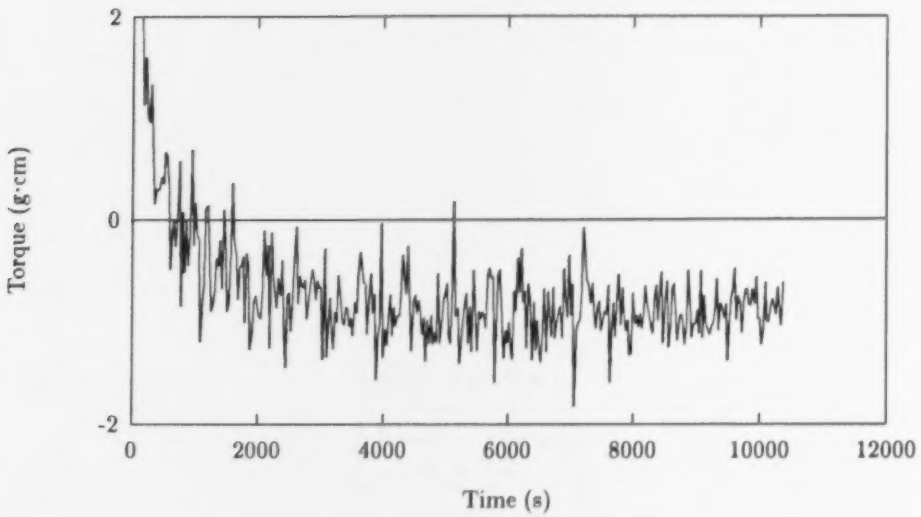

Figure 6.13: Torque relaxation for SBS2 at 110°C, $\gamma_N = 0.2\%$.

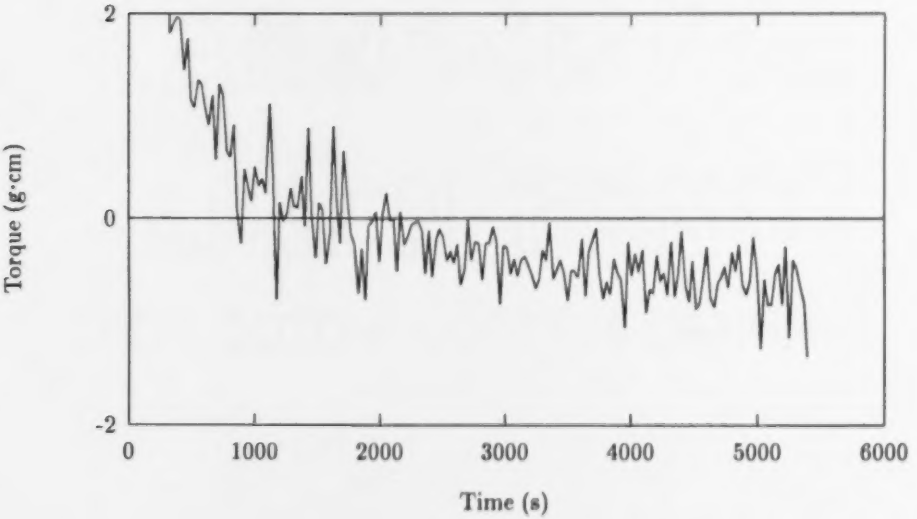

Figure 6.14: Torque relaxation for SBS2 at 110°C, $\gamma_N = 0.4\%$.

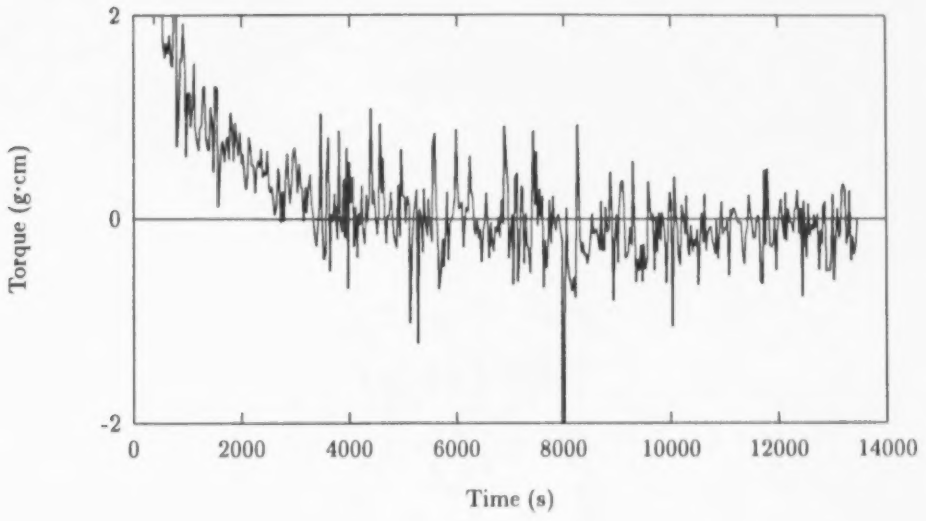

Figure 6.15: Torque relaxation for SBS2 at 110°C, $\gamma_N = 0.4\%$; no external data logging.

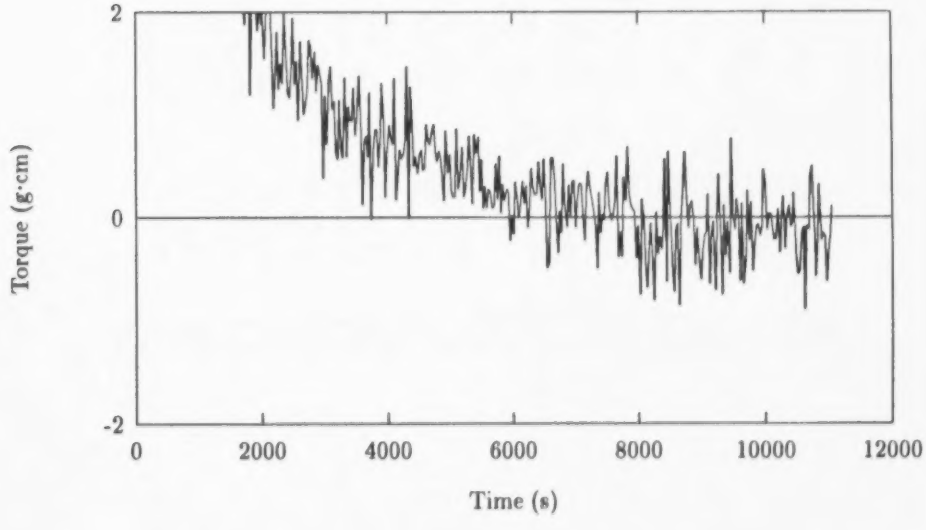

Figure 6.16: Torque relaxation for SBS2 at 110°C, $\gamma_N = 1\%$; no external data logging.

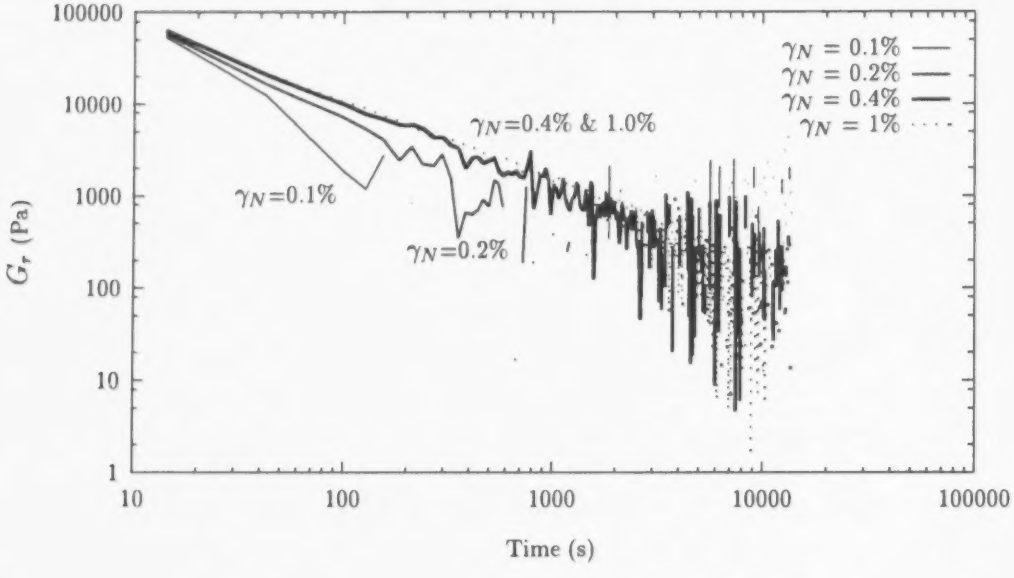

Figure 6.17: Relaxation modulus G_r(t) for SBS2 at 110°C.

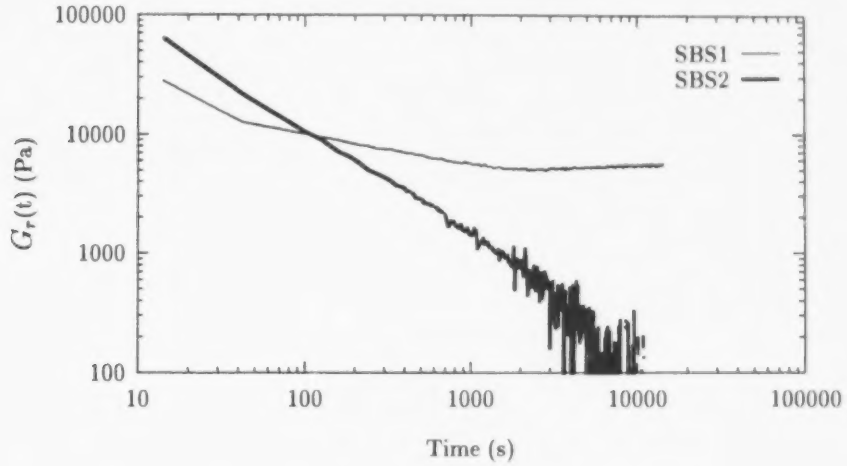

Figure 6.18: Relaxation modulus $G_r(t)$ comparison for SBS1 and SBS2 at 110°C, $\gamma_N = 1\%$.

Table 6.4: Peak stress and modulus for SBS2.

Commanded Strain (%)	Peak Stress (Pa)	Peak Modulus (Pa)
0.1	227	2.84×10^5
0.2	462	2.50×10^5
0.4	920	2.41×10^5

In Figure 6.18 the modulus of SBS2 is compared to that of SBS1 over the entire time range at γ_N=1% and 110°C. The modulus of SBS2 begins higher than that of SBS1 but rapidly drops below SBS1 in a straight-line fashion. Short-time data collected externally for γ_N=0.1 to 0.4% are compiled for SBS2 in Table 6.4 and it can be seen by comparison with Table 6.2 that the peak moduli for SBS2 are indeed higher than for SBS1 at each strain amplitude at the same temperature.

SBS2 could not be tested at temperatures below 110°C and SBS1 could not be tested at temperatures lower than 90°C. The reason for this lies in the ability of the

force rebalance transducer to balance itself. As the platens are more solidly coupled the transducer must work harder to rebalance itself. At a certain point a humming or buzzing can be heard from the transducer as it rapidly and repeatedly rezeros. This does not mean that torque measurements are any less accurate, but this buzzing introduces noise into the signal and the transducer is eventually burned out if it is operated in this condition for long. As SBS2 has a higher styrene content than SBS1 its network is more pervasive (barring any deformation) at low temperatures than that of SBS1, making it more solid. Hence the lowest practical operating temperature is higher for SBS2 than SBS1. The same problem is encountered [75] when testing polyethylenes in the vicinity of the crystalline melting point. Relaxation data were not collected at $T > 110°C$ because a broader T range could not be studied within the time scale of an M.Sc. research program.

6.1.3 SIS

Stress relaxation tests on SIS were performed at 90 and 110°C. Temperatures and strain amplitudes quoted in text or figures are nominal or commanded values while actual values are given in Table 6.5.

At 110°C (Figure 6.19), relaxation moduli at all strains tested superimpose closely at times between 15 seconds and 100-200 seconds. At roughly 200 seconds a classification is seen with higher strains relaxing to lower moduli. The modulus at γ_N=0.1% levels out and then recovers slightly before the end of the test at 8×10^3 seconds. At 0.2% commanded strain the curve levels to a plateau, while at 0.4, 1 and 4% the curves are still relaxing at the end of the test, each successively more steep than the next lowest strain. However, the curve at γ_N=0.4% is concave upwards and perhaps approaching a plateau at the end of the test while the other two are concave downwards. Peak moduli, from data collected externally which is compiled in Table 6.6, show the now familiar trend of decreasing values with increasing strain.

Table 6.5: Conditions for step strain tests on SIS.

Commanded Strain (%)	γ (actual, in %)	Gap (mm)	Temperature ($\pm$0.1°C)
Temperature Set Point = 90°C			
0.1	0.097	1.949	90.5
0.2	0.186	1.894	90.3
0.4	0.374	1.975	90.9
1	0.967	1.990	90.5
4	3.85	1.967	90.4
Temperature Set Point = 110°C			
0.1	0.090	1.978	110.5
0.2	0.183	1.980	109.9
0.4	0.378	2.031	110.5
1	0.950	1.975	110.5
4	3.83	1.982	110.3

Table 6.6: Peak stress and modulus and final torque for SIS.

Commanded Strain (%)	Peak Stress (Pa)	Peak Modulus (Pa)	Final Torque (g·cm)
Temperature Set Point = 90°C			
0.1	207	2.13×10^5	0.125
0.2	368	1.98×10^5	1.38
0.4	706	1.89×10^5	1
1	1764	1.82×10^5	5
4	7090	1.84×10^5	15.6
Temperature Set Point = 110°C			
0.1	174	1.93×10^5	0.3
0.2	319	1.74×10^5	0.35
0.4	635	1.68×10^5	0.38
1	1550	1.63×10^5	0.43
4	6387	1.67×10^5	0.5

The exception is the peak modulus at γ_N=4% which is slightly higher than that at 1% commanded strain.

The final (end-of-test) moduli in each case correspond to torques that are below the manufacturer-quoted range of the transducer. They are given in Table 6.6 and range from -0.3 to -0.5 g·cm. A calibration was done to determine the reliability of such torque measurements. This is fully explained in Appendix A. The trend in these torque values is consistent, going to increasing final torque with increasing strain amplitude.

At 90°C the relaxation behaviour does not follow the established patterns. Figure 6.20 shows that the curves again superimpose quite closely at short times. However, Table 6.6 shows that the peak moduli do decrease with increasing strain amplitude,

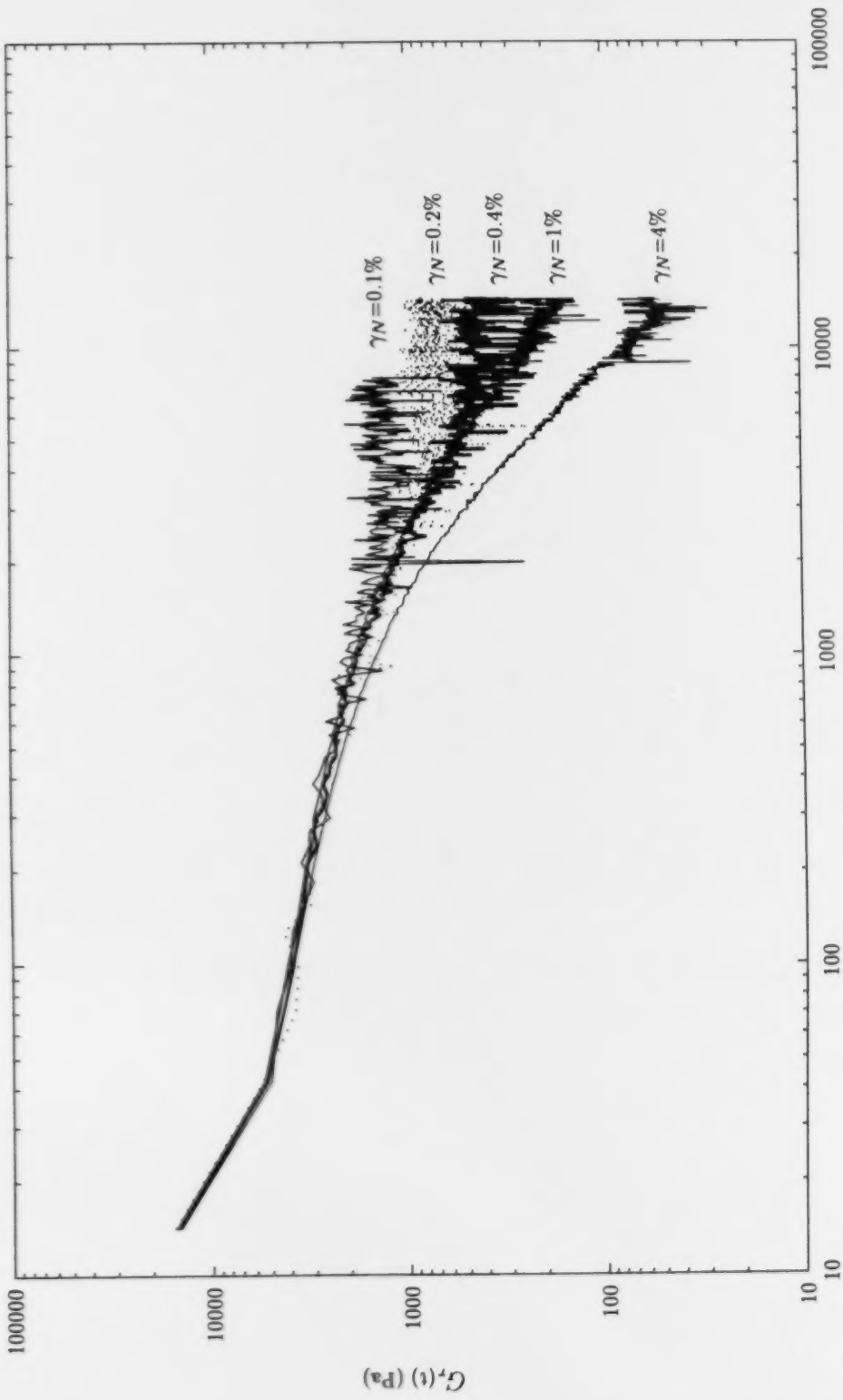

Figure 6.19: Relaxation modulus $G_r(t)$ for SIS at 110°C, $\gamma_N^o = 0.1\%$ to 4%.

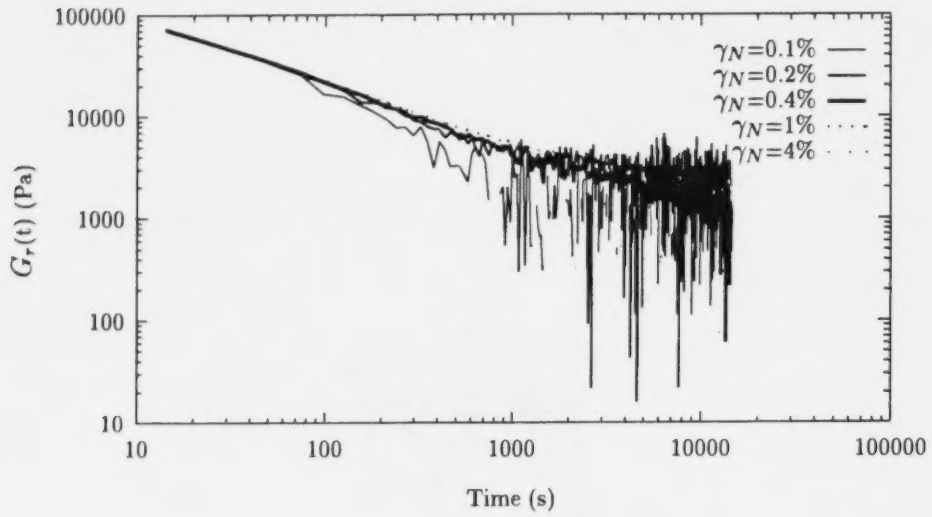

Figure 6.20: Relaxation modulus $G_r(t)$ for SIS at 90°C, γ_N = 0.1% to 4%.

except for that at 4% commanded strain which is anomalously higher than that at γ_N=1%.

The data are rather hard to interpret with all of the curves on the same plot as they are all so close together, even at long time scales. Therefore, γ_N=0.1 and 0.2% are plotted together in Figure 6.21 and γ_N=0.4, 1 and 4% are plotted together in Figure 6.22.

The torque levels at the final time of the test were again below the manufacturer quoted range of sensitivity for tests at 0.1 to 0.4% strain and are compiled in Table 6.6. However, torque did increase steadily with strain.

The final moduli at 90°C are compiled in Table 6.7. In order of magnitude from least to greatest they are: 0.4, 0.1, 4, 1 and 0.2% commanded strain. This does not follow the pattern of lower final modulus for higher strain. Comparing these to the actual test temperatures in Table 6.5 it can be seen that tests at 1 and 0.2% commanded strain had the lowest temperature (90.2°C) and the highest modulus,

Table 6.7: Final modulus for SIS at 90°C.

Commanded Strain (%)	$G_r(1.45\times10^4$ s) (Pa)
0.1	1200
0.2	3000
0.4	1100
1	2000
4	1750

while the test at γ_N=0.4% had the highest temperature (90.9°C) and the lowest modulus. Temperatures only varied by a fraction of a degree, but the trend seen in final modulus is consistent with temperature variations. These curves might in fact have superimposed if tested at exactly the same temperature.

6.1.4 SBS3 and SEBS

An attempt was made to load both SBS3 and SEBS into the rheometer. Problems were encountered in trying to achieve good contact over the entire surface of the upper platen. This was because the relaxation times for these polymers were so long that they would not relax in a reasonable time, even at 300°C. Therefore, the normal procedure of closing the gap by lowering the upper platen and squeezing out the sample could not be used. Note that both of these samples had very high predicted separation temperatures as seen in Table 5.1.

6.2 Step Rate Tests

In these tests, the operational mode titled "steady transient", which is also known as the "step rate" mode was used to perform step strain tests wherein the

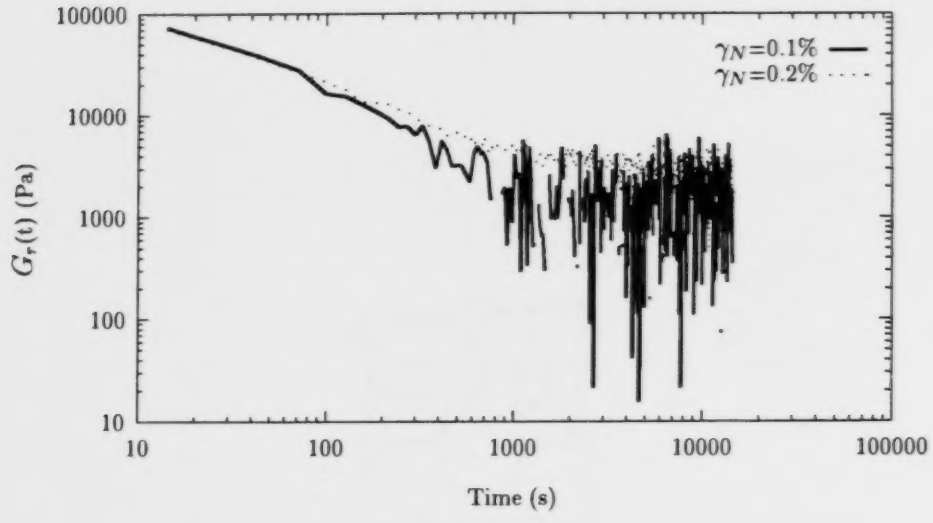

Figure 6.21: Relaxation modulus $G_r(t)$ for SIS at 90°C, γ_N = 0.1% to 0.2%.

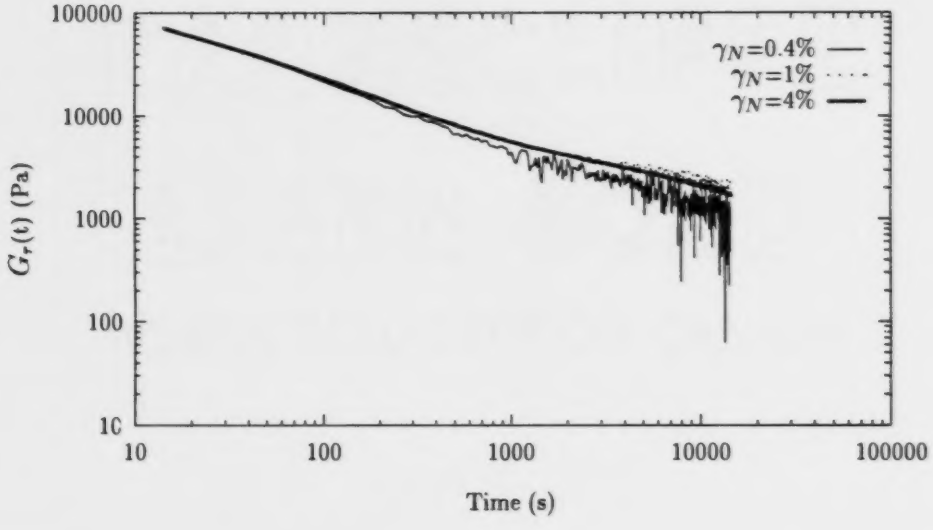

Figure 6.22: Relaxation modulus $G_r(t)$ for SIS at 90°C, γ_N = 0.4% to 4%.

transient occurred at a low rate. Only SBS1 was tested in this mode, and only at 90°C. The shear rate zones were programmed to displace the platen in the clockwise direction at 1×10^{-4} rad/s until the desired strain amplitude was achieved. Following this a zero shear rate zone was programmed in order to keep the platen at a fixed angular displacement for 1 hour. Finally, a rotation in the counterclockwise direction at 1×10^{-4} rad/s was used to return the platen to the zero position.

In steady mode, strain is not a measurable signal and so it is not possible to know for certain if the platen did move exactly as programmed. Therefore, quoted strain values are nominal values only and modulus could not be calculated. The data are plotted against linear time in Figure 6.23 and against a logarithmic time scale in Figure 6.24. From the logarithmic plots, unexpected jumps are seen in the stress at short times. The times of these jumps correspond to the end of the first shear rate zone. This seems to indicate that the platen did not hold the programmed position at the end of the first zone, but rather "skipped" to a higher strain than programmed. For this reason, only a qualitative discussion of this data will be given.

At 1% nominal strain there is a sudden drop in the stress at about 900 seconds. It is suspected that this was caused by some voltage irregularity on the circuit that powers the rheometer. This kind of drop has been seen when a computer in the same laboratory was turned off, although plugged into a different power bar than the rheometer, which should therefore have been a different circuit.

At nominal strains of 0.1%, 0.25% and 1% the stress relaxes from a maximum and then begins to rebound. The stress for a 0.25% strain drops below that for a 0.1% strain and then rebounds to a higher level, crossing over the second time at about 600 s. Stress relaxation data at 3 and 5% nominal strains display some sort of stress wave, the earlier cycles of which have a shorter wavelength and higher amplitude than subsequent cycles.

The 10% strain test was aborted at roughly 1600 seconds due to the oddity observed at about 1250 seconds, which may also have been a voltage irregularity

causing a fluctuation in platen position. The 10% response is qualitatively different from those at lower strains. However, the relaxation is not quite exponential. There appears to be a deviation from exponential behaviour between about 250 and 500 seconds.

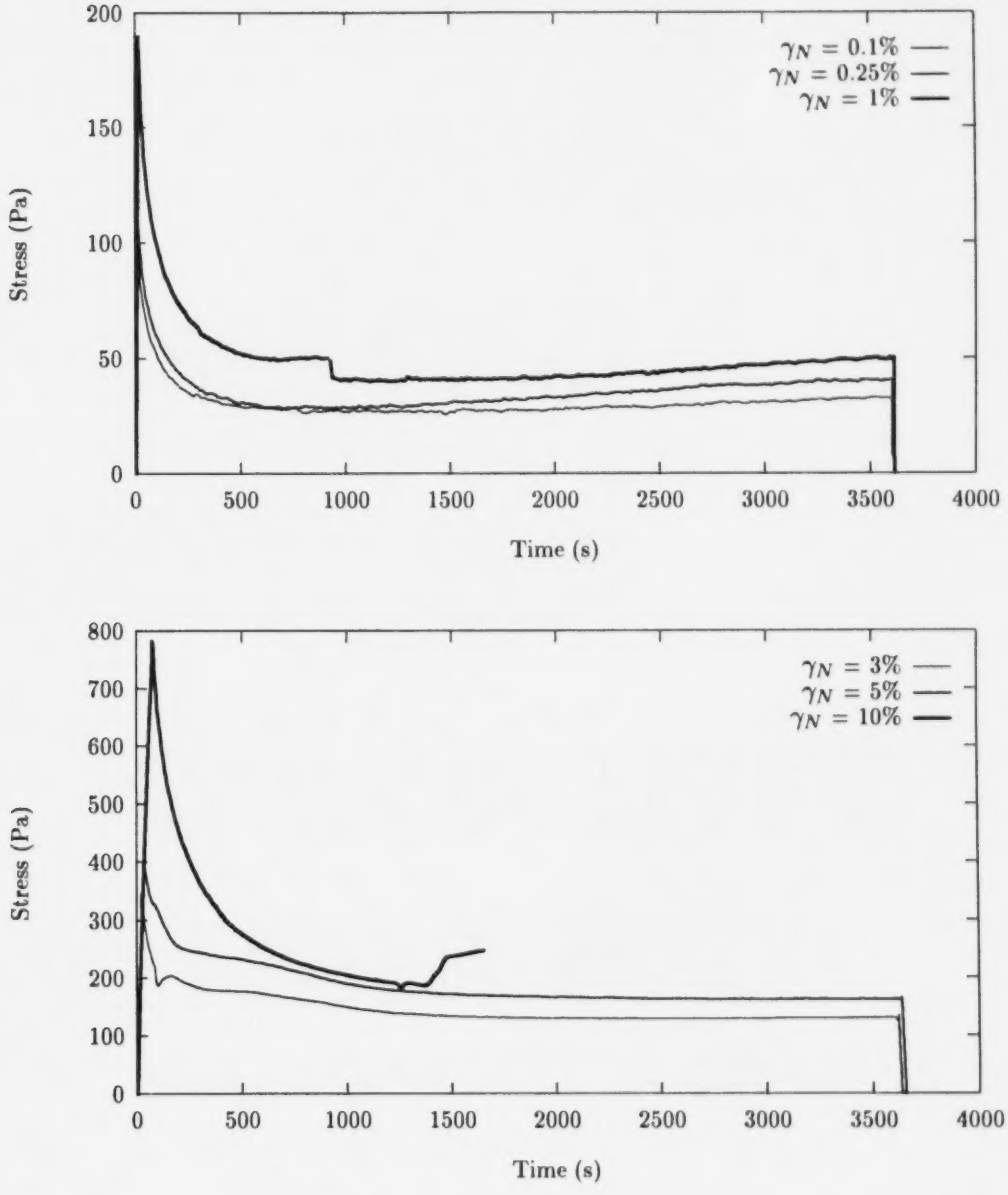

Figure 6.23: Stress relaxation for SBS1 at 90°C after step strains at 1×10^{-4} rad/s *vs.* linear time.

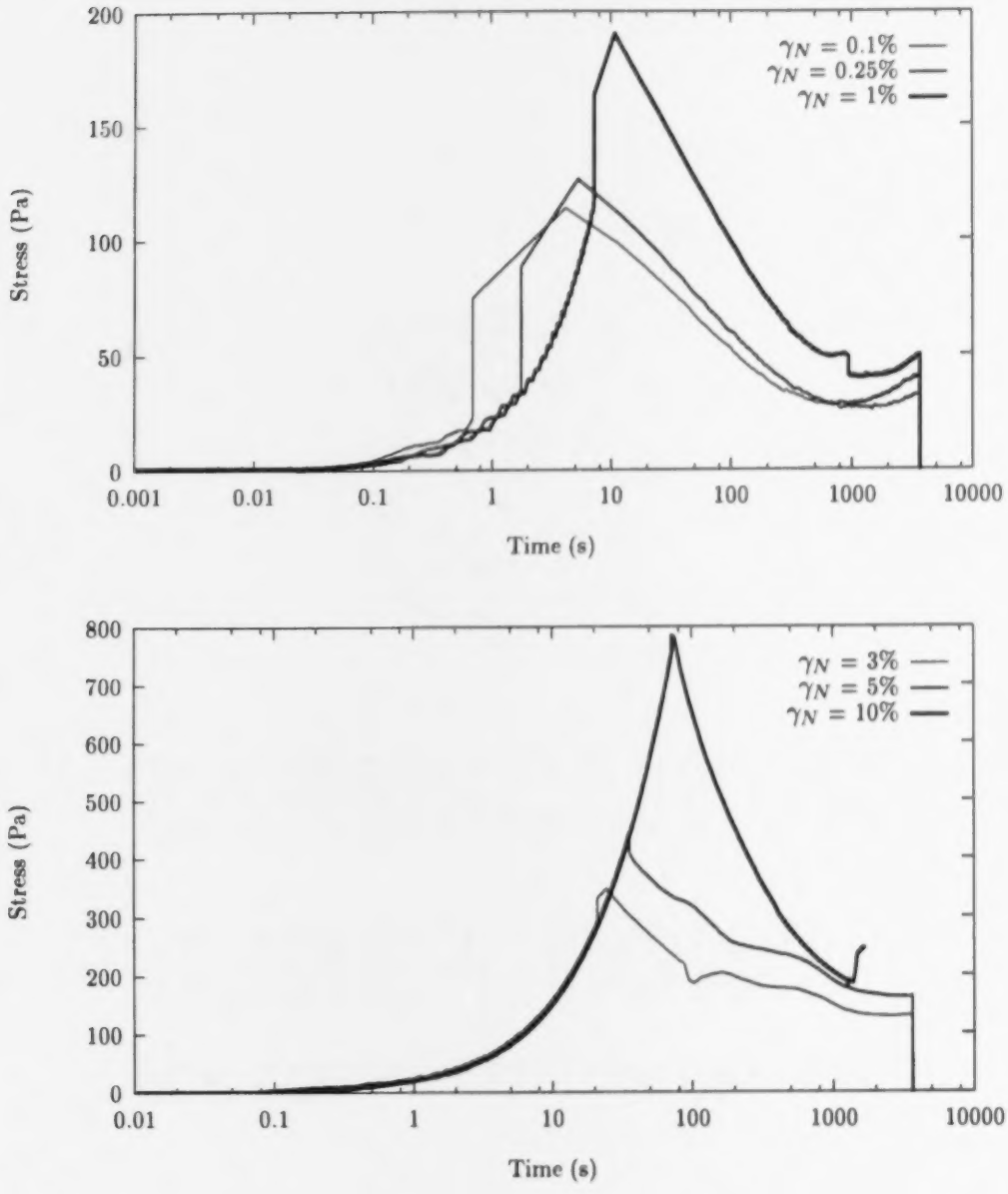

Figure 6.24: Stress relaxation for SBS1 at 90°C after step strains at 1×10^{-4} rad/s *vs.* logarithmic time.

Chapter 7

Results 2; Nonlinear Waveforms

In this chapter results from dynamic strain experiments are presented. The discussion of their meaning and significance is again deferred to a later chapter.

7.1 Strain Sweep

A strain sweep at 30°C and 1 rad/s was performed on SBS4. The results are shown in Figure 7.1. What is immediately obvious is that there is no range of linear viscoelasticity. The complex viscosity drops slightly from γ° =0.02% to 0.1%, followed by a more gradual downward slope from 0.1 to 1%. At 1% there is an abrupt change to a rather large negative slope. The onset of this drop I have termed the "crisis point" (γ_{cr}). It was found that above the crisis point the stress response is no longer sinusoidal, though the strain input is. All data points shown here are calculated values, derived by the computer fitting a sinusoidal function to the signals from the servo and transducer with a proprietary software package. Above γ_{cr} these numbers represent the computer's attempt to fit a sinusoid to data which are essentially non-sinusoidal. Therefore, these values cannot be trusted in any absolute sense.

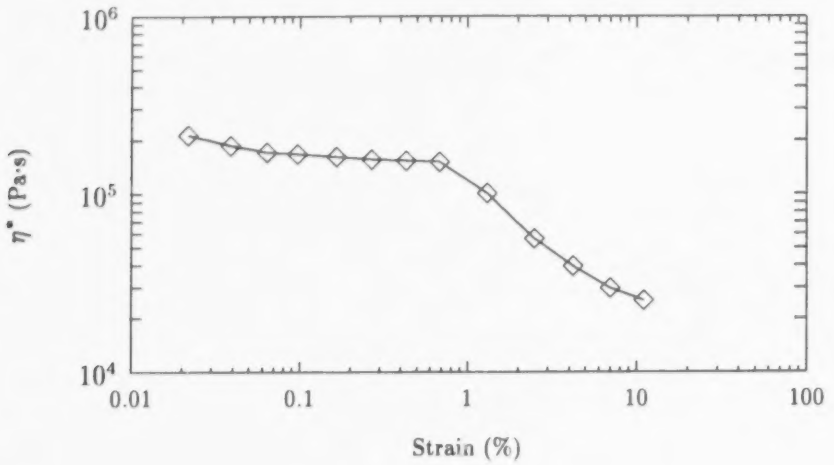

Figure 7.1: Strain sweep on SBS4, at 30°C and ω=1 rad/s.

In Figure 7.2 the same kind of behaviour is seen with SBS1 under the same conditions of temperature and frequency. The γ_{cr} is lower for SBS1, which has a slightly higher ϕ_S and lower overall MW. These data are insufficient to pinpoint γ_{cr} accurately; however, at γ^o =0.75% the response is non-sinusoidal and at γ^o =0.1 it is sinusoidal, and by extrapolation the data strongly suggest $0.1 < \gamma_{cr} < 0.2$ at this temperature.

7.2 Frequency/Temperature Sweep

SBS1 was tested in two frequency/temperature sweeps using the convection oven with nitrogen as the convection heating gas. The temperature was varied between 150°C and 221°C while the frequency was varied from 0.1 to 100 rad/s. A commanded strain amplitude of 0.5% was chosen; however, the actual strain amplitude γ^owhich the rheometer executes is not always the commanded, or nominal amplitude γ_N^o . Table 7.1 gives γ^o at each temperature and frequencies of 0.1, 1, 10 and 100 rad/s for γ_N^o =0.5. Note that data in Figures 7.1 and 7.2 are plotted against

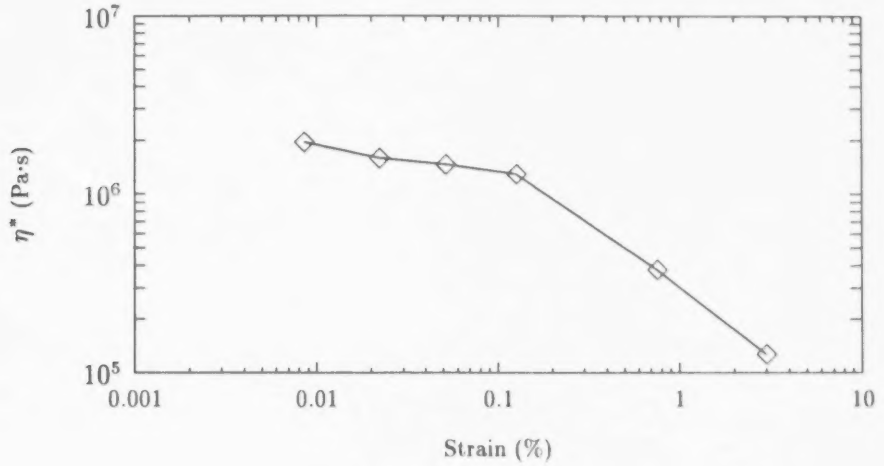

Figure 7.2: Strain sweep on SBS1, at 30°C and ω=1 rad/s.

actual strain amplitude. From Table 7.1 γ° at γ_N° =0.5% never exceeded 0.45%.

Figure 7.3 and 7.4 display η' and η'' respectively for the sweep at γ_N° =0.5%. At 150°C and higher the curves of both η' and η'' increase with decreasing frequency in the manner of the curve in Figure 2.9 for $\omega \leq 10$ rad/s. Above 10 rad/s the curves turn concave downwards at $T \leq$191.2°C for η' and $T \leq$170°C for η''. For both η' and η'' the curves at 211°C and 221°C are almost coincident.

7.3 Waveforms

Over a range of frequencies, strain amplitudes and temperatures, the servo (angular) displacement and torque were digitized directly using external data logging. This was performed only with SBS1. The same sample was used for the entire test series. Because these structured materials are in general sensitive to their shear history, the run number corresponding to the order in which it was performed is given in the caption of each figure. The RMS software automatically

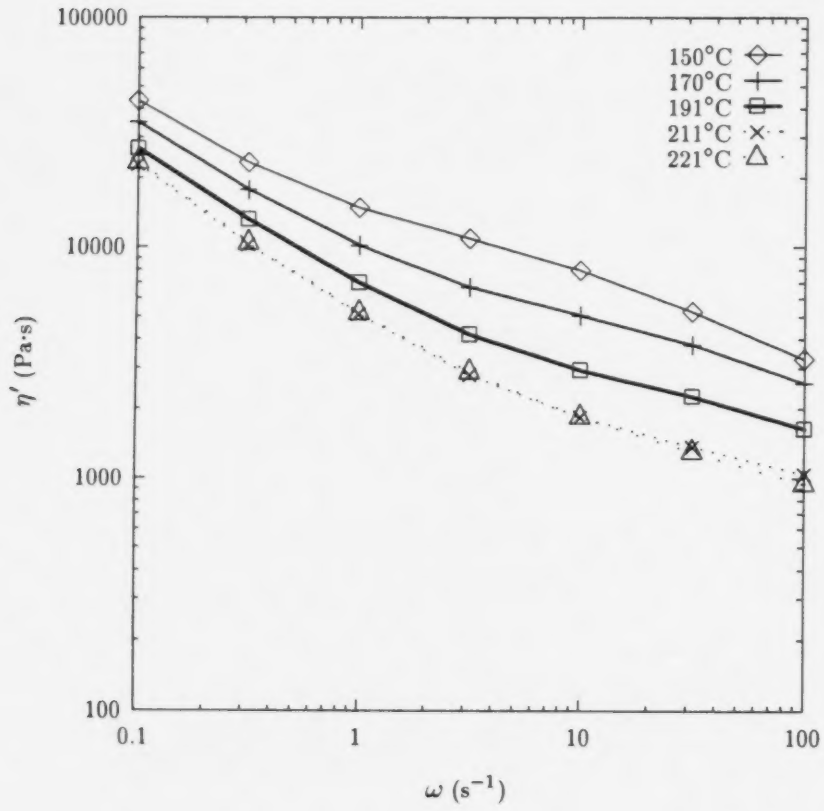

Figure 7.3: Dynamic viscosity frequency/temperature sweep on SBS1 γ_N° =0.5%.

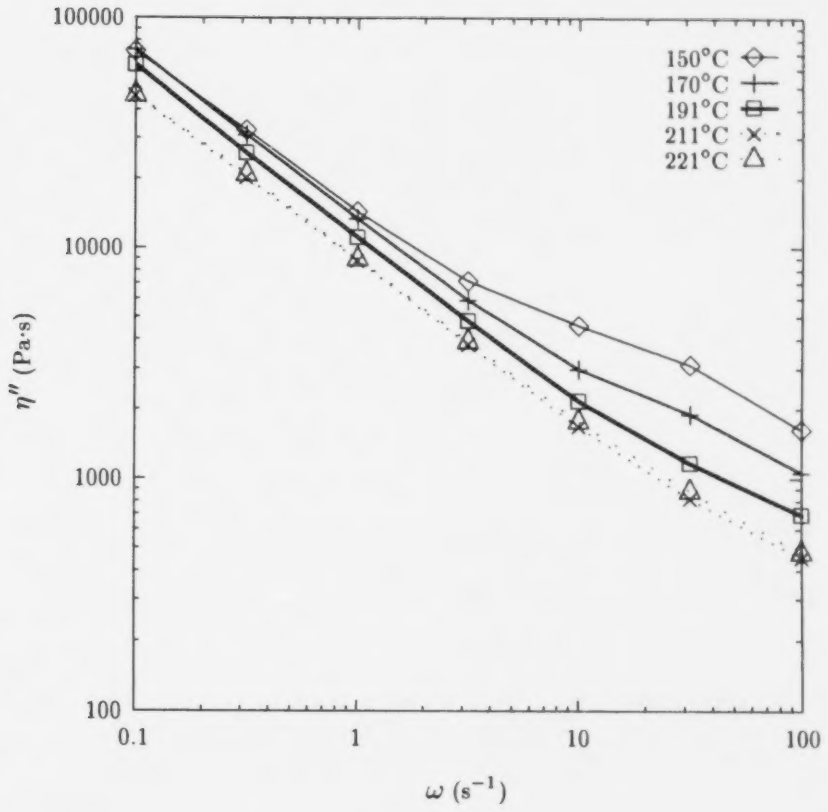

Figure 7.4: η'' frequency/temperature sweep on SBS1, γ_N° =0.5%.

Table 7.1: Actual γ° *vs.* nominal γ_N° for frequency/temperature sweep on SBS1.

$\gamma_N^\circ = 0.5\%$				
T(°C)	γ° (%)			
	ω=0.1	1	10	100 rad/s
150	0.44	0.42	0.35	0.14
170.8	0.44	0.42	0.38	0.17
191.2	0.44	0.43	0.41	0.23
211.4	0.45	0.44	0.42	0.29
221.5	0.45	0.44	0.42	0.30

zeros the signal so that curves oscillate around zero, whereas the external data logging does not. This is the reason why the curves do not oscillate around zero stress. Furthermore, in bypassing the manufacturers data aquisition and analysis system to obtain waveforms externally (it is not possible to obtain them with the internal data collection system) a phase shift was introduced in the curves. In each run, the strain lags (or else the stress leads) by an undetermined amount from their true phase. This is particularly evident with those curves which are sinusoidal, *eg.* Figure 7.20, where the stress peak *precedes* the strain peak. If this phase shift were real, then the physical interpretation would be that the fluid is predicting the deformation which it is about to experience. This is clearly not possible. However, none of the conclusions of this work depend on the phase of the waves, but only their shapes, so that this shift of unknown magnitude does not introduce interpretational difficulties. In many of these curves the first peak or trough is slightly different than those that follow. This is the transient at the beginning of the run in the first cycle.

Referring first to Figure 7.5, a test performed at 25.6°C, ω=1 rad/s and γ°=2%, it is immediately obvious that the stress response is not sinusoidal through the entire stress regime. In the mid-stress regime the curve is sinusoidal, but as the

stress builds a "bite" occurs in the curve beginning at about 1000 Pa. As the stress drops off on the far side of each peak the response is again sinusoidal. The curve is not symmetric in the peaks and troughs, although a similar bite can be seen in the troughs as well. Peaks are very reproducible in shape. This is demonstrated in Figures 7.6 and 7.7 where the same run is plotted from 30 to 45 seconds and 50 to 65 seconds. The troughs are less reproducible. At frequencies of 10 and 0.01 rad/s (Figures 7.9 and 7.10), at the same temperature and γ°, wave forms appear sinusoidal, while at ω=0.1 (Figure 7.8) the patterns are very similar to those at ω=1 rad/s.

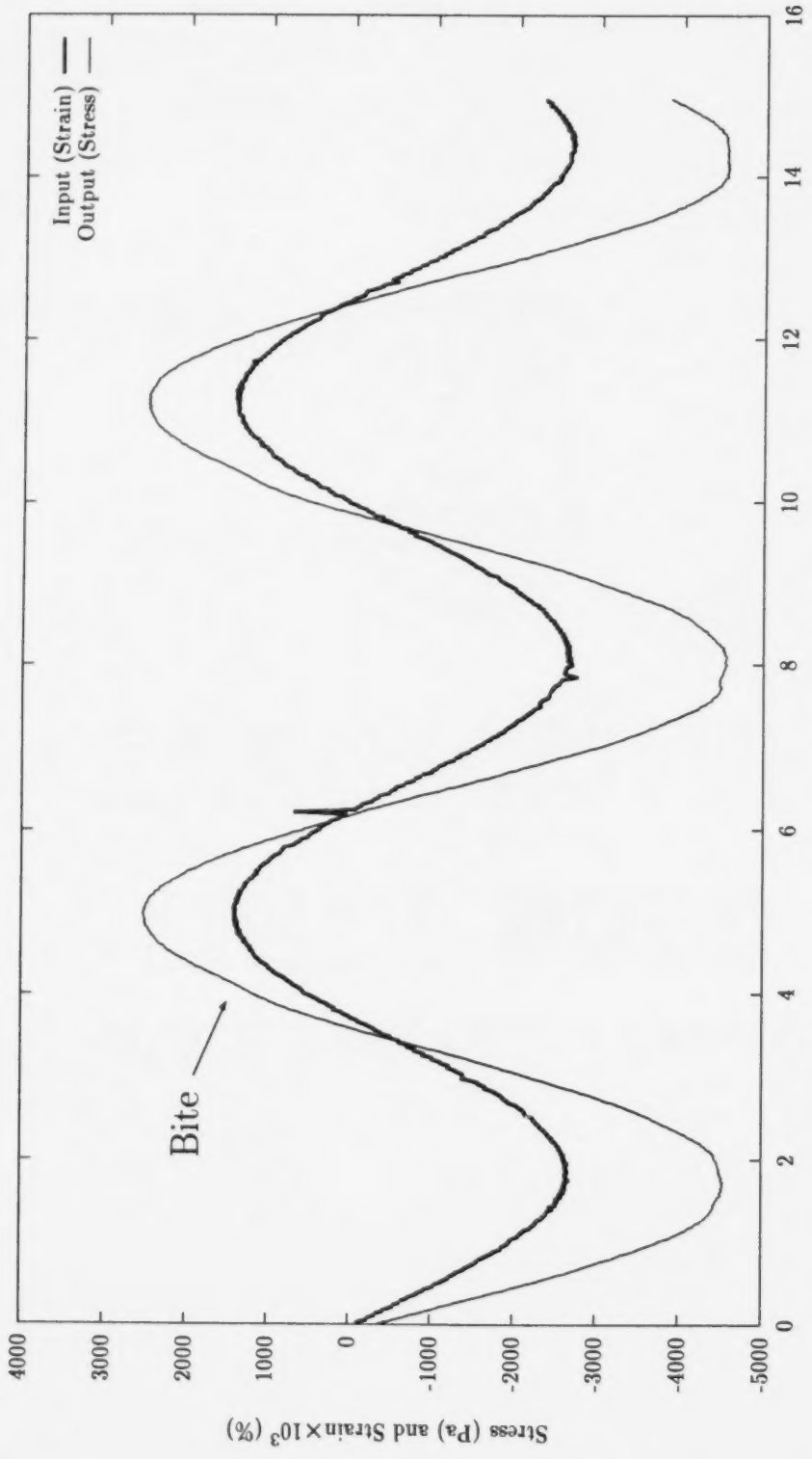

Figure 7.5: Run 2: Dynamic stress response of SBS1 at 25.6°C; $\gamma_N^\circ = \gamma^\circ = 2\%$, ω=1 rad/s.

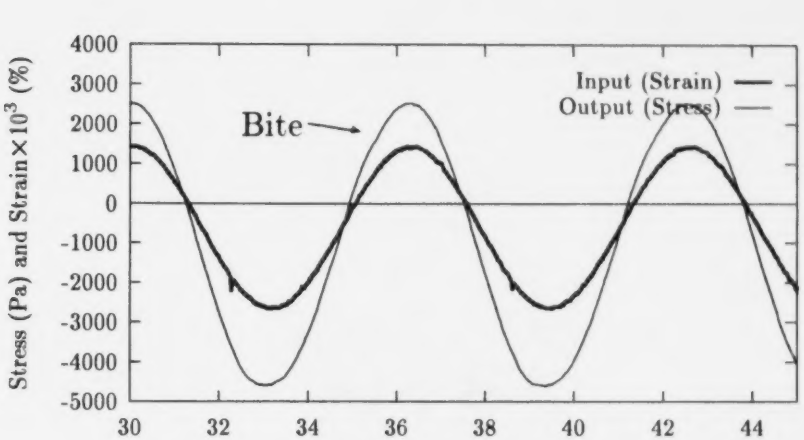

Figure 7.6: Run 2: Dynamic stress response of SBS1 at 25.6°C; $\gamma_N^\circ = \gamma^\circ = 2\%$, ω=1 rad/s from 30 to 45 seconds.

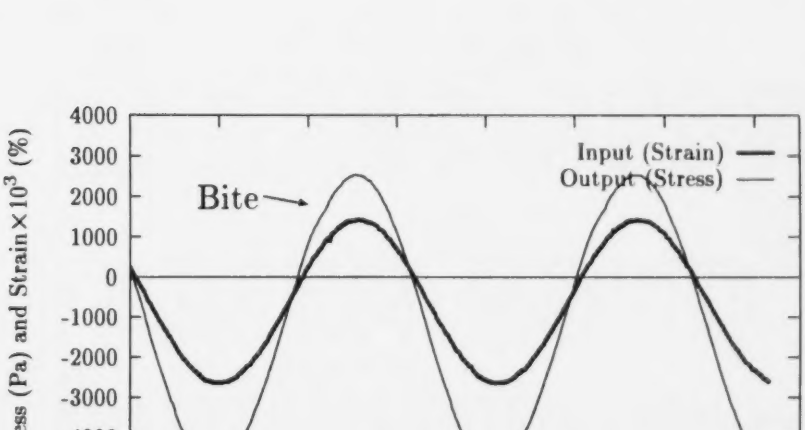

Figure 7.7: Run 2: Dynamic stress response of SBS1 at 25.6°C; $\gamma_N^\circ = \gamma^\circ = 2\%$, ω=1 rad/s from 50 to 65 seconds.

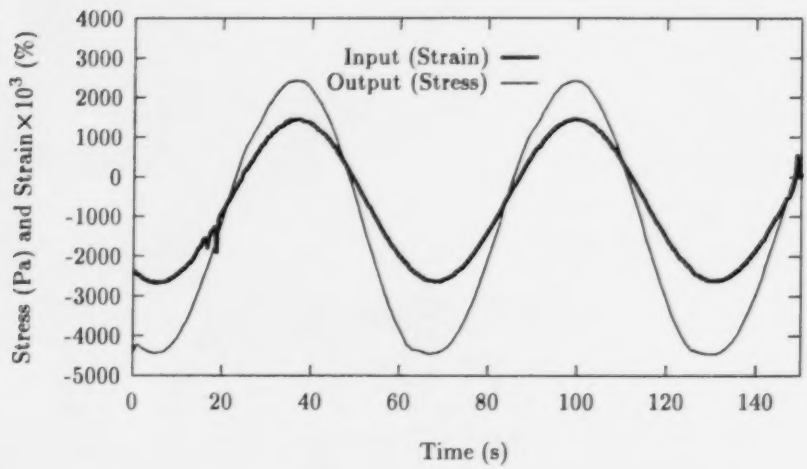

Figure 7.8: Run 1: Dynamic stress response of SBS1 at 25.6°C; $\gamma_N^\circ = \gamma^\circ = 2\%$, ω=0.1 rad/s.

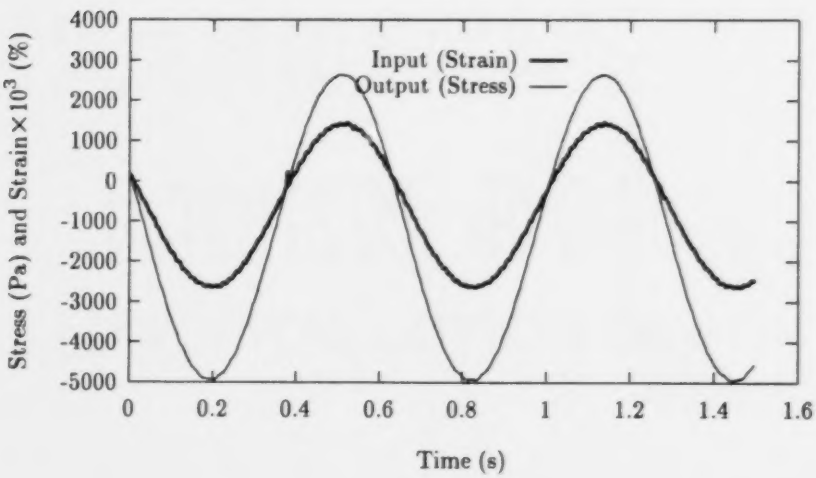

Figure 7.9: Run 3: Dynamic stress response of SBS1 at 25.6°C; $\gamma_N^\circ = \gamma^\circ = 2\%$, ω=10 rad/s.

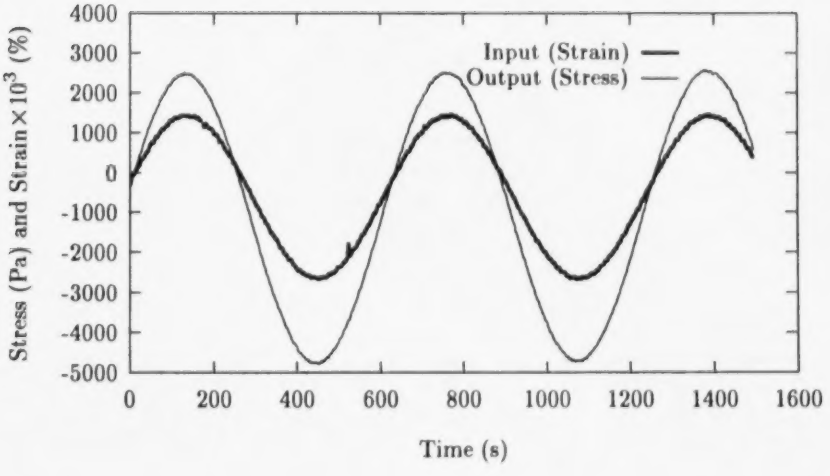

Figure 7.10: Run 5: Dynamic stress response of SBS1 at 25.6°C; $\gamma_N^o = \gamma^o = 2\%$, ω=0.01 rad/s.

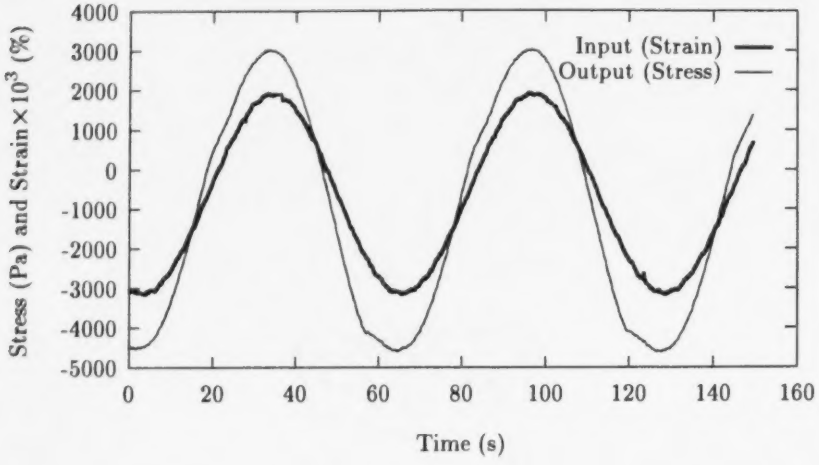

Figure 7.11: Run 6: Dynamic stress response of SBS1 at 43.2°C; $\gamma_N^o = \gamma^o = 2.5\%$, ω=0.1 rad/s.

Increasing the temperature to 43.2°C required a higher strain amplitude to reach the non-sinusoidal regime ($2\% < \gamma_{cr} < 2.5\%$). Figure 7.11 shows the response at ω=0.1 rad/s, $\gamma^o = 2.5\%$. The deviation from sinusoidal response is more pronounced than that at 25.6°C, both for the peaks and the troughs. On the peaks, or upswing of the stress, the bite in the curve begins at a lower stress, being around 100 or 200 Pa. Again the curve is not symmetric around zero. The response at 1 rad/s (Figure 7.12) is very similar to that at 0.1 rad/s. At 10 rad/s (Figure 7.13) the bite begins at a higher stress, somewhere around 1000 Pa, while at 0.01 rad/s (Figure 7.14) the response appears to be sinusoidal. The trough shapes are different than those seen at 25.6°C. At each frequency the bite appears more pronounced at the higher temperature. However, the shape is preserved at 43.2°C over a frequency range of 0.1 to 10 rad/s, or three orders of magnitude.

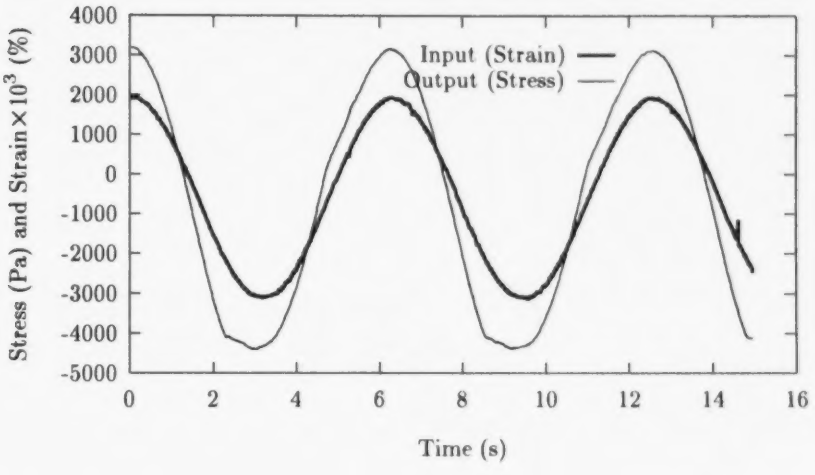

Figure 7.12: Run 7: Dynamic stress response of SBS1 at 43.2°C; $\gamma_N^\circ = \gamma^\circ = 2.5\%$, ω=1 rad/s.

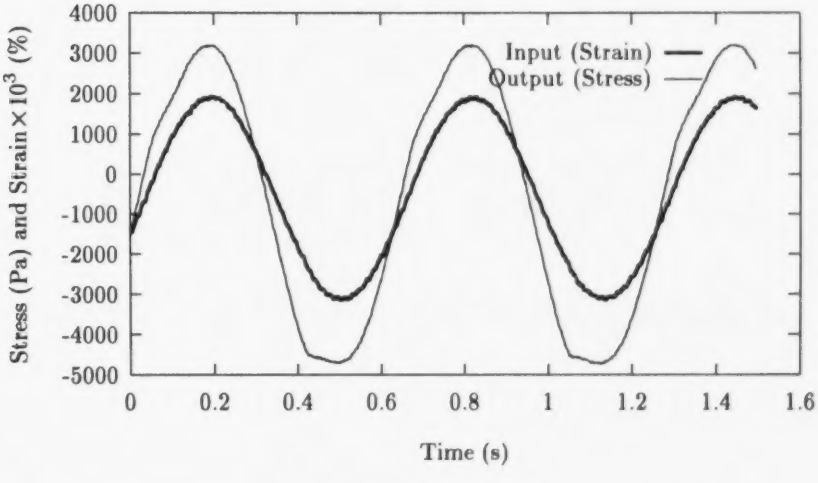

Figure 7.13: Run 8: Dynamic stress response of SBS1 at 43.2°C; $\gamma_N^\circ = \gamma^\circ = 2.5\%$, ω=10 rad/s.

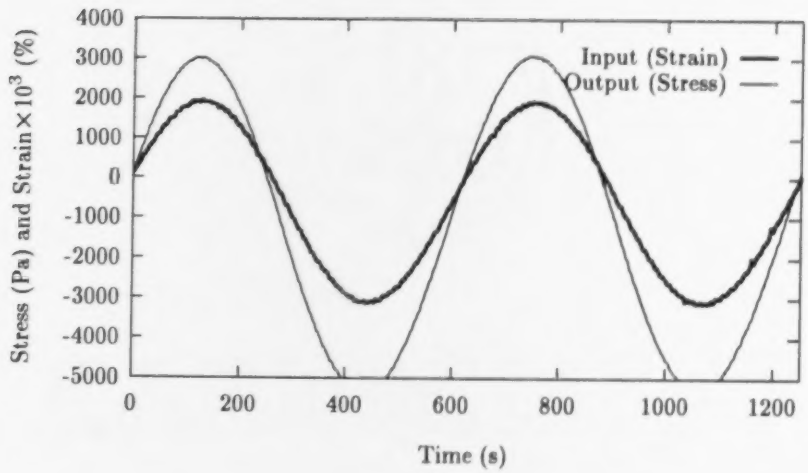

Figure 7.14: Run 10: Dynamic stress response of SBS1 at 43.2°C; $\gamma_N^\circ = \gamma^\circ = 2.5\%$, ω=0.01 rad/s.

At 60.5°C and γ^o=2.5% (Figures 7.15 to 7.19) the peak heights are lower than at 43.2°C, as is to be expected. At 0.1 rad/s (Figure 7.15) the bite in the peak begins at about 1200 Pa. At increasing frequencies the bite moves to progressively higher stresses, except at 100 rad/s where $\gamma^o < \gamma_N^o$, being only 1.89%. At 0.01 rad/s (Figure 7.19) the response appears to be almost sinusoidal. The shape of the bite in the troughs is again quite constant over the frequency range of 0.1 rad/s to 10 rad/s at the fixed temperature of 60.5°C and different than that at the lower temperatures. This suggests that the shape is unique to the material at a given temperature.

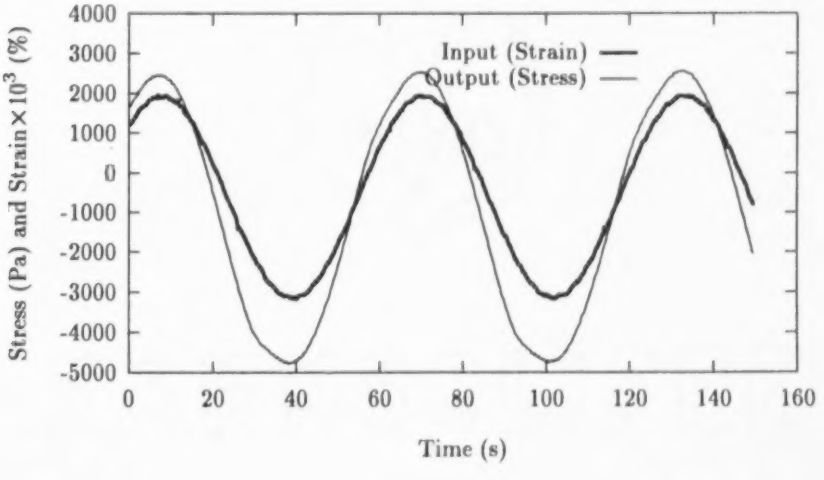

Figure 7.15: Run 11: Dynamic stress response of SBS1 at 60.5°C; $\gamma_N^o = \gamma^o$=2.5%, ω=0.1 rad/s.

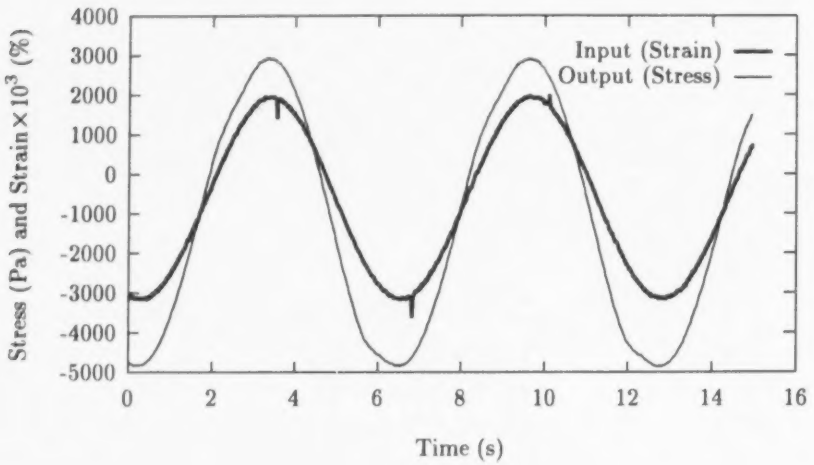

Figure 7.16: Run 12: Dynamic stress response of SBS1 at 60.5°C; $\gamma_N^\circ = \gamma^\circ = 2.5\%$, ω=1 rad/s.

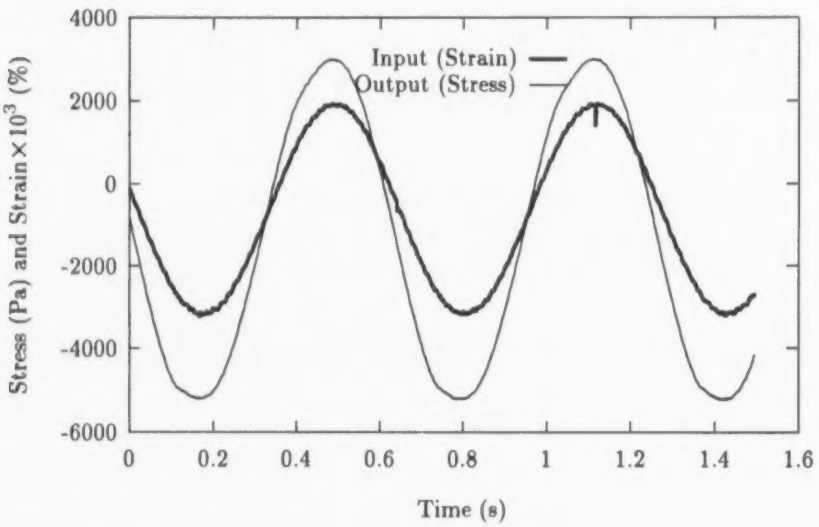

Figure 7.17: Run 13: Dynamic stress response of SBS1at 60.5°C; $\gamma_N^\circ = \gamma^\circ = 2.5\%$, ω=10 rad/s.

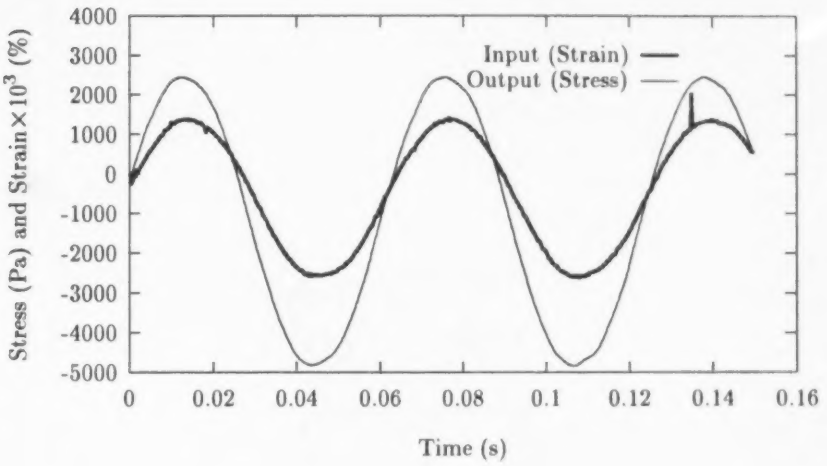

Figure 7.18: Run 14: Dynamic stress response of SBS1 at 60.5°C; γ^o =1.89%, ω=100 rad/s.

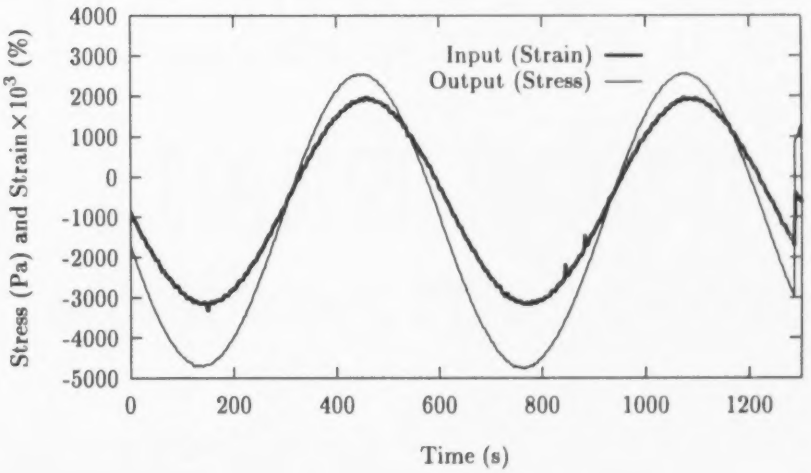

Figure 7.19: Run 15: Dynamic stress response of SBS1 at 60.5°C; $\gamma_N^o = \gamma^o$ =2.5%, ω=0.01 rad/s.

The next test temperature was 96.7°C, which was the only temperature in this test series greater than T_g of the dispersed phase. In order to see nonlinear waveforms at any frequency it was again necessary to increase the strain amplitude.

At γ° =2.9% and ω=0.1 rad/s (Figure 7.20) the stress response is sinusoidal with a peak to trough height of 2925 Pa. An increase of ω to 1 rad/s (Figure 7.21) causes the response to become dramatically nonlinear. The top of the waveform is almost a plateau, but the stress does still increase gradually until the strain reaches a maximum and then both drop off. The point at which the abrupt change in slope occurs in the upswing of the stress will be termed the shoulder. As the strain and stress increase in the *negative* direction the stress peaks at a very sharp shoulder and then drops off gradually with a concave curvature until the strain reaches its maximum in the negative direction at which point there is a second shoulder in the stress response followed by a linear drop-off. Curves are very reproducible except for the first peak ($\approx$0 time on this plot). Shoulder to shoulder height, measured from the shoulder on the positive and increasing side of the stress curve on the second peak to the negative and decreasing side of the stress curve on the second trough is 3300 Pa which is greater than the linear peak to trough height at 0.1 rad/s. The response at 10 rad/s was very similar, but shoulder to shoulder height was slightly greater at 3600 Pa.

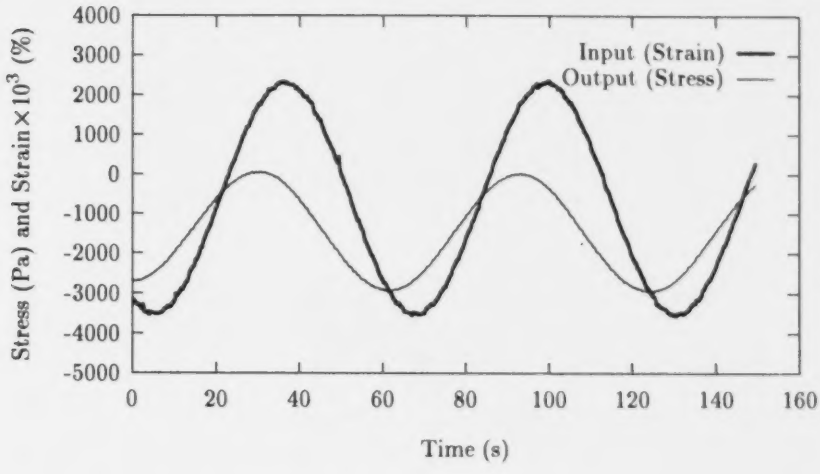

Figure 7.20: Run 16: Dynamic stress response of SBS1 at 96.7°C; $\gamma_N^o = \gamma^o = 2.9\%$, ω=0.1 rad/s.

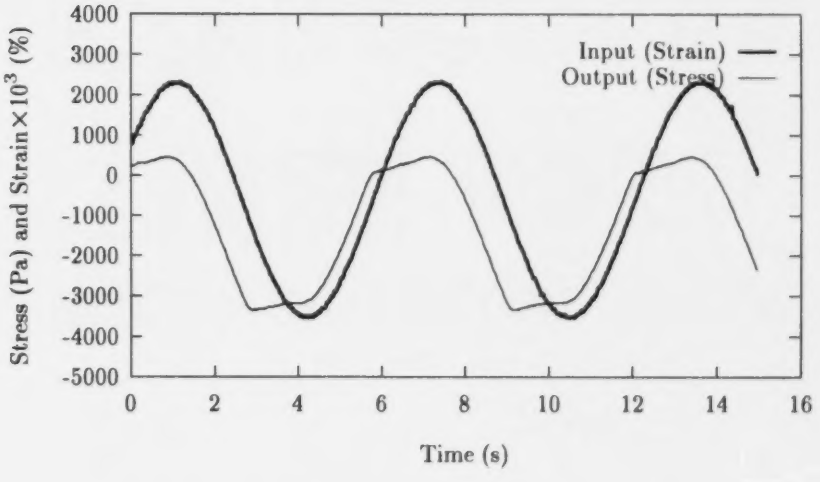

Figure 7.21: Run 17: Dynamic stress response of SBS1 at 96.7°C; $\gamma_N^o = \gamma^o = 2.9\%$, ω=1 rad/s.

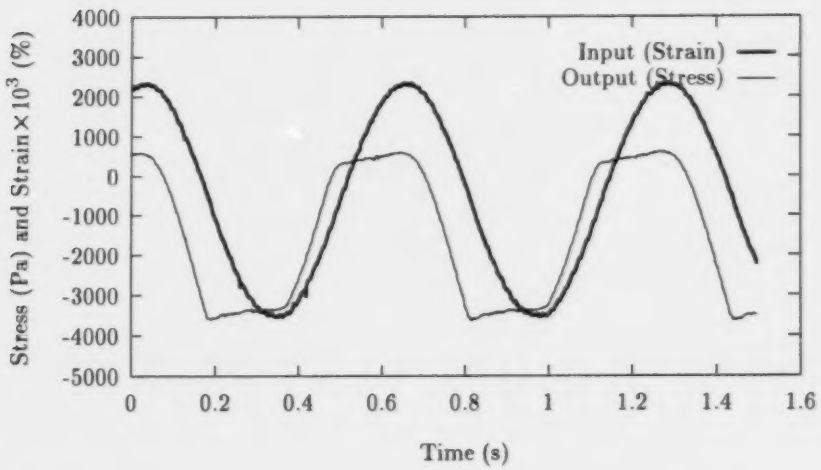

Figure 7.22: Run 18: Dynamic stress response of SBS1 at 96.7°C; $\gamma_N^\circ = \gamma^\circ = 2.9\%$, ω=10 rad/s.

Following the test at 96.7°C the temperature was dropped to 25.6°C again (same sample, allowed to soak overnight $\approx$ 12 hrs.). The tests at γ° =2% and ω=0.1 to 10 rad/s were repeated. The response was quite different from the first series. At 0.1 rad/s (Figure 7.23) the stress curve plateaus at the relatively low level of 4300 Pa (peak to trough), compared to the peak to trough heights of over 7000 Pa under the same conditions in the first series. Preceding the plateau there is a stress overshoot followed by a decaying stress wave. Here, and in many of the graphs to follow, there are seen "spikes" in the strain signal which are more prominent than in any previous such data. These are the result of electrical noise in the data, which is more severe under conditions where the transducer has more difficulty in re-zeroing (or balancing), resulting in an audible humming during the test. These spikes are not true excursions of the lower platen, as this would cause corresponding spikes or ripples in the stress waves. At ω=1 rad/s (Figure 7.24) the overshoot at the shoulder is followed by a slight increase in the stress to a short plateau. At 10 rad/s (Figure 7.25) the overshoot is again followed by a decaying stress wave and a plateau.

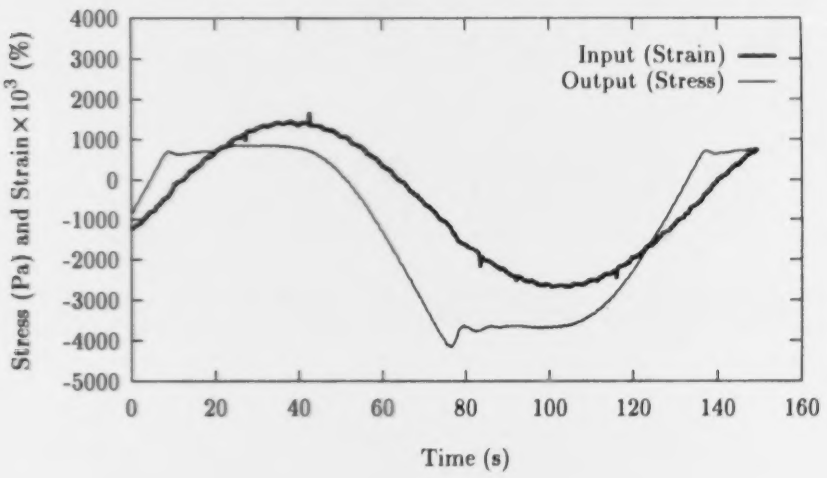

Figure 7.23: Run 20: Dynamic stress response of SBS1 at 25.6°C; γ_N° =γ° =2%, ω=0.1 rad/s, second cycle.

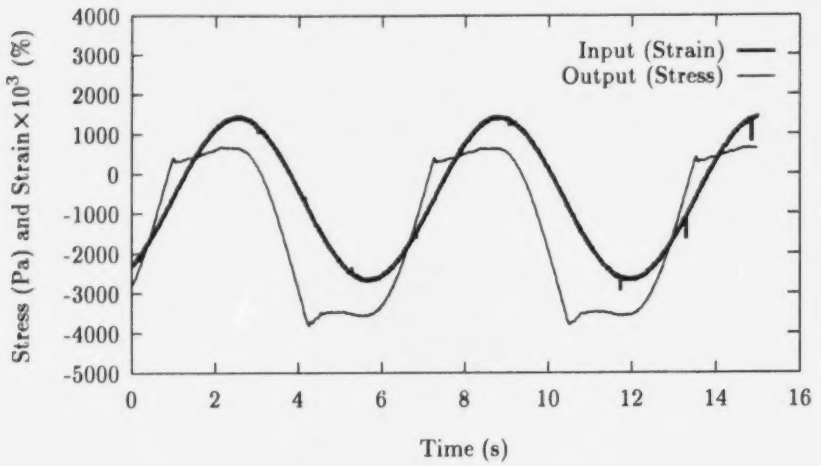

Figure 7.24: Run 21: Dynamic stress response of SBS1 at 25.6°C; $\gamma_N^\circ = \gamma^\circ = 2\%$, ω=1 rad/s, second cycle.

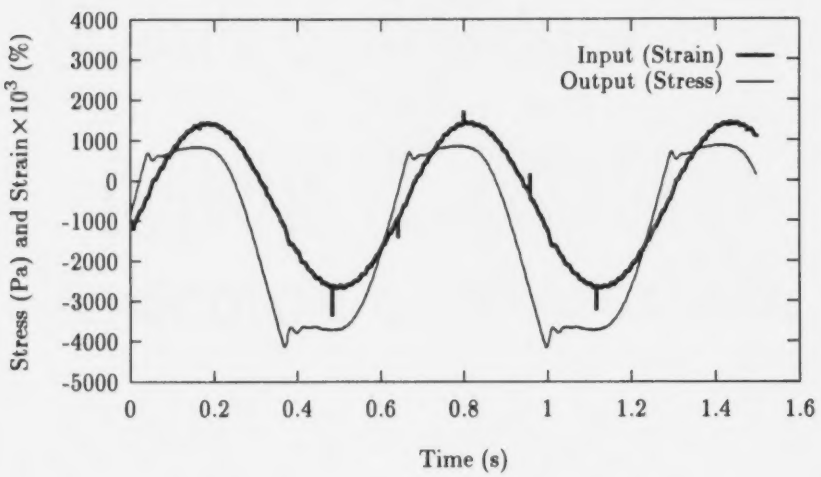

Figure 7.25: Run 22: Dynamic stress response of SBS1 at 25.6°C; $\gamma_N^\circ = \gamma^\circ = 2\%$, ω=10 rad/s, second cycle.

As γ° is increased to 3% at the same temperature (Figure 7.26) the overshoot at the shoulder becomes very sharp followed by a sharp oscillation in the stress to a short plateau. The shapes of other γ° =3% curves at 45.4°C (Figure 7.27 to 7.29) and 60.5°C (Figure 7.30 to 7.33) in the second series are very similar to those at 25.6°C and nothing more will be said about them here; the plots are included for completeness only.

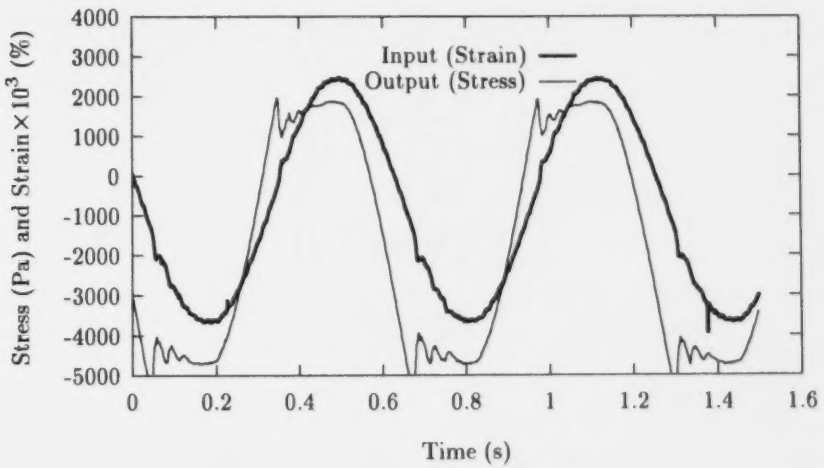

Figure 7.26: Run 27: Dynamic stress response of SBS1 at 25.6°C; γ_N° =γ° =3%, ω=10 rad/s, second cycle.

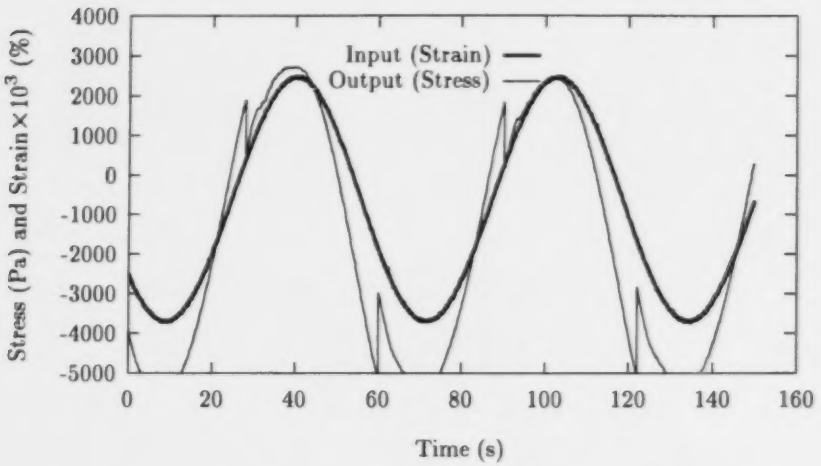

Figure 7.27: Run 29: Dynamic stress response of SBS1 at 45.4°C; $\gamma_N^\circ = \gamma^\circ = 3\%$, ω=0.1 rad/s, second cycle.

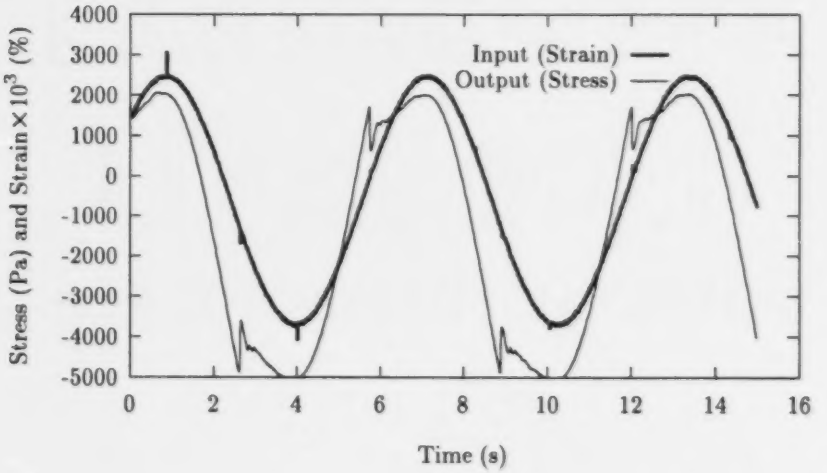

Figure 7.28: Run 30: Dynamic stress response of SBS1 at 45.4°C; $\gamma_N^\circ = \gamma^\circ = 3\%$, ω=1 rad/s, second cycle.

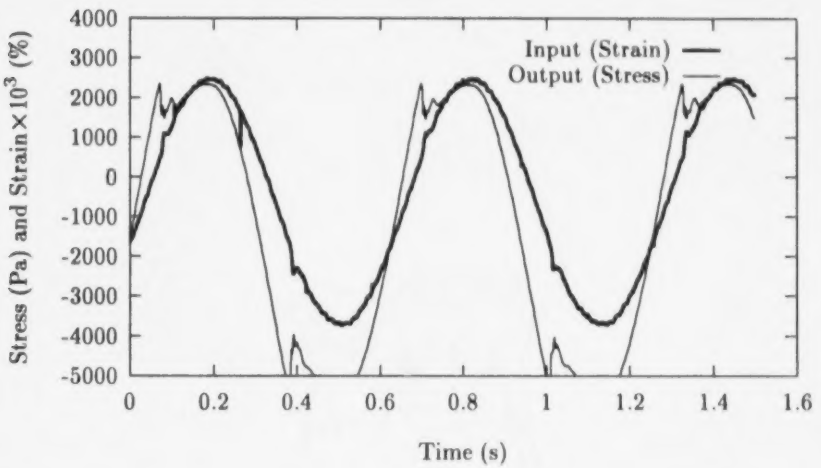

Figure 7.29: Run 31: Dynamic stress response of SBS1 at 45.4°C; $\gamma_N^o = \gamma^o = 3\%$, ω=10 rad/s, second cycle.

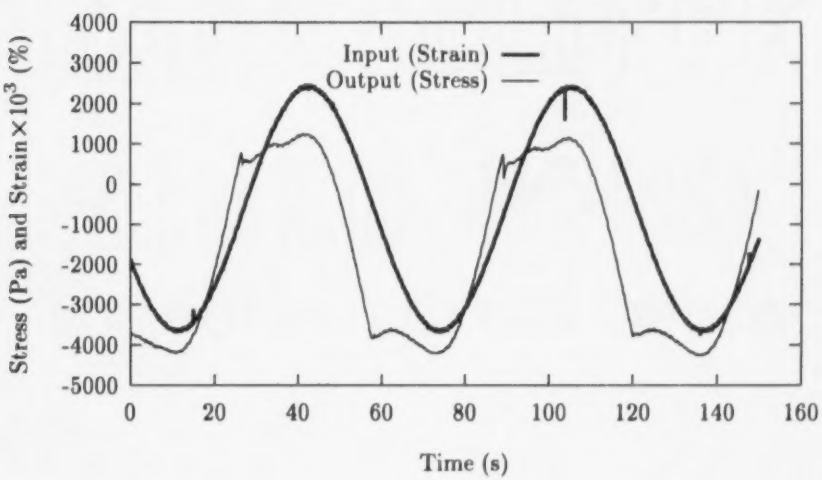

Figure 7.30: Run 34: Dynamic stress response of SBS1 at 60.5°C; $\gamma_N^o = \gamma^o = 3\%$, ω=0.1 rad/s, second cycle.

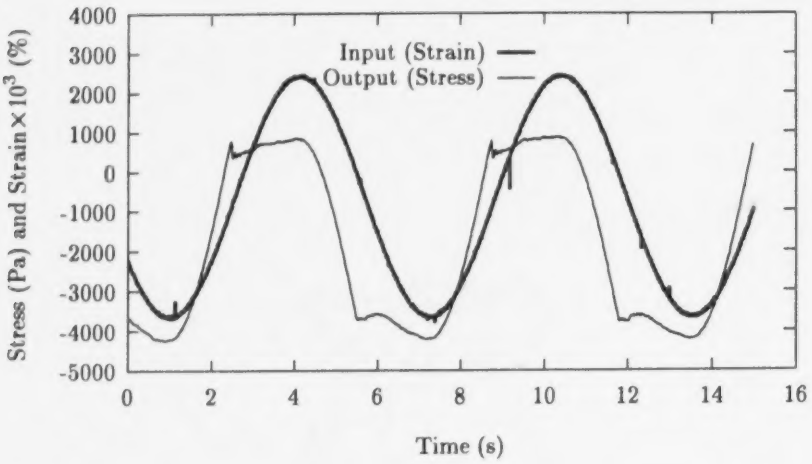

Figure 7.31: Run 35: Dynamic stress response of SBS1 at 60.5°C; $\gamma_N^\circ = \gamma^\circ = 3\%$, ω=1 rad/s, second cycle.

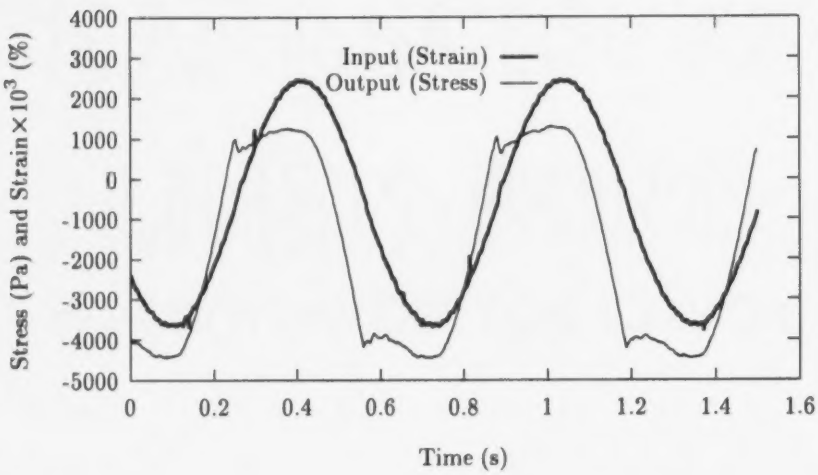

Figure 7.32: Run 36: Dynamic stress response of SBS1 at 60.5°C; $\gamma_N^\circ = \gamma^\circ = 3\%$, ω=10 rad/s, second cycle.

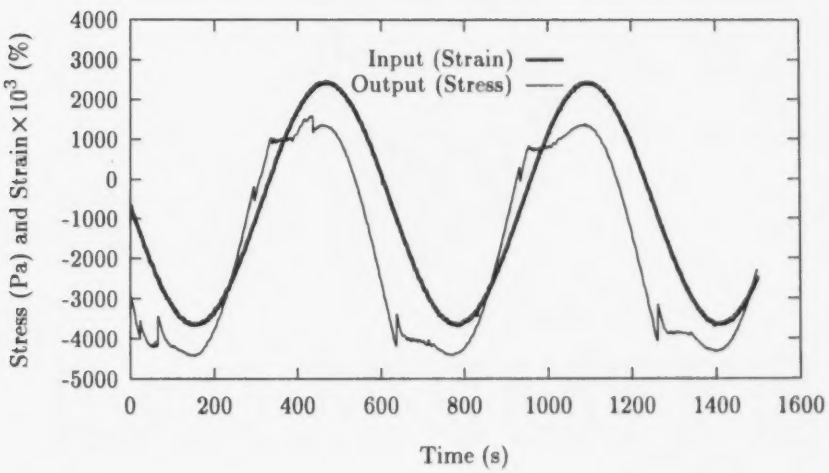

Figure 7.33: Run 38: Dynamic stress response of SBS1 at 60.5°C; $\gamma_N^\circ = \gamma^\circ = 3\%$, ω=0.01 rad/s, second cycle.

Increasing the temperature again to 96.5°C and the stress amplitude to 3.5% caused results parallel those at γ^o =3% in the first series. At low frequencies the response is sinusoidal (Figures 7.34 and 7.35), having a peak to trough height of 4160 Pa at 0.1 rad/s. At 1 rad/s (Figure 7.36) a shoulder followed by a gradual increase is seen on the stress peak. In the trough an overshoot on the shoulder is followed by a dip and a rise to a peak. Shoulder to shoulder height is 4240 Pa. At 10 rad/s (Figure 7.37) the peaks are almost flat while the troughs still show an overshoot and gradual drop to the descending shoulder, having a shoulder to shoulder height of 4500 Pa.

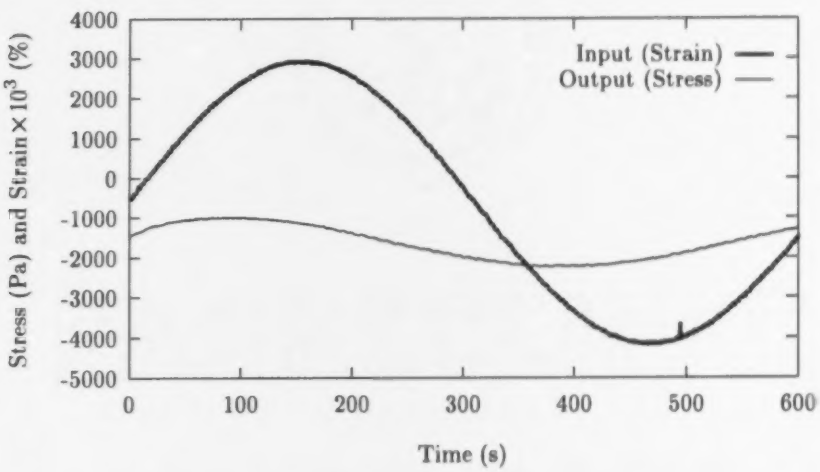

Figure 7.34: Run 39: Dynamic stress response of SBS1 at 96.5°C; $\gamma_N^o = \gamma^o$ =3.5%, ω=0.01 rad/s, second cycle.

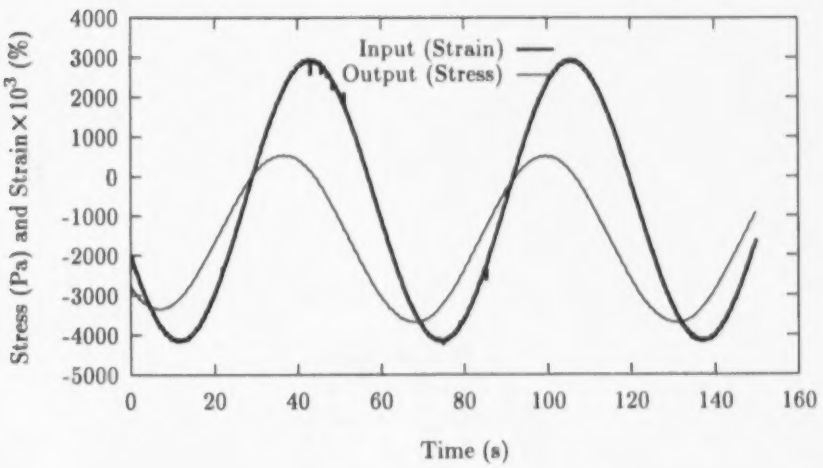

Figure 7.35: Run 40: Dynamic stress response of SBS1 at 96.5°C; $\gamma_N^o = \gamma^o = 3.5\%$, ω=0.1 rad/s, second cycle.

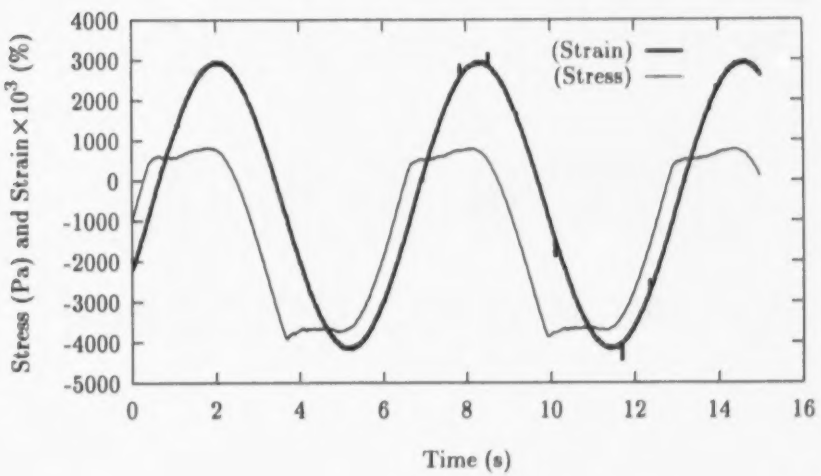

Figure 7.36: Run 41: Dynamic stress response of SBS1 at 96.5°C; $\gamma_N^o = \gamma^o = 3.5\%$, ω=1 rad/s, second cycle.

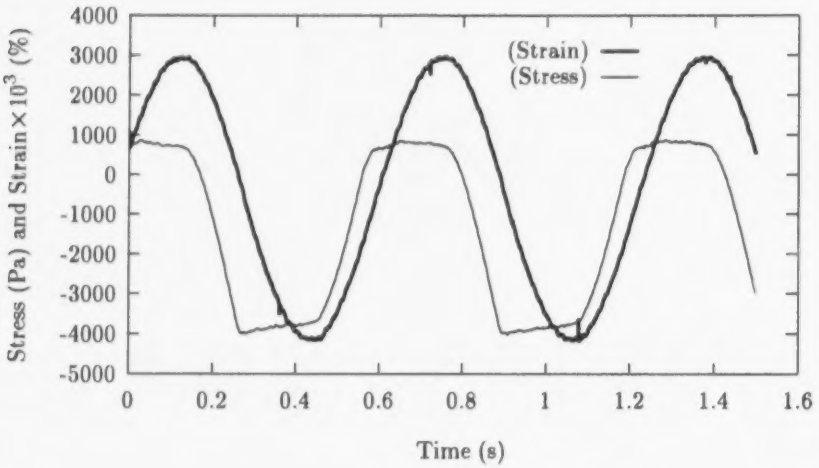

Figure 7.37: Run 42: Dynamic stress response of SBS1 at 96.5°C; $\gamma_N^\circ = \gamma^\circ = 3.5\%$, ω=10 rad/s, second cycle.

At γ^o =5% again low frequency response is sinusoidal while higher frequency responses are non-sinusoidal (Figures 7.38 to 7.41). The temperature for these tests is a fraction of a degree higher, being 96.8°C except at 0.1 rad/s (Figure 7.39) for which the temperature was 96.5°C. Peak to trough height at 0.01 rad/s is roughly 1860 Pa while shoulder to shoulder heights are about 4300 Pa at both 0.1 and 1 rad/s and 4700 Pa at 10 rad/s. At a strain amplitude of 5% non-linearity is very pronounced already at 0.1 rad/s, while for the earlier tests at γ^o =2.9%, sinusoidal response prevailed at this frequency. This serves to demonstrate again that the onset of non-linearity is correlated with stress amplitude, rather than frequency or strain amplitude, except insofar as these other parameters affect stress.

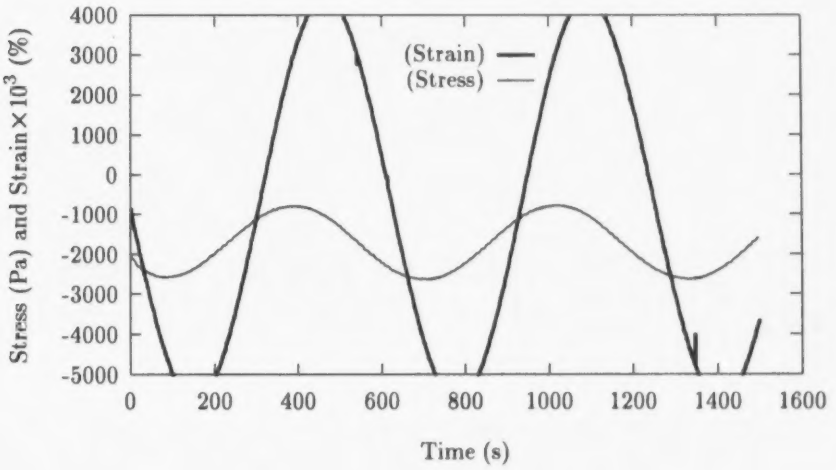

Figure 7.38: Run 43: Dynamic stress response of SBS1 at 96.8°C; γ_N^o =γ^o =5%, ω=0.01 rad/s, second cycle.

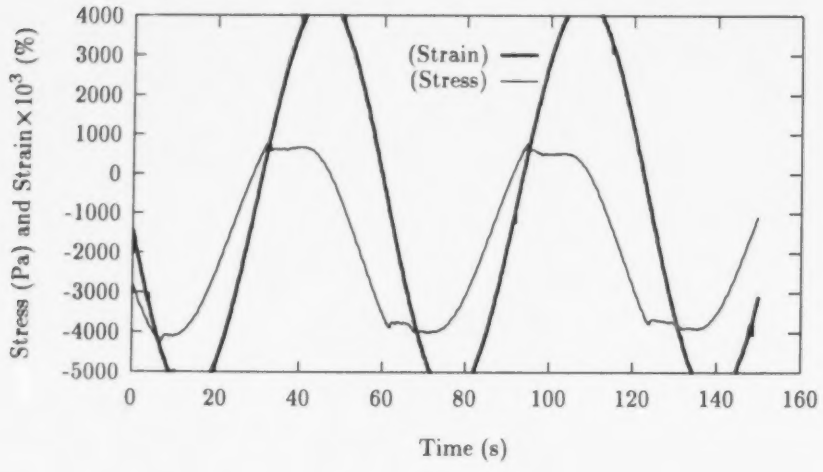

Figure 7.39: Run 44: Dynamic stress response of SBS1 at 96.5°C; $\gamma_N^\circ = \gamma^\circ = 5\%$, ω=0.1 rad/s, second cycle.

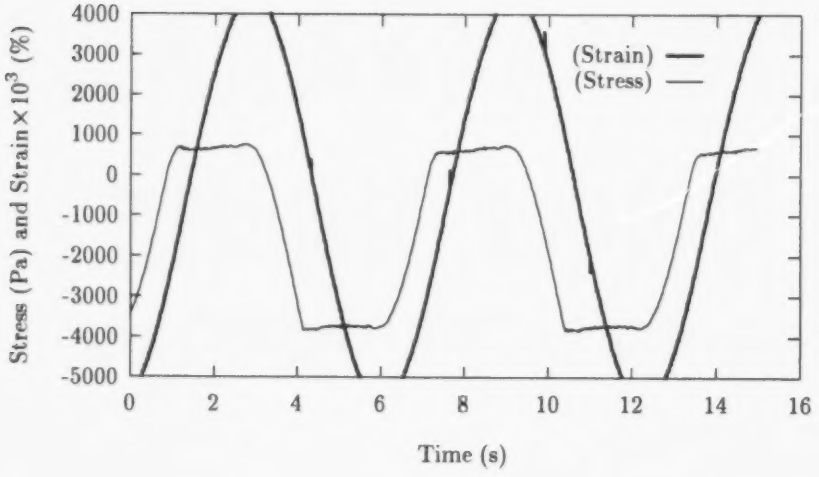

Figure 7.40: Run 45: Dynamic stress response of SBS1 at 96.8°C; $\gamma_N^\circ = \gamma^\circ = 5\%$, ω=1 rad/s, second cycle.

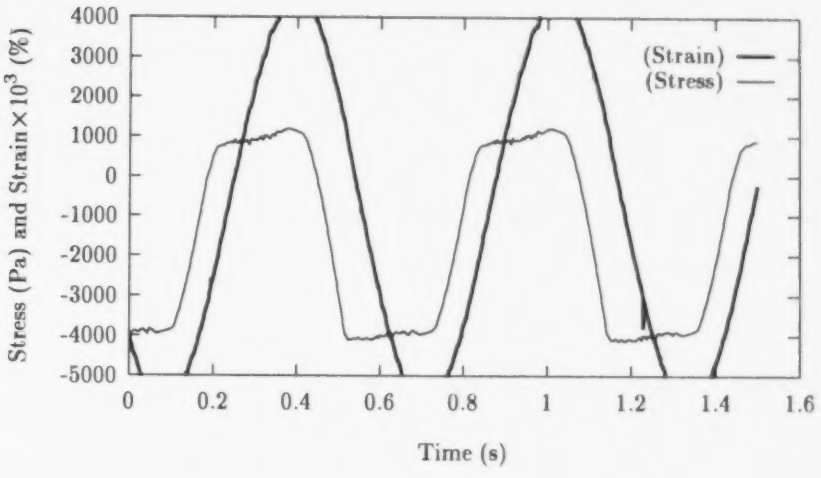

Figure 7.41: Run 46: Dynamic stress response of SBS1 at 96.8°C; $\gamma_N^\circ = \gamma^\circ = 5\%$, ω=10 rad/s, second cycle.

Chapter 8

Results 3; Phase Transition

In these experiments samples of SBS4 solvated with 50% (by weight) 5 base oil[1] were tested under dynamic oscillatory shear. Pico and Williams [59] predicted that the addition of solvent would depress the separation temperature of block copolymers. The convection oven was used for temperature control with air as the heating medium. Samples were hot-loaded [35]—loaded above T_s and allowed to cool, forming structure in situ—so that morphology was isotropic.

A strain sweep was performed at 30°C and ω=1 rad/s to determine the region of linear viscoelasticity. The plot of G' and η' *vs.* γ_N° (Figure 8.1) reveals a slight drop in both G' and η' at low strains followed by an almost flat region for 0.12% $<\gamma_N^\circ<$ 10%. Subsequent tests were performed at γ_N° =1%.

A temperature sweep at ω=10 rad/s and γ_N° =1% reveals a drastic drop in both modulus (Figure 8.2) and viscosity (Figure 8.3) through the region from 75°C to 90°C. This has been reported by several researchers [22, 10, 58] as an indication of a phase transition. Storage modulus starts out higher than loss modulus at low temperatures with an inversion occurring during the transition (Figure 8.2). The

[1] A refinery fraction provided by Esso from their Edmonton refinery—kerosene based, with a boiling point range of 130°C-288°C.

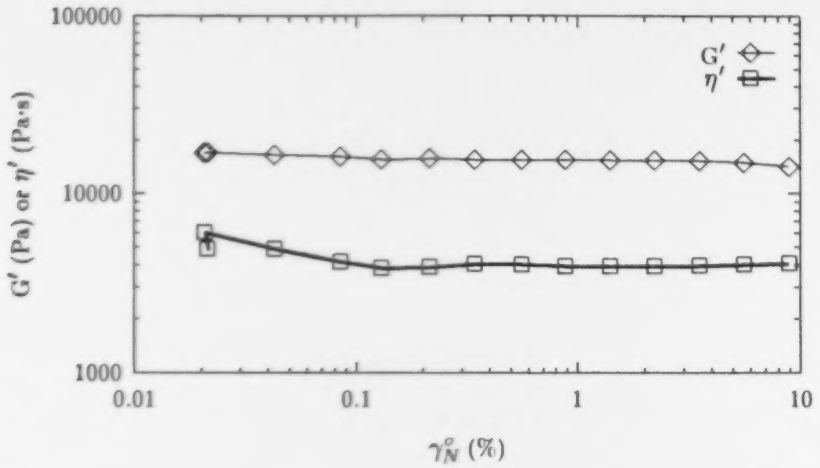

Figure 8.1: SBS4 solvated with 5 base oil, G' and η' strain sweep at 30°C and 1 rad/s.

same is demonstrated with η'' and η' in Figure 8.3.

Another sweep (fresh sample), concentrating on the transition region with smaller temperature steps and varying frequency, reveals unexpected behaviour at low frequencies (Figure 8.4). At ω=0.1 rad/s between 95°C and 105°C η^* jumps up and down in an apparently chaotic fashion. At 1 rad/s, η^* decreases rapidly through the transition region and then jumps unexpectedly at 104°C. At 10 and 100 rad/s the behaviour is qualitatively the same as that reported previously in the literature. The transition occurs at higher T than seen in Figures 8.2 and 8.3, which may be due to solvent concentration differences from thermal history variation.

Other evidence which points to odd behaviour in the transition region of temperature was encountered when heating a bulk (non-solvated) sample through this region. SBS1 was being tested in a manual frequency/temperature sweep, the results of which are presented in Figures 7.3 and 7.4. Recall that T_s for SBS1 was measured to be about 243°C (see Chapter 5). The sample was being heated in 10°C increments above 200°C with a 20 minute thermal soak time, using nitrogen as the

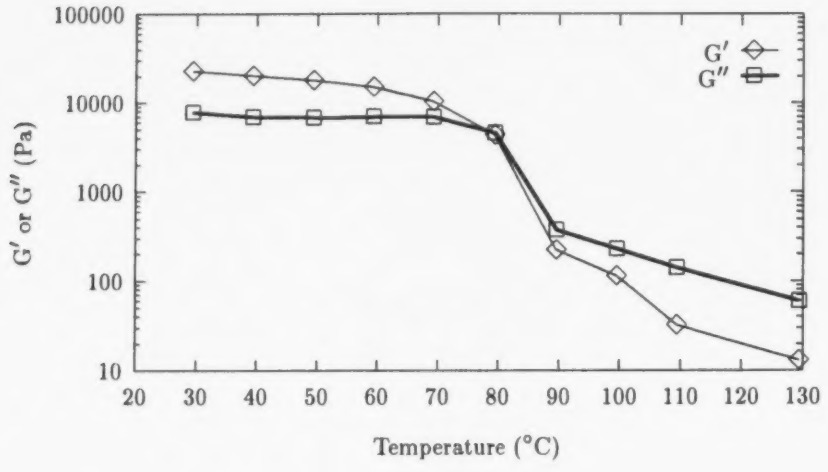

Figure 8.2: Dynamic moduli SBS4 solvated with 5 base oil temperature sweep at 10 rad/s.

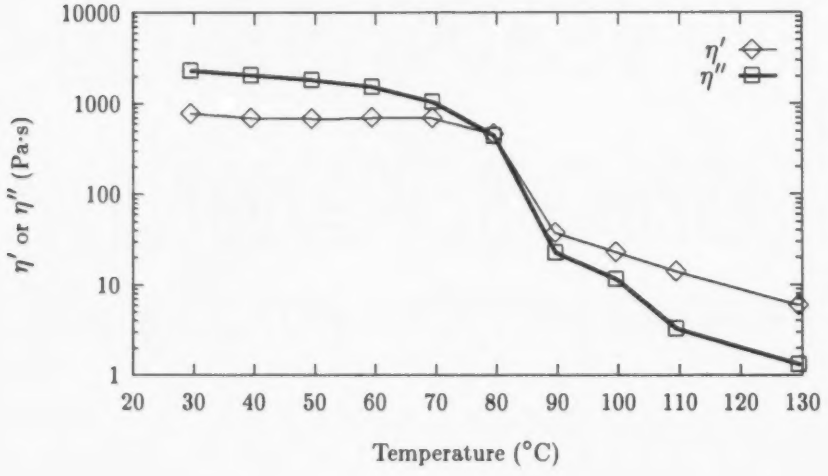

Figure 8.3: Dynamic viscosities for SBS4 solvated with 5 base oil temperature sweep at 10 rad/s.

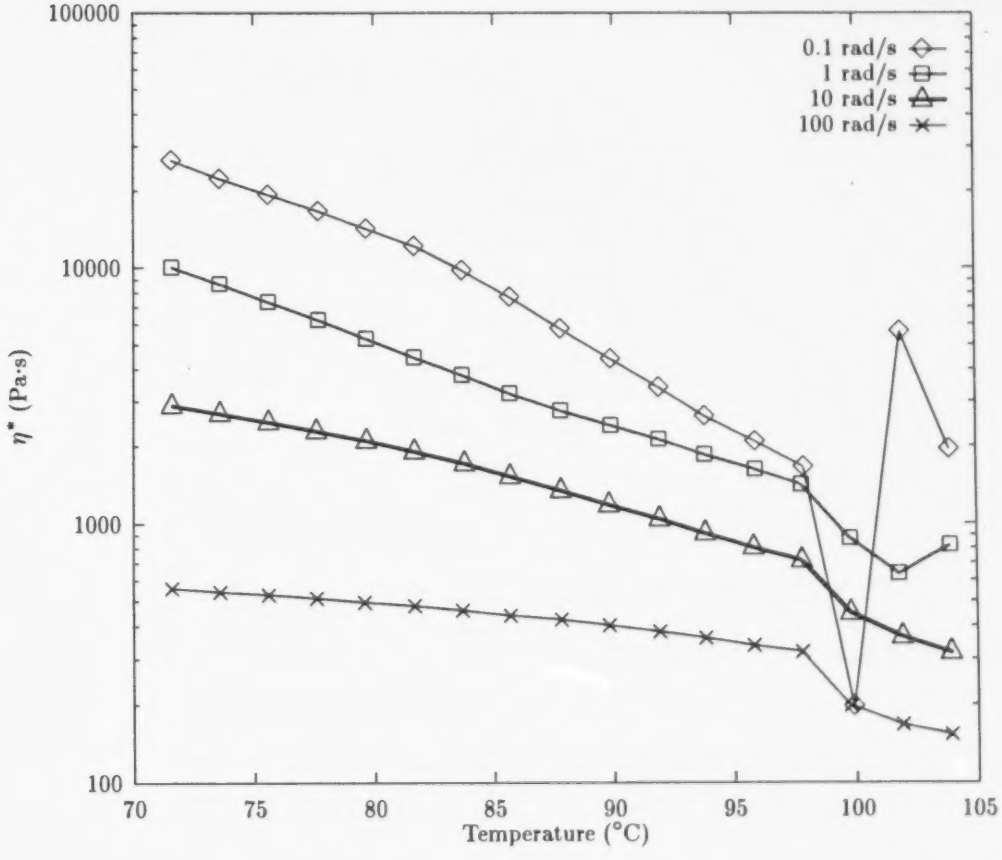

Figure 8.4: SBS4 solvated with 5 base oil η^*–frequency/temperature sweep.

heating gas. After testing at 221.5°C the sample was heated to 231.6°C. After 10 minutes at this temperature the autotension function on the RMS 800 appeared to enter an unstable control loop. Normal force would rise sharply causing the platform to rise abruptly. This in turn caused a negative normal force to which the machine responded by lowering the platform abruptly thus causing again a large positive normal force. This continued in ever-increasing normal force oscillations until the test had to be aborted and the transducer disconnected in order to protect the equipment from harm. It is not actually known whether the instability was started first by an increase or a decrease in the normal force, that is, an upwards thrust or a sudden relief of normal force.

The sample was removed by heating both platens with entrapped sample in a conventional oven until they could be pulled apart by hand. Only a bit of yellowing could be seen around the edges of the sample where it was not in contact with the platens. As the heating gas in the rheometer had been nitrogen it was suspected that the yellowing occurred largely while melting the sample out of the platens in the conventional oven.

This happened again with a second sample of SBS1, also at about 230°C. With SBS4 the same phenomenon was observed while heating to between 300 and 310°C. Recall that the predicted T_s for SBS4 is about 317°C (Table 5.1). However, with SBS4 the sample was significantly degraded after the test.

Chapter 9

Discussion

9.1 Theory

9.1.1 Yield Stress

There has been some debate staged over the concept of a true yield stress in liquid phase block copolymers. Several researchers have measured yield stresses in block copolymers [39, 48, 4, 12, 76, 27] and others have inferred its existence from their data [23, 26, 13] as reviewed in section 3.4.3. Henderson and Williams [31] established thermodynamic arguments for the existence of a true yield stress. Arnold and Meier [2] also proposed its existence from structural arguments. However, Vinogradov *et al.* [74] found no evidence of a liquid phase yield stress, as long time measurements suggested that flow continued (slowly) under even very low stresses. Ghijsels and Raadsen [72] measured viscous flow at stresses as low as 10 Pa and concluded that no true yield stress exists.

In recent years the debate over whether *any* material exhibits a true yield stress has resurfaced. I adopt here the classical definition of a yield stress as a stress below which, for a given material, no unrecoverable flow occurs. In the July/August

1993 issue of *Journal of Rheology*, De Kee and Fong [37] reviewed the most recent literature in this debate, dated between 1985 and 1992. Barnes and Walters [3] insisted that the yield stress is a "myth", since "if a material flows at high stresses it will also flow, however slowly, at low stresses." Schurz [63] suggested the use of the term "apparent yield stress" while Hartnett and Hu [28] demonstrated that the yield stress is an "engineering reality."

No one disputes the existence of an *apparent* yield stress. Rather, dispute arises over whether it truly represents the failure of a solid-like structure. An apparent (or *engineering*) yield stress would result from a relaxational process which is so slow that it can be considered infinitely long in comparison to the time scale of the process or measurement. Anyone in industry who has cleaned out a plugged pipe will tell you that such a yield stress exists. Overcoming these "apparent" or "engineering" yield stresses merely involves triggering a larger number of relaxational processes which are dormant at lower imposed stresses.

Measurements of yield stresses typically involve loading the sample with some finite stress and watching to see if flow is initiated. If no flow is detected after some given time, the length of which would be dependent on the researchers' patience, then the yield stress is known to be higher than the applied stress. Those who oppose on principle the concept of a true yield stress could always claim that not enough time was given to detect flow. The idea of "detection" also introduces controversy, as this brings in the question of instrument sensitivity.

The theory of linear viscoelasticity predicts that any stress, no matter how small, will eventually be relieved by viscous flow for non-crosslinked polymers. Your Tupperware bowl may seem quite solid, but in reality it is a highly viscous liquid. If left out on the counter long enough, say a few thousand years, it will eventually form a puddle on the countertop, barring any oxidative or radiative crosslinking[1].

[1] I am ignoring for the moment recent evidence that shows that solid phase catalysed homopolymers may have blocky type structures and by extension yield stresses, although very

However, block copolymers are not linear viscoelastic materials. The structure shown in Figure 3.2 (a) gives rise to free energy gradients as depicted in Figure 3.2 (b). Henderson and Williams proposed that any force imposed on a chain lower than the sum of the free energy and frictional forces would not be sufficient to pull a block junction from the interphase.

In terms of an Eyring type model, a segment of a homopolymer molecule is positioned in a potential well as shown in Figure 9.1 (a) with equal probability of making a segmental jump in any direction, unless a stress is imposed as in Figure 9.1 (b). This stress has the effect of lowering the potential (ΔE) in the direction of the imposed stress and raising it in the opposite direction, thus biasing the probability of a segmental jump in the direction of the stress. Note that any imposed stress, no matter how small, will bias the potential, and probability argues that eventually flow will occur.

Consider now such arguments with a junction between blocks or segments in a block copolymer residing in the interphase. It too is positioned in a potential well as in Figure 9.1 (a). When a stress is imposed, the potential is biased in the direction of the stress as in Figure 9.1 (b). However, as soon as the junction moves away from its rest point, there is a chemically-induced rise in chemical potential μ_A. Recall the work of Henderson and Williams (Section 3.1.3) wherein they proposed that the chemical potential gradient would cause a force on the chain (Equation 3.5). Therefore, the increase in μ_A biases the forces in the opposite direction, as depicted in Figure 9.1 (c). As long as these two biases are balanced, flow will not be initiated, *i.e.* the yield stress has not been exceeded. A large enough stress, of course, will bias the potential in the direction of the stress to a greater extent than the chemical potential gradient can counter, being limited by the physics of the system. With no external stress imposed on a chain, the junction (or rather the

small. The force of gravity on the sides of the Tupperware bowl may be lower than the yield stress.

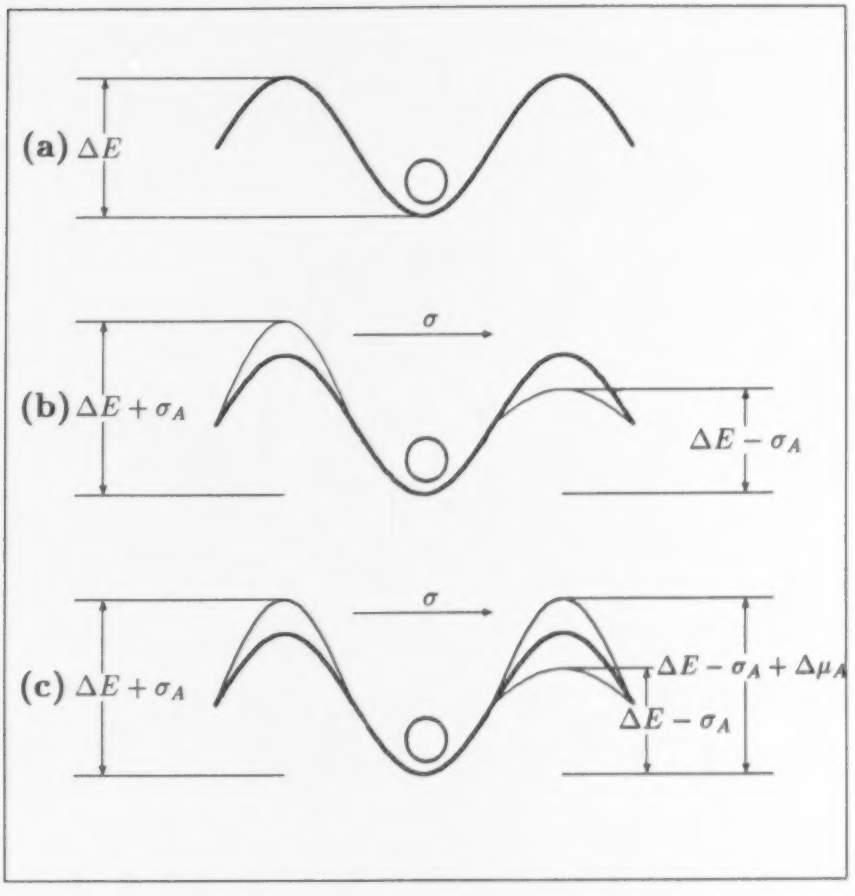

Figure 9.1: Eyring rate model for (a) homopolymer segment with no imposed stress, (b) homopolymer segment with imposed stress, (c) block copolymer segment junction with imposed stress. σ is an imposed stress and $\sigma_A \equiv \frac{1}{2}\sigma/n_A$, where n_A is the molar density of A units. $\Delta\mu_A$ is a chemical potential difference.

A and B monomer units on either side of the junction) would not individually be in a state of minimum μ_A or μ_B as both monomer units would be in a more stable state energetically residing in their respective pure phases. However, a move in either direction, towards the respective pure phase of one chemical species (A or B) would drag the other into a higher, less favoured chemical potential state. Therefore, the position of the junction with no external imposed stresses is determined by a thermodynamic balance of these forces.

Watanabe *et al.* [76] observed Bingham-type flow behaviour (steady shear) in solutions of SB (diblock) copolymers using a solvent selective to the PB phase. They also witnessed *dynamic* shear stresses containing higher-order odd harmonics (nonsinusoidal) under small amplitude oscillation. The data were found to suggest that the yield stress was the main cause of the nonlinearities and that the existence of the yield stress could be attributed to the driving force for "macrolattice formation" (phase separation). Hansen and Williams [27] correlated yield stress with the phase separation temperature, T_s. A higher T_s represents a stronger thermodynamic driving force towards the phase-separated state. As the thermodynamic driving force increases, more mechanical force is needed to overcome it and extract end blocks.

It should be noted that the yield stress in block copolymers would be unlike that in suspensions. In the latter case the yield stress represents the frictional hindrance of particle-particle interactions. Given enough stress the long range order or structure of these contacting particles would be catastrophically disrupted. In block copolymers, any deformation of the microstructure would alter to some extent the interphase and the nature of the composition gradient. This would then alter the free energy gradient and hence the yield stress. The yield stress is therefore a dynamic property of the microstructure, changing as the microstructure deforms. It would be different for each different shear, solvent and temperature history and could even change over the course of a test – or while it is being measured!

9.1.2 Phase Transition

Thermodynamic theories of phase transition in block copolymers are equilibrium theories giving T_s=$T_s(\phi_A, \phi_B, \overline{\phi'_A\phi'_B}, V_m, \Delta\delta)$. However, the above discussion introduces the role of strain (a non-equilibrium variable since γ=0 defines equilibrium) in determining the phase-separated character of the material. Mechanically-induced mixing of sufficient intensity could induce formation of a homogeneous mixture in the melt even if $T < T_s$.

Imagine a phase-separated structure at some T just fractionally below T_s. All phases would be liquid and easily deformable. If this structure is then strained in steady shear, the microstructure could be disrupted enough to disperse all microphases. If the shear is high enough then blocks pulled from domains could not establish themselves strongly in other neighboring domains before they are pulled out again. However, if T were dropped further, the driving force to microphase-separate would become stronger and the shear may not be sufficient to maintain a homogeneous state. Effectively, T_s has been lowered by the shearing. Thus $T_s = T_s(\gamma,\phi_A, \phi_B, \overline{\phi'_A\phi'_B}, V_m, \Delta\delta)$. Morrison and Winter [52] studied the effect of unidirectional shear on triblock copolymers, as reviewed in Section 3.4.2 and they concluded that the degree of microphase separation could be permanently altered by flow.

In this work I do not claim to present any comprehensive model for the role of strain as a thermodynamic variable. However, the interaction between thermodynamic and mechanical forces is central to the behaviour of block copolymers, particularly triblocks. Research on these materials is heading towards a definition of the effect of strain on microphase separation.

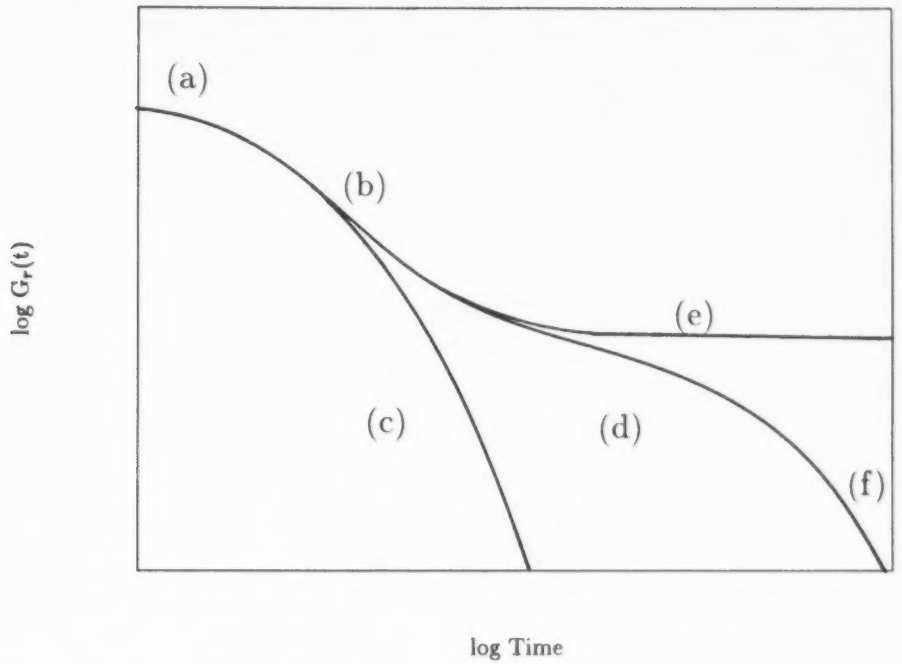

Figure 9.2: Stress relaxation curves for typical homopolymers.

9.2 Stress Relaxation Experiments

Stress relaxation master curves for typical homopolymers in response to a step strain are shown in Figure 9.2. The plateau labelled (a) is known as the glassy plateau. This initially high modulus at short times is the glassy response resulting when the shortest relaxation times are challenged. Following the glassy plateau is the relaxation labelled (b) which I will refer to as the initial relaxation. This is the rapid response of the shortest relaxation times in the polymer. Short chain polymers, *i.e.* , MW$< M_c$ (the chain entanglement molecular weight) , would follow the curve labelled (c), with modulus dropping off in a rapid fashion. Longer chain molecules with at least 2 entanglements per chain would follow the curve labelled (d), with

modulus levelling and merging for some time with the rubbery or entanglement "plateau" or "regime" (though it need not have a slope of zero). The modulus of a crosslinked rubber would continue to level out to a slope of zero and remain at that level indefinitely, as in (e). For an uncrosslinked entangled polymer at long times, the modulus would again drop off, eventually to zero as in (f). Along the line (f), the longest relaxation times associated with entanglements have been overcome and the now disentangled polymer chains relieve stress rapidly ([61], p.252).

9.2.1 SBS1

Starting our discussion with SBS1 at 90°C, it has already been pointed out that $G_r(t)$ curves at differing strain amplitudes do not superimpose, demonstrating that these materials are not linear in their response to shear. At 1 and 4% strain (Figure 6.4) the initial glassy plateau is evident as in Figure 9.2 (a), followed by a relaxation analogous to the initial relaxation (b) and then levelling off in a fashion similar to the entanglement regime (d) in the same figure. At lower strain amplitudes (γ=0.05 to 0.3%) the initial relaxation is not followed by an entanglement plateau, but by a *recovery* of the modulus as seen in Figure 6.5.

This recovery can only be explained by a microstructural- thermodynamic model. The stress resulting from a step strain tends to deform the local microstructure. The stress can only be relieved if flow occurs, which necessitates a disruption of the network structure. However, the network structure can only be disrupted if end blocks are pulled from their domains. Thermodynamic forces, and in particular those related to interphase composition gradients, oppose the extraction of blocks from their domains. Upon sudden imposition of a step strain, the microstructure is perturbed from its initial state. This may cause migration of segment junctions partially through the interphase or it may involve complete block extraction.

If a block is not entirely pulled out, but rather the position of the segment

junction is merely perturbed within the interphase, then the free energy gradients will tend to force it back in the direction from which it moved. This provides a mechanism for stress recovery. In Figure 9.3 the σ(t) curve for a 0.1% step strain at 90°C is compared to a curve of the form

$$\sigma(t) = C_1 e^{-t/a} + C_2 e^{-b/t}. \tag{9.1}$$

The first term is a single Maxwell element with a modulus C_1 at t=0 and a relaxation time a. The second term is an inverse exponential, beginning at high rates but low values at t→0, levelling and approaching some stable state C_2 as t→ ∞. This is typical of rate processes. The prefactor C_2 is a modulus at t=∞ while the exponential factor b is analagous to the relaxation time, but more appropriately termed the "recovery time". The second term therefore represents the reformation process, the rate of which is determined by the thermodynamic balance of the system. This reveals the nature of the σ(t) curve to be that of competing processes. The first is an exponential decay of stress and the second is an inverse exponential recovery of stress approaching some constant level. An attempt at modelling this process, or fitting these curves, would most likely require more than one relaxing element and several recovering elements, as there are sure to be several relaxation times each corresponding to a relaxation mode, and analogously, more than one recovery mode.

These data represent a direct mechanical measurement of thermodynamic forces. Kelterborn and Soong [38] followed the recovery of G' and G'' in block copolymers after the imposition and release of a tensile strain and interpreted these results in terms of microstructural recovery. However, no one has ever reported before this a direct, real-time measure of the thermodynamic microstructural reformation process.

If an end block were to be pulled completely out of its domain and interphase then it would encounter a locally homogeneous environment of matrix centre block

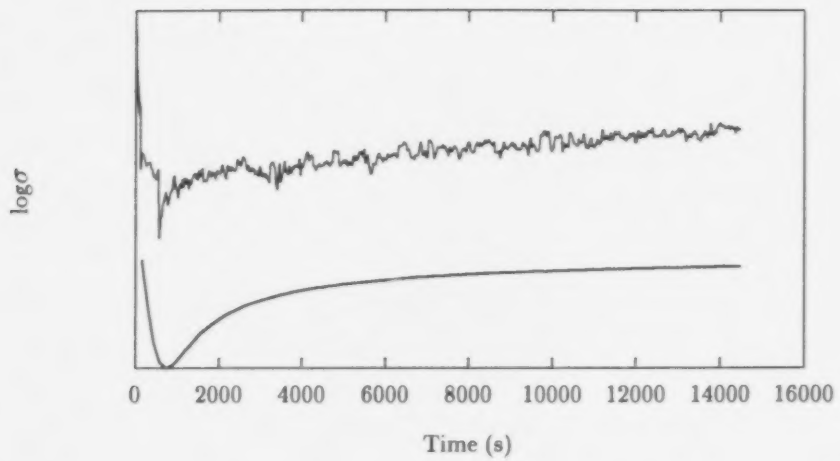

Figure 9.3: σ(t) for SBS1 at 90°C and γ=0.1% modeled as two competing exponentials.

molecules. It would then not experience any gradients which would tend to force it back towards its original position. Such an end block may by Brownian motion seek out another domain. Because of the considerable stress built up in the centre block it may recoil, like an elastic band, towards the domain in which its opposite end is anchored. Otherwise it may encounter another, closer domain. Whichever occurs, stress relaxation would be much more rapid after block pull-out, and stress recovery would not follow.

Furthermore, the trend would be towards a decrease in the number of interconnections between domains. The end block would not likely find its way back into the same domain from which it was extracted due to the recoil described above. Perhaps the block would tend to find its way into a domain in a different shear layer. What would follow would be smaller "chunks" consisting of a smaller number of interconnected domains which could move relative to other chunks. Such chunk flow would result in a lowering of modulus, and more liquid-like behaviour.

Considering the above arguments it becomes clear that the trend towards lower final modulus at higher step strains observed in these tests is due to greater microstructural damage. At strains of 0.3% and lower, end blocks are not fully extracted from their domains and so a microstructural recovery pulls the structure back towards its initial state. At higher strains, end blocks are pulled from their domains resulting in more chunk flow (liquid-like behaviour) and a relaxation which is not followed by a recovery. The drastic drop in $G_r(t)$ from 0.05% to 0.1% strain (Figure 6.5) may be explained by some critical degree of microstructural damage. Perhaps segment junctions are dragged over some locally steep portion of the composition gradient.

It was pointed out in Section 6.1.1 that for 0.1 to 0.3% step strains at 90°C the rate of recovery as indicated by the slope of the curve at long times is greater for lower strain amplitudes. To understand this result we must think not in terms of relaxation times, but rather analogous "recovery times". The time for blocks or segment junctions to migrate backwards over the composition gradient will be greater if more microstructural damage is done by the initial strain. It may then be asked why the recovery portion of the curve at γ=0.05% is not steeper than that at 0.1%. Rate processes tend to slow down approaching their equilibrium state. The $G_r(t)$ curve at 0.1% strain and 100°C (Figure 6.6) is a good example as it is recovering very quickly at intermediate times, but the slope of the curve levels off more near the end. Perhaps the curve at 0.05% strain and 90°C is closely approaching its equilibrium state and is therefore recovering at a lower rate.

It is not known whether, at each strain amplitude where stress recovery is observed, the modulus would recover to the same final value. If the 0.05% and 0.1% curves at 90°C continue to recover at the same rate as at 14,500 seconds, then they would reach the same value at approximately 2×10^6 seconds, or 23 hours. While it is not likely, as discussed above, that the curves will continue with the same slope until they intersect, the point is clear that it may require an exceptionally long test to

determine what the final state will be. If modulus would recover to the same value irrespective of strain amplitude, provided it was low enough that stress recovery was observed, then it would mean that segment junctions in general would return to their initial positions. I suspect that this is not *generally* the case, as the initial condition is probably not the equilibrium state.

So far I have discussed these effects as if each segment junction in a sample behaves the same in any given test. However, as Morrison and Winter have discussed [52], domains oriented in different directions will behave differently in shear. Just because stress recovery is observed in a test does not mean that no end blocks are extracted, but rather that fewer end blocks are extracted than at higher strains. The average microstructural damage over all domains in the sample is lower at lower strains. Therefore, I again would argue that $G_r(t)$ curves at different strain amplitudes would probably not recover to the same levels. Some stress would be permanently relieved by block pull-out and the curve would level out to a modulus, or stress, which represents the new balance of thermodynamic and mechanical forces. This then would be the yield stress which is unique to that sample history.

At 100°C (Figure 6.6) the same trend of lower final modulus with increasing strain is again followed, indicating greater microstructural damage. The exception to this trend is the curve at 0.4% strain which passes through a relaxation analogous to the entanglement regime of Figure 9.2 (d) and drops rapidly at long times in the straight line fashion of the disentangled relaxation in curve (f), which is also liquid-like behaviour. As mentioned in Section 6.1.1 the gap spacing for this test was anomalously small. During loading the sample has to be squeezed between the platens to obtain good contact with both platen surfaces. This represents a loading trauma. Although there was some variation in sample thickness after molding, the weight of polymer was kept constant to obtain a constant average thickness. If the gap is relatively small (because of greater sample "extrusion" during loading), this represents a greater loading trauma and hence more microstructural damage. That

sample was more severely damaged than others before the test was even begun.

The γ=0.2% curve at 100°C levels to a plateau like a crosslinked rubber except for a slight overshoot which may be a stress wave started by the step strain. This balance of forces represents the yield stress for this material *and sample history*. The 1% curve also levels to a yield stress, although at a lower modulus than that of the 0.2% test. As more microstructural damage was done in the higher amplitude strain, the plateau represents a different balance of thermodynamic and mechanical forces. These results are consistent with the model presented earlier. Both block pull-out resulting in stress relaxation and segment junction movement with subsequent recovery have occurred in differing ratios. At 4% strain the curve passes through the entanglement regime and into the disentangled relaxation, rapidly relaxing in a liquid like fashion towards zero. Again, much greater microstructural damage resulted from such a large strain, causing a solid-to-liquid transition.

These results demonstrate that there exists a strain magnitude (and corresponding material-dependent magnitude of shear stress) below which the solid-like structure of the material does not fail, but in fact recovers from its initial deformation. This stress level is history dependent, but it is unequivocally a true liquid phase yield stress. Since at some given shear stress the relaxation modulus first drops and then recovers it stands to reason that there also exists some shear stress for which the balance of forces results in a levelling out of the modulus to a plateau with no subsequent increase. This has been demonstrated by the tests at 100°C with strains of 0.2% and 1%.

The plots showing G_r(t) for SBS1 at constant γ_N but varying temperatures between 90°C and 110°C (Figures 6.8 to 6.11), reveal the strong temperature dependence of the properties of these materials. The curves differ significantly over what is only at 20°C range. The two most important temperatures for interpreting these dependencies are the glass transition temperature of the styrenic domains and the separation temperature. The T_g of the styrene domains is in the vicinity of

65°C—75°C as discussed in Chapter 5. The relaxation times (and by extension the viscosity), for the styrenic phase drop extremely quickly, more than exponentially, above T_g in the range of WLF behaviour (see Section 2.7) from T_g to T_g+100°C. Therefore, a 10 or 20°C increase in temperature in this case (from roughly T_g+20°C to T_g+40°C) could have a significant effect on the mobility of styrene blocks in their domains. This would allow more rapid relaxations, but also more rapid recovery. In addition, elastomeric forces become stronger at higher temperatures. This relationship is linear with temperature so that an increase from 90°C to 110°C would result in a 5% increase in elastomeric forces.

The second temperature of importance is T_s. Thermodynamic forces of structure formation would increase as temperature is dropped further below T_s. The "desire" to microphase-separate would be stronger at lower temperatures. This temperature dependence would in general be difficult to quantify; however, the test temperatures from 90 to 110°C were much further from T_s (=243°C) than from T_g, and so it is suspected that temperature variation effects associated with T_g would be stronger.

In reference to Figure 6.8, comparing relaxations at γ_N=0.1% for 90°C and 100°C, at 100°C modulus initially drops as much as four times lower than at 90°C, but by 3500 seconds the two curves are coincident until the end of the test. This indicates more rapid relaxations and recoveries at the higher temperature, due to lower viscosities and higher elastomeric forces. The fact that the curves are coincident from 3500 seconds seems to suggest that at γ_N=0.1 the same magnitude of structural damage is incurred at the two temperatures, so that temperature variations (over this narrow range) affect only the early rates of stress changes but not the recovered structure itself.

At γ_N=0.2% (Figure 6.9), modulus varies by a factor of 7 over a temperature range from 90°C to 110°C. For an ideal rubber, modulus would scale proportionally with temperature, but as noted above this would result in only a 5% variation. This suggests a temperature dependence more dominated by T_g effects.

When γ_N=1% we see in Figure 6.10 the full range of behaviour by the end of the test. At 90°C the curve is relaxing, while at 100°C the curve has levelled out, and at 110°C it is recovering. The data of Figure 6.8 at γ_N=0.1% suggested that the same magnitude of structural damage is incurred at the two test temperatures, provided that γ_N is constant, resulting in recovery to the same final state, though the rates are different. As relaxations and recoveries are both faster at higher temperatures, it seems likely—following the above reasoning—that at γ_N=1% the recovery observed at 110°C would also occur at 100°C and 90°C, but would be delayed to longer times.

At γ_N=4% (Figure 6.11) we despair of the curves ever recovering, as by the end of the test the 100°C and 110°C curves have passed the "entanglement" plateau and are curving downwards indicating liquid-like, rather than solid-like, character. By the above arguments (for γ_N=0.1% and 1%) it seems likely that the curve at 90°C will also drop off at longer times. As mentioned earlier, these curves come close to being superimposable by a shift along the time axis. Time-temperature superposition is generally considered invalid for phase separated block copolymers [2, 10, 20, 22]. Therefore, the potential for superposition after such large deformations is additional evidence that the long-range microstructural network has been fatally altered, as superposition by time-shifting should only be possible for "rheologically simple" materials.

A word should perhaps be said about "large" deformations in these materials. Immediately above, I spoke of "such large deformations", because 4% is the largest γ_N used in this test series. But remember that this is a fractional strain of only 0.04. It is incredible to think that such a small deformation can cause such a profound microstructural change. These materials are ultra-sensitive to their strain history.

9.2.2 SBS2

In Section 6.1.2 it was demonstrated that for all step strain amplitudes performed on SBS2 the stress dropped rapidly to zero and remained there. Plotting modulus against time on log-log coordinates as in Figure 9.2 produces in each case a straight line. The behaviour is that of an unentangled short chain polymer or else an entangled long chain polymer which has already relaxed beyond its glassy and entanglement regimes before the first data point is internally logged. In Figure 6.18 the relaxation of SBS2 is compared to the behaviour of SBS1 at the same temperature and strain. The peak modulus (approaching the short-time glassy limit) for SBS2 is significantly higher, as is consistent with the higher styrene content. At 44% styrene the structure of SBS2 would be lamellar while that of SBS1 at 30.4% styrene would be cylindrical. The lamellae, being continuous in two spacial dimensions, should have a greater reinforcing effect in the solid state than cylinders which are continuous in only one dimension (speaking in terms of flexural stiffness and shear modulus, not tensile strength) so it is not surprising to see a higher peak modulus in SBS2. What is surprising is how it rapidly drops below the curve for SBS1.

The styrene end blocks in SBS2 each have a molecular weight of 13,480, compared to only 10,550 in SBS1. The higher molecular weight of the styrenic blocks should result in a slower relaxation for SBS2 than SBS1. However, the reverse is observed. Therefore, the end block molecular weight cannot be the cause of the differences observed.

The molecular weight of the butadiene centre block in SBS2 is 34,320 while that in SBS1 is 48,320. The critical (entanglement-onset) molecular weight of bulk polybutadiene is 6380 [11] so that the centre blocks in both samples have MW> M_c. Therefore, viscosity and hence relaxation times would vary according to the 3.4 power rule. The relaxation times associated with the polybutadiene entanglements

would therefore be 3.2 times greater in SBS1 than SBS2. However, it will be demonstrated later that the relaxations associated with centre block entanglements are not the longest or controlling relaxation times of the material.

In addition to the greater *speed* of stress relaxation in SBS2, another qualitative difference relative to SBS2 is the apparent absence of microstructural repair. No recovery of modulus is seen in SBS2 while the recovery in SBS1 at the same temperature and strain amplitude is clearly evident. The degree of microstructural recovery would be dependent on the overall thermodynamic balance. The relative molecular weights of the end and centre blocks as well as the overall molecular weight would influence that balance; however, it is not suspected that the difference in centre block molecular weight is the direct cause of the difference in thermodynamic recovery. T_s would be the best overall measure of the thermodynamic balance, and that of SBS2 is more than 10°C higher than that of SBS1 (255°C *vs.* 243°C). This should lead to *stronger* thermodynamic driving forces in SBS2 than SBS1 at the same temperature, provided it was below T_s. This point also seems to be violated here. Therefore, the differences in the behaviour of these two samples are not primarily due to the centre block molecular weights.

The key to understanding this profound difference in the behaviour of these two polymers, which initially seem so similar, appears to be the differences in interphase character. Henderson and Williams [34] predicted that interphase thickness increases with increasing styrene content. The theory was only done for lamellar microstructures; however, there is no reason why interphase thickness would suddenly change on transition to a cylindrical morphology. Therefore, it can be concluded that the interphase thickness in SBS2 (44% PS) is greater than that in SBS1 (30.4% PS). With a broader interphase, the average composition gradient and hence force barriers in SBS2 would be lower. This would result in easier block extraction and smaller σ_y. Therefore, any strain amplitude in the range of SBS2 testing causes greater microstructural damage through a greater number of block

extractions than the same test performed on SBS1. This results in more rapid relaxations and little or no microstructural recovery.

9.2.3 SIS

For SIS at 110°C Figure 6.19 shows again that greater strain amplitudes do more microstructural damage resulting in lower final moduli. In the case of 0.2% and 0.4% strain the modulus reaches a plateau at long times. At 0.1% strain there appears to be a slight recovery, although the test was terminated early. Recovery in general is weaker for SIS than for SBS1. The final modulus was only 0.9% of the peak modulus for a 0.1% step strain and only 0.4% of peak modulus for a 0.2% step strain. This is much lower than 3.5% of peak modulus for a 0.2% strain at 110°C for SBS1. Furthermore, comparing G_r for both SBS1 and SIS at the same temperature and γ_N reveals that SIS relaxes faster than SBS1. At 110°C and γ_N=0.2% (Figures 6.7 and 6.19), at t = 100 s SIS has relaxed to a modulus of 4,700 Pa while that of SBS1 is 11,000 Pa, or more than twice as high though the peak modulus of SIS was only about 12% lower than that of SBS1. Therefore, relaxations are faster and recovery is weaker in SIS than in SBS1.

In order to explain this we compare the two polymers. The thermodynamic driving forces are characterized by both T_s and interphase characteristics. T_s of SIS (255°C) is higher than that of SBS1 (243°C). This would argue for stronger driving forces towards the phase separated state, thus longer relaxations and stronger recovery for SIS over SBS1, thus this is opposite to the trend observed. SIS, having an even lower styrene content than SBS1 (14% *vs.* 30.4%) should also have narrower interphases than SBS1, and thus higher average gradients in the interphase. this also would argue for longer relaxation times and stronger recovery in SIS than in SBS1. The styrene block molecular weights are around 10,000 for both SIS and SBS, so this cannot explain the difference.

The explanation appears to lie with the molecular weight of the centre blocks. In SIS the centre block has a molecular weight of 120,000, while in SBS1 it has a molecular weight of 48,000. This results in 2.5 times the density of entanglements in the SIS centre block over that in the SBS1 centre block. This greater entanglement density results in a more effective transmission of stress through the viscous medium *at the same strain amplitude*. At short times, as the glassy limit is approached, the stress resulting from the high strain rate during the initial strain tansient would be more effectively transmitted through the material, resulting in more block pull-out and more chunk formation. Therefore, the microstructure of SIS is more damaged than that of SBS1 (at the same strain amplitude) before the first data point is logged.

It was determined in Section 6.1.3 that at a nominal test temperature of 90°C the data at all γ_N in the range tested would likely superimpose, or come close to superimposing, if the temperature were consistently 90°C. In the discussion on the temperature dependence of relaxation behaviour in SBS1 the data indicated that the final state should be the same at all temperatures, provided that γ_N is kept constant, but that the rates of relaxation and recovery are temperature dependent. Figure 6.19 shows that the data at all γ_N at 110°C also superimpose very closely between t=14 and 200 seconds. Therefore, it is likely that the data at 90°C would show the same classification according to strain amplitude if the test were continued for a longer time.

9.2.4 Peak Moduli

In Chapter 6 a trend was noted in the magnitude of the modulus at the time of the peak stress *i.e.*, immediately at the end of the strain transient. The trend is consistently towards lower peak moduli with increasing strain for SBS1, SBS2 and SIS, the only exceptions being the peak moduli at γ_N=4%, which are always slightly

greater than those at the next-to-largest strain amplitude at the same temperature and for the same material, but still lower than those at the lowest γ_N in the series.

In the glassy limit the stress should scale proportionately with strain *i.e.*, Hookean behaviour. However, for viscoelastic materials this could only be achieved with an infinite strain rate from $\gamma = 0$ to $\gamma = \gamma_N$. In the case of my experimental data, there is already some degradation of structure by the time the peak is reached, resulting in a lower peak modulus. However, the strain rate $\dot{\gamma}$ is greater for each higher γ_N (since the time of deformation is about the same for all tests, $\Delta t \approx 0.1$ s), and modulus tends to increase with increasing $\dot{\gamma}$ for viscoelastic materials. This can explain the trend of increasing modulus from the next-to-largest γ_N to γ_N=4% in each test series. The ratio of γ_N=4% to the next-to-largest strain amplitude is in each case the largest ratio between successive strain amplitudes in the series, resulting in the largest ratio of $\dot{\gamma}$ also. Therefore, while the increased γ_N has indeed resulted in increased microstructural damage, the viscoelastic $\dot{\gamma}$ dependence has "caught up" with the loss in modulus due to strain amplitude.

9.2.5 Relaxation Times

Relaxation times were fit to several $G_r(t)$ curves by the method of Ferry. The method is described in detail in Appendix C. The fit in each case is of the form

$$G_r = G_1 e^{-t/\lambda_1} + G_2 e^{-t/\lambda_2} + G_3 e^{-t/\lambda_3} + \ldots \tag{9.2}$$

where λ_i's are relaxation times corresponding to a fluid model having several Maxwell elements. Figure 9.4 shows the fit of

$$G_r = 15,800 e^{-t/600,000} + 5,500 e^{-t/5,800} + 31,000 e^{-t/436} + 50,000 e^{-t/70} \tag{9.3}$$

to the curve at 90°C and 1% strain, where t and λ_i are in seconds and G_i are in Pa. However, Equation 9.3 is not an ideal fit as can be seen by the deviation between

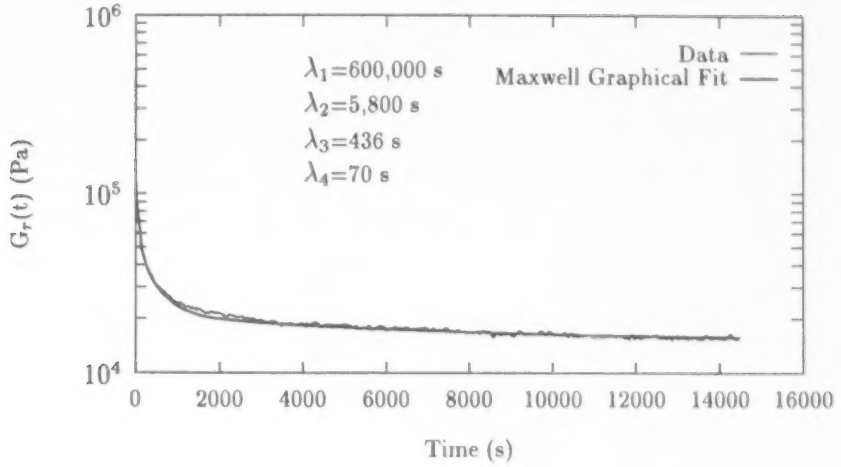

Figure 9.4: Graphical fit of relaxation times for SBS1 at 90°C and γ=1%.

roughly 200 and 3000 seconds. Because both relaxation and recovery are occurring, it is not surprising that a simple series of relaxing Maxwell elements will not fit the curve perfectly. The curve

$$G_r = 25,000e^{-t/12,500} + 30,000e^{-t/318} + 50,000e^{-t/47} \quad (9.4)$$

shown in Figure 9.5 fits the early relaxations better. In this time range the recovery is not dominant, and so a series of relaxing Maxwell elements fits the curve well. However, both short and long time portions of the data cannot be perfectly fit by a single curve representing relaxing Maxwell elements. Despite the deficiency of the fit, it can still be derived from Equation 9.3 that the longest relaxation time observed over the duration of the test was 6×10^5 seconds, or almost 7 days.

For a 4% step strain at 90°C the curve is well fit by

$$G_r = 12,800e^{-t/163,241} + 8,000e^{-t/3,654} + 20,000e^{-t/500} + 45,000e^{-t/131} \quad (9.5)$$

as shown in Figure 9.6. This reveals the longest relaxation time to be just over

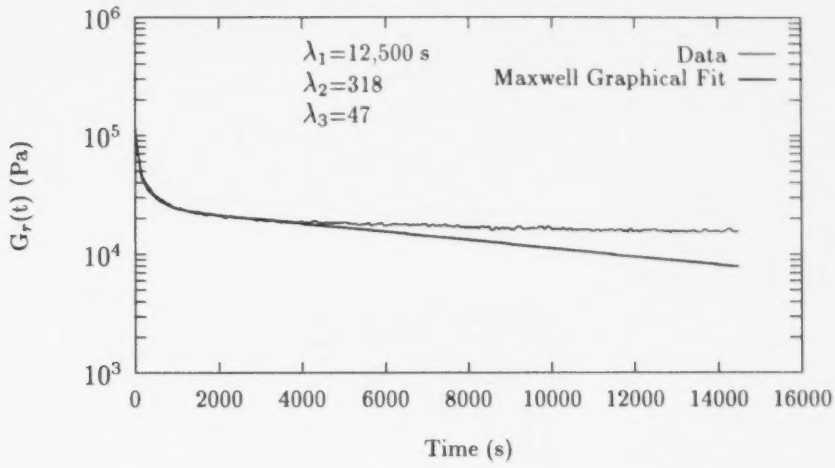

Figure 9.5: Graphical fit of short time relaxation for SBS1 at 90°C and γ=1%.

1.63×10^5, or less than 1/3 of the largest λ for a 1% strain. The more rapid relaxation is because of greater microstructural damage.

At 100°C and γ=1% the fit

$$G_r = 9,000e^{-t/231,866} + 5,000e^{-t/1,067} + 10,000e^{-t/160} + 19,000e^{-t/41} \quad (9.6)$$

shown in Figure 9.7 reveals the largest λ to be 231,866 s, or less than half that at 90°C and the same strain amplitude, which is a qualitatively expected trend. At 110°C and 4% strain Figure 9.8 shows an excellent fit to Equation 9.7

$$G_r = 4,250e^{-t/33,357} + 3,700e^{-t/2,500} + 5,500e^{-t/340} + 3,000e^{-t/99} \quad (9.7)$$

which reveals the longest relaxation time to be only 3.3×10^4 s, or roughly 20% of that at 90°C and the same strain. It is to be expected that relaxation times at higher temperatures would be shorter as viscosities drop.

The dramatic difference between SBS2 and SBS1 is again emphasized by

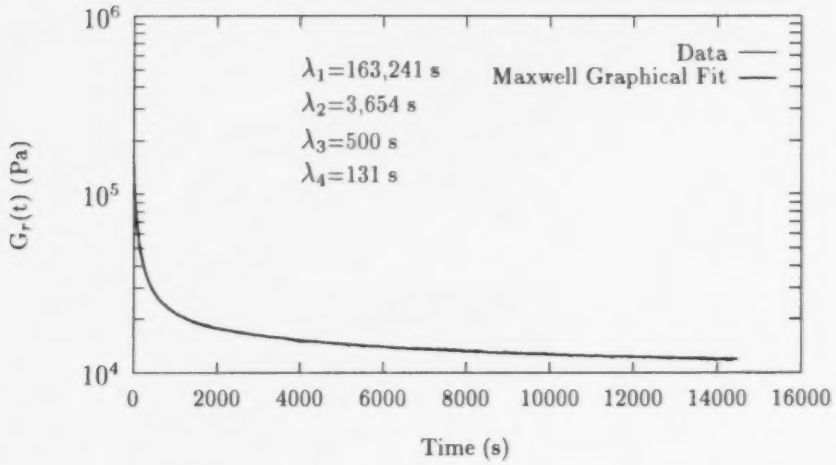

Figure 9.6: Graphical fit of relaxation times for SBS1 at 90°C and γ=4%.

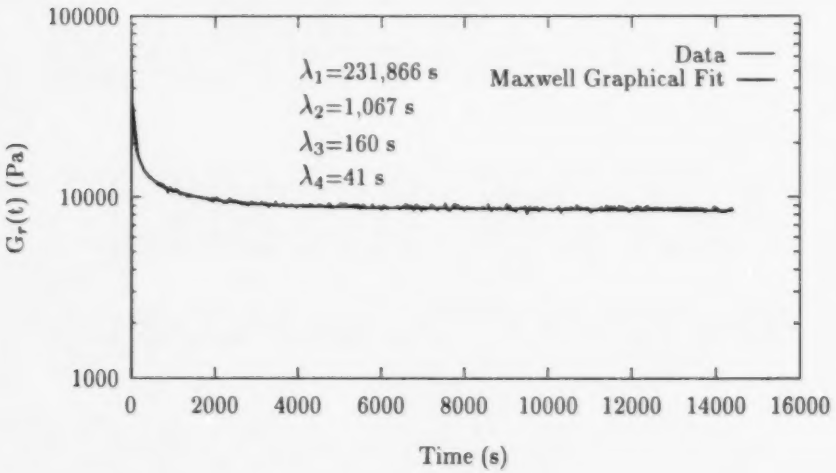

Figure 9.7: Graphical fit of relaxation times for SBS1 at 100°C and γ=1%.

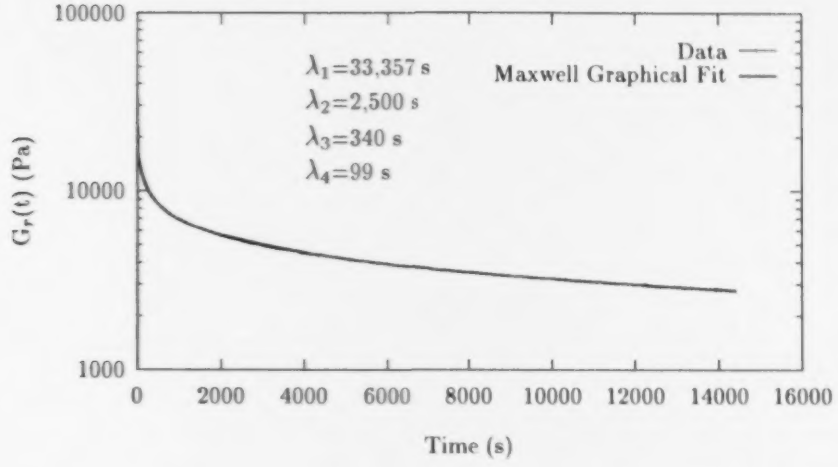

Figure 9.8: Graphical fit of relaxation times for SBS1 at 110°C and γ=4%.

considering the 110°C relaxation times. From the fit of SBS2 data by

$$G_r = 2,000e^{-t/2,100} + 7,000e^{-t/278} + 15,000e^{-t/72} \tag{9.8}$$

shown in Figure 9.9 for a 1% step strain at 110°C, we derive the largest λ to be only 2,100 s, much shorter than λ_1=33,357 of SBS1.

For SIS the curve at 110°C and 1% strain was best fit overall by

$$G_r = 600e^{-t/11,000} + 2,000e^{-t/1,905} + 2,000e^{-t/296} + 2,000e^{-t/62}. \tag{9.9}$$

However, as seen by Figure 9.10, Equation 9.9 was not a perfect fit.

The short time data, where the competing recovery is not dominant, is fit very well by

$$G_r = 1,450e^{-t/4,850} + 1,900e^{-t/979} + 35,000e^{-t/81} \tag{9.10}$$

as shown in Figure 9.11. Once again, pure relaxing Maxwell elements will not fit this curve.

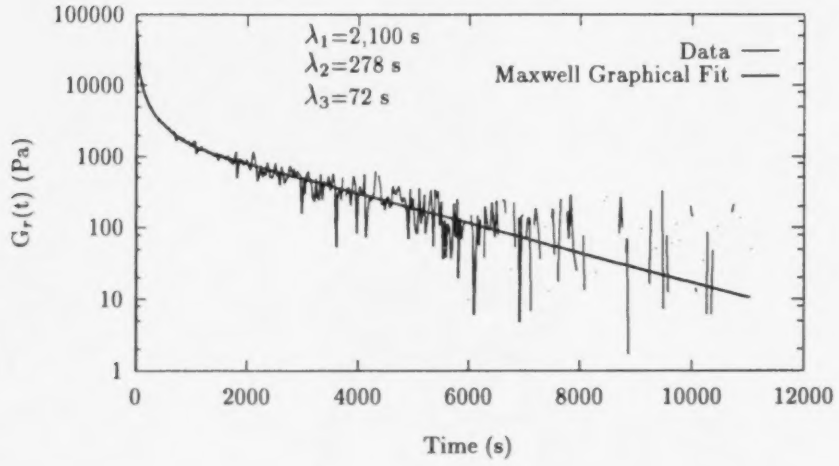

Figure 9.9: Graphical fit of relaxation times for SBS2 at 110°C and γ=1%.

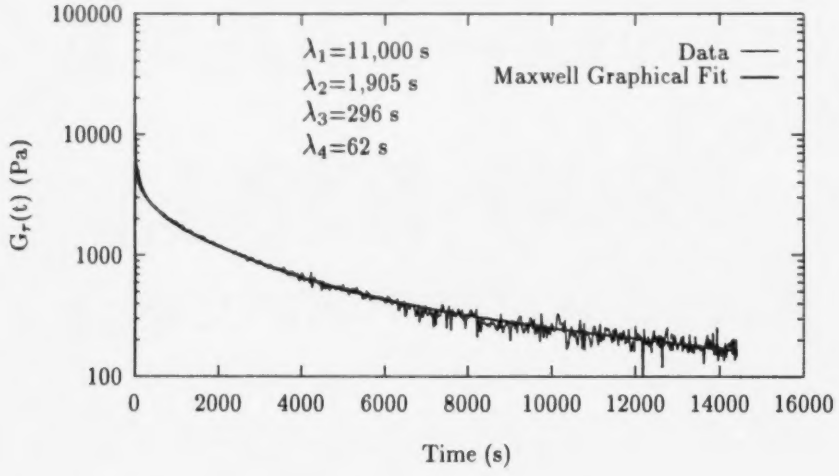

Figure 9.10: Graphical fit of relaxation times for SIS at 110°C and γ=1%.

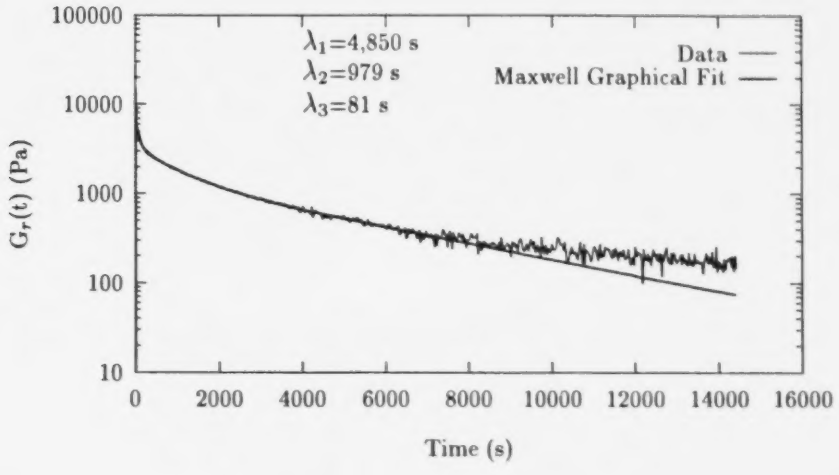

Figure 9.11: Graphical fit of short time relaxations for SIS at 110°C and γ=1%.

At 90°C and 1% strain the SIS curve is best fit by

$$G_r = 4,100e^{-t/18,458} + 6,000e^{-t/773} + 31,000e^{-t/124} \tag{9.11}$$

as shown in Figure 9.12. We can derive from equation 9.11 that the largest λ is 1.85×10^4. The rubbery (polyisoprene) centre block in SIS has a molecular weight of 120,000, much higher than that of the SBS1 centre block which is 34,320. Polyisoprene, with an extra pendant methyl group, would have a higher viscosity and longer relaxation times than polybutadiene of the same molecular weight. However, for the purposes of this comparison we will consider them identical and only consider molecular weight effects, as the higher viscosity of polyisoprene only serves to strengthen the following argument. Following the 3.4 power rule, the relaxation times of the rubbery centre block in SIS should be roughly 70 times as great as those of the rubbery centre block in SBS1. Instead, the largest relaxation time in SBS1 at 1% strain and 90°C is roughly 32 times that of SIS under the same conditions—opposite to the expected trend. This demonstrates unequivocally that

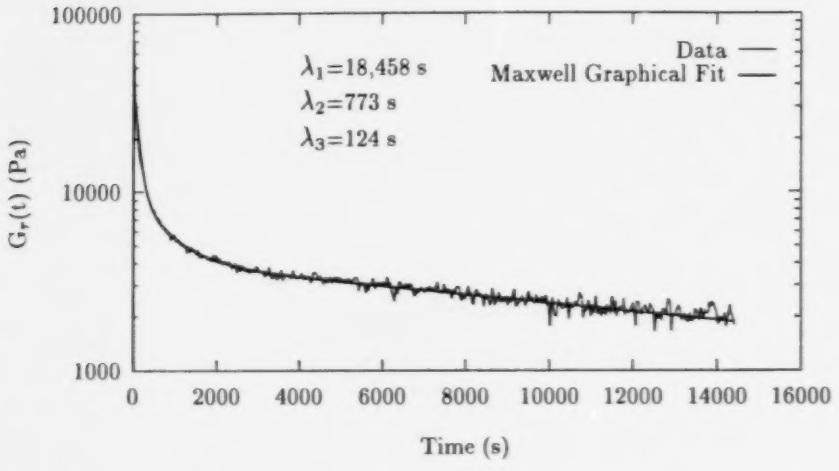

Figure 9.12: Graphical fit of relaxation times for SIS at 90°C and γ=1%.

the relaxation times associated with the entanglements in the rubbery centre block are not the controlling, or longest, relaxation times in these materials.

Earlier it was demonstrated that the relaxations associated with the viscosity of the styrenic phase are also not controlling, provided the sample is at a temperature above T_g. Therefore, the long "relaxation" times must be associated with the motion of segment junctions through the composition gradient of the interphase *i.e.*, with structural repair whose kinetics is dominated by the interphase force barriers.

9.2.6 SBS3 and SEBS

As described in Section 6.1.4, the relaxation times of SBS3 and SEBS are extremely long, so long that they cannot be effectively loaded into the rheometer. The overall molecular weight of SBS3 is 101,225, less than that of SIS. The styrene content is only 31%, or roughly the same as that in SBS1. For SEBS the molecular weight is even lower at 67,000 and the styrene content is again on par with that in

SBS1. Therefore, neither the molecular weights nor the styrene contents could be individually responsible for the long relaxation times.

However, the predicted separation temperatures listed in Table 5.1 are 482°C and 839°C respectively for SBS3 and SEBS. These are higher than for any other polymer tested. Such high separation temperatures reflect the very high thermodynamic driving forces towards the phase-separated state encountered at our loading temperatures, which went as high as 300°C in an attempt to load the samples. This results in very long relaxation times, as the driving forces retard the motion of blocks from the microphases into the matrix. The thermodynamic driving forces, and hence the separation temperature, are particularly high for SEBS because of the higher $\Delta\delta$ between the centre and end blocks. Futamura and Meineke [20] quote the value of $\Delta\delta$ between styrene and ethylene/butylene as 0.8 $(cal/cm^3)^{1/2}$ and between styrene and butadiene as 0.5 $(cal/cm^3)^{1/2}$. Leary and Williams [44] found 0.8 $(cal/cm^3)^{1/2}$ to be the most accurate value for $\Delta\delta$ between PS and PB; however, they did no calculations on SEBS.

9.3 Step Rate Tests

Other evidence of the network response of these materials to a shear strain was obtained from a series of step rate tests described in Section 6.2. At the lower strain rate of these tests the trauma to the network during the transient is much less severe. Therefore, less damage would be done to the network. However, what these data tell us about the character of the network is unclear at this time.

9.4 Nonlinear Waveforms

The strain sweeps in Figure 7.1 and Figure 7.2 reveal how sensitive the microstructures of block copolymers are to shear. The linear region is by definition

the region of strain in which the microstructure of the material being tested is unaffected by the test. This region is indicated by strain-invariance in a property such as η^* which is an effective probe of the structure. Many researchers studying block copolymer rheology claim to be testing in the linear viscoelastic region; however, test results presented here fail to display any truly linear range. A normal rule of thumb which is used in selecting the linear range is to define anything less than 5% variation in the property as being invariant. This would be acceptable if the variation were random around a mean, but that is not the case with this data.

Considering Figure 7.1, a strain sweep on SBS4 at 30°C, in the range from γ° =0.06% to 0.7% the complex viscosity drops only slightly. It would be tempting to select this as the linear region; however, the more drastic drop from γ° =0.02% to 0.06% indicates that at these amplitudes the structure is already affected by the test. Within the sensitivity of our equipment, which includes one of the most sensitive transducers on the market, it was not possible to reach the linear region with a bulk block copolymer sample at this temperature. A linear region was equally evasive with SBS1 at this temperature. As has already been discussed, any deformation of the interphase imposes a thermodynamic change, driving it into non-equilibrium. Therefore, a new microstructure prevails as soon as we make a measurement. For this reason, it may not be possible to reach a true linear range with these materials.

Above γ_{cr} something more drastic occurs. The waveforms cease to be sinusoidal. The nature of these waveforms will be discussed in detail shortly. As pointed out in Section 7.1 the exact magnitude of γ_{cr} is difficult to pinpoint from this data; however, for SBS1 at 30°C $0.1\% < \gamma_{cr} < 0.20\%$.

The frequency/temperature sweep on SBS1 displayed in Figures 7.3 and 7.4 was performed at γ_N° =0.5%. It was determined in Section 7.2 that γ° did not exceed 0.45% for γ_N° =0.5%. This is above γ_{cr} ($0.1\% < \gamma_{cr} < 0.20\%$) **at 30°C**. However, as will be demonstrated later, γ_{cr} in general increases at higher temperatures. Therefore, at all temperatures in this sweep ($T > 150$°C) γ° can be considered

to be below γ_{cr}.

For all $T \geq$150°C the SBS1 curves of $\eta'(\omega)$ and $\eta''(\omega)$ curve upwards at lower frequencies demonstrating the yield stress character of the material. Both η' and η'' gradually decrease with increasing temperature, as is to be expected since the microstructure is becoming more fluid. However, it is interesting that at 211°C and 221°C the curves are almost coincident, so that the viscosities seem to be approaching some limit. At lower temperatures the styrenic domains act as reinforcing fillers in the rubbery matrix, since their viscosity (η^S) is so high when T is not far from T_g^S. At higher temperatures their contribution is much different; since the molecular weight of the styrenic blocks is below M_c=37,400 [52], these end blocks are not entangled, hence there is no network enhancement of η^S according to the 3.4 power rule. The result is that $\eta^S(T)$ drops off rapidly, perhaps even dropping below that of the rubbery matrix, which is entangled, so that the contribution from the filler effect is negligable.

At temperatures of 150°C through 191°C the higher-frequency viscosity drops off, not levelling to a constant as in Figure 2.9. Similar behaviour occurs also in homopolymers as a consequence of normal viscoelasticity and perhaps nonlinear effects. We have already discussed the strain dependence of viscosity for structured materials; however; even for unstructured fluids there is a nonlinear strain rate effect as $\eta(\dot{\gamma}) = \eta(\gamma \cdot \omega)$. Therefore, high frequencies at constant γ^o can have the same nonlinear effect on viscosity as high strain amplitudes at constant ω.

We now turn our consideration to the shapes of the waveforms. Figure 7.5 shows the strain and stress response for a test at 25.6°C, γ^o =2% and ω=1 rad/s. The test was performed on SBS1 as were all of the tests discussed here. In the intermediate range of stress from roughly -4000 Pa to 1000 Pa (remembering that stress is not oscillating around zero) the response appears to be sinusoidal and roughly in phase with γ. The exact phase of the stress cannot be determined unless a zero line is established which is difficult to do with a nonsinusoidal waveform; however, the

input and output waves are very close to being in phase, indicating a solid-like response. At roughly 1000 Pa a bite becomes evident on the rising side of the stress wave. Rather abruptly stress ceases to increase as rapidly as it would if it followed a sinusoidal form. The falling side of the stress response is sinusoidal—or *linear*.

Here we are going to run into a problem in our terminology. Until now I have referred to the *linear* region as the region of strain invariance of a property. However, in a strain range where properties are not invarient the waveforms may still be pure, or sinusoidal. Herein lies the difficulty; nonsinusoidal waveforms are referred to as *nonlinear* waveforms, and will be so referred to in this discussion, because a sinusoid is a *linear* function.

Recall that the solid-like character of this material is a result of its network structure. If this network is stressed to some critical degree so that segment junctions in the interphase are suddenly able to move over some local free energy gradient then the rate of stress growth would abruptly decrease as is observed here. As stress decreases with strain (on the falling side of the waveform) then segment junctions would return to their original positions which are thermodynamically favoured. Another way of stating this is that the onset of nonlinearity represents the overcoming of the yield stress—that is, a yield stress related to a force barrier arising from a composition gradient.

An alternative interpretation of these data which may be proposed is based on slip at the platen surfaces. Above a critical stress the material may begin to slip, which would cause a lower rate of stress growth and, possibly, similar waveforms. However, it was found that after a sample had been loaded between the platens, it acted as such a strong adhesive that at low temperatures (below about 100°C) the platens could not be separated manually, in the limit of normal human strength. That is not meant to flatter myself, but my strength is certainly sufficient to send the transducer off scale (with ease), but not near sufficient to separate two platens stuck together by a block copolymer sample. Such strong adhesion seems to argue

strongly against any slip occurring at the platen surfaces.

The stress response is not symmetric about the zero axis. That is, peaks and troughs, or stress peaks in opposite directions, are not identical. This may represent an incompletely healed microstructure which is being stressed in the opposite direction and hence responding differently.

The role of ω is important and sometimes puzzling. We first consider the extreme values, ω=10 and 10^{-2}, for the same polymer (SBS1) at the same temperature and strain amplitude. Figures 7.9 and 7.10 show that the stress response is sinusoidal, or linear, at both 0.01 rad/s and 10 rad/s. At 0.1 and 1 rad/s it seems that a frequency range was found which probed the relaxations associated with junction motions through the composition gradient of the interphase.

At 43.2 °C it was necessary to increase γ^o to 2.5% in order to obtain nonlinear waveforms. The yield stress would decrease with increasing temperature as more thermal energy is provided to overcome the free energy gradient. However, stress amplitude decreases with increasing temperature at constant strain amplitude. Therefore, if the decrease in the yield stress on increasing the temperature is less than the decrease in stress amplitude at the same γ^o then a higher γ^o would be required to obtain nonlinear waveforms at higher temperatures.

At 43.2°C Figures 7.11 through 7.14 show that the onset of nonlinearity in the peaks at 0.01 rad/s and 1 rad/s occurs at around 100 Pa, a lower stress than at 25.6°C and 1 rad/s. This is consistent with the model proposed above. Higher temperature provides more thermal energy to lower the free energy gradient. The shape of the curve is different than that at 25.6°C. There are several inflection points on the rising side of the stress peak rather than just one as at 25.6°C. Remembering that any deformation changes the character of the interphase somewhat and thus influences the response immediately following, the shapes of these peaks are probes of what is happening to the interphase upon deformation. However, this time-varying fingerprint would in general be difficult to quantify.

At 10 rad/s (Figure 7.11) the onset of nonlinearity in the peaks is at a higher stress, about 1000 Pa. Relaxations associated with junction movement through the interphase would be more severely challenged at higher strain rates. Therefore, it stands to reason that stress would reach a higher level before these relaxations occur. At 0.01 rad/s (Figure 7.14) the response is linear. Again there exists a frequency at which the relaxations associated with the nonlinear phenomena are not probed.

For a temperature of 60.5°C at 2.5% strain and frequencies of 0.1 and 1 rad/s (Figures 7.15 and 7.16) the onset of nonlinearity in the peaks is around 1000 Pa. This is higher than the onset at 43.2°C , all other conditions being the same. This may be representative of the average over the specific portions of the composition gradient throughout the sample that are being challenged at this particular temperature, frequency and strain amplitude. At 10 rad/s (Figure 7.17) the onset is again higher at the same γ^o because the relaxations are challenged more severely. At 100 rad/s $\gamma^o < \gamma_N^o$ =2.5% and the nonlinearity is less pronounced. Figure 7.19 shows that at 0.01 rad/s the response is linear as the relaxations associated with the nonlinear phenomena are again not probed.

The only test temperatures above T_g^S at which waveforms were digitized were around 97°C. (Below T_g^S the styrenic domains are rigid rather than fluid.) Although the glassy domains are not solid, strictly speaking, the relaxations associated with end block motion through these microdomains are extremely slow. Therefore, motions of segment junctions can be accomplished only through a straightening of the randomly coiled chain segments local to the junctions. This complicates the matter somewhat and our understanding of these phenomena is admittedly incomplete. Above T_g^S, as will be demonstrated, the peaks and troughs are still not symmetric about the zero stress axis, but the trends are more regular and more easily interpreted.

At 96.7°C it was necessary again to increase the strain amplitude in order to obtain nonlinear waveforms. In Figures 7.20 through 7.22, then, γ^o =2.9%.

Comparing Figure 7.20, a test at 0.1 rad/s, to Figure 7.21 at 1 rad/s, it is immediately obvious that at the higher frequency the response is nonlinear while at the lower it is linear. The nonlinearity at 96.7°C and 1 rad/s is more pronounced than at any lower temperature; the tops and bottoms of the waveform are almost plateaus. At 0.1 rad/s the peak to trough stress is 2925 Pa. At 1 rad/s the magnitude of the stress from the onset of nonlinearity in one direction to that in the other is 3300 Pa, greater than the linear peak to trough height of 2925 Pa at 0.1 rad/s. In general, in dynamic polymer testing stress amplitude increases with increasing frequency at the same strain amplitude because the relaxations are more severely challenged.

Here then it is easy to see that nonlinearity is initiated above some critical yield stress. Above the yield stress, flow occurs readily as stress hardly increases at all beyond the stress necessary to reach σ_y. The flatness of the peak associated with post-yield flow ends abruptly when the strain reaches its maximum. At 10 rad/s (Figure 7.22) the response is very similar, with a slightly greater shoulder-to-shoulder height, as is consistent with a higher frequency challenging the relaxations to a greater extent.

The shear sensitivity of this material is demonstrated by the next series of test results. After tests at 96.7°C, the temperature was dropped to 25.6°C again. Tests were performed at the same amplitude as the first series: γ° =2%. However, the stress response was drastically different. Examining Figures 7.23 to 7.25, we see that the tops and bottoms of the waveforms are very flat, but that at the onset of nonlinearity there is a stress overshoot and a decaying wave. This is some kind of an elastic recoil associated with overcoming a barrier to flow. Straining the material when $T > T_g^S$ (*i.e.* , at 96.7°C) caused a morphological change which drastically altered the response at subsequent lower temperatures. At an increased strain amplitude of 3% the elastic recoil at the shoulders is even more drastic (Figure 7.26).

This general $\sigma(t)$ shape is displayed in stress responses from a series of tests which followed those discussed above. The results are displayed in Figures 7.27 through 7.33, but no further explanation is offered here for these complex waveforms.

The final series of tests was performed at 96.5°C, again above T_g^S. The strain amplitudes tested were 3.5% and 5%. The resulting curves follow the same pattern as previously discussed at a similar test temperature. Consider first the series at γ^o =3.5%, at frequencies of 0.01 and 0.1 rad/s (Figures 7.34 and 7.35): the stress amplitudes are low and waveforms are linear. Increasing ω to 1 rad/s Figure 7.36 shows that the stress amplitude exceeds the yield stress and the result is almost flat wave tops. The stress at which the material yields is higher at 3.5% strain than at 2.9%, which goes to demonstrate again that the yield stress is dependent on the shear history of the material and/or the conditions of testing because the material character changes as it deforms. At 10 rad/s (Figure 7.37) the shoulder to shoulder height is again slightly higher than at 1 rad/s due to the challenge to relaxation times which has already been discussed. At γ^o =5% the same patterns are followed (Figures 7.38 through 7.41) and no further explanation is needed.

9.5 Phase Transition Phenomena: A Speculative Discussion

In Chapter 8 rheological phenomena in the vicinity of the phase separation temperature were examined. Figure 8.2 shows the results of a temperature sweep on G' and G'' of SBS4 solvated with 50% 5 base oil. The solvation depresses T_s as predicted by Pico [59, 57]. The transition is evident between 75°C and 90°C. The microstructure is more solid below T_s and more fluid (or non-existent) above T_s as indicated by the initially high storage to loss modulus ratio, inverting above the transition.

As pointed out previously, these results have been reported before. However, a second sweep with smaller temperature steps (Figure 8.4) points to some odd behaviour in the transition region at low frequencies. At 0.1 rad/s η^* jumps erratically above T_s.

I offer here some provocative ideas for the interpretation of these results. In the transition region ($T \approx T_s$) microstructure is on the cusp of the thermodynamic balance which, when pushed in one direction, results in phase separation and in the other homogenization. Perhaps a low frequency (long wavelength) dynamic strain which challenges long relaxation times associated with large scale structure interacts with the thermodynamics to cause some kind of bifurcation between the two states. In such a state of transition the microstructure might not respond linearly. That is, the waveforms could be nonlinear resulting in spurious results. On the other hand, the values of η^* may be valid, derived from truly linear waveforms.

At higher frequencies the anomaly first diminishes in magnitude (1 rad/s) and then disappears altogether as the curves at 10 and 100 rad/s drop off directly as previously reported in the open literature. High frequencies probe shorter-range relaxations which would not be as much affected by the bifurcation between phase structures.

Further evidence of odd behaviour in the transition region was also described in Chapter 8. That is, the unstable normal force control loop which occurred while heating a bulk sample in the transition region. As the material passes through the transition from phase separated to homogeneous microstructure a volumetric change would occur. Specific volume should abruptly increase which would cause an abrupt increase in normal force. The normal force control may then over-compensate, raising the platen too far in an attempt to relieve this stress. This overcompensation would result in a large negative normal force which the control sequence would attempt to counteract by lowering the platen rapidly, once again overcompensating, and the process might continue with normal force oscillations of ever increasing

amplitude until the transducer is forced off scale and the instrument shuts down. At 230°C the material was certainly below the measured T_s of 243°C. However, only a truly monodisperse sample would have a sharp transition temperature and it is widely recognized that the phase transition is not sharp [62, 45]. Therefore, the transition (at least, the concentration fluctuations) would begin below the average T_s and end at some higher temperature.

There is another possible interpretation which is even more provocative. Perhaps the normal force on the sample was interacting with the thermodynamics of phase separation. In that case, not only would the normal force have been overcompensating, but the structure may have been bifurcating between the phase separated state and some stage of homogenization. That is, if the force on the sample had influenced the thermodynamic driving force towards homogenization then a sudden release of force, or even a negative force, would cause it to suddenly move back towards its equilibrium state at that temperature.

References

[1] G. Akovali, J. Diamant, and M. Shen. Polyblends of poly(styrene-b-butadiene-b-styrene) and polystyrene. i. mechanical properties. *Journal of Macromolecular Science: Physics Ed.*, B13:117–131, 1977.

[2] K. R. Arnold and D. J. Meier. A rheological characterization of sbs block copolymers. *Journal of Applied Polymer Science*, 14:427–440, 1970.

[3] H. A. Barnes and K. Walters. The yield stress myth? *Rheologica Acta*, 24:323–326, 1985.

[4] H. Bauer and G. Meerlender. Polymer solutions with threshold values of shear stress and shear rate in the flow curve. *Progress in Colloid & Polymer Science*, 72:106–111, 1986.

[5] James F. Beecher, L. Marker, and R. D. Bradford. Morphology and mechanical behaviour of block copolymers. *Journal of Polymer Science: Part C*, 26:117–134, 1969.

[6] V. Bianchi, E. Pedemonte, and A Torturro. Statistical thermodynamics of styrene-butadiene block copolymers. *Journal of Polymer Science: Polymer Letters*, 7:785–788, 1969.

[7] E. T. Bishop and S. Davidson. Network characteristics of the thermoplastic elastomers. *Journal of Polymer Science: Part C*, 26:59–79, 1969.

[8] D. M. Brunwin, E. Fischer, and J. F. Henderson. Developments in self-reinforced elastomers. *Journal of Polymer Science: Part C*, 29:135–147, 1969.

[9] Chan I. Chung and John C. Gale. Newtonian behaviour of a styrene-butadiene-styrene block copolymer. *Journal of Polymer Science: Polymer Physics Edition*, 14:1149–1156, 1976.

[10] Chan I Chung and Ming I. Lin. Nature of melt rheological transition in a styrene- butadiene-styrene block copolymer. *Journal of Polymer Science: Polymer Physics Edition*, 16:545–553, 1978.

[11] Ralph H. Colby, Lewis J. Fetters, Walter G. Funk, and William W. Graessley. Effects of concentration and thermodynamic interaction on the viscoelastic properties of polymer solutions. *Macromolecules*, 24:3873–3882, 1991.

[12] D. De Kee and P. Mohan. Yield stress determination of styrene-butadiene-styrene triblock copolymer solutions. *Journal of Macromolecular Science: Physics*, 25:153–169, 1986.

[13] J. Diamant, D. S. Soong, and M. C. Williams. Modeling the viscoelastic behaviour of sbs copolymer solids. In William J. Bailey and Teiji Tsuruta, editors, *Contemporary Topics in Polymer Science, Volume 4*, pages 599–627. Plenum Publishing Corporation, 1984.

[14] Joram Diamant, David Soong, and Michael C. Williams. The mechanical properties of styrene-butadiene-styrene (sbs) triblock copolymer blends with polystyrene (ps) and styrene- butadiene copolymer (sbr). *Polymer Engineering and Science*, 22(11):673–683, 1982.

[15] Joram Diamant and Michael C. Williams. Microstructural diagnosis of block copolymer nonlinear mechanical properties ii. free recovery from large tensile deformations. *Polymer Engineering and Science*, 29(4):227–234, 1989.

[16] Joram Diamant and Michael C. Williams. Microstructural diagnosis of block copolymer nonlinear mechanical properties. iii. cycling tensile tests. *Polymer Engineering and Science*, 29(4):235–243, 1989.

[17] Joram Diamant, Michael C. Williams, and David S. Soane. Microstructural diagnosis of block copolymer nonlinear mechanical properties i. uniaxial stress/strain. *Polymer Engineering and Science*, 28(4):207–220, 1988.

[18] John D. Ferry. *Viscoelastic Properties of Polymers.* John Wiley & Sons, Toronto, 1970.

[19] L. J. Fetters, B. H. Meyer, and D. McIntyre. The effect of diblock and homopolymer impurities on the morphology of triblock polymers. *Journal of Applied Polymer Science*, 16:2079–2089, 1972.

[20] Shingo Futamura and Eberhard A. Meinecke. Effect of center block structure on the physical and rheological properties of aba block copolymers. part ii. rheological properties. *Polymer Engineering and Science*, 17(8):563–569, 1977.

[21] E. T. Bishop G. Holden and N. R. Legge. Thermoplastic elastomers. *Journal of Polymer Science: Part C*, 26:37–57, 1969.

[22] Edward V. Gouinlock and Roger S. Porter. Linear dynamic mechanical properties of an sbs block copolymer. *Polymer Engineering and Science*, 17(8):535–543, 1977.

[23] Chang Dae Han, Deog Man Baek, Jin Kon Kim, Takeji Hashimoto, and Shigeru Okamoto. Viscoelastic behaviour of a homogeneous polystyrene-block- polyisoprene-block-polystyrene copolymer. *Macromolecules*, 24:5408–5413, 1991.

[24] Chang Dae Han, Deog Man Baek, Shinichi Sakurai, and Takeji Hashimoto. Determination of the order-disorder transition temperature of a styrene-

isoprene-styrene triblock copolymer using dynamic viscoelastic measurements and small-angle x-ray scattering technique. *Polymer Journal Tokyo*, 21(10):841–846, 1989.

[25] Chang Dae Han and Jinhwan Kim. Rheological technique for determining the order-disorder transition of block copolymers. *Journal of Polymer Science: Polymer Physics*, 25:1741–1764, 1987.

[26] Chang Dae Han, Deog man Baek, Jin Kon Kim, and Sung Gun Chu. Rheological behaviour of block copolymers in the disordered state: Effects of molecular weight and block length ratio. *Polymer*, 33(2):294–305, 1992.

[27] Paula J. Hansen and Michael C. Williams. Yield stress and flow measurements in aba block copolymer melts. *Polymer Engineering and Science*, 27(8):586–597, 1987.

[28] J. P. Hartnett and R. Y. Z. Hu. The yield stress—an engineering reality. *Journal of Rheology*, 33:671–679, 1984.

[29] T. Hashimoto, M. Fujimura, K. Saijo, H. Kawai, J. Diamant, and M. Shen. Strain-induced plastic-to-rubber transition of a sbs block copolymer and its blend with ps. In Stuart L. Cooper and Gerald M. Estes, editors, *Multiphase Polymers*, pages 257–275. American Chemical Society, Washington, D. C., 1979.

[30] E. Helfand and Z. R. Wasserman. Statistical thermodynamics of microdomain structures in block copolymer systems. *Polymer Engineering and Science*, 17:582–586, 1977.

[31] Clayton P. Henderson and Michael C. Williams. A model for triblock copolymer rheology. *Journal of Polymer Science: Polymer Letters Edition*, 17:257–261, 1979.

[32] Clayton P. Henderson and Michael C. Williams. Asymmetric composition profiles in block copolymer interphases: 1. experimental evidence. *Polymer*, 26:2021–2026, 1985.

[33] Clayton P. Henderson and Michael C. Williams. Asymmetric composition profiles on block copolymer interphases: 2. thermodynamic model predictions and implications. *Polymer*, 26:2026–2038, 1985.

[34] Clayton P. Henderson and Michael C. Williams. Influece of the interphase on block copolymer thermodynamics: Extension of the leary model. *Journal of Polymer Science: Polymer Physics Edition*, 23:1001–1029, 1985.

[35] G. Scott Hugenberger and Michael C. Williams. Complex viscosity of block copolymer solutions with models of microstructural degradation. *Macromolecules*, 21:1773–1783, 1988.

[36] Takashi Inoue, Toshiichi Soen, Takeji Hashimoto, and Hiromichi Kawai. Thermodynamic interpretation of domain structure in solvent-cast films of a-b type block copolymers of styrene and isoprene. *Journal of Polymer Science: Part A-2*, 7:1283–1302, 1969.

[37] D. De Kee and C. F. Chan Man Fong. A true yield stress? *Journal of Rheology*, 37:775–776, 1993.

[38] Jeffrey C. Kelterborn and David S. Soong. Time-dependent morphologies and viscoelastic properties of block copolymers. *Polymer Engineering and Science*, 22(11):654–672, 1982.

[39] T. Kotaka and J. L. White. Rheological properties of solutions of butadiene-styrene copolymers of varying microstructure. *Transactions of the Society of Rheology*, 17:587–615, 1973.

[40] Gerard Kraus and K. W. Rollmann. Dynamic viscoelastic behaviour of aba block polymers and the nature of the domain boundary. *Journal of Polymer Science: Polymer Physics Edition*, 14:1133–1148, 1976.

[41] Gerard Kraus, K. W. Rollmann, and J. O. Gardner. Effect of domain morphology of butadiene-styrene block copolymers on viscoelastic properties and in tension shear. *Journal of Polymer Science: Polymer Physics Edition*, 10:2061–2072, 1972.

[42] S. Krause. Microphase separation in block copolymers: Zeroeth approximation. *Journal of Polymer Science: Part A-2*, 7:249–252, 1969.

[43] David F. Leary and Michael C. Williams. Statistical thermodynamics of a-b-a block copolymers: I. *Polymer Letters*, 8:335–340, 1970.

[44] David F. Leary and Michael C. Williams. Statistical thermodynamics of aba block copolymers. ii. *Journal of Polymer Science: Polymer Physics Edition*, 11:345–358, 1973.

[45] David F. Leary and Michael C. Williams. Statistical thermodynamics of block copolymers. iii. microstructural transitions and model verification. *Journal of Polymer Science: Polymer Physics Edition*, 12:265–287, 1974.

[46] D. G. LeGrand. *Polymer Preprints of the American Chemical Society, Division of Polymer Chemistry*, 11:434, 1970.

[47] L. Marker. Phase equilibria and transition behavior of block copolymers - a simple model. *Polymer Preprints of the American Chemical Society, Division of Polymer Chemistry*, 10:524, 1969.

[48] T. Masuda, Y. Matsumoto, and S. Onogi. *Journal of Macromolecular Science: Physics*, 17:265, 1980.

[49] N. G. McCrum, C. P. Buckley, and C. B. Bucknall. *Principles of Polymer Engineering.* Oxford University Press, Oxford, 1988.

[50] D. J. Meier. Theory of block copolymers. i. domain formation in a-b block copolymers. *Journal of Polymer Science: Part C*, 26:81–98, 1969.

[51] D. J. Meier. A theory of the domain and interfacial properties of block copolymers. In *Polymer Colloquy*, Kyoto, Japan, September 1977.

[52] Faith A. Morrison and H. Henning Winter. Effect of unidirectional shear on the structure of triblock copolymers 1. polystyrene-polybutadiene-polystyrene. *Macromolecules*, 22:3533–3540, 1989.

[53] Faith A. Morrison, H. Henning Winter, Wolfram Gronski, and John D. Barnes. Effect of unidirectional shear on the structure of triblock copolymers. 2. polystyrene-polyisoprene-polystyrene. *Macromolecules*, 23:4200–4205, 1990.

[54] Maurice Morton, James E. McGrath, and Peter C. Juliano. Structure-property relationships for styrene-diene thermoplastic elastomers. *Journal of Polymer Science: Part C*, 26:99–115, 1969.

[55] D. R. Paul, J. E. St. Lawrence, and J. H. Troell. Flow behaviour of concentrated solutions of an sbs block copolymer. *Polymer Engineering and Science*, 10(2):70–78, 1970.

[56] Efrain R. Pico and Michael C. Williams. Viscosity in the phase transition region of triblock copolymer systems. *Nature*, 259(5542):388–389, February 5 1976.

[57] Efrain R. Pico and Michael C. Williams. Thermodynamics of plasticized triblock copolymers. i. theory. *Journal of Polymer Science: Polymer Physics Edition*, 15:1585–1600, 1977.

[58] Efrain R. Pico and Michael C. Williams. Thermodynamics of plasticized triblock copolymers. part ii: Model verification by light transmittance and rheology. *Polymer Engineering and Science*, 17(8), 1977.

[59] Efrain R. Pico and Michael C. Williams. Solvation and phase separation in aba block copolymers. *Journal of Applied Polymer Science*, 22:445–457, 1978.

[60] Rheometrics Inc., One Possumtown Road, Piscataway, NJ 08854. *RMS 800 Owner's Manual*, september 1990 edition.

[61] Ferdinand Rodriguez. *Principles of Polymer Systems.* Hemisphere Publishing Corporation, New York, 1989.

[62] Ryong-Joon Roe, M. Fishkis, and J. C. Chang. Small-angle x-ray diffraction study of thermal transition in styrene-butadiene block copolymers. *Macromolecules*, 14:1091–1103, 1981.

[63] J. Schurz. A yield value in a true solution? *Journal of Rheology*, 36:1319–1321, 1992.

[64] M. Shen and D. H. Kaelble. On the viscoelastic behaviour of a styrene-butadiene- styrene (s-b-s) block copolymer. *Polymer Letters*, 8:149–153, 1970.

[65] Mitchel Shen and David R. Hansen. Viscoelastic relaxation times of a homogeneous block copolymer. *Journal of Polymer Science: Symposium*, 46:55–67, 1974.

[66] Naomi Sivashinsky, Tak Jin Moon, and David S. Soong. Transient structures and rheological properites of sbs block copolymer melts. *Journal of Macromolecular Science: Physics*, 1983:213–229, 1983.

[67] D. S. Soong, N. Sivashinsky, and J. C. Kelterborn. Dynamic mechanical and rheological properties of sbs block copolymers and their blends with sbr. *Journal of Elastomers and Plastics*, 15:193–206, 1983.

[68] Richard J. Spontak and Michael C. Williams. Prediction of microstructures for polydisperse block copolymers, using continuous thermodynamics. *Journal of Polymer Science: Polymer Physics*, 28:1379–1407, 1990.

[69] Richard J. Spontak, Michael C. Williams, and David A. Agard. Interphase composition profile in sb/sbs block copolymers, measured with electron microscopy, and microstructural implications. *Macromolecules*, 21:1377–1387, 1988.

[70] Richard J. Spontak, Michael C. Williams, and Caroline N. Schooley. Morphology of bulk sbs block copolymers prepared by wet cryo-ultramicrotomy. *Journal of Materials Science*, 21:3173–3178, 1986.

[71] Zehev Tadmor and Costas G. Gogos. *Principles of Polymer Processing.* John Wiley and Sons, New York, 1979.

[72] The IUPAC Working Party on "Structure and Properties of Commercial Polymers". Development of a residual shear stress in an sbs block copolymer during stress relaxation following steady-state flow. *Journal of Polymer Science: Polymer Physics Edition*, 18:397–399, 1980.

[73] Takanori Uchida, Toshinichi Soen, Takashi Inoue, and Hiromichi Kawai. Domain structure and bulk properties of solvent cast films of a-b-a block copolymers of styrene-isoprene-styrene. *Journal of Polymer Science: Part A-2*, 10:101–121, 1972.

[74] G. V. Vinogradov, V. E. Dreval, A. Ya. Malkin, Yu. G. Yanovsky, V. V. Barancheeva, E. K. Borisenkova, M. P. Zabugina, E. P. Plotinkova, and O. Yu. Sabsai. Viscoelastic properties of butadiene-styrene block copolymers. *Rheologica Acta*, 17:258–263, 1978.

[75] Leigh Wardhaugh. Work on the rheology of polyolefins. University of Alberta Department of Chemical Engineering, 1993.

[76] Hiroshi Watanabe, Tadao Kotaka, Mitsuhiro Shibayama, and Hiromichi Kawai. Rheological and morphological behaviour of styrene-butadiene diblock copolymer solutions in selective solvents. *Journal of Rheology*, 26:153–179, 1982.

[77] A. Weill and R. Pixa. Styrene-diene triblock copolymers: Orientation conditions and mechanical properties of the oriented materials. *Journal of Polymer Science: Polymer Symposium*, 58:381–394, 1977.

Appendix A

Calibrations

A.1 Torque

Torque calibrations on the RMS 800 transducer are done by hanging a known weight on a monofilament line which loops over a pulley to a 5 cm moment arm mounted on the transducer. The arrangement is shown in Figure A.1.

A 200 g weight (supplied with the rheometer calibration kit) should result in a 1000 g·cm ± 3% torque (according to manufacturer specifications). The torque values resulting from several weights were measured to determine the calibration and linearity of the transducer in the normal (or high-torque) range. These are shown in Table A.1. As a consequence of verification of the manufacturers calibration, within the 3% tolerances specified, the RMS 800 values for torque and related physical properties were used without any correction factors being applied.

In order to determine the reliability of measured torque values below the quoted lower limit of 2 g·cm a calibration was also performed with small weights.

First, the zero was determined. With no weight or line on the moment arm (6, Figure A.1) many readings of the zero were taken to determine the average "zero" reading. Weights of 500 mg, 200 mg and 50 mg were then hung on the moment

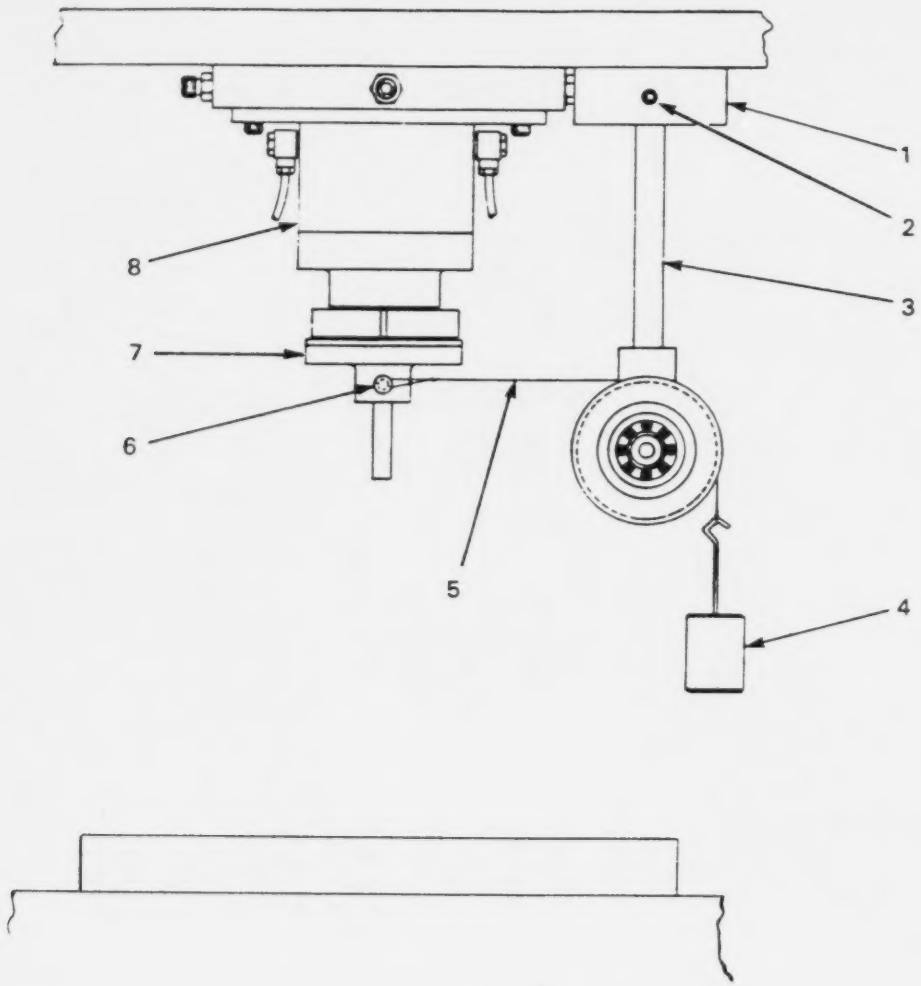

LEGEND

1. Pulley Mounting Bracket
2. Set Screw
3. Calibration Pulley
4. Weight
5. Monofilament Line
6. Moment Arm
7. Calibration Collar
8. Mid Range FRT

Figure A.1: Transducer calibration set-up.

Table A.1: Normal torque range calibration.

Weight (g)	Torque (g·cm)*	Error
200	1001	+0.1%
100	504.4	+0.88%
50	252.7	+1.08%

* Average of three readings

arm and many torque readings were recorded. At these low weights the weight of the monofilament line may have had a measurable effect on the reading. The line was weighed on an electronic balance with a precision of 10^{-4}g. The weight of the line was 0.0205 g. Roughly half the line extends from the high point of the pulley wheel to the weight. Therefore, only half the weight of the line was included in the calculation of total weight. The results are given in Table A.2 along with statistical analysis.

For the 500 mg and 200 mg weights, the mean indicated torque was 2.2% higher than the true torque (calculated from the weight and length of the moment arm). The standard deviations relative to the mean were 0.7% and 1.5% respectively. This level of uncertainty is acceptable, as the quoted accuracy of the transducer is only ±3% in the normal torque range (this being a conservative manufacturer quote, as the transducer is generally more accurate than that). Therefore, torques as low as 1 g·cm can be measured with sufficient accuracy and confidence.

For the 50 mg weight, the mean indicated torque was high by 20%. The relative standard deviation was almost 30%. Such high error and standard deviation throws into question the reliability of numerical results in this torque range (3×10^{-1} g·cm). However, since the mean indicated torque for the "zero" was one order of magnitude lower it can be concluded that torques in the range of 10^{-1} can be considered non-zero with confidence.

Table A.2: Low torque range calibration.

Weight (including $\frac{1}{2}$ line)	0	510 mg	210 mg	60 mg
True Torque (g·cm)	0	2.55	1.05	0.3
Indicated Torque (g·cm)	0.01400	2.65000	1.11000	0.41610
	0.00860	2.62000	1.09900	0.25990
	0.00422	2.62100	1.08300	0.37870
	0.01390	2.61900	1.07300	0.31520
	0.00741	2.61800	1.08600	0.47790
	0.00801	2.60700	1.06700	0.19390
	0.02500	2.59600	1.06200	0.19390
	0.00490	2.60800	1.06900	0.42610
	0.00067	2.60900	1.06700	0.32010
	0.00062	2.60300	1.05000	0.45950
	0.00339	2.61000	1.05800	0.22010
	0.01900	2.59100	1.06600	0.31520
	0.00342	2.58000	1.06600	0.47870
	0.01041	2.57500		0.45640
	0.01800			0.48120
	0.02140			
	0.02020			
	0.02020			
	0.00901			
	0.00550			
	0.01000			
Statistical Analysis				
Mean	0.01085	2.60764	1.07354	0.35953
Standard Deviation	0.00735	0.01888	0.01676	0.10694

A.2 Gap

The gap, or spacing between the surfaces of the platens in contact with the sample (H in Equation 4.1), must be known accurately in order to calculate the strain. A problem therefore arises because the platens expand and contract with temperature, thereby changing the gap. In order to account for this a calibration was performed to determine the change in gap with temperature.

The gap was first zeroed at room temperature by lowering the upper platen until a positive normal force was detected by the first deflection of the normal force analogue meter. The upper platen was then raised and the platens were heated a few degrees using the convection oven, allowing a 5 minute thermal soak time after steady temperature had been reached. At the new temperature the upper platen was again lowered until the first deflection of the normal force analogue meter was detected. The gap reading then indicated the combined expansion of both platens and hence the decrease in the gap. The results are given in tabular form in Table A.3 and graphically in Figure A.2. This expansion of the platens decreases the true gap by the same amount. Therefore, if the gap is zeroed at some temperature T_1, then the true gap at T_2 can be obtained by subtracting the "gap" reading from Table A.3 or Figure A.2 at T_2 minus that at T_1 from the gap indicated by the dial guage.

A.3 Circulation Jacket

The circulation jacket was described in Section 4.10. A calibration was performed to determine sample temperature *vs.* tool temperature. A polydimethylsiloxane (silicone) fluid was loaded between the platens with a 2 mm gap and three thermocouples of diameter 0.020 inch were inserted at different points in the sample. One thermocouple was very close to one of the nitrogen ports in the jacket. The

Table A.3: Tool expansion calibration.

Temperature (°C)	Gap (Microns)	Temperature (°C)	Gap (Microns)
26.3	0	140.3	352
29.4	25	144.9	372
34.2	35	150.5	392
39.2	50	155.5	412
44.3	62	160.7	427
49.4	76	165.9	442
54.4	88	170.9	454
59.4	88	176.1	468
64.4	100	181.2	490
69.5	122	185.6	506
74.6	140	190.6	516
79.6	160	195.8	524
84.8	184	200.9	548
90	204	206.2	580
95	230	211.1	590
100.1	242	216.2	600
105.1	256	221.3	618
110.1	268	226	622
115.1	282	231.5	634
119.8	298	236.2	640
125.1	304	241.6	658
130.3	326	246.6	678
135.3	340	250.8	690

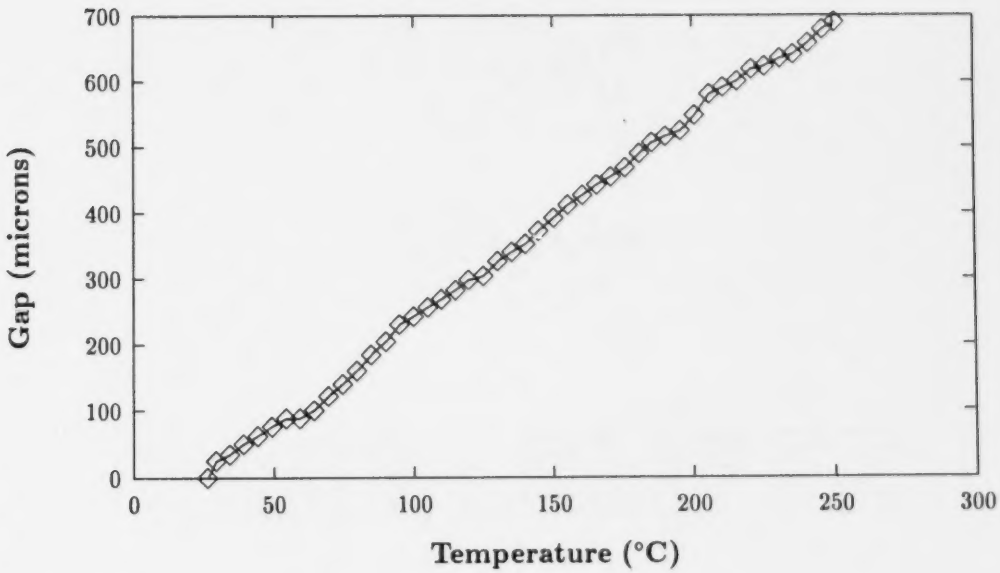

Figure A.2: Tool expansion calibration.

thermocouples were read on a DVM and referenced to an ice point in a 1 L beaker of distilled water and ice made from distilled water, chilled overnight. The ice was replenished frequently to maintain the temperature within 0.2°C of zero as read on a mercury thermometer with 0.1°C divisions. It was found that temperatures at steady state never varied more than two tenths of a degree between the three thermocouples.

With the circulator set for minimum temperature (-30°C) the nitrogen flowrate was gradually increased to achieve minimum sample temperature. It was found that a N_2 flowrate of 5 L per minute as measured on a Matheson 603 rotameter yielded the sample temperature closest to the temperature set point. At this N_2 flowrate the circulator temperature set point was gradually increased and both tool temperature and sample temperature were recorded. The results of this calibration are given in tabular form in Table A.4 and graphically in Figure A.3. In Table A.4, where several tool and sample temperatures are given at one set point, these are temperatures evolving over time so that the last temperature is the steady state temperature.

Table A.4: Circulation jacket temperature calibration.

All Temperatures in °C					
Set Point	**Tool**	**Sample**	**Set Point**	**Tool**	**Sample**
-30	-24.6	-22.85	25	24.7	24.53
	-23.6	-22.06	30	29.4	28.65
-28	-23.3	-21.59	35	34.0	33.66
	-20.8	-19.11		38.4	38.13
	-19.3	-17.84	40	38.7	38.35
	-19.0	-17.62	45	43.4	43.06
	-18.8	-17.54		47.7	47.43
-23	-18.9	-17.52		48.1	47.82
	-14.5	-13.62		48.2	47.89
	-14.3	-13.32	50	48.3	47.82
-18	-14.4	-13.35	55	52.8	52.71
	-10.2	-9.49		57.2	57.10
-13	-9.9	-9.22		57.4	57.32
	-5.7	-5.32	60	57.6	57.37
	-5.4	-5.00	65	62.3	62.18
-8	-5.3	-4.90		66.8	66.87
	-0.8	-0.73	70	67.0	66.97
-3	-0.6	-0.61	75	71.7	71.83
0	2.0	2.02		76.3	76.54
	6.4	6.24	80	76.5	76.61
5	6.5	6.22		81.1	81.28
10	11.0	10.98	85	81.2	81.45
15	15.5	15.37	90	85.9	86.31
20	20.1	19.89		90.6	90.97
			95	90.7	91.12
				95.4	95.85

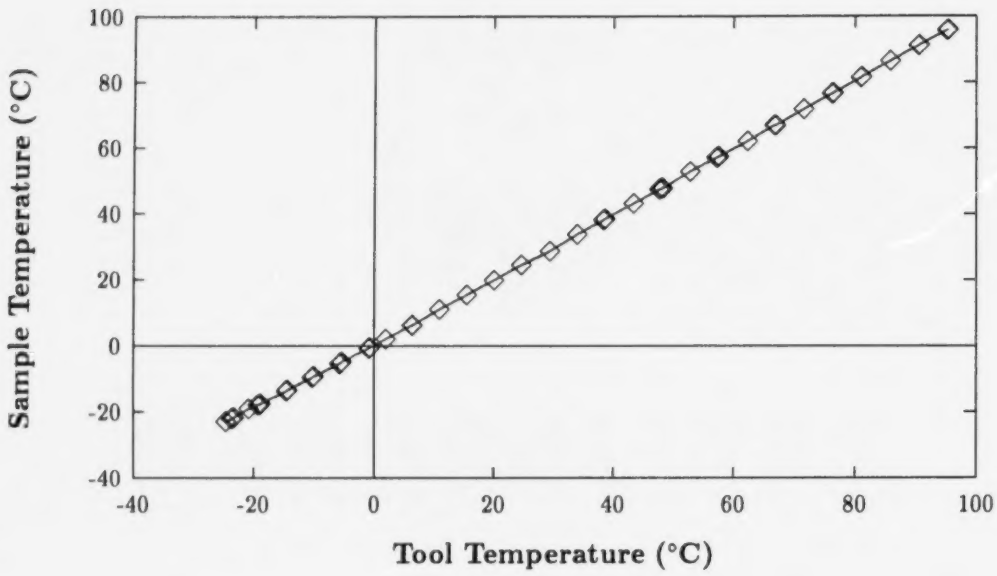

Figure A.3: Circulation oven temperature calibration.

Appendix B

Compression Mold

The design of the mold is given in Figures B.1 and B.2. The disc heater used has a power rating of 600 W.

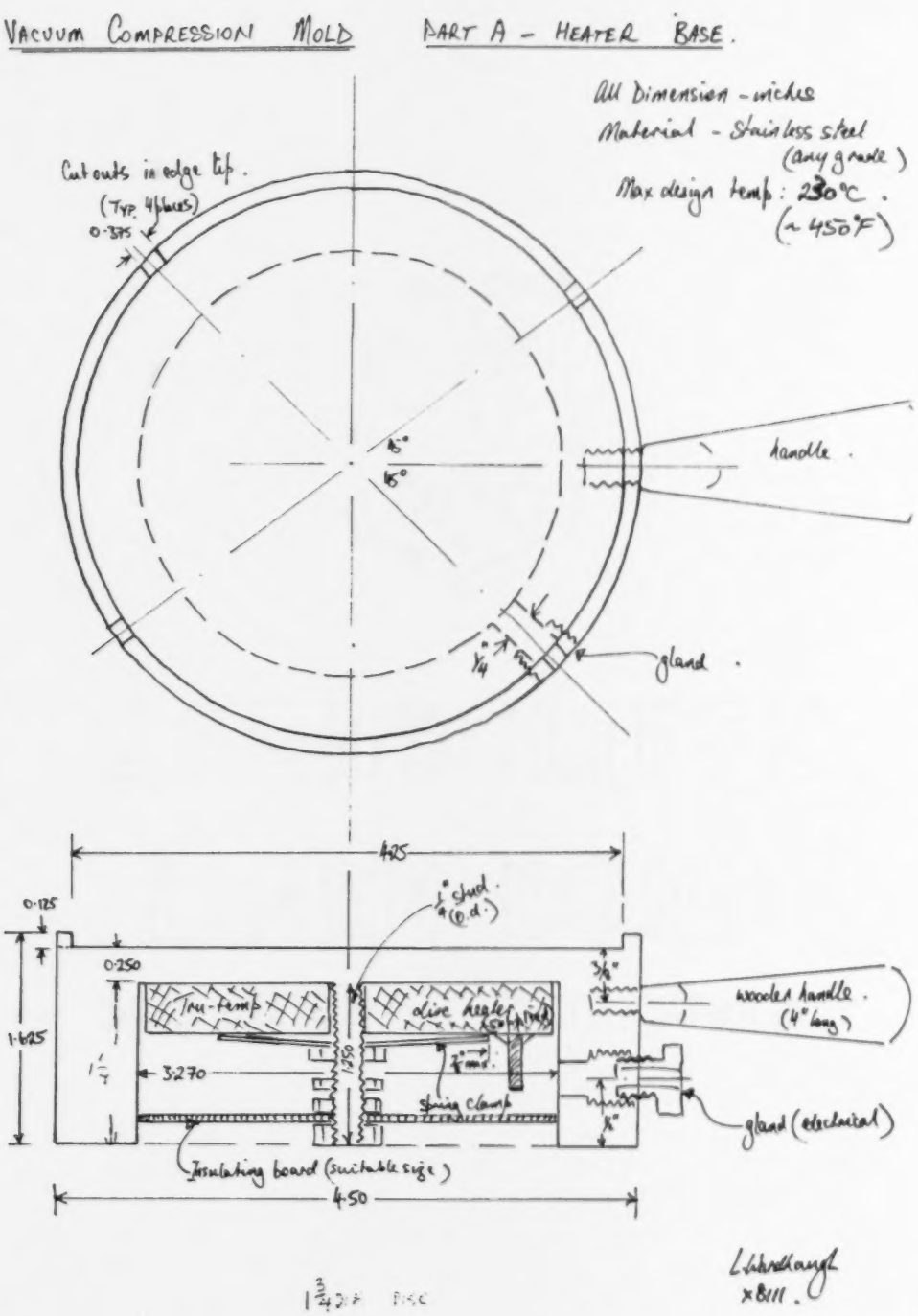

Figure B.1: Compression mold (a); heater base.

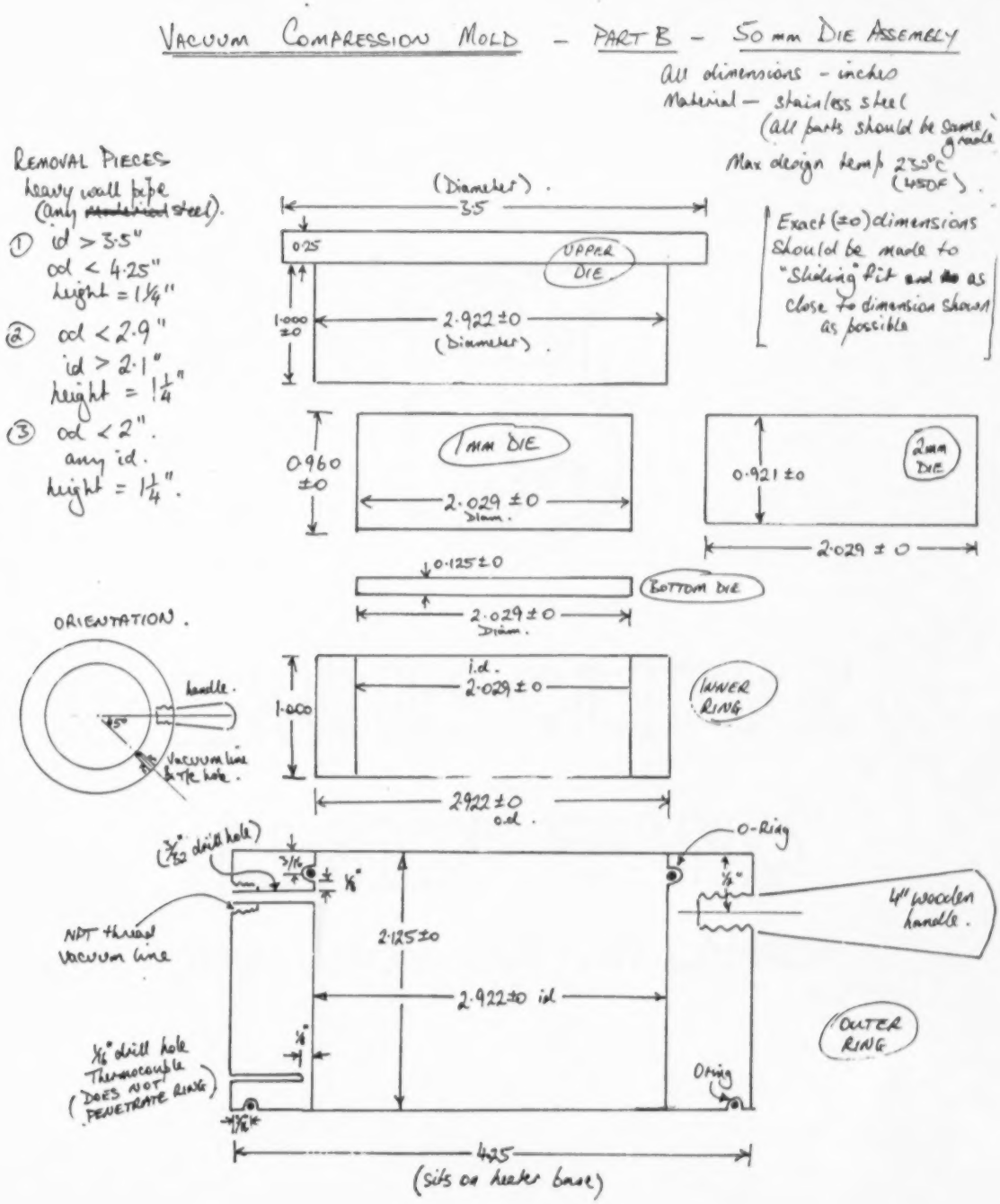

Figure B.2: Compression mold (b); 50 mm die assembly.

Appendix C

Graphical Curve Fitting

The method of Ferry ([18], Chapter 5) for the graphical fitting of relaxation times is described here. The method is demonstrated step by step for the plot of relaxation modulus for SBS1 following a 1% step strain at 90°C.

We begin with an equation of the form

$$G_r(t) = G_1 e^{-t/\lambda_1} + G_2 e^{-t/\lambda_2} + G_3 e^{-t/\lambda_3} + \ldots \tag{C.1}$$

which is a simple series of Maxwell elements and, by convention, $\lambda_1 > \lambda_2 > \lambda_3 \ldots$.

The stress relaxation data, or $G_r(t)$, from a step strain experiment is plotted on a logarithmic abscissa against a linear time scale. To obtain the longest relaxation time (λ_1) we fit a tangent to the curve at the longest test times:

$$G_r(t)|_{t\to\infty} \approx G_1 e^{-t/\lambda_1} + negl. \tag{C.2}$$

so that:

$$2.3 \log G_r = 2.3 \log G_1 - \frac{t}{\lambda_1}. \tag{C.3}$$

The slope of the tangent then gives the relaxation

$$\lambda_1 = \frac{-1}{2.303 * slope}. \tag{C.4}$$

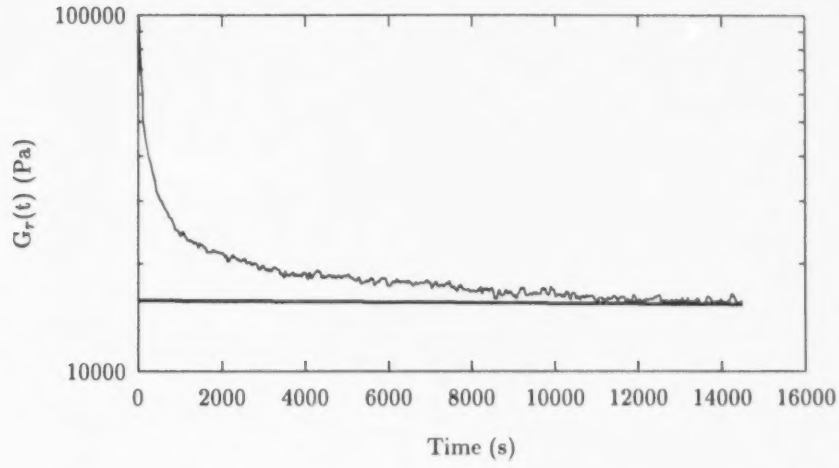

Figure C.1: First (longest) relaxation fit to $G_r(t)$ for SBS1 at 1% strain and 90°C.

The intercept of the tangent gives G_1, which would be $G_r(0)$ *assuming only one relaxation time,* λ_1. This is shown in Figure C.1 where

$$G_r(t)|_{t\to\infty} = 15,800e^{-t/600,000} = G_1e^{-t/\lambda_1} \tag{C.5}$$

is fit to the curve, giving a relaxation time of 6×10^5 seconds and an intercept of 15,800 Pa.

The influence of that relaxation can then be subtracted from the curve of $G_r(t)$ to obtain the next shorter relaxation time

$$G_r'(t) = G_r(t) - G_1e^{-t/\lambda_1} = G_2e^{-t/\lambda_2} + G_3e^{-t/\lambda_3} + \ldots \tag{C.6}$$

so,

$$G_r'(t)|_{t\to\infty} \approx G_2e^{-t/\lambda_2}. \tag{C.7}$$

Figure C.2 shows the longest relaxation (Equation C.5) stripped off by Equation C.6 and a second relaxation fit by the tangent

$$G_r'(t)|_{t\to\infty} = 5,500e^{-t/5,800} = G_2e^{-t/\lambda_2}. \tag{C.8}$$

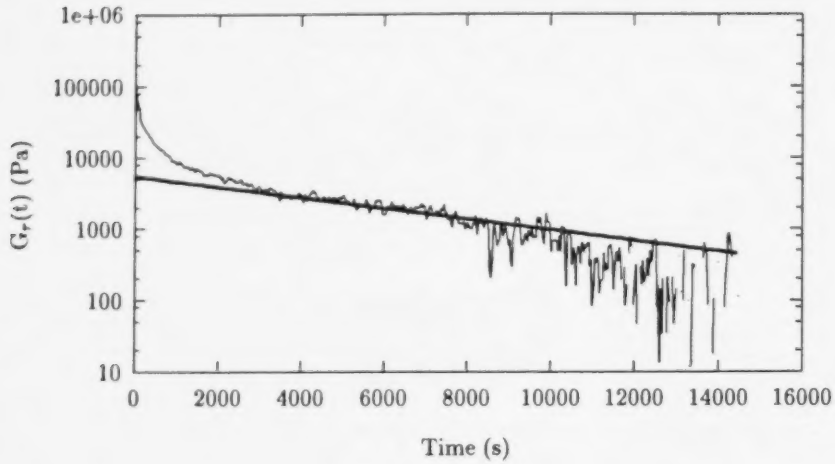

Figure C.2: Second relaxation fit to $G_r(t)$ for SBS1 at 1% strain and 90°C.

This is repeated twice again in Figures C.3 and C.4, giving the relaxations

$$G_r''(t)|_{t\to\infty} = 31,000e^{-t/436} = G_3e^{-t/\lambda_3} \tag{C.9}$$

and

$$G_r'''(t)|_{t\to\infty} = 50,000e^{-t/70} = G_4e^{-t/\lambda_4}. \tag{C.10}$$

The four relaxations fit to the curve are shown together with the data in Figure C.5

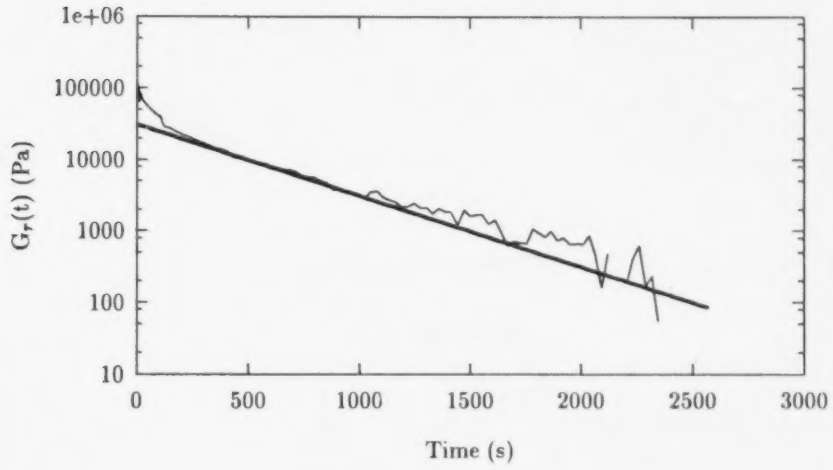

Figure C.3: Third relaxation fit to $G_r(t)$ for SBS1 at 1% strain and 90°C.

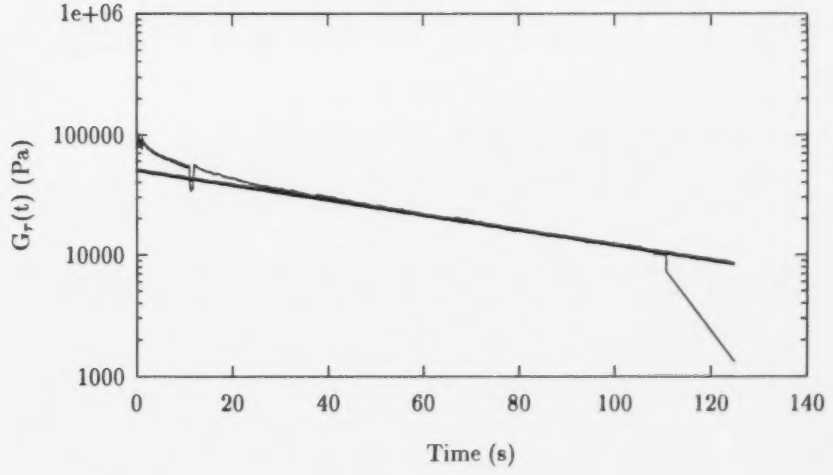

Figure C.4: Fourth relaxation fit to $G_r(t)$ for SBS1 at 1% strain and 90°C.

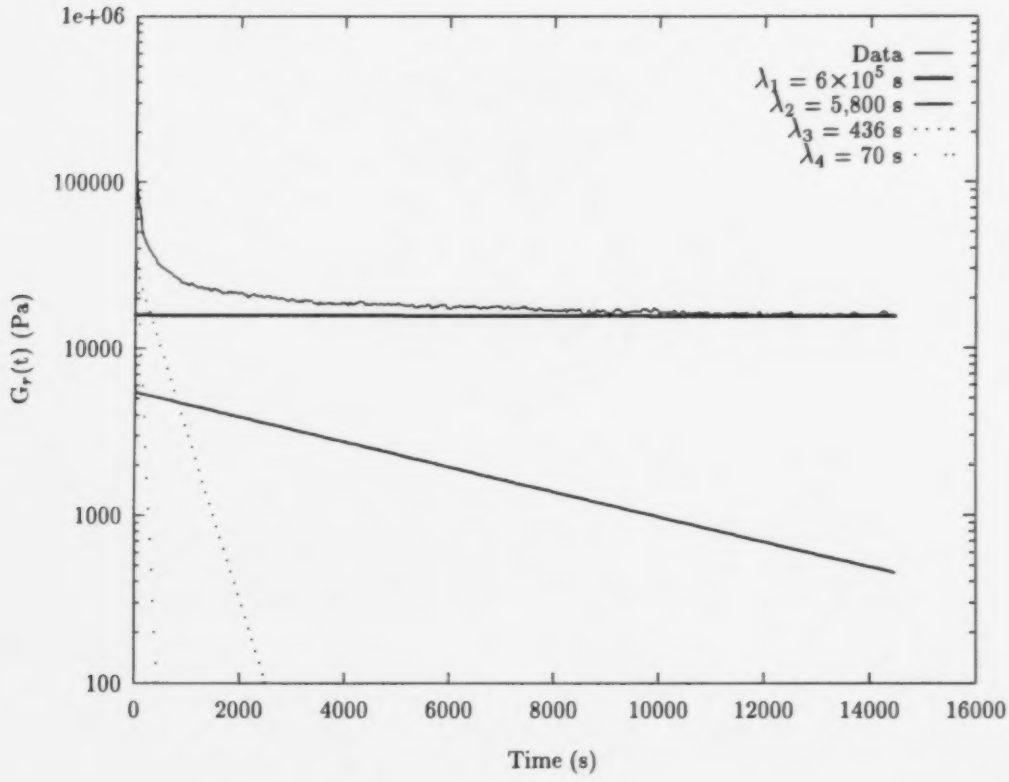

Figure C.5: Composite of relaxations fit to $G_r(t)$ for SBS1 at 1% strain and 90°C.

Appendix D

Copyrighted Materials

Figures 2.3, 4.1 and A.1 were each taken from the Rheometrics September 1990 RMS 800 Owners Manual, which is copyrighted material. A letter of permission from Rheometrics to use this material is included on the next page.

Rheometrics

Rheometrics, Inc.
One Possumtown Road
Piscataway, NJ 08854
Phone (908) 560-8550
Telex 219107 RHEO UR
Telefax (908) 560-7451

June 16, 1993

Mr. Robert Spaans
University of Alberta
Department of Chemical Engineering
536 Chemical-Mineral Engineering Building
Edmonton, Alberta
T6G 2R3, Canada

Dear Mr. Spaans:

This is in response to your request to include several figures from Rheometrics' September 1990 RMS Owners Manual in your thesis. On behalf of Rheometrics, I grant you permission to use Figures 4-5 on page 4-9, 6-32 on page 6-73 and 8-7 on page 8-13.

I would appreciate receiving a copy of your thesis for our files. It is always intriguing to see how Rheometrics instrumentation helps today's scholars become tomorrow's scientists.

Congratulations on the completion of your Master of Science.

Sincerely,

Alberto Correa
Director/Technical Services